**Title**

The impact of autism spectrum disorder risk gene mutations on striatal circuit function



**Author**

Cording, Katherine Rose

**Publication Date**

2024

Peer reviewed|Thesis/dissertation

# The impact of autism spectrum disorder risk gene mutations on striatal circuit function

By

Katherine Rose Cording

A dissertation submitted in partial satisfaction of the

requirements for the degree of

Doctor of Philosophy

in

Neuroscience

in the

Graduate Division

of the

University of California, Berkeley

Committee in Charge:

Professor Helen Bateup, Chair
Professor Daniel Feldman
Professor Andrea Gomez
Professor Linda Wilbrecht

Spring 2024

Abstract

The impact of autism spectrum disorder risk gene mutations on striatal circuit function

by

Katherine Rose Cording

Doctor of Philosophy in Neuroscience

University of California, Berkeley

Professor Helen Bateup, Chair

Autism spectrum disorder (ASD) is a neurodevelopmental disorder characterized by persistent deficits in social communication and interaction, and the presentation of restricted repetitive patterns of behavior. The prevalence of ASD has increased steadily in the last 40 years, with a recent study from the Center for Disease Control (CDC) indicating that roughly 1 in 36 children in America is diagnosed with ASD. The disorder has a strong genetic component, and there have now been over 100 high confidence ASD risk genes identified through genetic sequencing of those with ASD. As improved genetic tools allow for these genes to be identified, genetic access in animal models has also improved, allowing for the development of many mouse models of ASD that harbor mutations in these identified genes. ASD risk genes vary greatly in the types of proteins for which they encode, including ion channels, neurotransmitter receptors, cell adhesion molecules, and machinery implicated in all aspects of transcription and translation. Despite this genetic heterogeneity, the major diagnostic criteria of ASD still fit within the two symptom domains listed above. Given this shared symptomology, much work in ASD research has focused on identifying brain regions that may be commonly impacted across a range of underlying genetic alterations. The basal ganglia, in particular the striatum, the primary input center of the basal ganglia, has arisen as one such brain region. We believe that dysfunction of the striatum, given its known role in action selection, motor learning, and habit formation, may be particularly implicated in the restricted, repetitive behavior domain of ASD. However, whether altered striatal function is a shared pathophysiology across genetically diverse ASD mouse models has yet to be comprehensively assessed.

For this dissertation project, I investigated this question in two unique ASD mouse models. First, I developmentally deleted the ASD risk gene *Tsc1* selectively from the two primary types of striatal projection neurons (SPNs). I found that loss of Tsc1 selectively from SPNs of the direct pathway (dSPNs), but not the indirect pathway (iSPNs), increases cortical drive of these neurons, likely through increased glutamate release from cortical inputs onto these cells. This increased corticostriatal drive of the direct pathway increases motor learning, measured through enhanced performance in

the accelerating rotarod assay. Altered cortical input to the striatum has arisen as a potential convergent change across a number of ASD mouse models, an idea that is reviewed and expanded upon in the second chapter of this dissertation.

To investigate whether striatal function and striatum-associated behaviors are altered in a genetically distinct mouse model, I utilized mice with brainwide loss of the ASD risk gene *Cntnap2*. I found that mice lacking *Cntnap2* also exhibited increased cortical drive, of both dSPNs and iSPNs. In this model however, cortical synaptic input onto SPNs was unchanged. Instead, the intrinsic excitability of SPNs in *Cntnap2*$^{-/-}$ mice was significantly increased, in particular in dSPNs, which likely underlies the increased cortical drive of these cells. Behaviorally, *Cntnap2*$^{-/-}$ mice also exhibit increased performance in the accelerating rotarod task, as well as increased spontaneous repetitive behaviors, and cognitive inflexibility in a reversal learning task. Together, these findings support a role for striatal dysfunction in the manifestation of stereotyped, inflexible behaviors across ASD mouse models with varying genetic causes. In particular, this data supports an emerging theory that corticostriatal alterations, in particular enhanced cortical activation of the movement-initiating direct pathway, may occur commonly in the case of ASD-associated repetitive behaviors.

**Acknowledgments**

First, thank you to Helen, for being a fantastic, kind and generous mentor. You've always struck the perfect balance of giving me the space and encouragement to learn and grow on my own, while also pushing me to achieve more with my work than I thought possible. I'm leaving graduate school far more confident in myself as a scientist, and as a person, and I have you to thank for a lot of that. I am incredibly grateful.

Thank you to my committee members – Dan Feldman, Linda Wilbrecht, Andrea Gomez. You've been a great resource over the years. The thoughtful advice that you brought to our meetings has helped me immensely.

Thank you to my fellow Bateup lab members, for being a community of friendly people always willing to help. I benefitted greatly from working alongside colleagues asking such a diverse range of scientific questions and have learned a lot from all of you as a result. Thank you in particular to Emilie Tu – I couldn't have asked for a better mentee. Your interest and eagerness reignited in me a youthful love of research. Your help was crucial to getting our project over the finish line, and I'm very proud of the work that we did together. I'm so excited to see what you do in the rest of your scientific career, as I have the utmost faith that it will be spectacular.

Thank you to my friends in the Bay Area – Cameron Baker, Alex Naka, Charles Frye, Dylan Paiton, Christine Hopkins, Kelsey Howard and all of the rest of the Very Best Friends. I am so lucky to have found this fantastic group of people early in graduate school. You made all the tough times easier. Seeing the former graduate students in the group (Cam, Alex, Charles, Dylan) do amazing things after their PhDs helped me see what could be out there for me on the other side, and that made the work easier, too. Science advice, life advice, cookbook club, movie nights and river floats – graduate school would've been a lot harder without the VBFs.

Thank you to my fellow FentCheck comrades and Skeeball teammates, Alison Heller and Holly Gore. It's been a blast getting to know you guys while becoming mutually obsessed with competitive Skeeball, a hobby that we only recently realized exists. If the science thing doesn't work out, now I know I've got Skeeball talent to fall back on. In seriousness, thank you especially to Ali. Doing harm reduction work with you through FentCheck has been one of the most meaningful experiences of my life. You're a truly inspiring person and I'm so happy to work alongside you while you make our corner of the world better.

Thank you to my far-away friend but forever anchor, Ben Miller. You've been with me for every step of this research journey. You continue to be the most supportive, curious, empathetic, thoughtful friend that I could ask for and nine-hour time difference be damned, you're always right there when I need you.

Finally, to my family – Mom, Dad, Becka, Annie, Devin and Ada – I couldn't have done any of this without you. Your unwavering belief in me has buoyed me through it all. From the trips home to Colorado to spend time with you all, to the innumerable anxiety-ridden phone calls to Mom, you guys were the unshakeable lifeline. Words can't express how grateful I am for your support and your love, thank you.

## Table of Contents

# Chapter 1: The striatum as a common site of functional change across a diverse range of genetic autism spectrum disorder mouse models

Katherine Cording

Helen Wills Neuroscience Institute
University of California, Berkeley

## Introduction

Autism spectrum disorder (ASD) is a neurodevelopmental disorder characterized by persistent deficits in social communication and interaction, and the presentation of restricted, repetitive behaviors (APA, 2022). First described by physician Leo Kanner in the 1940's (Kanner, 1968), ASD was not considered a diagnosable disorder, nor was it considered to be biological, until the 1980's (Geschwind, 2011). Since that time, the estimated prevalence of ASD has grown continuously, with estimates of 1 in 100 children having ASD globally, and Centers for Disease Control and Prevention (CDC) reports suggesting an even greater prevalence of 1 in 36 children in America (Maenner et al., 2023; Talantseva et al., 2023; Zeidan et al., 2022). Studies suggest that this increase is likely due not to significant changes or increases in ASD risk factors over time, but rather an increased awareness and understanding of ASD symptomology amongst parents, caretakers and physicians such that diagnoses are more accessible (Lord et al., 2020; Taylor et al., 2020). Changes to the diagnostic criteria during this time, in particular the categorization of autism as a spectrum disorder beginning in the early 2000's, also contributed greatly to changes in diagnosis (Volkmar & McPartland, 2014). While a diagnosis of ASD does require the presentation of multiple behaviors within both the social and repetitive behavior symptom domains (APA, 2022), the presentation of ASD is heterogeneous. Before children learn to speak, delayed development of early social communication skills such as following social stimuli with eye contact, or joint attention, the sharing of attention on an object or event with an individual, may indicate future communication deficits (DeQuinzio et al., 2016). Later, these deficits may include avoiding eye contact during interaction, decreased use of communicative gestures, reduced sharing of interests, or overall difficulty in developing, understanding and maintaining relationships (APA, 2022). In some cases, individuals on the autism spectrum are completely non-verbal. However, many others may have no detectable language problems (Eigsti et al., 2011).

Restricted, repetitive patterns of behavior can include motor stereotypies (i.e. hand-flapping, self-hitting, echolalia, lining up or flipping objects) or overarching insistence on sameness in life, resulting in difficulties with changes in routines, or intensely fixated interests (APA, 2022). In addition to motor stereotypies, there is also evidence that gross motor changes in balance, gait, posture as well as motor skill learning occur commonly in ASD (Chukoskie et al., 2013). Although criteria within the social communication and repetitive behavior symptom domains differ, a number of studies have shown that motor skill deficits relate to social communication functions within individuals with ASD (MacDonald et al., 2013; West, 2019), such that in some cases, motor delays were predictive of future communication deficits (Bhat et al., 2012). Following from that, a number of studies have found that early physical activity interventions for motor delays has a positive effect on later social functioning (Busti Ceccarelli et al., 2020; Healy et al., 2018). Increased understanding of the clinical presentation of ASD symptoms, and functional relationships between them, will continue to improve the holistic understanding of ASD.

With increasing estimated prevalence and diagnosis, so too has grown the understanding of the biological and genetic basis of ASD. Twin studies have shown that ASD is highly heritable, with heritability of the disorder estimated at 83% (Sandin et al., 2017). Increased accessibility of DNA sequencing has allowed for investigation into this

genetic basis, resulting in the identification of genetic mutations that are likely to confer increased risk of developing ASD. Recently, a large-scale exome sequencing study of over 30,000 samples identified just over 100 high confidence ASD risk genes (Satterstrom et al., 2020). As access to the genetic roots of ASD has expanded, so has the ability to develop genetic mouse models of ASD (Bey & Jiang, 2014). Many modern ASD mouse models exhibit good construct validity, where the mutation used to generate the model of ASD is one that has been identified in individuals with ASD (Nestler & Hyman, 2010). Availability of these models has allowed for more direct investigation into the consequences on cellular function that occur as a result of gene mutations. Although there are many ASD risk genes that encode diverse types of proteins, they can be grouped based on similar functionality, leading to a more cohesive understanding of some of the cellular processes that may be commonly altered in ASD.

**Genetic functional domains commonly altered in ASD**

*Intrinsic and synaptic physiological function*

A large number of high confidence ASD risk genes can be broadly grouped into two functional domains: (1) regulation of neuronal excitability and synaptic function/stabilization, and (2) transcriptional and translational regulation. The former group includes genes that encode proteins implicated at every level of intrinsic neuronal physiology and synaptic transmission, including ion channels, neurotransmitter receptors, scaffolding proteins and cell adhesion molecules (Delorme et al., 2013). Both genes for ion channels involved in regulating intrinsic cell physiology (*SCN1A, SCN2A*) and those for receptors involved in synaptic signaling (*GRIN2B, GABRB3*) are implicated in ASD (Schmunk & Gargus, 2013). While alteration of these genes impacts neuronal excitability directly, ASD-associated mutations in genes encoding proteins involved in the localization of channels and receptors (*SYNGAP1, CNTNAP2*) and synaptic stabilization (*SHANK* genes, *NLGN3*) also impact neuronal communication (De Rubeis et al., 2014).

Considering many ASD risk gene mutations alter the synaptic and/or intrinsic physiological function of neurons, one of the earliest theories explaining circuit dysfunction in ASD was the inability for excitatory and inhibitory neurons to communicate properly and maintain appropriate balance of activity (Rubenstein & Merzenich, 2003). More specifically, a number of ASD mouse model studies have identified deficits in inhibitory neurons across cortex and hippocampus, a change that may result in overly excitable, “noisier” circuits and thus less efficient information processing (Lee et al., 2017). Indeed optogenetic manipulations that decrease inhibitory neuron function and/or promote excitatory neuron function have been shown to evoke ASD-associated behaviors in mice, such as cognitive inflexibility and social deficits (Cardin et al., 2009; Yizhar et al., 2011). In other cases where both excitatory and inhibitory activity are dampened, lower circuit activity in general is theorized to reduce the proper signal to noise ratio needed to differentiate meaningful input/information (Sohal & Rubenstein, 2019). However, more recent work suggests that circuit changes in ASD are likely more complicated, especially when accounting for second-order homeostatic changes to excitatory/inhibitory balance that likely occur in order to preserve, rather than alter, appropriate depolarization and spiking (Antoine et al., 2019; Nelson & Valakh, 2015).

*Transcriptional control*

Within the domain of risk genes involved in transcriptional and translational control, broader theories of the neurobiology of ASD have also arisen. Genes encoding proteins involved in chromatin remodeling and regulating transcription like *CHD8*, *CTNNB1* and *MECP2* are high confidence syndromic ASD risk genes, implicating transcriptional changes in the etiology of ASD (Ebert & Greenberg, 2013). Dysregulation of transcriptional programs as a result of these mutations may lead to altered neural and circuit development. *CHD8* and *CTNNB1* for example both converge on the Wnt signaling network, an intracellular signaling pathway important at multiple stages of neurodevelopment for cell proliferation, synaptic growth and maturation (Kwan et al., 2016). Mutations in *MECP2*, a transcriptional regulator that covers nearly the whole genome, can increase overall transcription and widespread modifications to chromatin structure (Guy et al., 2011). Activity-dependent gene transcription is crucial for synaptic development and plasticity, such that mutations in regulators of transcription are likely to alter the ability of circuits to grow and adapt to incoming information (Ebert & Greenberg, 2013; Jiang et al., 2022). Beyond risk genes that regulate transcription itself, post-mortem transcriptomic analysis of brains from individuals with ASD support the idea that ASD may converge at a genome-wide transcriptional level, with a shared transcriptional signature of commonly up- and downregulated genes across a range of cases (Voineagu, 2012). Upregulation of immune response genes, for example, has been identified in a number of studies of brain tissue and cerebrospinal fluid from subjects with ASD, suggesting that across genetic variants of ASD, transcriptional responses may be shared (Garbett et al., 2008; Lintas et al., 2012; Voineagu et al., 2011). However, as is the case with excitation/inhibition balance, it is unclear to what extent transcriptional changes are second-order, or how they impact cell and circuit function broadly.

*Translational control*

A similar theory to that of convergent transcriptional change in ASD exists regarding translation, specifically that there are translational regulators present in the list of high confidence ASD risk genes (e.g. *FMRP*, mTOR pathway genes), and that ASD could also be a disorder driven by aberrant protein synthesis broadly (Hooshmandi et al., 2020; Kelleher & Bear, 2008). Just as activity-dependent gene transcription must occur properly in order for adequate synaptic development and plasticity, the translation of synaptic proteins is crucial to the neuron's ability to update with changing activity at an even shorter timescale (Darnell & Klann, 2013). In the case of *FMRP* and *TSC1* (a negative regulator of mTOR signaling), mutations lead to widespread increases in protein translation (Darnell & Klann, 2013; Ma & Blenis, 2009) (although others find reduced translation in $Tsc2^{+/-}$ mice (Auerbach et al., 2011)). This change may lead to increased availability of synaptic proteins such that plasticity is enhanced or consolidated at synapses where it otherwise might not have been, reducing the specificity of signal to noise needed for proper learning (Kelleher & Bear, 2008). However, hypoconnectivity and decreased synaptic plasticity or function in the case of some ASD mutations, such as *MECP2*, suggest that while protein translation could still be a process of convergent change, the direction and impact varies (Chao et al., 2007).

Taken together, similarities in the functional roles of the genes implicated in ASD has allowed for the development of several hypotheses regarding ASD pathophysiology. Although a decisive theory is yet to emerge, progress in this approach has led to increased understanding of convergent systemic changes across a number of ASD models.

**Brain regions of convergent change in ASD**

An approach to understanding the etiology of ASD is to identify brain regions that may be convergently changed. Although there are many identified risk genes for ASD, the behavioral symptomology of the disorder still consists of two domains: deficits in social communication and interaction, and the presence of persistent, pervasive repetitive motor behaviors (APA, 2022). As ASD mouse models increasingly provide good construct validity of the disorder, harboring patient-specific gene mutations, they have also been shown to demonstrate good face validity, exhibiting behavioral changes that are similar to those comprising the symptom domains above. Mice are social animals, and thus perform reciprocal social interactions with other mice, respond strongly to social olfactory cues, and exhibit communication with other mice through ultrasonic vocalizations that vary by context (Portfors, 2007; Winslow, 2003). Taking advantage of this, several behavioral assays have been developed and verified to measure potential changes to these social behaviors in mouse models of ASD (Kazdoba et al., 2016). Similarly, changes to motor behavior sequences that occur naturally in mice, such as self-grooming, digging, rearing, and general aspects of locomoting are utilized as a proxy of the restricted, repetitive behaviors present in ASD (Lewis et al., 2007). Brain regions, then, that play a role in these behaviors present good targets for potential convergent change across genetically diverse ASD mouse models.

*Cortical and subcortical structures implicated in ASD*

The cortex, a region involved in complex cognitive functions through its processing and integration of internal and external information, has long been a primary brain region of study in mouse models of ASD (Gustafsson, 1997; Hill, 2004; Minshew & Williams, 2007). Higher order functions like theory of mind, the understanding of mental states in reference to self and others, or cognitive flexibility, as well as lower order basic processing of sensory and motor information require proper cortical function (Kana et al., 2011). Both of these types of processes are likely to be altered in ASD. Autism risk genes are also highly enriched in the cortex, further supporting the potential importance of the region in ASD etiology (Xu et al., 2014).

Altered function of some subcortical structures, often those situated as integrators of information from cortical and other regions, have also been implicated in ASD (Fuccillo, 2016; Kelly et al., 2021; Sweeten et al., 2002; Thabault et al., 2022). The amygdala, for example, while often thought of as detecting or assessing potential threats or dangers in the environment, may be important for more broad interpretation of self-relevant information for decision making (Sander et al., 2003). Altered amygdala function then may make orienting to and integrating environmental cues more difficult, which is theorized to play a role in ASD, in particular the social interaction deficits associated with ASD (Zalla & Sperduti, 2013). The cerebellum has also been implicated

in ASD-associated behaviors, both in the repetitive motor domain and in altered social function (Kelly et al., 2021). As a region that utilizes sensorimotor information to control the timing, dynamics and effectors of movements, constantly updating to adjust to environmental changes, it is straightforward to see how altered cerebellar function may result in aberrant motor behavior (Mosconi et al., 2015). However, the cerebellum is also theorized to use this highly adaptive feedback loop to more generally integrate internal states and external stimuli in order to guide behavior, which if altered, also impacts social interactions (Kelly et al., 2021). Finally, the basal ganglia, in particular the striatum, is another subcortical region that has arisen as a point of potential convergent change in ASD, as it likely plays a role in both social and motor ASD symptom domains, and it rivals the cortex in enrichment of ASD risk genes (Fuccillo, 2016; Xu et al., 2014). The role of basal ganglia circuits in ASD is the focus of this dissertation and will be discussed further below.

**The basal ganglia**

*Architecture of the basal ganglia*

The basal ganglia are a group of subcortical structures implicated in motor learning, action selection and habit formation, as well as limbic and associative functions in reward, motivation and executive function (Fig. 1) (Nelson & Kreitzer, 2014; Packard & Knowlton, 2002; Yin, 2017). The striatum, the primary input center of the basal ganglia, receives glutamatergic input from nearly all functional subregions of the cortex, as well as from thalamus (Fig. 1A, B) (Huerta-Ocampo et al., 2014; Johansson & Silberberg, 2020). This excitatory input onto striatal projection neurons (SPNs), the predominant cell type in the striatum, together with neuromodulatory input from midbrain dopamine neurons, shapes striatal plasticity and function (Gerfen & Surmeier, 2011). Based largely on the types of cortical input they receive; regions of the striatum can be functionally subdivided. The dorsal striatum receives glutamatergic input from sensorimotor and associative cortices as well as dopaminergic input from substantia nigra pars compacta (SNc) and is implicated in sensorimotor goal-directed and habitual behavior (Fig. 1A) (Balleine et al., 2007). The ventral striatum (or nucleus accumbens, NAc) receives input from prefrontal cortex, as well as the amygdala and hippocampus, and dopaminergic input from ventral tegmental area (VTA), and is implicated in limbic function (Fig.1B) (Voorn et al., 2004).

*Cell types of the basal ganglia*

SPNs, GABAergic neurons that make up ~95% of striatal cells, are evenly distributed in a salt-and-pepper fashion throughout the striatum, but can be separated into two subtypes: D1 dopamine receptor expressing cells of the direct pathway (dSPNs) and D2 dopamine receptor expressing cells of the indirect pathway (iSPNs) (Calabresi et al., 2014). While grossly similar in the inputs that they receive (Huerta-Ocampo et al., 2014; Johansson & Silberberg, 2020) (although some evidence challenges this (Klug et al., 2023)), dSPNs and iSPNs differ in a number of ways that impact their role in the striatal circuit. $G_{s/olf}$-coupled D1 receptors on dSPNs and $G_{i/o}$-coupled D2 receptors on iSPNs result in the activation and inhibition of adenylyl cyclase in the presence of dopamine, respectively (Girault & Greengard, 2004). As a result, dSPNs exhibit increased cell activity and iSPNs exhibit decreased activity as a result of

dopamine signaling (Surmeier et al., 2007). Intrinsically, however, iSPNs are more excitable than dSPNs, likely due to the smaller total dendritic area of iSPNs (Gertler et al., 2008). While all SPNs utilize GABA as their primary neurotransmitter, they can be distinguished by the neuropeptides that they express: dSPNs express substance P and dynorphin, while iSPNs express enkephalin (Steiner & Gerfen, 1998). Despite being GABAergic, SPNs exhibit minimal local inhibitory connectivity with other nearby SPNs (Czubayko & Plenz, 2002; Tunstall et al., 2002). Instead, the remaining ~5% of striatal cells comprises an array of interneurons that exhibit inhibitory or modulatory control over SPNs (Fig. 1C, D).

Interneurons in the striatum make up two groups: cholinergic interneurons and GABAergic interneurons. Cholinergic interneurons can alter SPN excitability directly through the action of acetylcholine at muscarinic receptors (Oldenburg & Ding, 2011), as well as indirectly through modulation of dopamine release from midbrain terminals (Threlfell et al., 2012), and GABA both from GABAergic interneuron and midbrain terminals (Faust et al., 2016; Nelson et al., 2014). In particular because of this role in dopaminergic modulation, cholinergic interneurons are important regulators of striatal plasticity (Wang et al., 2006). GABAergic interneurons, although making up only ~4% of all striatal cells, can be subdivided into many types (Fig. 1D) (Burke et al., 2017). Parvalbumin (PV) or fast-spiking interneurons (FSIs), the most well studied of striatal GABAergic interneurons, are driven by glutamatergic cortical input to provide the fastest, largest feedforward inhibitory controls over SPNs (Koos & Tepper, 1999). Neurogliaform GABAergic interneurons, a subtype of neuropeptide Y-expressing interneurons, provide a large but much slower inhibition onto SPNs, primarily within a disynaptic circuit including cholinergic interneurons (Faust et al., 2015). Another subtype of neuropeptide Y-expressing interneurons, low-threshold spiking interneurons (LTSIs) evoke sparse and weak responses in SPNs, but also release the neuropeptides somatostatin (SOM) and nitric oxide synthase (NOS), which may have more indirect modulatory effects (Gittis et al., 2010). Finally, tyrosine hydroxylase interneurons (THINs), which despite expressing the rate limiting enzyme for dopamine synthesis, are GABAergic, are an understudied GABAergic interneuron (Xenias et al., 2015). However, it has been shown that THINs are the only identified striatal GABAergic interneurons that receive inputs from SPNs, suggesting a potentially unique functional role in inhibitory signaling in the striatum (Ibanez-Sandoval et al., 2010). Taken together, the unique functional differences of dSPNs and iSPNs, together with a complex intrastriatal inhibitory network, work in concert to shape the output of the striatum.

*Output circuits of the basal ganglia*

In addition to physiological and morphological differences, SPNs can also be functionally separated into two pathways based on their projection targets: dSPNs comprise the direct pathway and iSPNs comprise the indirect pathway (Calabresi et al., 2014). In the dorsal striatum, dSPNs project directly to substantia nigra pars reticulata (SNr) output nuclei, and are broadly thought to initiate movement when activated in bulk, while iSPNs project to the external segment of the globus pallidus, and are generally thought to inhibit movement or inhibit competing movements when activated in bulk (Kravitz et al., 2010; Parent & Hazrati, 1995; Takakusaki et al., 2004). However, recent work showing that dorsal striatal iSPNs are active alongside dSPNs during

movement initiation (Cui et al., 2013) and directly inhibiting globus pallidus does not suppress movement (Isett et al., 2023), supports the need for a revised model of the indirect pathway. Output in the ventral striatum is more complex, however, with some dSPNs projecting directly to VTA output nuclei, while others project together with iSPNs to the ventral pallidum, an intermediate structure (Kupchik et al., 2015). When stimulated in bulk, dSPNs of the ventral striatum increase motivation, drug sensitization, and conditioned place preference (Lobo et al., 2010; Soares-Cunha, Coimbra, David-Pereira, et al., 2016), suggesting a role in reinforcement. As the anatomy suggests, bulk stimulation of ventral striatal iSPNs reveals a less explicit role, but may be broadly thought of as aversive in most contexts (Soares-Cunha, Coimbra, Sousa, & Rodrigues, 2016). That the stimulation of the direct and indirect pathways in the ventral striatum can so directly alter aspects of motivation and aversion emphasizes the importance of proper function of this circuit in limbic processes. Deficits in social communication and interaction, complex cognitive behaviors shaped by the valence and rewarding quality of social cues, support a potential role for this ventral circuit in ASD etiology. Similarly for the dorsal striatum, that direct and indirect pathway stimulation can strongly alter motor behavior emphasizes the importance of proper function of this region in the execution of movements. In ASD, given that repetitive motor behaviors are a hallmark symptom domain, altered dorsal striatal circuit function is also likely to play a role in ASD etiology.

## The role of the basal ganglia in ASD etiology

### *Basal ganglia and social behaviors*

Evidence from both human and animal studies supports a role for the striatum in altered social behavior. Imaging studies have revealed that a number of aspects of social behavior such as acquiring social information, observing pictures of partners and friends, mutual cooperation, and seeing others succeed strongly modulate striatal activity, often in ventral striatum, as social behavior in humans is regarded as in itself rewarding (Baez-Mendoza & Schultz, 2013; Gunaydin & Deisseroth, 2014). *In vivo* recordings in rats have shown that whisker contact and sniffing behavior during social interaction with unfamiliar conspecifics correlates with increased dopamine transients in the NAc, as would be expected for a rewarding stimulus (Robinson et al., 2002). In individuals with ASD, a metanalysis of human imaging studies revealed that hypoactivation of both dorsal and ventral striatum in response to social stimuli was commonly identified (Clements et al., 2018). In rodents, altering striatal function can bidirectionally impact social behavior: inducing social deficits in wildtype (WT) rodents, or rescuing social deficits in rodent ASD models (Aragona et al., 2006; Dolen et al., 2013; Gunaydin et al., 2014; Rapanelli et al., 2017). Modulating activity of SPNs in NAc can alter both pair-bond formation in voles, as well as time spent with same-sex conspecifics in mice (Aragona et al., 2006; Gunaydin et al., 2014). Blocking either oxytocin or serotonin receptors in the NAc is sufficient to inhibit formation of a preference for social cues: whereas WT animals will spend more time in a context previously associated with group housing compared to a context associated with isolate housing, blocking either oxytocin or serotonin signaling in NAc eliminates this preference (Dolen et al., 2013). Finally, depletion of parvalbumin and cholinergic interneurons, interestingly in dorsal striatum, was sufficient to evoke deficits in social interaction in WT mice (Rapanelli et al., 2017). In a mouse model of ASD-linked copy

number variant 16p11.2, which exhibits deficits in social interaction, activation of 5HT1b serotonin receptors in the NAc was sufficient to rescue social deficits (Walsh et al., 2018). Conversely, knockdown of the ASD risk genes *Mecp2* or *Tsc1* in the dorsal striatum was sufficient to induce social interaction deficits in mice (Lee et al., 2018). It should be noted that social behaviors are complex, and evidence suggests that a number of brain regions, including the cortex and cerebellum, are also implicated in social function, including in ASD mouse models (Bey et al., 2018; Fernandez et al., 2018; Thabault et al., 2022). Continued study of the role of the striatum in social behaviors in ASD is likely to identify more convergent brain region changes.

*Basal ganglia and motor behaviors*

Appropriate modulation of the activity of striatal neurons, in particular in dorsal striatum, is associated with the acquisition and performance of intentional movements, motor sequences and habits, across multiple species including humans, primates and mice (Cui et al., 2013; Graybiel & Grafton, 2015; Hassler, 1978; Lopez-Huerta et al., 2021). Due to this role in the control and execution of intentional movement, altered function of the striatum is associated with the restricted, repetitive behavior domain of ASD (Comparan-Meza et al., 2021; Evans et al., 2024). Many of the characteristics of repetitive behaviors, like stereotyped movements, cognitive inflexibility and perseverative interests map neatly onto both the more rote and higher order functions of the striatum (Fuccillo, 2016). Evidence from human imaging studies supports this connection, as structural and functional imaging has identified changes in striatal morphology and connectivity in individuals with ASD, in some cases strongly correlating with the presentation of repetitive behaviors (Dichter, 2012; Estes et al., 2011; Hollander et al., 2005). In mouse studies, similar evidence exists, with a diverse genetic range of ASD mouse models also exhibiting changes in striatal morphology and connectivity, revealed by MRI (Ellegood & Crawley, 2015; Lai et al., 2016; Portmann et al., 2014; Wei et al., 2012). Changes in the number or distribution of some striatal cell types, striatal cell morphology and transcriptomic or protein expression changes in striatum have also been reported in ASD mouse models (Evans et al., 2024). Mouse studies that deleted the ASD risk genes *Chd8* or *Nlgn3* specifically in cells of the striatum found that this was sufficient to increase the formation of fixed motor routines or patterns (Platt et al., 2017; Rothwell et al., 2014), further strengthening the direct link between striatal function and repetitive behavior. As is the case with social behavior, the complexity of motor behaviors necessarily recruits brain regions beyond the striatum, like motor cortex and cerebellum (Dayan & Cohen, 2011; Sathyamurthy et al., 2020; Tian & Chen, 2021). However, altered striatal circuit function resulting in increased repetitive motor behaviors should continue to be pursued as a potentially convergent change across ASD.

**Conclusions and caveats**

Our understanding of the neurodevelopmental disorder ASD has expanded greatly in the last 50 years. Increased understanding and awareness of ASD symptomology has likely aided in increased diagnosis, and increased access to genetic sequencing tools has led to the identification of many genes that confer risk of developing ASD (Geschwind, 2011; Satterstrom et al., 2020). Improved genetic tools

have also greatly improved the ability to develop animal models of ASD, leading to a wide range of mouse models that harbor mutations in ASD risk genes identified in the human population. The development and validation of mouse behavioral assays that assess social and motor behaviors, which resemble those seen in people with ASD have also lent face validity to many of these models. However, it should be acknowledged that behaviors in a mouse should not be regarded as precisely phenocopying those seen in humans. The behavioral manifestations of ASD in humans are complex and heterogeneous, in some cases employing cognitive processes that do not exist in mice (i.e. primarily verbal communication, emphasis on the visual system for sensory processing, etc.). Relying too heavily on the assumed face validity of a behavioral manifestation in a mouse model of ASD is not likely to lead to mechanistic understanding. Instead, the suite of behavioral changes observed in each ASD mouse model should be considered in concert with the construct validity of the model (Silverman et al., 2022).

While improved understanding of ASD at the genetic and behavioral level has led to greater understanding of the common functional systems that may be altered in ASD, it remains unclear what comprises the shared pathogenesis of the disorder (if one exists). As outlined above, clustering of ASD risk genes by their functional roles has contributed to theories of convergence at the level of excitatory/inhibitory synaptic balance, common transcriptional signatures or similarly altered protein translation (Ebert & Greenberg, 2013; Kelleher & Bear, 2008; Rubenstein & Merzenich, 2003). While these theories differ, and highlight different genes and cellular processes, they all include some emphasis on the role of synaptic function; excitatory/inhibitory synaptic balance focuses most on this, but changes in activity-dependent gene transcription and protein translation necessarily alter the ability for neurons to carry out proper synaptic plasticity and function. The mechanistic molecular and cellular changes that underlie neuronal function in the context of gene mutation are important to know, but it is possible that these differ widely across ASD. Indeed across cell types, brain regions and developmental timepoints within a single ASD mouse model, molecular and cellular changes can vary (Maloney et al., 2013). However, the recognition and diagnosis of ASD is carried out through the identification of behaviors, phenotypes that occur as an emergent consequence of the function of and communication between brain regions involved in carrying out those behaviors. It seems likely then that despite varying mechanistic underpinnings mentioned above, ASD is likely to converge upon similar circuit changes. The studies that follow in this dissertation support this theory, as they identify heterogeneous changes to cell physiology and function across two genetically distinct ASD mouse models that converge to impact circuit output of the basal ganglia.

The basal ganglia, in particular the striatum, is a strong candidate for convergent change in ASD. When primarily using behavior phenotypes to identify potential circuit convergence in ASD, the striatum stands out as a region that plays a functional role in both social and motor behaviors. However, even from a cellular and molecular approach to convergence, studies that identify changes to striatal cells across a range of ASD models (Cording & Bateup, 2023; Evans et al., 2024; Fuccillo, 2016; Li & Pozzo-Miller, 2020) and the finding that ASD risk genes are highly enriched in the striatum (Xu et al., 2014) support the striatum as a candidate. Although, as outlined above, other brain regions including the cortex, amygdala, and cerebellum are also involved in the

behavioral manifestations of ASD, and have been shown to exhibit altered function in the context of ASD (Kana et al., 2011; Kelly et al., 2021; Sweeten et al., 2002; Thabault et al., 2022). It is worth noting, however, that all of these brain regions exist within or parallel to a striatal circuit loop (Dayan & Cohen, 2011; Packard & Knowlton, 2002; Voorn et al., 2004). Taken together, continued study of the ways in which a diverse number of ASD risk gene mutations alter striatal function, and in turn striatal-associated social and motor behaviors, is likely to increase understanding of a potentially convergent pathophysiology in ASD.

**Dissertation research questions**

The striatum has been implicated in both the social and motor phenotypes of ASD, albeit often due to dysfunction in different subregions. For the restricted, repetitive motor behaviors associated with ASD, dorsal striatal dysfunction is more commonly implicated, due to the role of this region in action selection and motor learning. Increasingly, alterations in cortical inputs in this region has been identified across a number of ASD mouse models (Li & Pozzo-Miller, 2020). Alteration of this pathway, which carries sensory, motor and associative information to the striatum, is emerging as a possible point of convergence across mouse models of ASD, but has yet to be comprehensively assessed. Thus, the focus of my dissertation is to both summarize existing literature in regard to corticostriatal alterations in ASD, and experimentally define changes in corticostriatal function across two genetically distinct ASD mouse models.

The second chapter of this dissertation reviews the relationship between striatal function and motor performance across a diverse genetic range of ASD mouse models, through the lens of a common corticostriatal-dependent behavioral assay of motor coordination and learning, the accelerating rotarod. Chapters three and four then define how mutations in the ASD risk genes *Tsc1* and *Cntnap2* affect striatal cellular function and striatum-associated behaviors. These genes exist within distinct functional families of ASD risk genes: *Tsc1*, which encodes a negative regulator of mTORC1, a cell signaling hub involved in cell growth and protein synthesis, fits into the transcriptional/translational regulation family outlined above, while *Cntnap2*, a cell adhesion molecule of the neurexin family that stabilizes voltage-gated potassium channels, fits into the neuronal excitability and synaptic function/stabilization family. Taken together, the results of these studies identify points of striatal convergence that help to illuminate the pathophysiology of motor behaviors across ASD mouse models with unique genetic bases.

## Figures

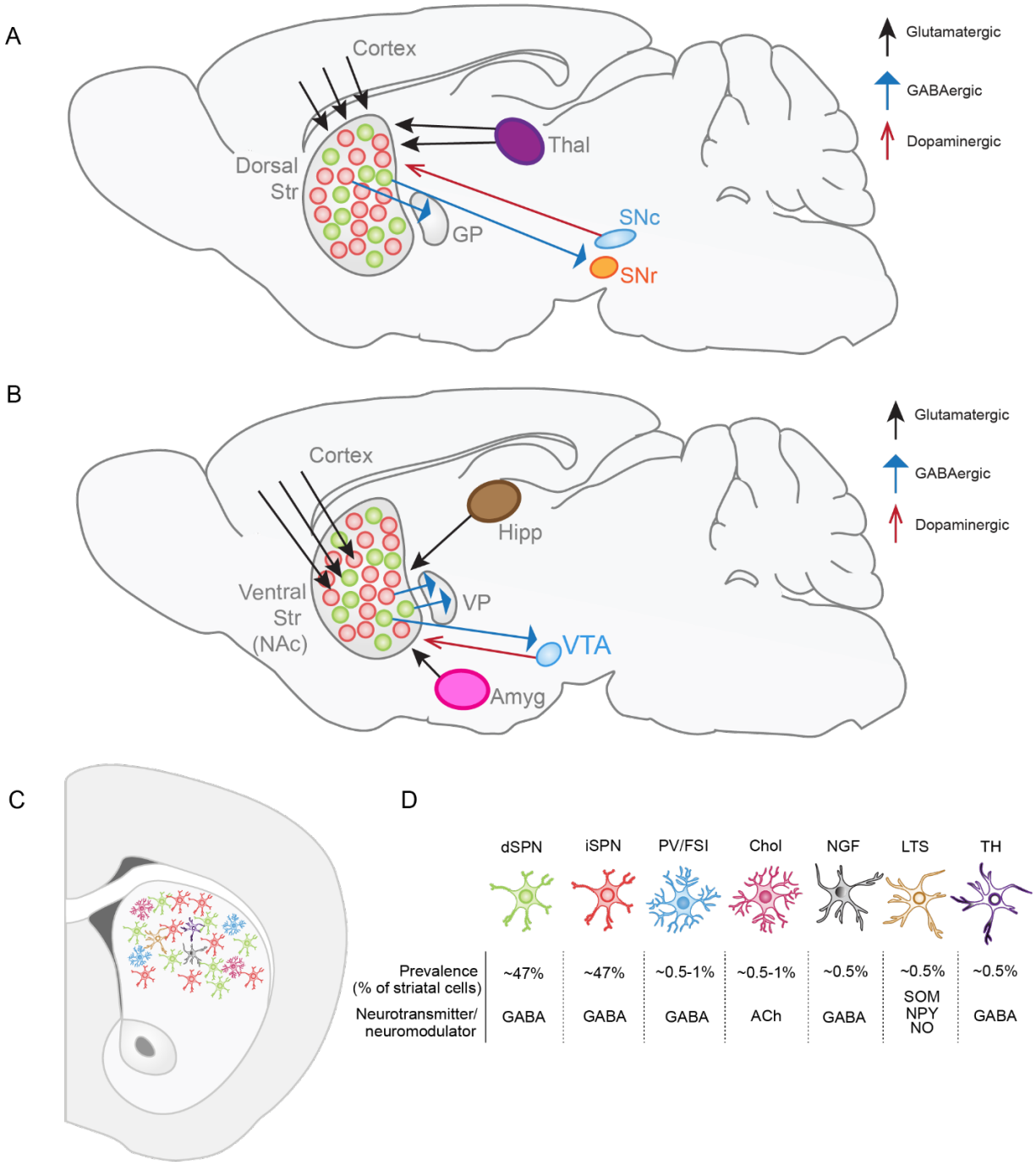


**Figure 1. Primary cell types and circuits of the basal ganglia**
(A) Schematic of a sagittal mouse brain slice depicting the primary inputs and outputs of the dorsal striatal circuit; Str, striatum; GP, globus pallidus; Thal, thalamus; SNc, substantia nigra pars compacta; SNr, substantia nigra pars reticulata. (B) Schematic of a sagittal mouse brain slice depicting the primary inputs and outputs of the ventral striatal or nucleus accumbens circuit; Str, striatum; NAc, nucleus accumbens; VP,

ventral pallidum; Hipp, hippocampus; Amyg, amygdala; VTA, ventral tegmental area. Brain region locations are approximate and simplified. (C) Schematic of a coronal mouse brain slice depicting the proportional distribution of cell types in dorsal striatum. (D) Estimated prevalence of striatal cell types and the primary neurotransmitter/neuromodulator that each cell type releases; dSPN, D1-receptor expressing direct pathway striatal projection neuron; iSPN, D2-receptor expressing indirect pathway striatal projection neuron; PV/FSI, parvalbumin/fast-spiking interneuron; Chol, cholinergic interneuron; NGF, neurogliaform interneuron; LTS, low-threshold spike interneuron; TH, tyrosine hydroxylase interneuron. Schematic is not comprehensive for all GABAergic interneuron types.

**References**


Antoine, M. W., Langberg, T., Schnepel, P., & Feldman, D. E. (2019). Increased Excitation-Inhibition Ratio Stabilizes Synapse and Circuit Excitability in Four Autism Mouse Models. *Neuron*, *101*(4), 648-661 e644. https://doi.org/10.1016/j.neuron.2018.12.026

APA. (2022). *Diagnostic and Statistical Manual of Mental Disorders* (5th ed., text rev. ed.). https://doi.org/https://doi.org/10.1176/appi.books.9780890425787

Aragona, B. J., Liu, Y., Yu, Y. J., Curtis, J. T., Detwiler, J. M., Insel, T. R., & Wang, Z. (2006). Nucleus accumbens dopamine differentially mediates the formation and maintenance of monogamous pair bonds. *Nat Neurosci*, *9*(1), 133-139. https://doi.org/10.1038/nn1613

Auerbach, B. D., Osterweil, E. K., & Bear, M. F. (2011). Mutations causing syndromic autism define an axis of synaptic pathophysiology. *Nature*, *480*(7375), 63-68. https://doi.org/10.1038/nature10658

Baez-Mendoza, R., & Schultz, W. (2013). The role of the striatum in social behavior. *Front Neurosci*, *7*, 233. https://doi.org/10.3389/fnins.2013.00233

Balleine, B. W., Delgado, M. R., & Hikosaka, O. (2007). The role of the dorsal striatum in reward and decision-making. *J Neurosci*, *27*(31), 8161-8165. https://doi.org/10.1523/JNEUROSCI.1554-07.2007

Bey, A. L., & Jiang, Y. H. (2014). Overview of Mouse Models of Autism Spectrum Disorders. *Current Protocols in Pharmacology*, *66*(1). https://doi.org/10.1002/0471141755.ph0566s66

Bey, A. L., Wang, X., Yan, H., Kim, N., Passman, R. L., Yang, Y., Cao, X., Towers, A. J., Hulbert, S. W., Duffney, L. J., Gaidis, E., Rodriguiz, R. M., Wetsel, W. C., Yin, H. H., & Jiang, Y. H. (2018). Brain region-specific disruption of Shank3 in mice reveals a dissociation for cortical and striatal circuits in autism-related behaviors. *Transl Psychiatry*, *8*(1), 94. https://doi.org/10.1038/s41398-018-0142-6

Bhat, A. N., Galloway, J. C., & Landa, R. J. (2012). Relation between early motor delay and later communication delay in infants at risk for autism. *Infant Behav Dev*, *35*(4), 838-846. https://doi.org/10.1016/j.infbeh.2012.07.019

Burke, D. A., Rotstein, H. G., & Alvarez, V. A. (2017). Striatal Local Circuitry: A New Framework for Lateral Inhibition. *Neuron*, *96*(2), 267-284. https://doi.org/10.1016/j.neuron.2017.09.019

Busti Ceccarelli, S., Ferrante, C., Gazzola, E., Marzocchi, G. M., Nobile, M., Molteni, M., & Crippa, A. (2020). Fundamental Motor Skills Intervention for Children with Autism Spectrum Disorder: A 10-Year Narrative Review. *Children (Basel)*, *7*(11). https://doi.org/10.3390/children7110250

Calabresi, P., Picconi, B., Tozzi, A., Ghiglieri, V., & Di Filippo, M. (2014). Direct and indirect pathways of basal ganglia: a critical reappraisal. *Nat Neurosci*, *17*(8), 1022-1030. https://doi.org/10.1038/nn.3743

Cardin, J. A., Carlen, M., Meletis, K., Knoblich, U., Zhang, F., Deisseroth, K., Tsai, L. H., & Moore, C. I. (2009). Driving fast-spiking cells induces gamma rhythm and controls sensory responses. *Nature*, *459*(7247), 663-667. https://doi.org/10.1038/nature08002

Chao, H. T., Zoghbi, H. Y., & Rosenmund, C. (2007). MeCP2 controls excitatory synaptic strength by regulating glutamatergic synapse number. *Neuron*, *56*(1), 58-65. https://doi.org/10.1016/j.neuron.2007.08.018

Chukoskie, L., Townsend, J., & Westerfield, M. (2013). Motor skill in autism spectrum disorders: a subcortical view. *Int Rev Neurobiol*, *113*, 207-249. https://doi.org/10.1016/B978-0-12-418700-9.00007-1

Clements, C. C., Zoltowski, A. R., Yankowitz, L. D., Yerys, B. E., Schultz, R. T., & Herrington, J. D. (2018). Evaluation of the Social Motivation Hypothesis of Autism: A Systematic Review and Meta-analysis. *JAMA Psychiatry*, *75*(8), 797-808. https://doi.org/10.1001/jamapsychiatry.2018.1100

Comparan-Meza, M., Vargas de la Cruz, I., Jauregui-Huerta, F., Gonzalez-Castaneda, R. E., Gonzalez-Perez, O., & Galvez-Contreras, A. Y. (2021). Biopsychological correlates of repetitive and restricted behaviors in autism spectrum disorders. *Brain Behav*, *11*(10), e2341. https://doi.org/10.1002/brb3.2341

Cording, K. R., & Bateup, H. S. (2023). Altered motor learning and coordination in mouse models of autism spectrum disorder. *Front Cell Neurosci*, *17*, 1270489. https://doi.org/10.3389/fncel.2023.1270489

Cui, G., Jun, S. B., Jin, X., Pham, M. D., Vogel, S. S., Lovinger, D. M., & Costa, R. M. (2013). Concurrent activation of striatal direct and indirect pathways during action initiation. *Nature*, *494*(7436), 238-242. https://doi.org/10.1038/nature11846

Czubayko, U., & Plenz, D. (2002). Fast synaptic transmission between striatal spiny projection neurons. *Proc Natl Acad Sci U S A*, *99*(24), 15764-15769. https://doi.org/10.1073/pnas.242428599

Darnell, J. C., & Klann, E. (2013). The translation of translational control by FMRP: therapeutic targets for FXS. *Nature Neuroscience*, *16*(11), 1530-1536. https://doi.org/10.1038/nn.3379

Dayan, E., & Cohen, L. G. (2011). Neuroplasticity subserving motor skill learning. *Neuron*, *72*(3), 443-454. https://doi.org/10.1016/j.neuron.2011.10.008

De Rubeis, S., He, X., Goldberg, A. P., Poultney, C. S., Samocha, K., Cicek, A. E., Kou, Y., Liu, L., Fromer, M., Walker, S., Singh, T., Klei, L., Kosmicki, J., Shih-Chen, F., Aleksic, B., Biscaldi, M., Bolton, P. F., Brownfeld, J. M., Cai, J., . . . Buxbaum, J. D. (2014). Synaptic, transcriptional and chromatin genes disrupted in autism. *Nature*, *515*(7526), 209-215. https://doi.org/10.1038/nature13772

Delorme, R., Ey, E., Toro, R., Leboyer, M., Gillberg, C., & Bourgeron, T. (2013). Progress toward treatments for synaptic defects in autism. *Nat Med*, *19*(6), 685-694. https://doi.org/10.1038/nm.3193

DeQuinzio, J. A., Poulson, C. L., Townsend, D. B., & Taylor, B. A. (2016). Social Referencing and Children with Autism. *Behav Anal*, *39*(2), 319-331. https://doi.org/10.1007/s40614-015-0046-1

Dichter, G. S. (2012). Functional magnetic resonance imaging of autism spectrum disorders. *Dialogues Clin Neurosci*, *14*(3), 319-351. https://doi.org/10.31887/DCNS.2012.14.3/gdichter

Dolen, G., Darvishzadeh, A., Huang, K. W., & Malenka, R. C. (2013). Social reward requires coordinated activity of nucleus accumbens oxytocin and serotonin. *Nature*, *501*(7466), 179-184. https://doi.org/10.1038/nature12518

Ebert, D. H., & Greenberg, M. E. (2013). Activity-dependent neuronal signalling and autism spectrum disorder. *Nature*, *493*(7432), 327-337. https://doi.org/10.1038/nature11860
Eigsti, I. M., Weitzman, C., Schuh, J., de Marchena, A., & Casey, B. J. (2011). Language and cognitive outcomes in internationally adopted children. *Dev Psychopathol*, *23*(2), 629-646. https://doi.org/10.1017/S0954579411000204
Ellegood, J., & Crawley, J. N. (2015). Behavioral and Neuroanatomical Phenotypes in Mouse Models of Autism. *Neurotherapeutics*, *12*(3), 521-533. https://doi.org/10.1007/s13311-015-0360-z
Estes, A., Shaw, D. W., Sparks, B. F., Friedman, S., Giedd, J. N., Dawson, G., Bryan, M., & Dager, S. R. (2011). Basal ganglia morphometry and repetitive behavior in young children with autism spectrum disorder. *Autism Res*, *4*(3), 212-220. https://doi.org/10.1002/aur.193
Evans, M. M., Kim, J., Abel, T., Nickl-Jockschat, T., & Stevens, H. E. (2024). Developmental Disruptions of the Dorsal Striatum in Autism Spectrum Disorder. *Biol Psychiatry*, *95*(2), 102-111. https://doi.org/10.1016/j.biopsych.2023.08.015
Faust, T. W., Assous, M., Shah, F., Tepper, J. M., & Koos, T. (2015). Novel fast adapting interneurons mediate cholinergic-induced fast GABAA inhibitory postsynaptic currents in striatal spiny neurons. *Eur J Neurosci*, *42*(2), 1764-1774. https://doi.org/10.1111/ejn.12915
Faust, T. W., Assous, M., Tepper, J. M., & Koos, T. (2016). Neostriatal GABAergic Interneurons Mediate Cholinergic Inhibition of Spiny Projection Neurons. *J Neurosci*, *36*(36), 9505-9511. https://doi.org/10.1523/JNEUROSCI.0466-16.2016
Fernandez, M., Mollinedo-Gajate, I., & Penagarikano, O. (2018). Neural Circuits for Social Cognition: Implications for Autism. *Neuroscience*, *370*, 148-162. https://doi.org/10.1016/j.neuroscience.2017.07.013
Fuccillo, M. V. (2016). Striatal Circuits as a Common Node for Autism Pathophysiology. *Front Neurosci*, *10*, 27. https://doi.org/10.3389/fnins.2016.00027
Garbett, K., Ebert, P. J., Mitchell, A., Lintas, C., Manzi, B., Mirnics, K., & Persico, A. M. (2008). Immune transcriptome alterations in the temporal cortex of subjects with autism. *Neurobiol Dis*, *30*(3), 303-311. https://doi.org/10.1016/j.nbd.2008.01.012
Gerfen, C. R., & Surmeier, D. J. (2011). Modulation of striatal projection systems by dopamine. *Annu Rev Neurosci*, *34*, 441-466. https://doi.org/10.1146/annurev-neuro-061010-113641
Gertler, T. S., Chan, C. S., & Surmeier, D. J. (2008). Dichotomous anatomical properties of adult striatal medium spiny neurons. *J Neurosci*, *28*(43), 10814-10824. https://doi.org/10.1523/JNEUROSCI.2660-08.2008
Geschwind, D. H. (2011). Genetics of autism spectrum disorders. *Trends Cogn Sci*, *15*(9), 409-416. https://doi.org/10.1016/j.tics.2011.07.003
Girault, J. A., & Greengard, P. (2004). The neurobiology of dopamine signaling. *Arch Neurol*, *61*(5), 641-644. https://doi.org/10.1001/archneur.61.5.641
Gittis, A. H., Nelson, A. B., Thwin, M. T., Palop, J. J., & Kreitzer, A. C. (2010). Distinct roles of GABAergic interneurons in the regulation of striatal output pathways. *J Neurosci*, *30*(6), 2223-2234. https://doi.org/10.1523/JNEUROSCI.4870-09.2010

Graybiel, A. M., & Grafton, S. T. (2015). The striatum: where skills and habits meet. *Cold Spring Harb Perspect Biol*, *7*(8), a021691. https://doi.org/10.1101/cshperspect.a021691

Gunaydin, L. A., & Deisseroth, K. (2014). Dopaminergic Dynamics Contributing to Social Behavior. *Cold Spring Harb Symp Quant Biol*, *79*, 221-227. https://doi.org/10.1101/sqb.2014.79.024711

Gunaydin, L. A., Grosenick, L., Finkelstein, J. C., Kauvar, I. V., Fenno, L. E., Adhikari, A., Lammel, S., Mirzabekov, J. J., Airan, R. D., Zalocusky, K. A., Tye, K. M., Anikeeva, P., Malenka, R. C., & Deisseroth, K. (2014). Natural neural projection dynamics underlying social behavior. *Cell*, *157*(7), 1535-1551. https://doi.org/10.1016/j.cell.2014.05.017

Gustafsson, L. (1997). Inadequate cortical feature maps: a neural circuit theory of autism. *Biol Psychiatry*, *42*(12), 1138-1147. https://doi.org/10.1016/s0006-3223(97)00141-8

Guy, J., Cheval, H., Selfridge, J., & Bird, A. (2011). The role of MeCP2 in the brain. *Annu Rev Cell Dev Biol*, *27*, 631-652. https://doi.org/10.1146/annurev-cellbio-092910-154121

Hassler, R. (1978). Striatal control of locomotion, intentional actions and of integrating and perceptive activity. *J Neurol Sci*, *36*(2), 187-224. https://doi.org/10.1016/0022-510x(78)90082-5

Healy, S., Nacario, A., Braithwaite, R. E., & Hopper, C. (2018). The effect of physical activity interventions on youth with autism spectrum disorder: A meta-analysis. *Autism Res*, *11*(6), 818-833. https://doi.org/10.1002/aur.1955

Hill, E. L. (2004). Executive dysfunction in autism. *Trends Cogn Sci*, *8*(1), 26-32. https://doi.org/10.1016/j.tics.2003.11.003

Hollander, E., Anagnostou, E., Chaplin, W., Esposito, K., Haznedar, M. M., Licalzi, E., Wasserman, S., Soorya, L., & Buchsbaum, M. (2005). Striatal volume on magnetic resonance imaging and repetitive behaviors in autism. *Biol Psychiatry*, *58*(3), 226-232. https://doi.org/10.1016/j.biopsych.2005.03.040

Hooshmandi, M., Wong, C., & Khoutorsky, A. (2020). Dysregulation of translational control signaling in autism spectrum disorders. *Cell Signal*, *75*, 109746. https://doi.org/10.1016/j.cellsig.2020.109746

Huerta-Ocampo, I., Mena-Segovia, J., & Bolam, J. P. (2014). Convergence of cortical and thalamic input to direct and indirect pathway medium spiny neurons in the striatum. *Brain Struct Funct*, *219*(5), 1787-1800. https://doi.org/10.1007/s00429-013-0601-z

Ibanez-Sandoval, O., Tecuapetla, F., Unal, B., Shah, F., Koos, T., & Tepper, J. M. (2010). Electrophysiological and morphological characteristics and synaptic connectivity of tyrosine hydroxylase-expressing neurons in adult mouse striatum. *J Neurosci*, *30*(20), 6999-7016. https://doi.org/10.1523/JNEUROSCI.5996-09.2010

Isett, B. R., Nguyen, K. P., Schwenk, J. C., Yurek, J. R., Snyder, C. N., Vounatsos, M. V., Adegbesan, K. A., Ziausyte, U., & Gittis, A. H. (2023). The indirect pathway of the basal ganglia promotes transient punishment but not motor suppression. *Neuron*, *111*(14), 2218-2231 e2214. https://doi.org/10.1016/j.neuron.2023.04.017

Jiang, C. C., Lin, L. S., Long, S., Ke, X. Y., Fukunaga, K., Lu, Y. M., & Han, F. (2022). Signalling pathways in autism spectrum disorder: mechanisms and therapeutic

implications. *Signal Transduct Target Ther*, *7*(1), 229. https://doi.org/10.1038/s41392-022-01081-0
Johansson, Y., & Silberberg, G. (2020). The Functional Organization of Cortical and Thalamic Inputs onto Five Types of Striatal Neurons Is Determined by Source and Target Cell Identities. *Cell Rep*, *30*(4), 1178-1194 e1173. https://doi.org/10.1016/j.celrep.2019.12.095
Kana, R. K., Libero, L. E., & Moore, M. S. (2011). Disrupted cortical connectivity theory as an explanatory model for autism spectrum disorders. *Phys Life Rev*, *8*(4), 410-437. https://doi.org/10.1016/j.plrev.2011.10.001
Kanner, L. (1968). Autistic disturbances of affective contact. *Acta Paedopsychiatr*, *35*(4), 100-136. https://www.ncbi.nlm.nih.gov/pubmed/4880460
Kazdoba, T. M., Leach, P. T., & Crawley, J. N. (2016). Behavioral phenotypes of genetic mouse models of autism. *Genes Brain Behav*, *15*(1), 7-26. https://doi.org/10.1111/gbb.12256
Kelleher, R. J., 3rd, & Bear, M. F. (2008). The autistic neuron: troubled translation? *Cell*, *135*(3), 401-406. https://doi.org/10.1016/j.cell.2008.10.017
Kelly, E., Escamilla, C. O., & Tsai, P. T. (2021). Cerebellar Dysfunction in Autism Spectrum Disorders: Deriving Mechanistic Insights from an Internal Model Framework. *Neuroscience*, *462*, 274-287. https://doi.org/10.1016/j.neuroscience.2020.11.012
Klug, J. R., Yan, X., Hoffman, H. A., Engelhardt, M. D., Osakada, F., Callaway, E. M., & Jin, X. (2023). Asymmetric cortical projections to striatal direct and indirect pathways distinctly control actions. *bioRxiv*. https://doi.org/10.1101/2023.10.02.560589
Koos, T., & Tepper, J. M. (1999). Inhibitory control of neostriatal projection neurons by GABAergic interneurons. *Nat Neurosci*, *2*(5), 467-472. https://doi.org/10.1038/8138
Kravitz, A. V., Freeze, B. S., Parker, P. R., Kay, K., Thwin, M. T., Deisseroth, K., & Kreitzer, A. C. (2010). Regulation of parkinsonian motor behaviours by optogenetic control of basal ganglia circuitry. *Nature*, *466*(7306), 622-626. https://doi.org/10.1038/nature09159
Kupchik, Y. M., Brown, R. M., Heinsbroek, J. A., Lobo, M. K., Schwartz, D. J., & Kalivas, P. W. (2015). Coding the direct/indirect pathways by D1 and D2 receptors is not valid for accumbens projections. *Nat Neurosci*, *18*(9), 1230-1232. https://doi.org/10.1038/nn.4068
Kwan, V., Unda, B. K., & Singh, K. K. (2016). Wnt signaling networks in autism spectrum disorder and intellectual disability. *J Neurodev Disord*, *8*, 45. https://doi.org/10.1186/s11689-016-9176-3
Lai, J. K., Lerch, J. P., Doering, L. C., Foster, J. A., & Ellegood, J. (2016). Regional brain volumes changes in adult male FMR1-KO mouse on the FVB strain. *Neuroscience*, *318*, 12-21. https://doi.org/10.1016/j.neuroscience.2016.01.021
Lee, E., Lee, J., & Kim, E. (2017). Excitation/Inhibition Imbalance in Animal Models of Autism Spectrum Disorders. *Biol Psychiatry*, *81*(10), 838-847. https://doi.org/10.1016/j.biopsych.2016.05.011

Lee, Y., Kim, H., & Han, P. L. (2018). Striatal Inhibition of MeCP2 or TSC1 Produces Sociability Deficits and Repetitive Behaviors. *Exp Neurobiol*, *27*(6), 539-549. https://doi.org/10.5607/en.2018.27.6.539

Lewis, M. H., Tanimura, Y., Lee, L. W., & Bodfish, J. W. (2007). Animal models of restricted repetitive behavior in autism. *Behav Brain Res*, *176*(1), 66-74. https://doi.org/10.1016/j.bbr.2006.08.023

Li, W., & Pozzo-Miller, L. (2020). Dysfunction of the corticostriatal pathway in autism spectrum disorders. *J Neurosci Res*, *98*(11), 2130-2147. https://doi.org/10.1002/jnr.24560

Lintas, C., Sacco, R., & Persico, A. M. (2012). Genome-wide expression studies in autism spectrum disorder, Rett syndrome, and Down syndrome. *Neurobiol Dis*, *45*(1), 57-68. https://doi.org/10.1016/j.nbd.2010.11.010

Lobo, M. K., Covington, H. E., 3rd, Chaudhury, D., Friedman, A. K., Sun, H., Damez-Werno, D., Dietz, D. M., Zaman, S., Koo, J. W., Kennedy, P. J., Mouzon, E., Mogri, M., Neve, R. L., Deisseroth, K., Han, M. H., & Nestler, E. J. (2010). Cell type-specific loss of BDNF signaling mimics optogenetic control of cocaine reward. *Science*, *330*(6002), 385-390. https://doi.org/10.1126/science.1188472

Lopez-Huerta, V. G., Denton, J. A., Nakano, Y., Jaidar, O., Garcia-Munoz, M., & Arbuthnott, G. W. (2021). Striatal bilateral control of skilled forelimb movement. *Cell Rep*, *34*(3), 108651. https://doi.org/10.1016/j.celrep.2020.108651

Lord, C., Brugha, T. S., Charman, T., Cusack, J., Dumas, G., Frazier, T., Jones, E. J. H., Jones, R. M., Pickles, A., State, M. W., Taylor, J. L., & Veenstra-VanderWeele, J. (2020). Autism spectrum disorder. *Nat Rev Dis Primers*, *6*(1), 5. https://doi.org/10.1038/s41572-019-0138-4

Ma, X. M., & Blenis, J. (2009). Molecular mechanisms of mTOR-mediated translational control. *Nat Rev Mol Cell Biol*, *10*(5), 307-318. https://doi.org/10.1038/nrm2672

MacDonald, M., Lord, C., & Ulrich, D. (2013). The relationship of motor skills and adaptive behavior skills in young children with autism spectrum disorders. *Res Autism Spectr Disord*, *7*(11), 1383-1390. https://doi.org/10.1016/j.rasd.2013.07.020

Maenner, M. J., Warren, Z., Williams, A. R., Amoakohene, E., Bakian, A. V., Bilder, D. A., Durkin, M. S., Fitzgerald, R. T., Furnier, S. M., Hughes, M. M., Ladd-Acosta, C. M., McArthur, D., Pas, E. T., Salinas, A., Vehorn, A., Williams, S., Esler, A., Grzybowski, A., Hall-Lande, J., . . . Shaw, K. A. (2023). Prevalence and Characteristics of Autism Spectrum Disorder Among Children Aged 8 Years — Autism and Developmental Disabilities Monitoring Network, 11 Sites, United States, 2020. *MMWR. Surveillance Summaries*, *72*(2), 1-14. https://doi.org/10.15585/mmwr.ss7202a1

Maloney, S. E., Rieger, M. A., & Dougherty, J. D. (2013). Identifying essential cell types and circuits in autism spectrum disorders. *Int Rev Neurobiol*, *113*, 61-96. https://doi.org/10.1016/B978-0-12-418700-9.00003-4

Minshew, N. J., & Williams, D. L. (2007). The new neurobiology of autism: cortex, connectivity, and neuronal organization. *Arch Neurol*, *64*(7), 945-950. https://doi.org/10.1001/archneur.64.7.945

Mosconi, M. W., Wang, Z., Schmitt, L. M., Tsai, P., & Sweeney, J. A. (2015). The role of cerebellar circuitry alterations in the pathophysiology of autism spectrum disorders. *Front Neurosci*, *9*, 296. https://doi.org/10.3389/fnins.2015.00296

Nelson, A. B., Hammack, N., Yang, C. F., Shah, N. M., Seal, R. P., & Kreitzer, A. C. (2014). Striatal cholinergic interneurons Drive GABA release from dopamine terminals. *Neuron*, *82*(1), 63-70. https://doi.org/10.1016/j.neuron.2014.01.023

Nelson, A. B., & Kreitzer, A. C. (2014). Reassessing models of basal ganglia function and dysfunction. *Annu Rev Neurosci*, *37*, 117-135. https://doi.org/10.1146/annurev-neuro-071013-013916

Nelson, S. B., & Valakh, V. (2015). Excitatory/Inhibitory Balance and Circuit Homeostasis in Autism Spectrum Disorders. *Neuron*, *87*(4), 684-698. https://doi.org/10.1016/j.neuron.2015.07.033

Nestler, E. J., & Hyman, S. E. (2010). Animal models of neuropsychiatric disorders. *Nat Neurosci*, *13*(10), 1161-1169. https://doi.org/10.1038/nn.2647

Oldenburg, I. A., & Ding, J. B. (2011). Cholinergic modulation of synaptic integration and dendritic excitability in the striatum. *Curr Opin Neurobiol*, *21*(3), 425-432. https://doi.org/10.1016/j.conb.2011.04.004

Packard, M. G., & Knowlton, B. J. (2002). Learning and memory functions of the Basal Ganglia. *Annu Rev Neurosci*, *25*, 563-593. https://doi.org/10.1146/annurev.neuro.25.112701.142937

Parent, A., & Hazrati, L. N. (1995). Functional anatomy of the basal ganglia. I. The cortico-basal ganglia-thalamo-cortical loop. *Brain Res Brain Res Rev*, *20*(1), 91-127. https://doi.org/10.1016/0165-0173(94)00007-c

Platt, R. J., Zhou, Y., Slaymaker, I. M., Shetty, A. S., Weisbach, N. R., Kim, J. A., Sharma, J., Desai, M., Sood, S., Kempton, H. R., Crabtree, G. R., Feng, G., & Zhang, F. (2017). Chd8 Mutation Leads to Autistic-like Behaviors and Impaired Striatal Circuits. *Cell Rep*, *19*(2), 335-350. https://doi.org/10.1016/j.celrep.2017.03.052

Portfors, C. V. (2007). Types and functions of ultrasonic vocalizations in laboratory rats and mice. *J Am Assoc Lab Anim Sci*, *46*(1), 28-34. https://www.ncbi.nlm.nih.gov/pubmed/17203913

Portmann, T., Yang, M., Mao, R., Panagiotakos, G., Ellegood, J., Dolen, G., Bader, P. L., Grueter, B. A., Goold, C., Fisher, E., Clifford, K., Rengarajan, P., Kalikhman, D., Loureiro, D., Saw, N. L., Zhengqui, Z., Miller, M. A., Lerch, J. P., Henkelman, M., . . . Dolmetsch, R. E. (2014). Behavioral abnormalities and circuit defects in the basal ganglia of a mouse model of 16p11.2 deletion syndrome. *Cell Rep*, *7*(4), 1077-1092. https://doi.org/10.1016/j.celrep.2014.03.036

Rapanelli, M., Frick, L. R., Xu, M., Groman, S. M., Jindachomthong, K., Tamamaki, N., Tanahira, C., Taylor, J. R., & Pittenger, C. (2017). Targeted Interneuron Depletion in the Dorsal Striatum Produces Autism-like Behavioral Abnormalities in Male but Not Female Mice. *Biol Psychiatry*, *82*(3), 194-203. https://doi.org/10.1016/j.biopsych.2017.01.020

Robinson, D. L., Heien, M. L., & Wightman, R. M. (2002). Frequency of dopamine concentration transients increases in dorsal and ventral striatum of male rats during introduction of conspecifics. *J Neurosci*, *22*(23), 10477-10486. https://doi.org/10.1523/JNEUROSCI.22-23-10477.2002

Rothwell, P. E., Fuccillo, M. V., Maxeiner, S., Hayton, S. J., Gokce, O., Lim, B. K., Fowler, S. C., Malenka, R. C., & Sudhof, T. C. (2014). Autism-associated neuroligin-3 mutations commonly impair striatal circuits to boost repetitive behaviors. *Cell*, *158*(1), 198-212. https://doi.org/10.1016/j.cell.2014.04.045

Rubenstein, J. L., & Merzenich, M. M. (2003). Model of autism: increased ratio of excitation/inhibition in key neural systems. *Genes Brain Behav*, *2*(5), 255-267. https://doi.org/10.1034/j.1601-183x.2003.00037.x

Sander, D., Grafman, J., & Zalla, T. (2003). The human amygdala: an evolved system for relevance detection. *Rev Neurosci*, *14*(4), 303-316. https://doi.org/10.1515/revneuro.2003.14.4.303

Sandin, S., Lichtenstein, P., Kuja-Halkola, R., Hultman, C., Larsson, H., & Reichenberg, A. (2017). The Heritability of Autism Spectrum Disorder. *JAMA*, *318*(12), 1182-1184. https://doi.org/10.1001/jama.2017.12141

Sathyamurthy, A., Barik, A., Dobrott, C. I., Matson, K. J. E., Stoica, S., Pursley, R., Chesler, A. T., & Levine, A. J. (2020). Cerebellospinal Neurons Regulate Motor Performance and Motor Learning. *Cell Rep*, *31*(6), 107595. https://doi.org/10.1016/j.celrep.2020.107595

Satterstrom, F. K., Kosmicki, J. A., Wang, J., Breen, M. S., De Rubeis, S., An, J.-Y., Peng, M., Collins, R., Grove, J., Klei, L., Stevens, C., Reichert, J., Mulhern, M. S., Artomov, M., Gerges, S., Sheppard, B., Xu, X., Bhaduri, A., Norman, U., . . . Walters, R. K. (2020). Large-Scale Exome Sequencing Study Implicates Both Developmental and Functional Changes in the Neurobiology of Autism. *Cell*, *180*(3), 568-584.e523. https://doi.org/10.1016/j.cell.2019.12.036

Schmunk, G., & Gargus, J. J. (2013). Channelopathy pathogenesis in autism spectrum disorders. *Front Genet*, *4*, 222. https://doi.org/10.3389/fgene.2013.00222

Silverman, J. L., Thurm, A., Ethridge, S. B., Soller, M. M., Petkova, S. P., Abel, T., Bauman, M. D., Brodkin, E. S., Harony-Nicolas, H., Wohr, M., & Halladay, A. (2022). Reconsidering animal models used to study autism spectrum disorder: Current state and optimizing future. *Genes Brain Behav*, *21*(5), e12803. https://doi.org/10.1111/gbb.12803

Soares-Cunha, C., Coimbra, B., David-Pereira, A., Borges, S., Pinto, L., Costa, P., Sousa, N., & Rodrigues, A. J. (2016). Activation of D2 dopamine receptor-expressing neurons in the nucleus accumbens increases motivation. *Nat Commun*, *7*, 11829. https://doi.org/10.1038/ncomms11829

Soares-Cunha, C., Coimbra, B., Sousa, N., & Rodrigues, A. J. (2016). Reappraising striatal D1- and D2-neurons in reward and aversion. *Neurosci Biobehav Rev*, *68*, 370-386. https://doi.org/10.1016/j.neubiorev.2016.05.021

Sohal, V. S., & Rubenstein, J. L. R. (2019). Excitation-inhibition balance as a framework for investigating mechanisms in neuropsychiatric disorders. *Mol Psychiatry*, *24*(9), 1248-1257. https://doi.org/10.1038/s41380-019-0426-0

Steiner, H., & Gerfen, C. R. (1998). Role of dynorphin and enkephalin in the regulation of striatal output pathways and behavior. *Exp Brain Res*, *123*(1-2), 60-76. https://doi.org/10.1007/s002210050545

Surmeier, D. J., Ding, J., Day, M., Wang, Z., & Shen, W. (2007). D1 and D2 dopamine-receptor modulation of striatal glutamatergic signaling in striatal medium spiny

neurons. *Trends Neurosci*, *30*(5), 228-235. https://doi.org/10.1016/j.tins.2007.03.008
Sweeten, T. L., Posey, D. J., Shekhar, A., & McDougle, C. J. (2002). The amygdala and related structures in the pathophysiology of autism. *Pharmacol Biochem Behav*, *71*(3), 449-455. https://doi.org/10.1016/s0091-3057(01)00697-9
Takakusaki, K., Saitoh, K., Harada, H., & Kashiwayanagi, M. (2004). Role of basal ganglia-brainstem pathways in the control of motor behaviors. *Neurosci Res*, *50*(2), 137-151. https://doi.org/10.1016/j.neures.2004.06.015
Talantseva, O. I., Romanova, R. S., Shurdova, E. M., Dolgorukova, T. A., Sologub, P. S., Titova, O. S., Kleeva, D. F., & Grigorenko, E. L. (2023). The global prevalence of autism spectrum disorder: A three-level meta-analysis. *Front Psychiatry*, *14*, 1071181. https://doi.org/10.3389/fpsyt.2023.1071181
Taylor, M. J., Rosenqvist, M. A., Larsson, H., Gillberg, C., D'Onofrio, B. M., Lichtenstein, P., & Lundstrom, S. (2020). Etiology of Autism Spectrum Disorders and Autistic Traits Over Time. *JAMA Psychiatry*, *77*(9), 936-943. https://doi.org/10.1001/jamapsychiatry.2020.0680
Thabault, M., Turpin, V., Maisterrena, A., Jaber, M., Egloff, M., & Galvan, L. (2022). Cerebellar and Striatal Implications in Autism Spectrum Disorders: From Clinical Observations to Animal Models. *Int J Mol Sci*, *23*(4). https://doi.org/10.3390/ijms23042294
Threlfell, S., Lalic, T., Platt, N. J., Jennings, K. A., Deisseroth, K., & Cragg, S. J. (2012). Striatal dopamine release is triggered by synchronized activity in cholinergic interneurons. *Neuron*, *75*(1), 58-64. https://doi.org/10.1016/j.neuron.2012.04.038
Tian, W., & Chen, S. (2021). Neurotransmitters, Cell Types, and Circuit Mechanisms of Motor Skill Learning and Clinical Applications. *Front Neurol*, *12*, 616820. https://doi.org/10.3389/fneur.2021.616820
Tunstall, M. J., Oorschot, D. E., Kean, A., & Wickens, J. R. (2002). Inhibitory interactions between spiny projection neurons in the rat striatum. *J Neurophysiol*, *88*(3), 1263-1269. https://doi.org/10.1152/jn.2002.88.3.1263
Voineagu, I. (2012). Gene expression studies in autism: moving from the genome to the transcriptome and beyond. *Neurobiol Dis*, *45*(1), 69-75. https://doi.org/10.1016/j.nbd.2011.07.017
Voineagu, I., Wang, X., Johnston, P., Lowe, J. K., Tian, Y., Horvath, S., Mill, J., Cantor, R. M., Blencowe, B. J., & Geschwind, D. H. (2011). Transcriptomic analysis of autistic brain reveals convergent molecular pathology. *Nature*, *474*(7351), 380-384. https://doi.org/10.1038/nature10110
Volkmar, F. R., & McPartland, J. C. (2014). From Kanner to DSM-5: autism as an evolving diagnostic concept. *Annu Rev Clin Psychol*, *10*, 193-212. https://doi.org/10.1146/annurev-clinpsy-032813-153710
Voorn, P., Vanderschuren, L. J., Groenewegen, H. J., Robbins, T. W., & Pennartz, C. M. (2004). Putting a spin on the dorsal-ventral divide of the striatum. *Trends Neurosci*, *27*(8), 468-474. https://doi.org/10.1016/j.tins.2004.06.006
Walsh, J. J., Christoffel, D. J., Heifets, B. D., Ben-Dor, G. A., Selimbeyoglu, A., Hung, L. W., Deisseroth, K., & Malenka, R. C. (2018). 5-HT release in nucleus accumbens rescues social deficits in mouse autism model. *Nature*, *560*(7720), 589-594. https://doi.org/10.1038/s41586-018-0416-4

Wang, Z., Kai, L., Day, M., Ronesi, J., Yin, H. H., Ding, J., Tkatch, T., Lovinger, D. M., & Surmeier, D. J. (2006). Dopaminergic control of corticostriatal long-term synaptic depression in medium spiny neurons is mediated by cholinergic interneurons. *Neuron*, *50*(3), 443-452. https://doi.org/10.1016/j.neuron.2006.04.010

Wei, H., Mori, S., Hua, K., & Li, X. (2012). Alteration of brain volume in IL-6 overexpressing mice related to autism. *Int J Dev Neurosci*, *30*(7), 554-559. https://doi.org/10.1016/j.ijdevneu.2012.08.007

West, K. L. (2019). Infant Motor Development in Autism Spectrum Disorder: A Synthesis and Meta-analysis. *Child Dev*, *90*(6), 2053-2070. https://doi.org/10.1111/cdev.13086

Winslow, J. T. (2003). Mouse social recognition and preference. *Curr Protoc Neurosci*, *Chapter 8*, Unit 8 16. https://doi.org/10.1002/0471142301.ns0816s22

Xenias, H. S., Ibanez-Sandoval, O., Koos, T., & Tepper, J. M. (2015). Are striatal tyrosine hydroxylase interneurons dopaminergic? *J Neurosci*, *35*(16), 6584-6599. https://doi.org/10.1523/JNEUROSCI.0195-15.2015

Xu, X., Wells, A. B., O'Brien, D. R., Nehorai, A., & Dougherty, J. D. (2014). Cell type-specific expression analysis to identify putative cellular mechanisms for neurogenetic disorders. *J Neurosci*, *34*(4), 1420-1431. https://doi.org/10.1523/JNEUROSCI.4488-13.2014

Yin, H. H. (2017). The Basal Ganglia in Action. *Neuroscientist*, *23*(3), 299-313. https://doi.org/10.1177/1073858416654115

Yizhar, O., Fenno, L. E., Prigge, M., Schneider, F., Davidson, T. J., O'Shea, D. J., Sohal, V. S., Goshen, I., Finkelstein, J., Paz, J. T., Stehfest, K., Fudim, R., Ramakrishnan, C., Huguenard, J. R., Hegemann, P., & Deisseroth, K. (2011). Neocortical excitation/inhibition balance in information processing and social dysfunction. *Nature*, *477*(7363), 171-178. https://doi.org/10.1038/nature10360

Zalla, T., & Sperduti, M. (2013). The amygdala and the relevance detection theory of autism: an evolutionary perspective. *Front Hum Neurosci*, *7*, 894. https://doi.org/10.3389/fnhum.2013.00894

Zeidan, J., Fombonne, E., Scorah, J., Ibrahim, A., Durkin, M. S., Saxena, S., Yusuf, A., Shih, A., & Elsabbagh, M. (2022). Global prevalence of autism: A systematic review update. *Autism Research*, *15*(5), 778-790. https://doi.org/10.1002/aur.2696

# Chapter 2: Altered motor learning and coordination in mouse models of autism spectrum disorder*

Katherine Cording

Helen Wills Neuroscience Institute
University of California, Berkeley

*The following chapter includes previously published work:
Cording, K. R., & Bateup, H. S. (2023). Altered motor learning and coordination in mouse models of autism spectrum disorder. *Front Cell Neurosci*, *17*, 1270489. https://doi.org/10.3389/fncel.2023.1270489

## Introduction

An estimated 1 in 100 children globally have autism spectrum disorder (ASD), and CDC estimates indicate even greater prevalence in America, where roughly 1 in 36 children is diagnosed with ASD (Maenner et al., 2023; Talantseva et al., 2023; Zeidan et al., 2022). As ASD is highly heritable (Sandin et al., 2017), much work has been done in recent years to identify genes that confer risk of developing ASD. Increased accessibility of DNA sequencing has allowed for the identification of hundreds of ASD risk genes, which range widely in the types of proteins for which they code (Satterstrom et al., 2020). Despite this molecular heterogeneity, ASD is still diagnosed through identification of behaviors that fall into two primary domains: deficits in social communication and interaction, and the presence of restricted, repetitive patterns of behavior (RRBs) (APA, 2022).

In individuals with ASD, RRBs can span a range of “lower order” and “higher level” behaviors. “Lower order” motor presentations may include self-stimulation or self-injury like head banging, hand flapping, twirling, lining up or manipulating objects, or repeatedly pressing buttons. “Higher level” repetitive behaviors include rituals, perseverative interests and insistence on sameness in a variety of situations (Caldwell-Harris, 2021). In addition to the repetitive behaviors recognized as core ASD symptoms, other motor presentations can include changes to gross motor skills such as balance, gait and posture, as well as alterations in fine motor skills and motor skill learning (Chukoskie et al., 2013). In studies of balance, individuals with ASD exhibit reduced postural control, in particular when somatosensory or visual challenges are introduced. This could occur when a subject is instructed to close their eyes, stand on one leg, or balance on a swaying platform, for example (Minshew et al., 2004; Travers et al., 2013). Atypical gait, which several studies have reported in individuals with ASD, may occur as a result of difficulties with balance and posture (Chukoskie et al., 2013). While specific changes in gait parameters are heterogenous across studies, a lack of smoothness, irregular trunk movements, and shorter stride length are commonly identified in individuals with ASD (Vernazza-Martin et al., 2005; Weiss et al., 2013). Foundational motor movements such as reaching and grasping have also been shown to be altered in children with ASD (David et al., 2012; Haswell et al., 2009), which may underlie some of the deficits seen in executing gross motor skills like throwing and catching, as well as fine motor skills like buttoning, manipulating small objects, and handwriting (Battah et al., 2023; Chukoskie et al., 2013; Green et al., 2009). Notably, handwriting has been reported to be significantly altered in those with ASD since the earliest descriptions of the disorder (Asperger, 1991). Although the early presence of motor symptoms is highly predictive of later overall ASD symptom severity, this remains an understudied and undertreated symptom domain (Troyb et al., 2016; Zampella et al., 2021). The use of common behavioral assays in tractable animal models of ASD can greatly assist in the identification of circuits that may underlie motor changes in autism.

Increasingly, the basal ganglia, and in particular the striatum, has been implicated in the manifestation of repetitive behaviors in ASD, because of the role of

these circuits in motor learning, action selection, and habit formation (Fuccillo, 2016). Indeed, both structural and functional imaging studies identify aberrant striatal morphology and connectivity in individuals with ASD, in some cases strongly correlating with the presentation of repetitive behaviors (Dichter, 2012; Estes et al., 2011; Hollander et al., 2005). Magnetic resonance imaging (MRI) studies in mice support these findings, where a diverse range of genetic ASD mouse models exhibit altered striatal morphology and connectivity (Ellegood et al., 2015; Lai et al., 2016; Portmann et al., 2014; Wang et al., 2016). In this review we will discuss the relationship between striatal function and motor performance in mouse models of ASD, which has been illuminated through the use of a common behavioral assay of motor coordination and learning, the accelerating rotarod.

**Mouse models of ASD**

An increase in the identification of genes implicated in ASD risk paired with the genetic accessibility of animal models has allowed for the development of many genetic mouse models of ASD (Bey & Jiang, 2014). Targeting mutations in these mouse models to risk genes that have been identified in individuals with ASD provides construct validity (where the perturbation used to generate the disease model recapitulates the known etiology of the disease in people) (Nestler & Hyman, 2010). Face validity of these models (where the model displays key clinical manifestations of the disease) is more challenging to achieve given the heterogeneity and variability of ASD presentations in people. That said, a range of assays have been developed with the goal of measuring mouse behaviors analogous to those comprising the symptom domains of ASD (Bey & Jiang, 2014).

For the RRB domain of ASD, mouse behavioral assays primarily fit into the “lower order” and “higher level” domain distinctions detailed above. The former is typically measured with the open-field assay, allowing for detection of changes in general locomotor features such as speed and distance traveled, as well as the presence of motor stereotypies such as repetitive grooming, rearing, circling or jumping (Gandhi & Lee, 2020). Other assays like the marble burying test and the hole board take advantage of natural exploratory mouse behaviors like digging and head poking to detect increased repetition of these spontaneous behaviors (Bey & Jiang, 2014). More complex, “higher level” aspects of RRBs can also be assessed in mice, measuring resistance to change, cognitive inflexibility and perseveration in a range of reversal learning, set-shifting and response extinction tasks (Gandhi & Lee, 2020). The changes to gross motor function and coordination that appear to coincide with the repetitive behavior domain in individuals with ASD can also be assessed in mice using balance beams and commercially available systems for measuring and analyzing gait parameters (e.g. DigiGait, Neurocube) (Simmons et al., 2021). The recent development of deep-learning-based platforms such as DeepLabCut and MoSeq allows for unsupervised, data-driven detection and analysis of mouse behavioral parameters (Mathis et al., 2018; Wiltschko et al., 2020).

One behavioral assay commonly utilized in mouse models, the accelerating rotarod task, can be used both as a measure of gross motor coordination, as well as motor skill learning. Below we will outline the structure and parameters of the rotarod task, the way that learning occurs over the course of trials, and the brain regions and circuits implicated in rotarod performance.

**The rotarod task measures motor coordination and learning**

First described in the 1950's (Dunham & Miya, 1957), the accelerating rotarod task has historically been used as a measure of motor coordination and function in animal models of disease (Hamm et al., 1994; Heng et al., 2008; Lubrich et al., 2022) (Figure 1). However, performance on this test can also be used as a measure of motor skill learning. In the task, mice are trained to walk on a rotating rod as it increases in speed at a constant rate. Protocols utilized in the task vary, but typically the rod increases from 5 to 40 revolutions per minute over the course of 5 minutes. The latency to fall, or rotate backwards off the rod, is used to determine the terminal velocity in each trial, with increases in this measure indicating better performance. Over several trials, animals exhibit improvement both within a given training day, and over the course of training sessions (Luft & Buitrago, 2005). In this way, initial performance in the task can be isolated as a measure of basic motor coordination, with differences between mouse models at this early stage indicating gross motor deficits or altered baseline motor function. If initial performance is similar, but there are differences in improvement within a given training day and/or across training days, this indicates a difference in motor learning. Many different versions of this extended protocol have been used, ranging from 3-5 trials for one day up to ten trials a day for eight days in longer versions of the task (Yin et al., 2009). Most common is to utilize 3-4 trials per day across 3-4 days of testing (Benthall et al., 2021; Le Merrer et al., 2023; Lynch et al., 2020; Rothwell et al., 2014) (Figure 1).

When given home cage access to a running wheel, animals perform better on the rotarod overall, but the rate of both intra- and intersession improvement remains the same, indicating that increasing performance in the task goes beyond gains in locomotor fitness (Buitrago et al., 2004). Instead, animals develop and optimize a sequence of movements that allows them to stay on the rod at faster speeds, which is exemplified by shifts in gait patterns across training from stepping to running (Buitrago et al., 2004). In some cases, differences in performance between models is only revealed in versions of the task that utilize faster speeds, up to 80 revolutions per minute, which necessitates even greater motor program optimization (Benthall et al., 2021; DiCarlo et al., 2019; Lynch et al., 2020; Rothwell et al., 2014).

Given the multiphasic nature of the accelerating rotarod task, several brain regions are implicated in task performance, including the cortex (Ash, Park, et al., 2021; Fu et al., 2012; Yang et al., 2009), basal ganglia (Costa et al., 2004; Durieux et al., 2012; Yin et al., 2009), and cerebellum (Sathyamurthy et al., 2020; Simmons et al., 2021). In this review, we highlight the role of the basal ganglia, in particular the striatum,

in the motor learning that occurs during rotarod training. Given the involvement of the striatum in a number of other motor learning functions, such as instrumental learning and extinction (Santos et al., 2015; Yin et al., 2005, 2006), active avoidance, response-based procedural learning (Pittenger et al., 2006), and shifting from action-outcome to stimulus-response performance (Hawes et al., 2015), altered rotarod performance, which is easily assessed in mice, likely translates into changes in these more difficult to measure corticostriatal-dependent behaviors. In this way, performance in the accelerating rotarod task is an informative indicator of the function of a frequently altered circuit in mouse models of ASD (Li & Pozzo-Miller, 2020).

**Motor learning depends on corticostriatal circuits**

The striatum, the main input center of the basal ganglia, is composed of GABAergic striatal projection neurons (SPNs) and local interneurons. SPNs, which make up over 95% of striatal neurons, send their outputs to downstream nuclei via two largely parallel pathways. Dopamine D1-receptor expressing SPNs of the direct pathway (dSPNs) send their primary projections to the substantia nigra pars reticulata and globus pallidus internal segment (SNr/GPi) and broadly facilitate movement when activated in bulk (Gerfen & Surmeier, 2011; Kravitz et al., 2010; Tai et al., 2012). D2-receptor expressing SPNs of the indirect pathway (iSPNs) send their primary projections to the globus pallidus external segment (GPe) and generally inhibit movement or suppress competing actions when activated as a population (Calabresi et al., 2014; Gerfen & Surmeier, 2011; Kravitz et al., 2010; Tai et al., 2012). During behavior, both populations of SPNs are activated in a coordinated way to orchestrate movement and decision-making. SPNs are innervated by a variety of inputs, most notably glutamatergic input from the cortex and thalamus, and dopamine input from the midbrain (Ding et al., 2008; Doig et al., 2010; Gerfen & Surmeier, 2011). Despite overall similar cytoarchitecture, the dorsal and ventral regions of the striatum are thought to be implicated in different functions, with the former controlling motor and cognitive functions, and the latter mediating limbic functions such as appetitive behavior and reward (Voorn et al., 2004) (Figure 1).

Further parsing of striatal regions, based primarily on differences in cortical inputs, implicates the dorsomedial striatum (DMS) as an associative region involved in the initial stages of learning action-outcome pairings and the dorsolateral striatum (DLS) as a sensorimotor region involved in the acquisition of habitual or procedural behaviors (Voorn et al., 2004). In both subregions, SPN ensemble activity and plasticity at striatal synapses is important for a variety of learning tasks, including motor skill learning (Barnes et al., 2005; Costa et al., 2004; Dang et al., 2006; Kupferschmidt et al., 2019; Yin et al., 2009). In the accelerating rotarod task, *in vivo* electrophysiological recordings showed that neurons in the striatum exhibit task-related activity that is highly correlated with performance (Barnes et al., 2005; Costa et al., 2004). Within the striatum, different subregions exhibit dynamic activity patterns throughout different phases of motor learning. In the DMS, positive modulation of firing rate in task-related SPNs

predominantly occurs early in rotarod training, while in DLS, this firing rate modulation occurs after extensive training. Consistent with this, lesions of the DMS impair early learning while lesions of the DLS impair both early and late learning (Yin et al., 2009). Together this work establishes a key role for dorsal striatal circuits in rotarod learning.

While initial work highlighted the importance of the dorsal striatum in motor skill learning, several studies suggest that the ventral striatum may also play a role. In particular, a recent study showed that ablation of iSPNs in the nucleus accumbens (NAc) is sufficient to impair rotarod learning (Le Merrer et al., 2023). In addition, as discussed below, ventral striatal-specific manipulation of some ASD risk genes is sufficient to impact rotarod performance (Platt et al., 2017; Rothwell et al., 2014). This fits within the theory first introduced by Haber and colleagues that the ventral and dorsal striatum interact dynamically over the course of learning (Haber et al., 2000). Just as varying cortical inputs form a gradient across dorsolateral and ventromedial striatum, so too do the inputs to and outputs from dopaminergic substantia nigra. Ventral striatal subregions are proposed to influence behavioral gating in dorsal striatal regions through an ascending “spiral” of information through these striatonigrostriatal connections (Belin et al., 2007; Haber et al., 2000). Dynamic changes in the activity and functional roles of different SPN subtypes across this spiral likely occur during rotarod training.

In terms of the striatal cell types involved in motor learning, studies using *ex vivo* electrophysiology showed that D2-receptor expressing iSPNs of the DLS undergo significant synaptic potentiation during late training and that administration of a D2R antagonist late in training impairs rotarod performance (Yin et al., 2009). This suggests that plasticity of dorsal striatal indirect pathway activity may be important for rotarod learning. A study using adult neurotoxin-induced ablation of iSPNs throughout the striatum confirmed the importance of iSPNs for rotarod performance, particularly for early learning (Durieux et al., 2012). However, it was also shown that ablation of dSPNs throughout the striatum (Durieux et al., 2012), or selectively in the dorsal striatum (Durieux et al., 2012; Le Merrer et al., 2023), impairs rotarod performance, resulting in severe motor learning deficits. This is consistent with other studies showing that manipulations of dorsal striatal dSPNs can impact rotarod performance (Benthall et al., 2021; Ma et al., 2022). In terms of the ventral striatum, Le Merrer and colleagues showed that ablation of iSPNs (but not dSPNs) in the NAc disrupts rotarod performance (Le Merrer et al., 2023). Furthermore, reducing the excitability of dSPNs in the NAc has also been shown to impair motor learning (Rothwell et al., 2014). Together these studies provide evidence that multiple striatal circuits and subregions are required for motor learning and likely play a coordinated role in motor skill acquisition and maintenance.

The differential roles of striatal sub-regions as well as SPN subtypes during different stages of rotarod learning is likely driven by changes in cortical drive (Yin et al., 2009). Indeed, intact glutamatergic corticostriatal transmission is necessary for rotarod learning. Loss of the presynaptic scaffolding protein RIM1 from corticostriatal neurons, which disrupts excitatory transmission in the dorsal striatum, impairs rotarod learning (Kupferschmidt et al., 2019). In addition, striatal-specific deletion of glutamatergic

NMDARs results in a significant deficit in learning in the task (Dang et al., 2006). Taken together, these studies show that changes in the synaptic properties of direct and indirect pathway neurons, throughout dorsal and ventral striatum, shape rotarod performance throughout different stages of the task. Our emerging understanding of the synaptic and circuit mechanisms that underlie rotarod learning make it a useful assay to apply to mouse models of disease.

**Altered rotarod performance in mice with mutations in ASD risk genes**

Rotarod performance has been assessed across numerous mouse models with mutations in ASD risk genes, making it a useful assay for identifying potential convergent phenotypes. In surveying the literature, we find that many (but not all) ASD mouse models exhibit altered performance in this task, which can include altered initial performance, a global change in performance, or a difference in learning rate across trials (Table 1). One challenge with making general conclusions from this assessment is that multiple different rotarod protocols have been used. While utilizing a rod that increases in speed from 5-40 RPM over the course of 5 minutes per trial is most common, the number of trials implemented per day, and the total number of days of the task vary greatly across studies. In some cases where multiple protocols have been used, mice can show changes in one version of the rotarod task but not another (Benthall et al., 2021; DiCarlo et al., 2019; Lynch et al., 2020; Rothwell et al., 2014). Therefore, if no phenotype is reported with one rotarod protocol, it's possible that performance would be altered if the acceleration speed, number of trials, and/or number of testing days were different.

With this caveat noted, we do find a group of models, including mice with loss-of-function mutations in *Mecp2*, *Shank3* and *Ube3a*, which show consistent deficits in rotarod performance (Table 1). Some of these models exhibit poor performance from the first trial of the task, exemplified by decreased latency to fall from the rod in trial 1 compared to wild-type (WT) controls, owing to baseline deficits in motor coordination (see Table 1 - models with a deficit in coordination). In other models, trial 1 performance resembles that of WT controls, suggesting intact coordination, however, the latency to fall across trials either does not increase, or increases less than WT controls, indicating a deficit in motor learning (see Table 1 - models with a deficit in learning).

In the case of many loss-of-function *Mecp2*, *Shank3* and *Ube3a* mutations, mice exhibit deficits in both initial coordination and motor learning. The phenotypes observed in these mouse models may reflect the motor deficits that occur in individuals with mutations in these genes (Caldwell-Harris, 2021; Chukoskie et al., 2013; Troyb et al., 2016). Specifically, while motor function can be quite variable across individuals with ASD as a whole, one of the core diagnostic criteria of Rett syndrome, which is caused by loss-of-function mutations in the *MECP2* gene, is the deterioration of motor function, often resulting in complete loss of mobility in patients (Chahrour & Zoghbi, 2007). Similarly, patients with Angelman syndrome, a neurodevelopmental disorder caused by mutations in the *UBE3A* gene, generally exhibit severe motor dysfunction including

orthopedic and movement difficulties, walking that is stiff or jerky, and a lack of coordination or development of complex motor skills (Rotaru et al., 2020). A comprehensive clinical assessment of 17 individuals with point mutations in the *SHANK3* gene, a gene located within the 22q13.3 chromosomal region implicated in the neurodevelopmental disorder Phelan-McDermid syndrome, identified less severe motor dysfunction than typically seen in the above syndromes; however, nearly all individuals assessed exhibited hypotonia and gait abnormalities (De Rubeis et al., 2018). The identification of motor dysfunction as a common clinical presentation caused by mutations in these genes, alongside the consistently decreased rotarod performance seen in models of these syndromes lends face validity to the rotarod assay.

Notably, while phenotypic analysis of animal models of disease often focuses on identifying deficits, there is a cohort of ASD mouse models that show increased performance on the rotarod task (Table 1). The enhanced performance in these models can either be apparent from initial testing onward or revealed over the course of training. In the remainder of this review, we will focus specifically on these “gain-of-function” cases and discuss how enhanced motor learning may reflect changes in striatal circuit function that could facilitate the development of RRBs.

**Enhanced rotarod performance in mice with ASD risk gene mutations**

*Copy number variations*

Many different copy number variations (CNVs) and genomic deletions, duplications or inversions, have been found in individuals with ASD (Takumi & Tamada, 2018). The 16p11.2 variant is one of the most common CNVs associated with ASD (Weiss et al., 2008). Mice with a syntenic 16p11.2 microdeletion (16p11.2 $Del^{m}$) have been generated and shown to exhibit increased performance on the rotarod, in particular, in a version of the task that utilizes higher speeds (8-80 RPM) (Lynch et al., 2020). Another 16p11.2 microdeletion mouse model exhibits cellular changes in the striatum including an increased number of iSPNs, increased relative volume of the ventral striatum (in particular the NAc), and excitatory synapse deficits onto SPNs in the NAc. While this mouse model has gross motor alterations such as tremors and gait changes, rotarod performance is unchanged, although the higher speeds utilized in Lynch et al. were not tested (Portmann et al., 2014). Another study found that stride and stance duration in adult 16p11.2 heterozygous mice (16p11.2 $Del^{m}$) are significantly shorter than in controls, which are features that positively correlate with increased speed (Brunner et al., 2015). These gait changes may contribute to the increased performance on the rotarod task seen in some models of this CNV.

Another CNV implicated in ASD spans the 15q11-13 region, and is most commonly identified as a duplication (Takumi & Tamada, 2018). Mice with a paternal duplication in the 15q11-13 region exhibit increased rotarod performance compared to controls, staying on the rod for significantly longer in every trial after the first, reaching near ceiling performance (Nakatani et al., 2009). Gait assessment in another model of this CNV using a transparent treadmill identified significant changes in the motor

program of these mice, which may contribute to their increased performance on the rotarod (Piochon et al., 2014).

*Cell adhesion molecules*

Several of the rare genetic variants that have been identified as conferring ASD risk impact synaptic cell adhesion molecules, which are proteins involved in the formation and stabilization of synaptic contacts (Betancur et al., 2009). The best characterized synaptic cell adhesion molecules implicated in ASD are those of the neurexin and neuroligin families of proteins. *Nrxn1* (neurexin 1a) mutant mice exhibit increased performance on the accelerating rotarod, to the point of near peak performance after ten trials at 4-45 RPM over five minutes (Etherton et al., 2009). This type of enhancement has been observed in another *Nrxn1* mutant mouse model as well (Xu et al., 2023). With testing over two additional trials at five times the rate of acceleration (4-45 RPM over one minute), *Nrxn1* knockout (KO) mice continue to perform significantly better than WT mice (Etherton et al., 2009).

Multiple *Nlgn3* (neuroligin 3) mutant mouse models also exhibit enhanced performance on the accelerating rotarod, in particular at higher speeds (8-80 RPM) (Cao et al., 2022; Chadman et al., 2008; Rothwell et al., 2014; Yoshida et al., 2021). Video analysis of one such model revealed that *Nlgn3* KO mice have reduced variability in their motor performance, streamlining step location, timing, and length significantly more than WT counterparts throughout the task. Variability in these measures negatively correlates with time to fall off the rod, indicating that they represent a valid measure of acquisition of this stereotyped behavior (Rothwell et al., 2014).

Mice lacking another ASD risk gene of the neurexin family, *Cntnap2*, which encodes a cell adhesion molecule implicated in the stabilization of potassium channels, perform significantly better than WT littermates in a single-trial version of the accelerating rotarod task (Penagarikano et al., 2011), and in a constant speed rotarod task (Dawes et al., 2018). In another study of *Cntnap2*$^{-/-}$ mice, gait analysis found that KO mice are faster than WT controls. KO mice also exhibit shorter strides, which may contribute to their increased performance in the rotarod task (Brunner et al., 2015). A few studies identified alterations in the development or function of inhibitory interneuron populations in the striatum of *Cntnap2*$^{-/-}$ mice (Ahmed et al., 2023; Penagarikano et al., 2011), a change that may alter SPN excitability and in turn the propensity to form motor routines.

*KIRREL3* is an ASD risk gene that codes for a transmembrane protein implicated in synapse formation (Martin et al., 2015). Mice with complete loss of *Kirrel3* exhibit enhanced performance on the rotarod, particularly in later trials of the task (Hisaoka et al., 2018). Loss of the ASD risk gene *IL1RAPL1* (interleukin 1 receptor accessory protein-like 1), which also encodes a protein that mediates synapse formation, results in enhanced performance on the accelerating rotarod. *Il1rapl1*$^{-/-}$ mice are able to stay on the rod significantly longer than WT controls for all six trials of the task, demonstrating

significantly increased baseline coordination, as well as motor learning (Yasumura et al., 2014).

In the space surrounding synapses, extracellular matrix proteins like reelin aid in the stabilization of cell-cell interactions. Mice with a C-terminal domain mutation in *Reln*, a gene implicated in a number of neuropsychiatric disorders such as bipolar disorder, schizophrenia, and ASD, exhibit significantly enhanced performance in the accelerating rotarod (Sakai et al., 2016). At the cellular level, another study found that a protocol used to induce synaptic long-term depression (LTD) at corticostriatal synapses in WT mice instead induces long-term potentiation (LTP) in mice with homozygous loss of *Reln*. This effect is partially explained by a loss of GABAergic tone due to decreased numbers of striatal GABAergic interneurons in *Reln* mutant mice (Marrone et al., 2006). This enhanced corticostriatal excitability could underlie the increased rotarod performance seen in some *Reln* mutant models.

*mTOR regulators*

The mechanistic target of rapamycin (mTOR) serves as a central signaling hub involved in cellular metabolic processes such as protein and lipid synthesis and autophagy (Saxton & Sabatini, 2017). Several genes encoding proteins involved in the mTOR pathway are ASD risk genes, and dysregulation of mTOR signaling may occur in multiple forms of ASD (Winden et al., 2018). *TSC2*, which codes for an inhibitor of mTOR complex 1 (mTORC1) signaling, is one such ASD risk gene (Curatolo et al., 2015; Davis et al., 2015). Mice with heterozygous loss of *Tsc2* have normal initial performance but exhibit increased motor learning on the accelerating rotarod (Benthall et al., 2021). Notably, increased performance is only revealed at higher rotarod speeds (10-80 RPM), as *Tsc2*$^{+/-}$ mice perform similarly to WT littermates on 5-40 RPM trials (Benthall et al., 2021). This may reflect a ceiling effect, as WT mice can often stay on the rotarod for the entire 5-minute trial with speeds up to 40 RPM.

Mice with altered function of Pten, another inhibitor of mTOR signaling, also exhibit changes in rotarod behavior. While global heterozygous loss of *Pten* does not alter rotarod performance (Clipperton-Allen & Page, 2014), Kwon et al. found that conditional loss of *Pten* results in increased performance on the accelerating rotarod compared to controls. In this model, *Pten* loss occurs in a subset of cortical and hippocampal neurons (Kwon et al., 2006). *Pten* deletion in interneurons is likely not the driver of this enhanced performance, as cell-type specific loss of *Pten* in parvalbumin (PV) and/or somatostatin (SST) interneurons led to impaired rotarod performance (Shin et al., 2021). Instead, increased local and long range excitatory input onto *Pten* KO cells in sensory cortex suggests that increased excitatory drive of corticostriatal neurons could underlie increased rotarod performance (Xiong et al., 2012).

*Transcriptional and translational regulators*

Neural development requires precise coordination of molecular programs and several genes involved in transcriptional and translational control are implicated in ASD

(Longo & Klann, 2021). *CHD8*, which encodes the chromatin remodeling factor chromodomain helicase DNA binding protein 8, has been identified as one of the genes with the strongest association with ASD (Weissberg & Elliott, 2021). *Chd8*$^{+/-}$ mice perform significantly better than WT counterparts on the accelerating rotarod, regardless of whether mice were trained at 4-40 RPM once a day for five days, or three times a day for two days (Platt et al., 2017). Enhanced rotarod performance was also observed in a different *Chd8* mutant model (Hulbert et al., 2020). In this study, *Chd8*$^{+/E31T}$ mice performed significantly better than WT controls on all 4 trials of both accelerating (4-40 RPM over 5 min) and steady state (32 RPM) rotarod tasks.

As discussed above, loss of the transcriptional regulator MECP2 results in Rett syndrome, which is characterized by motor deficits in people and in mouse models. However, duplication of the *MECP2* locus causes *MECP2* duplication syndrome, which is a neurodevelopmental disorder highly comorbid with ASD (Qiu, 2018). In contrast to *Mecp2* deficient mice, mice with duplication of *Mecp2* exhibit significantly enhanced performance on the rotarod task, a phenotype that has been observed in several different *Mecp2* duplication models (Collins et al., 2004; Sztainberg et al., 2015). At the cellular level, following rotarod training, *Mecp2* duplication mice have significantly more new dendritic spines, as well as more stabilized spines on layer V pyramidal neurons in the motor cortex (M1), which project to the dorsal striatum (Ash, Park, et al., 2021). Newly stabilized spines tend to cluster in *Mecp2* duplication mice, a characteristic associated with increased motor skill learning (Fu et al., 2012; Yang et al., 2009). Indeed, Ash et al. found that the formation and stabilization of new spine clusters is significantly correlated with increased performance on the rotarod in both *Mecp2* duplication mice and WT controls (Ash, Park, et al., 2021).

To interrogate the molecular mechanisms driving the enhanced rotarod learning in *Mecp2* duplication mice, Ash et al. targeted Ras-ERK signaling by intraperitoneally injecting the ERK inhibitor SL327 daily preceding rotarod training. This reversed the enhanced performance of *Mecp2* duplication mice, without altering WT performance in the task (Ash, Buffington, et al., 2021). Together these findings suggest that increased synaptic stability within the corticostriatal sensorimotor loop may underlie enhanced motor learning in the context of *Mecp2* duplication. Notably, mice with a loss-of-function mutation in *Mecp2* exhibit significantly decreased spine density in pyramidal cells of both motor (Tropea et al., 2009) and somatosensory cortex, as well as altered short-term structural plasticity of spines in the latter region (Landi et al., 2011). These gene dose-dependent changes in synaptic stability within sensorimotor circuitry may contribute to the opposing impact of *Mecp2* mutations on rotarod performance.

Mutations in the *FMR1* gene result in Fragile X syndrome, a neurodevelopmental disorder with high comorbidity with ASD. *FMR1* mutations alter the expression of Fragile X Messenger Ribonucleoprotein (FMRP), an RNA binding protein involved in translational control (Jin & Warren, 2003). In one *Fmr1* KO mouse model, accelerating rotarod performance is enhanced compared to WT controls across all three sessions of the task, indicating both enhanced baseline coordination as well as increased learning

over trials (Roy et al., 2011). Another *Fmr1* model exhibits similar initial coordination as WT controls, but significantly increased learning across the eight trials of the rotarod task (Nolan et al., 2017). Other studies of this model identified changes in striatal endocannabinoid-mediated long-term depression (eCB-LTD) (Jung et al., 2012; Maccarrone et al., 2010), a form of synaptic plasticity altered in other genetic mouse models with enhanced performance in the rotarod task (Benthall et al., 2021; Martella et al., 2018). In the dorsal striatum, eCB-LTD is enhanced at GABAergic synapses in the context of FMRP loss (Maccarrone et al., 2010), whereas eCB-LTD at excitatory synapses in the ventral striatum of *Fmr1* KO mice is abolished (Jung et al., 2012). Taken together, this loss of LTD at excitatory synapses and enhanced LTD at inhibitory synapses may culminate in unchecked corticostriatal drive in *Fmr1* KO mice, which could underlie the convergent motor phenotype across these models.

*Dopamine and rotarod performance*

Dopamine is a potent modulator of cortical and striatal synapses (Tritsch & Sabatini, 2012) and functional dopamine signaling is important for motor performance and learning (Packard & Knowlton, 2002). Mice lacking dopaminergic neurons of the substantia nigra pars compacta, leading to 90% reductions in dorsal striatal dopamine, are unable to increase performance on the rotarod over trials, a deficit that is rescued by treatment with the dopamine precursor L-DOPA (Beeler et al., 2010). Several mouse models of ASD exhibit alterations in dopaminergic function (Kosillo & Bateup, 2021). A *de novo* mutation in *SLC6A3,* which results in a T356M amino acid substitution in the gene encoding the dopamine transporter (DAT), has been linked to ASD (Neale et al., 2012). *In vitro* characterization shows that this mutation results in efflux, rather than typical influx, of dopamine when expressed, potentially leading to greater synaptic dopamine (Hamilton et al., 2013). Mice expressing one copy of the *Slc6a3* mutation perform similarly to WT controls in early training; however, T356M$^{+/-}$ mice exhibit significantly enhanced performance in later trials of the task. DAT expression levels are normal in these mice, but striatal dopamine (DA) reuptake is impaired and increased extracellular dopamine in the striatum results in increased striatal DA metabolism and reduced striatal DA synthesis (DiCarlo et al., 2019). Appropriate regulation of extracellular dopamine is important for rotarod performance, as administration of the dopamine reuptake blocker nomifensine increases performance, while the dopamine agonist apomorphine diminishes performance (Shiotsuki et al., 2010). Nomifensine increases extracellular dopamine (Cragg & Rice, 2004), while apomorphine's action at presynaptic D2 autoreceptors suppresses dopamine release (Schmitz et al., 2002). The opposing impacts of these drugs on rotarod performance highlight the importance of proper dopamine signaling in motor learning.

**Striatal changes drive altered rotarod performance**

The majority of studies assessing accelerating rotarod performance have used mouse models with global mutations in ASD risk genes; therefore, the brain region or

circuit responsible for the phenotype is difficult to ascertain. As discussed above, striatal circuits have been identified as a key node in rotarod motor learning. To directly test the contribution of striatal neurons to rotarod phenotypes, conditional KO mice have been generated in which the ASD risk gene is manipulated selectively in striatal neurons. These studies have revealed a direct link between striatal function and rotarod performance.

In the case of *Nlgn3,* conditional deletion in cells of the direct, but not the indirect, pathway of the striatum results in increased rotarod performance (Rothwell et al., 2014). A deficit in inhibition specifically onto dSPNs in these mice, which is expected to enhance excitability of the direct pathway, likely contributes to their increased rotarod performance. Indeed, in WT mice, a manipulation that reduces the activity of indirect pathway cells, which would have the net effect of facilitating direct pathway activation of downstream basal ganglia nuclei, results in increased performance in the task. In addition, rotarod performance is restored to WT levels in *Nlgn3* dSPN conditional KO mice via expression of the potassium channel Kir2.1, which decreases dSPN excitability (Rothwell et al., 2014). This study provides compelling evidence that altered balance between the striatal direct and indirect pathways can contribute to altered motor learning in ASD mouse models. Interestingly, conditional deletion of *Nlgn3* in the NAc, and not broadly in the dorsal striatum, is sufficient to recapitulate the enhanced rotarod performance (Rothwell et al., 2014). This finding supports a potentially underappreciated role for the ventral striatum in motor learning. A possible explanation for the cell type and anatomical specificity of *Nlgn3* deletion is that *Nlgn3* is preferentially expressed in dSPNs of the NAc and therefore expected to have a greater effect when disrupted in these cells (Rothwell et al., 2014).

As discussed above, multiple studies of *Chd8* mouse models have identified enhanced rotarod performance (Hulbert et al., 2020; Platt et al., 2017). One such study performed gene expression analysis across brain regions in *Chd8*$^{+/-}$ mice, identifying the NAc as a region with significant gene dysregulation. Following this, Platt et al. injected *Chd8*-targeting sgRNA into the NAc in a Cas9 knock-in mouse to determine the impact of *Chd8* reduction specifically in this region. Similar to the findings in the *Nlgn3* study (Rothwell et al., 2014), reduction of *Chd8* specifically in the NAc, and not the dorsal striatum, recapitulated the increased rotarod performance seen in constitutive heterozygous mice (Platt et al., 2017; Rothwell et al., 2014). Electrophysiological assessment of these mice found that SPNs of the NAc core have increased frequency and amplitude of spontaneous excitatory synaptic currents, as well as decreased amplitude of miniature inhibitory synaptic currents, suggesting overall increased excitatory drive of SPNs in the region (Platt et al., 2017). A distinction between dSPNs and iSPNs was not made in this study.

While the above studies implicate altered NAc function as a driver of enhanced rotarod performance, a recent study identified increased motor learning in a mouse model with dorsal striatum-selective *Tsc1* loss (Benthall et al., 2021). In this study, dSPN-specific deletion of the ASD-risk gene *Tsc1* resulted in increased performance on

the accelerating rotarod, in particular at higher speeds (10-80 RPM). Mice with loss of *Tsc1* in iSPNs did not exhibit changes in rotarod performance, consistent with the findings in *Nlgn3* mice (Benthall et al., 2021; Rothwell et al., 2014). The D1-Cre line utilized in this study to target dSPNs is relatively restricted to dSPNs of the dorsal striatum, sparing the majority of NAc cells (Benthall et al., 2021). This, together with the results described above, indicate that altered direct pathway activity in either the dorsal or ventral striatum is sufficient to alter motor learning.

In *Tsc1* dSPN KO mice, electrophysiology experiments revealed that *Tsc1*-KO dSPNs have increased glutamate release probability at cortical inputs, resulting in enhanced corticostriatal drive. This study also found a deficit in eCB-LTD onto *Tsc1* KO dSPNs, which may explain the change in presynaptic release probability (Benthall et al., 2021). This prominent form of striatal synaptic depression works through the release of postsynaptic endocannabinoids that act on cortical presynaptic CB1 receptors, ultimately reducing the probability of neurotransmitter release (Kreitzer & Malenka, 2008; Lovinger, 2010). Loss of eCB-LTD onto *Tsc1* KO dSPNs likely renders these cells unable to depress excitatory inputs, leading to increased corticostriatal drive over time. Interestingly, a similar deficit in eCB-LTD was identified in the dorsal striatum of a *Nlgn3* mutant mouse model that exhibit enhanced performance in the rotarod task (Martella et al., 2018).

Here we have highlighted several examples of mouse models that exhibit enhanced rotarod performance. In a few of these models, striatal-specific manipulation of an ASD-risk gene was sufficient to induce changes in rotarod motor learning. In several studies, synaptic changes were reported that are expected to enhance striatal activation, particularly increase corticostriatal drive and/or excitability of the direct pathway. (Benthall et al., 2021; Platt et al., 2017; Rothwell et al., 2014). Given the importance of striatal circuits for not only motor skill leaning but also habit learning etc., it seems plausible that gain-of-function at the neural circuit level facilitates the formation of fixed motor routines or perseverative behaviors. These circuit changes that imbue mice with an increased ability to learn and execute the rotarod motor sequence may similarly underlie RRBs, as persistent, repetitive behaviors are likely to also be carried out through primed corticostriatal activation. For ASD models where motor deficits predominate, the neural circuitry underlying the presence of repetitive behaviors remains to be established. In these cases, basic motor circuits may be disrupted such that rotarod deficits arise, but gain-of-function in other motor control circuitry likely drives the emergence of RRBs, for example in the case of *Shank3* models (Drapeau et al., 2018). Further investigation into the motor phenotypes of ASD mouse models and the synaptic and circuit basis of repetitive behaviors will provide additional insight into this core aspect of ASD.

**Other considerations**

*Genetic background influences rotarod performance*

There are several factors beyond a targeted genetic manipulation that contribute to differences in rotarod performance, which should be considered when comparing across ASD mouse models. A study assessing 16 mouse strains from the “Collaborative Cross” (CC), a large panel of inbred mice that captures 90% of the known variation among laboratory mice, found that rotarod performance varies widely across the strains (Mao et al., 2015). 45 gene loci associated with rotarod performance were identified using genetic linkage analysis, many of which overlap with human GWAS-nominated genes associated with neuropsychiatric disorders including ASD and ADHD. A similar study assessing a range of behaviors across 10 inbred mouse strains also found wide variability in rotarod performance across strains (Moy et al., 2007). Two of these inbred mouse strains, BTBR $T^{+}$tf/J (BTBR) and BALB/cByJ (BALB), have been utilized for over a decade as models of ASD, owing to their strong and consistent displays of autism-relevant behaviors, including social behavior deficits and/or repetitive behaviors or stereotypies (Ellegood & Crawley, 2015). While BTBR mice exhibit deficits in the rotarod task, BALB mice perform similarly to C57BL/6J controls (Moy et al., 2007). Since these models are inbred strains that lack known genetic abnormalities and do not recapitulate known genetic causes of human ASD, it can be difficult to link neurodevelopmental changes to ASD-like behavior. However, continued study of these inbred models that demonstrate good face validity for ASD-like manifestations may uncover their potential construct and predictive validity.

Along with genetic background, body weight also significantly impacts rotarod performance, with weight being strongly negatively correlated with performance (Mao et al., 2015). Variability in these factors across studies, may contribute to some of the heterogeneity in rotarod outcomes reported in the literature (see Table 1).

*Environmental risk factors*

Here we have focused on rotarod performance in genetic mouse models of ASD; however, there is a growing body of work implicating exposure to certain environmental factors in the manifestation of autism, including factors that illicit an immune response (Meltzer & Van de Water, 2017). In mice, this is often modeled with a maternal immune activation paradigm. Briefly, pregnant dams are directly infected with a pathogen (e.g. influenza virus, *Escherichia coli*), or injected with a substance that mimics a pathogen to evoke a large immune response. Subsequently, significant immunological, behavioral and neurodevelopmental changes can then be observed in offspring (Careaga et al., 2017). As brain development continues after birth, models of postnatal infections and postnatal immune activation have also been shown to lead to some of these changes (Depino, 2013). While some immune activation mouse models exhibit enhanced performance on the accelerating rotarod (Carlezon et al., 2019), other models have no change in performance (Wei et al., 2012), or deficits in the task (Naviaux et al., 2014).

*In utero* exposure to certain medications has also been linked to the development of ASD, including the antiepileptic and bipolar medication valproic acid (VPA) (Roullet et al., 2013). The mechanism of VPA that may increase the risk of ASD is unknown, and

prenatal exposure to the drug, like other implicated environmental factors, could modify existing genetic risk (Wang et al., 2017). Mouse models of VPA exposure are typically achieved through injection of VPA into a pregnant dam roughly midway through gestation, resulting in offspring that exhibit both neurodevelopmental and behavioral alterations (Roullet et al., 2013). Rotarod phenotypes across studies of VPA models vary, with some identifying enhanced rotarod performance (Hernandez et al., 2023), and others identifying no difference from WT (Gandal et al., 2010), or a deficit in the task (Wang et al., 2018), owing potentially to variability in VPA exposure protocols.

*Genetic rat models of ASD*

Finally, while this review focuses on mouse models, there is a growing body of literature on genetic rat models of ASD (Berg et al., 2021; Dey & Chattarji, 2022; Harris et al., 2021), including models with mutations in ASD risk genes linked to enhanced rotarod performance discussed above, such as *Fmr1* (D'Elia et al., 2022; Schiavi et al., 2023; Till et al., 2015) and *Nlgn3* (Anstey et al., 2022; Thomas et al., 2017). However, as genetic accessibility of rat models is a recent development, assessment of rotarod performance in these models remains to be performed. Given the more expansive behavioral repertoire of rats, and the technical benefits that their larger size affords, increased study of genetic rat models of ASD is likely to benefit the understanding of rotarod behavior and motor skill learning in the context of ASD risk gene mutations in the coming years (Ellenbroek & Youn, 2016).

*Interactions between the basal ganglia and other motor control circuits*

This review highlights the ways that striatal, and in particular corticostriatal, circuits play a role in accelerating rotarod performance. However, cerebellar circuits are also implicated in motor skill learning. Different cerebellar subcircuits are implicated in early versus late stages of motor skill learning, and a number of studies suggest that cerebellar relays exist within or parallel to the cortico-basal ganglia-thalamic loop controlling motor learning (Dayan & Cohen, 2011). In the rotarod specifically, a subpopulation of excitatory cerebellospinal neurons in deep cerebellar nuclei that project to the spinal cord were identified as being necessary for learning, but not the execution, of rotarod behavior (Sathyamurthy et al., 2020). The specific inputs to these neurons are yet unclear, but they may receive direct input from the cortex and/or thalamus. In the context of ASD, the cerebellum is frequently implicated as a region of potential convergent change. Postmortem studies in humans reveal cellular and structural cerebellar abnormalities in individuals with ASD (Bolduc et al., 2012; Ecker et al., 2012; Schumann & Nordahl, 2011). In addition, mouse models that target mutation of ASD risk genes specifically to cerebellar cell types can recapitulate ASD-like phenotypes (Hampson & Blatt, 2015; Tsai et al., 2012). However, we note that in the case of cerebellar-specific ASD risk gene mutations, mouse models most often exhibit deficits in accelerating rotarod performance (Kawamura et al., 2021; Liu et al., 2022; Reith et al., 2013; Tsai et al., 2012), even in cases where constitutive mutation of the

gene leads to enhanced performance (Platt et al., 2017; Reith et al., 2013). Thus, while cerebellar circuits may participate in rotarod performance, it seems unlikely that they would contribute to the enhanced rotarod phenotype seen in the mouse models described above. Rather, we posit that synaptic gain-of-function in corticostriatal circuits is more likely to drive increased motor learning in the context of ASD mouse models.

**Conclusions**

As the number and heterogeneity of identified ASD risk genes continues to expand, the utilization of common behavioral assays to identify convergent phenotypes in mouse models of ASD is of great benefit. When it comes to assessing motor symptom domains of ASD in mouse models, the accelerating rotarod task has proved very useful for identifying phenotypes. The task is relatively fast and straightforward to carry out, reveals information about gross motor coordination and motor learning, and has established underlying neural circuitry. Corticostriatal circuits are key regulators of rotarod performance and are increasingly implicated as a point of convergent alteration across a range of mouse models of ASD (Li & Pozzo-Miller, 2020). If these circuits are found to consistently contribute to altered behavior, they represent a potential site for targeted therapeutics, which may be applicable across ASDs of different genetic origin.

**Tables**

**Table 1. Summary of rotarod performance in mouse models with mutations in ASD risk genes.**

| Human gene/CNV | Mouse model | Rotarod phenotype (reference) |
|---|---|---|
| 15q11-13 | patDp/+ (6.3 Mb duplication on chromosome 7) | similar coordination, enhanced learning (Nakatani et al., 2009) |
| 16p11.2 | $Del^{m}$ (Mills model) | similar coordination, enhanced learning (Lynch et al., 2020; Ouellette et al., 2020) similar coordination, deficit in learning (Yin et al., 2021) |
| | Dup/+ (*Sult1a1-Spn* interval) | similar coordination, deficit in learning (Arbogast et al., 2016) |
| 17p11.2 | *Dp(11)17/+* | similar coordination, deficit in learning (Ricard et al., 2010) |
| | *Df(11)17/+* | deficit in coordination, similar learning (Ricard et al., 2010) |
| *ARHGAP32* (*PX-RICS*) | *PX-RICS*$^{-/-}$ | deficit in coordination, deficit in learning (Nakamura et al., 2016) |
| *ARID1B* | *Arid1b* hKO | deficit in coordination, deficit in learning (Shibutani et al., 2017) |
| | *Arid1b*$^{+/-}$ | similar coordination, deficit in learning (Jung et al., 2017) |
| *ARX* | *Arx*$^{(GCG)10+7}$ | enhanced overall performance (Price et al., 2009) |
| | *Arx*$^{dup24/0}$ | increased average latency to fall across 3 trials (Dubos et al., 2018) |
| *ATP1A3* | *Atp1a3*$^{+/-}$ | enhanced overall performance (Ikeda et al., 2013) |
| *CACNA1G* | *Cacna1g*-Arg1723His-KI$^{+/-}$ *Cacna1g*-Arg1723His-KI$^{-/-}$ | deficit in coordination, deficit in learning (Hashiguchi et al., 2019) |
| *CADM1* | *Cadm1*-KO | deficit in coordination, deficit in learning (Takayanagi et al., 2010) |
| *CDKL5* | *Cdkl5*$^{-/y}$ | similar coordination, deficit in learning (Adhikari et al., 2022; Gao et al., 2020; Wang et al., 2012) deficit in coordination, deficit in learning (Jhang et al., 2017) |
| | *Cdkl5*$^{+/-}$, *Cdkl5*$^{-/-}$ | similar coordination, deficit in learning (Fuchs et al., 2018) |
| *CHD8* | *Chd8*$^{+/E31T}$ | enhanced overall performance (Hulbert et al., 2020) |
| | *Chd8*$^{+/-}$ | similar coordination, enhanced |

| | | |
|---|---|---|
| | | learning (Platt et al., 2017) |
| *CNTNAP2* | *Cntnap2*$^{-/-}$ | increased performance on a single trial (Penagarikano et al., 2011)<br>increased latency to fall from constant speed rotarod (Dawes et al., 2018) |
| *CTNNB1* | *Bfc/+* | deficit in coordination, deficit in learning (Tucci et al., 2014) |
| *CYFIP1* | *Cyfip1*$^{+/tm2a(EUCOMM)Wtsi}$ | similar coordination, deficit in learning (Bachmann et al., 2019) |
| | *Cyfip*$^{+/-}$ | deficit in coordination, similar learning (Dominguez-Iturza et al., 2019) |
| *DDX3X* | *Ddx3x*$^{+/-}$ | similar coordination, deficit in learning (Boitnott et al., 2021) |
| *DLG4* | *Dlg4*$^{-/-}$ | deficit in coordination, deficit in learning (Feyder et al., 2010) |
| *DSCAM* | *Dscam*$^{del17/del17}$ | deficit in coordination, deficit in learning (Xu et al., 2011) |
| *DYRK1A* | mBACtgDyrk1a (186n3) | similar coordination, deficit in learning (Souchet et al., 2014) |
| *EN2* | *En2*$^{-/-}$ | similar coordination, deficit in learning (Brielmaier et al., 2012)<br>deficit in coordination, deficit in learning (Cheh et al., 2006) |
| *FOXP2* | *Foxp2*$^{R552H/+}$ | similar coordination, deficit in learning (Groszer et al., 2008)<br>deficit in coordination, deficit in learning (French et al., 2012) |
| | *Foxp2*$^{wt/ko}$ | similar coordination, deficit in learning (Enard et al., 2009) |
| *FMR1* | *Fmr1*$^{-/-}$ | similar coordination, enhanced learning (Nolan et al., 2017)<br>enhanced overall performance (Roy et al., 2011)<br>similar coordination, deficit in learning (Bhattacharya et al., 2012; Li et al., 2023; Uutela et al., 2012) |
| | *Fmr1* CGG KI | similar coordination, deficit in learning (Van Dam et al., 2005) |
| *GABRB3* | *Gabrb3*$^{-/-}$ | similar coordination, deficit in learning (DeLorey et al., 1998) |
| | p+/m- | similar coordination, deficit in learning (DeLorey et al., 2011) |
| | p-/m+ | similar coordination, deficit in |

| | | |
|---|---|---|
| | | learning (DeLorey et al., 2011) |
| *IL1RAPL1* | *Il1rapl1*$^{-/Y}$ | enhanced overall performance (Yasumura et al., 2014) |
| *KDM5C* | *Kdm5c*$^{-/y}$ | decreased performance on a single trial (Scandaglia et al., 2017) |
| *KIRREL3* | *Kirrel3*$^{-/-}$ | similar coordination, enhanced learning (Hisaoka et al., 2018) |
| *LRRC4* | *Lrrc4*$^{-/-}$ | similar coordination, deficit in learning (Um et al., 2018) |
| *MECP2* | *Mecp2-308* | similar coordination, deficit in learning (De Filippis et al., 2010) |
| | *Mecp2*$^{tm1Tam}$ | deficit in coordination, deficit in learning (Pelka et al., 2006) |
| | *Mecp2*$^{tm1.1Jae}$ | deficit in coordination, deficit in learning (Morello et al., 2018) |
| | *Tau-Mecp2* (overexpression) | similar coordination, deficit in learning (Na et al., 2012) |
| | *Mecp2*$^{tm1.Bird}$ | similar coordination, deficit in learning (Pratte et al., 2011)<br>deficit in coordination, deficit in learning (Kao et al., 2015; Vogel Ciernia et al., 2017)<br>decreased performance on a single trial (Santos et al., 2007) |
| | *Mecp2*$^{T158A}$ | deficit in coordination, deficit in learning (Goffin et al., 2011) |
| | *Mecp2*$^{R168X}$ | decreased average latency to fall across 3 trials (Schaevitz et al., 2013) |
| | *Mecp2*$^{R294X}$ | deficit in coordination, deficit in learning (Collins et al., 2022) |
| | *Mecp2*$^{R306C}$ | decreased average latency to fall across 3 trials (Lyst et al., 2013)<br>decreased average latency to fall across 2-4 trials (Ebert et al., 2013) |
| | *Mecp2*$^{\Delta AT\text{-}hook1}$ | decreased average latency to fall across 3 trials (Xu et al., 2018) |
| | *Mecp2*$^{TG}$ (overexpression) | similar coordination, enhanced learning (Ash, Buffington, et al., 2021; Ash, Park, et al., 2021; Collins et al., 2004; Collins et al., 2022; Sztainberg et al., 2015) |

| | | |
|---|---|---|
| *MYT1L* | *Myt1l*$^{+/-}$ | similar coordination, deficit in learning (Wohr et al., 2022) |
| *NRXN1* | *Nrxn1α* KO | similar coordination, enhanced learning (Etherton et al., 2009) |
| | *Nrxn1α*$^{+/\Delta Exon1}$, *Nrxn1α*$^{\Delta Exon1/\Delta Exon1}$ | similar coordination, enhanced learning (Xu et al., 2023) |
| | *Nrxn1α*$^{+/\Delta Exon9}$, *Nrxn1α*$^{\Delta Exon9/\Delta Exon9}$ | similar coordination, enhanced learning (Xu et al., 2023) |
| *NLGN2* | *Nlgn2*$^{-/-}$ | deficit in coordination, similar learning (Blundell et al., 2009) |
| | *Nlgn2*$^{+/-}$ | similar coordination, enhanced learning (Wohr et al., 2013) |
| *NLGN3* | *Nlgn3*$^{-/-}$ | similar coordination, enhanced learning (Rothwell et al., 2014) |
| | *Nlgn3* R451C KI | similar coordination, enhanced learning (Cao et al., 2022; Chadman et al., 2008; Rothwell et al., 2014) |
| | *Nlgn3*$^{mf}$ | similar coordination, enhanced learning (Yoshida et al., 2021) |
| *NF1* | *Nf1*$^{+/-}$ | similar coordination, deficit in learning (van der Vaart et al., 2011) |
| | *Nf1*$^{23a-/-}$ | similar coordination, deficit in learning (Costa et al., 2001) |
| *NRP2* | *Nrp2*$^{-/-}$ | similar coordination, deficit in learning (Shiflett et al., 2015) |
| *NTNG1* | *Ntng2*$^{-/-}$ | enhanced overall performance (Zhang et al., 2016) |
| *OTUD7A* | *Otud7a*$^{-/-}$ | similar coordination, deficit in learning (Yin et al., 2018) |
| *PAX5* | *Pax*$^{5R31Q/-}$ | deficit in coordination, deficit in learning (Kaiser et al., 2022) |
| *PTCHD1* | *Ptchd1*$^{-/y}$ | decreased average latency to fall across 3 trials (Ung et al., 2018) |
| *PTEN* | *Pten*$^{m3m4/m3m4}$ | deficit in coordination, deficit in learning (Tilot et al., 2014) |
| *RAB39B* | *Rab39b*$^{-/-}$ | decreased average latency to fall across 3 trials (Wang et al., 2023) similar coordination, deficit in learning (Niu et al., 2020; Zhang et al., 2020) |
| *RELN* | *Reln* ΔC-KI | enhanced overall performance (Sakai et al., 2016) |
| | *Reln*$^{+/rl\text{-}Orl}$ | similar coordination, deficit in |

| | | |
|---|---|---|
| | | learning (Sobue et al., 2018)<br>deficit in coordination, deficit in learning (Lalonde et al., 2004) |
| *SCN1A* | *Scn1a*$^{+/-}$ | similar coordination, deficit in learning (Beretta et al., 2022) |
| | *Scn1a*$^{+/R1407X}$ | enhanced coordination, similar learning (Ito et al., 2013) |
| | *Scn1a*$^{+/A1783V}$ | similar coordination, enhanced learning (Miljanovic et al., 2021)<br>decreased average latency to fall across 3 trials (Fadila et al., 2020; Ricobaraza et al., 2019) |
| *SCN2A* | *Scn2a*$^{+/-}$ | similar coordination, enhanced learning (Lena & Mantegazza, 2019)<br>deficit in coordination, deficit in learning (Tatsukawa et al., 2019) |
| | *Scn2a*$^{+/K1422E}$ | similar coordination, enhanced learning (Echevarria-Cooper et al., 2022) |
| *SHANK1* | *Shank1*$^{-/-}$ | similar coordination, deficit in learning (Hung et al., 2008; Silverman et al., 2011) |
| *SHANK3* | *Shank3*$^{+/E13}$ | similar coordination, enhanced learning (Jaramillo et al., 2017) |
| | *Shank3*$^{+/\Delta 4\text{-}22}$ | similar coordination, deficit in learning (Drapeau et al., 2018) |
| | *Shank3*$^{e4\text{-}9/e4\text{-}9}$ | deficit in coordination, deficit in learning (Wang et al., 2011) |
| | *Shank3*$^{E13/E13}$ | similar coordination, deficit in learning (Jaramillo et al., 2017) |
| | *Shank3* $^{\Delta 13\text{-}16/\Delta 13\text{-}16}$ | similar coordination, deficit in learning (Peixoto et al., 2019) |
| | *Shank3*$^{fx/fx}$ | deficit in coordination, deficit in learning (Mei et al., 2016) |
| | *Shank3*$^{InsG3680/}$ InsG3680 | deficit in coordination, deficit in learning (Speed et al., 2015; Zhou et al., 2016) |
| | *Shank3*$^{\Delta 11/\Delta 11}$ | similar coordination, deficit in learning (Vicidomini et al., 2017) |
| | *Shank3*$^{\Delta C/\Delta C}$ | deficit in coordination, deficit in learning (Kouser et al., 2013) |
| | *Shank3*$^{-/-}$ | deficit in coordination, deficit in learning (Drapeau et al., 2018; Yang et al., 2012) |

| | | |
|---|---|---|
| *SLC6A3* | DAT$^{T356M/T356M}$ | similar coordination, enhanced learning (DiCarlo et al., 2019) |
| *SYNGAP1* | *Syngap1*$^{+/-}$ | deficit in coordination, deficit in learning (Nakajima et al., 2019) deficit in coordination, similar learning (Muhia et al., 2010) |
| *TOP3B* | *Top3β*$^{-/-}$ | deficit in coordination, deficit in learning (Rahman et al., 2021) |
| *TSC2* | *Tsc2*$^{+/-}$ | similar coordination, enhanced learning (Benthall et al., 2021) |
| | *Tsc2*$^{\Delta RG}$ | similar coordination, deficit in learning (Chevere-Torres et al., 2012) |
| *UBE3A* | *Ube3a*$^{m-/p+}$ | deficit in coordination, deficit in learning (Born et al., 2017; Heck et al., 2008; Huang et al., 2013; Jiang et al., 1998; Leach & Crawley, 2018; Miura et al., 2002; Mulherkar & Jana, 2010; Sonzogni et al., 2018) |
| | *Ube3a*$^{m-/p-}$ | deficit in coordination, deficit in learning (Heck et al., 2008) |
| | *Ube3a*$^{Genedel}$ | deficit in coordination, deficit in learning (Syding et al., 2022) |
| | *Ube3a*$^{OE}$ (overexpression) | enhanced overall performance (Punt et al., 2022) |
| | *Ube3a*$^{matT503A}$ (gain of function) | similar coordination, enhanced learning (Xing et al., 2023) |
| *WDFY3* | *Wdfy3*$^{+/lacZ}$ | deficit in coordination, deficit in learning (Le Duc et al., 2019) |

***Table 1 footnote**: ASD risk genes/CNVs depicted and references for a given model are representative and not exhaustive. Mouse models were chosen using the Simons Foundation Autism Research Initiative (SFARI) Gene mouse models module. Mouse models of ASD risk genes designated as Category 1 (high confidence gene) or Category 2 (strong candidate gene) by SFARI's gene scoring system were considered. More information about SFARI gene and their gene scoring system can be found at gene.sfari.org. Mouse studies that failed to detect a phenotype are not presented, nor are models that utilized cell-type specific perturbation.*

## Figures

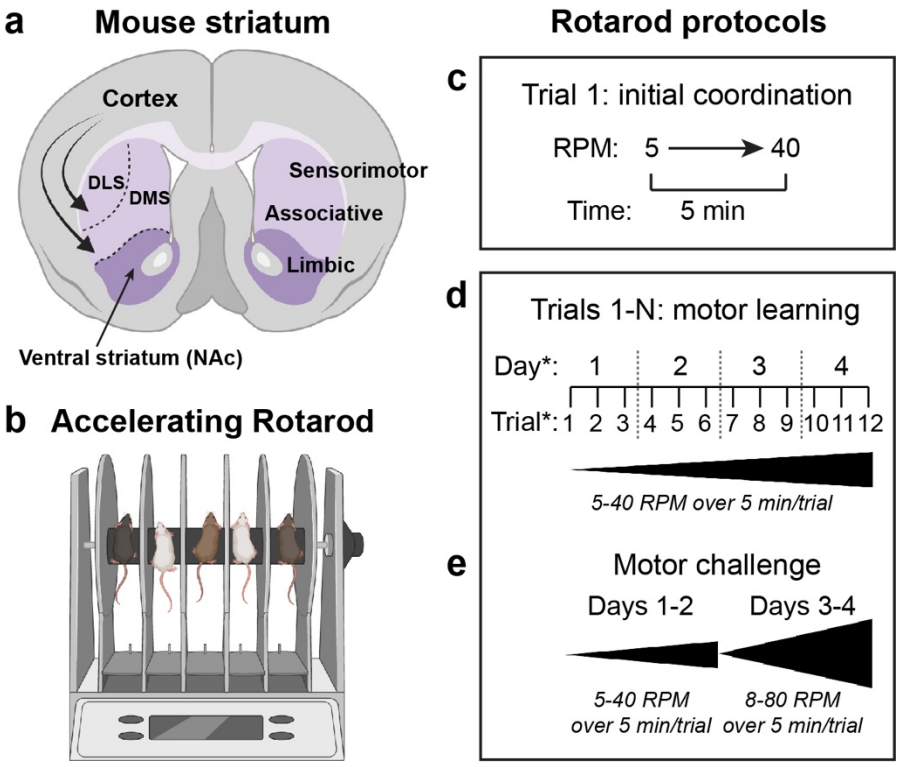


**Figure 1. Striatal circuits drive motor learning in the accelerating rotarod task.** (A) Schematic of a coronal mouse brain section showing the major subdivisions of the striatum (purple). DLS=dorsolateral striatum, DMS=dorsomedial striatum, NAc=nucleus accumbens. Curved arrows depict glutamatergic inputs from the cortex to all striatal subregions. (B) Schematic of the rotarod apparatus used to measure motor coordination and motor learning in rodents. (C-E) Various rotarod protocols have been used. In the simplest version of the task (C), the rod accelerates from 5-40 revolutions per minute (RPM) over the course of five minutes. The time to fall off or rotate off the rod is a measure of motor coordination. (D) To measure motor learning, multiple trials are used and the gain in performance from the first to last trial is assessed for each mouse. The number of trials per day and number of testing days can vary. A common version of the task uses three trials per day across four testing days. (E) In some cases, a more challenging version of the task can reveal phenotypes. In this protocol, the rod is accelerated from 8-10 RPM up to 80 RPM over 5 minutes. Schematics in panels A and B were created with bioRender.com.

**References**


Adhikari, A., Buchanan, F. K. B., Fenton, T. A., Cameron, D. L., Halmai, J., Copping, N. A., Fink, K. D., & Silverman, J. L. (2022). Touchscreen cognitive deficits, hyperexcitability and hyperactivity in males and females using two models of Cdkl5 deficiency. *Hum Mol Genet*, *31*(18), 3032-3050. https://doi.org/10.1093/hmg/ddac091

Ahmed, N. Y., Knowles, R., Liu, L., Yan, Y., Li, X., Schumann, U., Wang, Y., Sontani, Y., Reynolds, N., Natoli, R., Wen, J., Del Pino, I., Mi, D., & Dehorter, N. (2023). Developmental deficits of MGE-derived interneurons in the Cntnap2 knockout mouse model of autism spectrum disorder. *Front Cell Dev Biol*, *11*, 1112062. https://doi.org/10.3389/fcell.2023.1112062

Anstey, N. J., Kapgal, V., Tiwari, S., Watson, T. C., Toft, A. K. H., Dando, O. R., Inkpen, F. H., Baxter, P. S., Kozic, Z., Jackson, A. D., He, X., Nawaz, M. S., Kayenaat, A., Bhattacharya, A., Wyllie, D. J. A., Chattarji, S., Wood, E. R., Hardt, O., & Kind, P. C. (2022). Imbalance of flight-freeze responses and their cellular correlates in the Nlgn3(-/y) rat model of autism. *Mol Autism*, *13*(1), 34. https://doi.org/10.1186/s13229-022-00511-8

APA. (2022). *Diagnostic and Statistical Manual of Mental Disorders* (5th ed., text rev. ed.). https://doi.org/https://doi.org/10.1176/appi.books.9780890425787

Arbogast, T., Ouagazzal, A. M., Chevalier, C., Kopanitsa, M., Afinowi, N., Migliavacca, E., Cowling, B. S., Birling, M. C., Champy, M. F., Reymond, A., & Herault, Y. (2016). Reciprocal Effects on Neurocognitive and Metabolic Phenotypes in Mouse Models of 16p11.2 Deletion and Duplication Syndromes. *PLoS Genet*, *12*(2), e1005709. https://doi.org/10.1371/journal.pgen.1005709

Ash, R. T., Buffington, S. A., Park, J., Suter, B., Costa-Mattioli, M., Zoghbi, H. Y., & Smirnakis, S. M. (2021). Inhibition of Elevated Ras-MAPK Signaling Normalizes Enhanced Motor Learning and Excessive Clustered Dendritic Spine Stabilization in the MECP2-Duplication Syndrome Mouse Model of Autism. *eNeuro*, *8*(4). https://doi.org/10.1523/ENEURO.0056-21.2021

Ash, R. T., Park, J., Suter, B., Zoghbi, H. Y., & Smirnakis, S. M. (2021). Excessive Formation and Stabilization of Dendritic Spine Clusters in the MECP2-Duplication Syndrome Mouse Model of Autism. *eNeuro*, *8*(1). https://doi.org/10.1523/ENEURO.0282-20.2020

Asperger, H. (1991). 'Autistic psychopathy' in childhood (U. Frith, Trans.). In *Autism and Asperger syndrome* (pp. 37-70). Cambridge University Press.

Bachmann, S. O., Sledziowska, M., Cross, E., Kalbassi, S., Waldron, S., Chen, F., Ranson, A., & Baudouin, S. J. (2019). Behavioral training rescues motor deficits in Cyfip1 haploinsufficiency mouse model of autism spectrum disorders. *Transl Psychiatry*, *9*(1), 29. https://doi.org/10.1038/s41398-018-0338-9

Barnes, T. D., Kubota, Y., Hu, D., Jin, D. Z., & Graybiel, A. M. (2005). Activity of striatal neurons reflects dynamic encoding and recoding of procedural memories. *Nature*, *437*(7062), 1158-1161. https://doi.org/10.1038/nature04053

Battah, H. W., Lotan, M., & Moran, D. S. (2023). The Need for a Motor Assessment Tool for Children with Autism-An Opinion Article. *Diagnostics (Basel)*, *13*(12). https://doi.org/10.3390/diagnostics13122095

Beeler, J. A., Cao, Z. F., Kheirbek, M. A., Ding, Y., Koranda, J., Murakami, M., Kang, U. J., & Zhuang, X. (2010). Dopamine-dependent motor learning: insight into levodopa's long-duration response. *Ann Neurol*, *67*(5), 639-647. https://doi.org/10.1002/ana.21947

Belin, D., Deroche-Gamonet, V., & Jaber, M. (2007). Cocaine-induced sensitization is associated with altered dynamics of transcriptional responses of the dopamine transporter, tyrosine hydroxylase, and dopamine D2 receptors in C57Bl/6J mice. *Psychopharmacology (Berl)*, *193*(4), 567-578. https://doi.org/10.1007/s00213-007-0790-3

Benthall, K. N., Cording, K. R., Agopyan-Miu, A., Wong, C. D., Chen, E. Y., & Bateup, H. S. (2021). Loss of Tsc1 from striatal direct pathway neurons impairs endocannabinoid-LTD and enhances motor routine learning. *Cell Rep*, *36*(6), 109511. https://doi.org/10.1016/j.celrep.2021.109511

Beretta, S., Gritti, L., Ponzoni, L., Scalmani, P., Mantegazza, M., Sala, M., Verpelli, C., & Sala, C. (2022). Rescuing epileptic and behavioral alterations in a Dravet syndrome mouse model by inhibiting eukaryotic elongation factor 2 kinase (eEF2K). *Mol Autism*, *13*(1), 1. https://doi.org/10.1186/s13229-021-00484-0

Berg, E. L., Jami, S. A., Petkova, S. P., Berz, A., Fenton, T. A., Lerch, J. P., Segal, D. J., Gray, J. A., Ellegood, J., Wohr, M., & Silverman, J. L. (2021). Excessive Laughter-like Vocalizations, Microcephaly, and Translational Outcomes in the Ube3a Deletion Rat Model of Angelman Syndrome. *J Neurosci*, *41*(42), 8801-8814. https://doi.org/10.1523/JNEUROSCI.0925-21.2021

Betancur, C., Sakurai, T., & Buxbaum, J. D. (2009). The emerging role of synaptic cell-adhesion pathways in the pathogenesis of autism spectrum disorders. *Trends Neurosci*, *32*(7), 402-412. https://doi.org/10.1016/j.tins.2009.04.003

Bey, A. L., & Jiang, Y. H. (2014). Overview of Mouse Models of Autism Spectrum Disorders. *Current Protocols in Pharmacology*, *66*(1). https://doi.org/10.1002/0471141755.ph0566s66

Bhattacharya, A., Kaphzan, H., Alvarez-Dieppa, A. C., Murphy, J. P., Pierre, P., & Klann, E. (2012). Genetic removal of p70 S6 kinase 1 corrects molecular, synaptic, and behavioral phenotypes in fragile X syndrome mice. *Neuron*, *76*(2), 325-337. https://doi.org/10.1016/j.neuron.2012.07.022

Blundell, J., Tabuchi, K., Bolliger, M. F., Blaiss, C. A., Brose, N., Liu, X., Sudhof, T. C., & Powell, C. M. (2009). Increased anxiety-like behavior in mice lacking the inhibitory synapse cell adhesion molecule neuroligin 2. *Genes Brain Behav*, *8*(1), 114-126. https://doi.org/10.1111/j.1601-183X.2008.00455.x

Boitnott, A., Garcia-Forn, M., Ung, D. C., Niblo, K., Mendonca, D., Park, Y., Flores, M., Maxwell, S., Ellegood, J., Qiu, L. R., Grice, D. E., Lerch, J. P., Rasin, M. R., Buxbaum, J. D., Drapeau, E., & De Rubeis, S. (2021). Developmental and Behavioral Phenotypes in a Mouse Model of DDX3X Syndrome. *Biol Psychiatry*, *90*(11), 742-755. https://doi.org/10.1016/j.biopsych.2021.05.027

Bolduc, M. E., du Plessis, A. J., Sullivan, N., Guizard, N., Zhang, X., Robertson, R. L., & Limperopoulos, C. (2012). Regional cerebellar volumes predict functional outcome in children with cerebellar malformations. *Cerebellum*, *11*(2), 531-542. https://doi.org/10.1007/s12311-011-0312-z

Born, H. A., Dao, A. T., Levine, A. T., Lee, W. L., Mehta, N. M., Mehra, S., Weeber, E. J., & Anderson, A. E. (2017). Strain-dependence of the Angelman Syndrome phenotypes in Ube3a maternal deficiency mice. *Sci Rep*, *7*(1), 8451. https://doi.org/10.1038/s41598-017-08825-x

Brielmaier, J., Matteson, P. G., Silverman, J. L., Senerth, J. M., Kelly, S., Genestine, M., Millonig, J. H., DiCicco-Bloom, E., & Crawley, J. N. (2012). Autism-relevant social abnormalities and cognitive deficits in engrailed-2 knockout mice. *PLoS One*, *7*(7), e40914. https://doi.org/10.1371/journal.pone.0040914

Brunner, D., Kabitzke, P., He, D., Cox, K., Thiede, L., Hanania, T., Sabath, E., Alexandrov, V., Saxe, M., Peles, E., Mills, A., Spooren, W., Ghosh, A., Feliciano, P., Benedetti, M., Luo Clayton, A., & Biemans, B. (2015). Comprehensive Analysis of the 16p11.2 Deletion and Null Cntnap2 Mouse Models of Autism Spectrum Disorder. *PLoS One*, *10*(8), e0134572. https://doi.org/10.1371/journal.pone.0134572

Buitrago, M. M., Schulz, J. B., Dichgans, J., & Luft, A. R. (2004). Short and long-term motor skill learning in an accelerated rotarod training paradigm. *Neurobiol Learn Mem*, *81*(3), 211-216. https://doi.org/10.1016/j.nlm.2004.01.001

Calabresi, P., Picconi, B., Tozzi, A., Ghiglieri, V., & Di Filippo, M. (2014). Direct and indirect pathways of basal ganglia: a critical reappraisal. *Nat Neurosci*, *17*(8), 1022-1030. https://doi.org/10.1038/nn.3743

Caldwell-Harris, C. L. (2021). An Explanation for Repetitive Motor Behaviors in Autism: Facilitating Inventions via Trial-and-Error Discovery. *Front Psychiatry*, *12*, 657774. https://doi.org/10.3389/fpsyt.2021.657774

Cao, W., Li, J. H., Lin, S., Xia, Q. Q., Du, Y. L., Yang, Q., Ye, Y. Z., Zeng, L. H., Li, X. Y., Xu, J., & Luo, J. H. (2022). NMDA receptor hypofunction underlies deficits in parvalbumin interneurons and social behavior in neuroligin 3 R451C knockin mice. *Cell Rep*, *41*(10), 111771. https://doi.org/10.1016/j.celrep.2022.111771

Careaga, M., Murai, T., & Bauman, M. D. (2017). Maternal Immune Activation and Autism Spectrum Disorder: From Rodents to Nonhuman and Human Primates. *Biol Psychiatry*, *81*(5), 391-401. https://doi.org/10.1016/j.biopsych.2016.10.020

Carlezon, W. A., Jr., Kim, W., Missig, G., Finger, B. C., Landino, S. M., Alexander, A. J., Mokler, E. L., Robbins, J. O., Li, Y., Bolshakov, V. Y., McDougle, C. J., & Kim, K. S. (2019). Maternal and early postnatal immune activation produce sex-specific effects on autism-like behaviors and neuroimmune function in mice. *Sci Rep*, *9*(1), 16928. https://doi.org/10.1038/s41598-019-53294-z

Chadman, K. K., Gong, S., Scattoni, M. L., Boltuck, S. E., Gandhy, S. U., Heintz, N., & Crawley, J. N. (2008). Minimal aberrant behavioral phenotypes of neuroligin-3 R451C knockin mice. *Autism Res*, *1*(3), 147-158. https://doi.org/10.1002/aur.22

Chahrour, M., & Zoghbi, H. Y. (2007). The story of Rett syndrome: from clinic to neurobiology. *Neuron*, *56*(3), 422-437. https://doi.org/10.1016/j.neuron.2007.10.001

Cheh, M. A., Millonig, J. H., Roselli, L. M., Ming, X., Jacobsen, E., Kamdar, S., & Wagner, G. C. (2006). En2 knockout mice display neurobehavioral and neurochemical alterations relevant to autism spectrum disorder. *Brain Res*, *1116*(1), 166-176. https://doi.org/10.1016/j.brainres.2006.07.086

Chevere-Torres, I., Maki, J. M., Santini, E., & Klann, E. (2012). Impaired social interactions and motor learning skills in tuberous sclerosis complex model mice expressing a dominant/negative form of tuberin. *Neurobiol Dis*, *45*(1), 156-164. https://doi.org/10.1016/j.nbd.2011.07.018

Chukoskie, L., Townsend, J., & Westerfield, M. (2013). Motor skill in autism spectrum disorders: a subcortical view. *Int Rev Neurobiol*, *113*, 207-249. https://doi.org/10.1016/B978-0-12-418700-9.00007-1

Clipperton-Allen, A. E., & Page, D. T. (2014). Pten haploinsufficient mice show broad brain overgrowth but selective impairments in autism-relevant behavioral tests. *Hum Mol Genet*, *23*(13), 3490-3505. https://doi.org/10.1093/hmg/ddu057

Collins, A. L., Levenson, J. M., Vilaythong, A. P., Richman, R., Armstrong, D. L., Noebels, J. L., David Sweatt, J., & Zoghbi, H. Y. (2004). Mild overexpression of MeCP2 causes a progressive neurological disorder in mice. *Hum Mol Genet*, *13*(21), 2679-2689. https://doi.org/10.1093/hmg/ddh282

Collins, B. E., Merritt, J. K., Erickson, K. R., & Neul, J. L. (2022). Safety and efficacy of genetic MECP2 supplementation in the R294X mouse model of Rett syndrome. *Genes Brain Behav*, *21*(1), e12739. https://doi.org/10.1111/gbb.12739

Costa, R. M., Cohen, D., & Nicolelis, M. A. L. (2004). Differential Corticostriatal Plasticity during Fast and Slow Motor Skill Learning in Mice. *Current Biology*, *14*(13), 1124-1134. https://doi.org/10.1016/j.cub.2004.06.053

Costa, R. M., Yang, T., Huynh, D. P., Pulst, S. M., Viskochil, D. H., Silva, A. J., & Brannan, C. I. (2001). Learning deficits, but normal development and tumor predisposition, in mice lacking exon 23a of Nf1. *Nat Genet*, *27*(4), 399-405. https://doi.org/10.1038/86898

Cragg, S. J., & Rice, M. E. (2004). DAncing past the DAT at a DA synapse. *Trends Neurosci*, *27*(5), 270-277. https://doi.org/10.1016/j.tins.2004.03.011

Curatolo, P., Moavero, R., & de Vries, P. J. (2015). Neurological and neuropsychiatric aspects of tuberous sclerosis complex. *Lancet Neurol*, *14*(7), 733-745. https://doi.org/10.1016/S1474-4422(15)00069-1

D'Elia, A., Schiavi, S., Manduca, A., Rava, A., Buzzelli, V., Ascone, F., Orsini, T., Putti, S., Soluri, A., Galli, F., Soluri, A., Mattei, M., Cicconi, R., Massari, R., & Trezza, V. (2022). FMR1 deletion in rats induces hyperactivity with no changes in striatal dopamine transporter availability. *Sci Rep*, *12*(1), 22535. https://doi.org/10.1038/s41598-022-26986-2

Dang, M. T., Yokoi, F., Yin, H. H., Lovinger, D. M., Wang, Y., & Li, Y. (2006). Disrupted motor learning and long-term synaptic plasticity in mice lacking NMDAR1 in the striatum. *Proc Natl Acad Sci U S A*, *103*(41), 15254-15259. https://doi.org/10.1073/pnas.0601758103

David, F. J., Baranek, G. T., Wiesen, C., Miao, A. F., & Thorpe, D. E. (2012). Coordination of precision grip in 2-6 years-old children with autism spectrum disorders compared to children developing typically and children with developmental disabilities. *Front Integr Neurosci*, *6*, 122. https://doi.org/10.3389/fnint.2012.00122

Davis, P. E., Peters, J. M., Krueger, D. A., & Sahin, M. (2015). Tuberous Sclerosis: A New Frontier in Targeted Treatment of Autism. *Neurotherapeutics*, *12*(3), 572-583. https://doi.org/10.1007/s13311-015-0359-5

Dawes, J. M., Weir, G. A., Middleton, S. J., Patel, R., Chisholm, K. I., Pettingill, P., Peck, L. J., Sheridan, J., Shakir, A., Jacobson, L., Gutierrez-Mecinas, M., Galino, J., Walcher, J., Kuhnemund, J., Kuehn, H., Sanna, M. D., Lang, B., Clark, A. J., Themistocleous, A. C., . . . Bennett, D. L. (2018). Immune or Genetic-Mediated Disruption of CASPR2 Causes Pain Hypersensitivity Due to Enhanced Primary Afferent Excitability. *Neuron*, *97*(4), 806-822 e810. https://doi.org/10.1016/j.neuron.2018.01.033

Dayan, E., & Cohen, L. G. (2011). Neuroplasticity subserving motor skill learning. *Neuron*, *72*(3), 443-454. https://doi.org/10.1016/j.neuron.2011.10.008

De Filippis, B., Ricceri, L., & Laviola, G. (2010). Early postnatal behavioral changes in the Mecp2-308 truncation mouse model of Rett syndrome. *Genes Brain Behav*, *9*(2), 213-223. https://doi.org/10.1111/j.1601-183X.2009.00551.x

De Rubeis, S., Siper, P. M., Durkin, A., Weissman, J., Muratet, F., Halpern, D., Trelles, M. D. P., Frank, Y., Lozano, R., Wang, A. T., Holder, J. L., Jr., Betancur, C., Buxbaum, J. D., & Kolevzon, A. (2018). Delineation of the genetic and clinical spectrum of Phelan-McDermid syndrome caused by SHANK3 point mutations. *Mol Autism*, *9*, 31. https://doi.org/10.1186/s13229-018-0205-9

DeLorey, T. M., Handforth, A., Anagnostaras, S. G., Homanics, G. E., Minassian, B. A., Asatourian, A., Fanselow, M. S., Delgado-Escueta, A., Ellison, G. D., & Olsen, R. W. (1998). Mice lacking the beta3 subunit of the GABAA receptor have the epilepsy phenotype and many of the behavioral characteristics of Angelman syndrome. *J Neurosci*, *18*(20), 8505-8514. https://doi.org/10.1523/JNEUROSCI.18-20-08505.1998

DeLorey, T. M., Sahbaie, P., Hashemi, E., Li, W. W., Salehi, A., & Clark, D. J. (2011). Somatosensory and sensorimotor consequences associated with the heterozygous disruption of the autism candidate gene, Gabrb3. *Behav Brain Res*, *216*(1), 36-45. https://doi.org/10.1016/j.bbr.2010.06.032

Depino, A. M. (2013). Peripheral and central inflammation in autism spectrum disorders. *Mol Cell Neurosci*, *53*, 69-76. https://doi.org/10.1016/j.mcn.2012.10.003

Dey, R., & Chattarji, S. (2022). The same stress elicits different effects on anxiety-like behavior in rat models of Fmr1(-/y) and Pten(+/). *Behav Brain Res*, *428*, 113892. https://doi.org/10.1016/j.bbr.2022.113892

DiCarlo, G. E., Aguilar, J. I., Matthies, H. J., Harrison, F. E., Bundschuh, K. E., West, A., Hashemi, P., Herborg, F., Rickhag, M., Chen, H., Gether, U., Wallace, M. T., & Galli, A. (2019). Autism-linked dopamine transporter mutation alters striatal dopamine neurotransmission and dopamine-dependent behaviors. *J Clin Invest*, *129*(8), 3407-3419. https://doi.org/10.1172/JCI127411

Dichter, G. S. (2012). Functional magnetic resonance imaging of autism spectrum disorders. *Dialogues Clin Neurosci*, *14*(3), 319-351. https://doi.org/10.31887/DCNS.2012.14.3/gdichter

Ding, J., Peterson, J. D., & Surmeier, D. J. (2008). Corticostriatal and thalamostriatal synapses have distinctive properties. *J Neurosci*, *28*(25), 6483-6492. https://doi.org/10.1523/JNEUROSCI.0435-08.2008

Doig, N. M., Moss, J., & Bolam, J. P. (2010). Cortical and thalamic innervation of direct and indirect pathway medium-sized spiny neurons in mouse striatum. *J Neurosci*, *30*(44), 14610-14618. https://doi.org/10.1523/JNEUROSCI.1623-10.2010

Dominguez-Iturza, N., Lo, A. C., Shah, D., Armendariz, M., Vannelli, A., Mercaldo, V., Trusel, M., Li, K. W., Gastaldo, D., Santos, A. R., Callaerts-Vegh, Z., D'Hooge, R., Mameli, M., Van der Linden, A., Smit, A. B., Achsel, T., & Bagni, C. (2019). The autism- and schizophrenia-associated protein CYFIP1 regulates bilateral brain connectivity and behaviour. *Nat Commun*, *10*(1), 3454. https://doi.org/10.1038/s41467-019-11203-y

Drapeau, E., Riad, M., Kajiwara, Y., & Buxbaum, J. D. (2018). Behavioral Phenotyping of an Improved Mouse Model of Phelan-McDermid Syndrome with a Complete Deletion of the Shank3 Gene. *eNeuro*, *5*(3). https://doi.org/10.1523/ENEURO.0046-18.2018

Dubos, A., Meziane, H., Iacono, G., Curie, A., Riet, F., Martin, C., Loaec, N., Birling, M. C., Selloum, M., Normand, E., Pavlovic, G., Sorg, T., Stunnenberg, H. G., Chelly, J., Humeau, Y., Friocourt, G., & Herault, Y. (2018). A new mouse model of ARX dup24 recapitulates the patients' behavioral and fine motor alterations. *Hum Mol Genet*, *27*(12), 2138-2153. https://doi.org/10.1093/hmg/ddy122

Dunham, N. W., & Miya, T. S. (1957). A note on a simple apparatus for detecting neurological deficit in rats and mice. *J Am Pharm Assoc Am Pharm Assoc*, *46*(3), 208-209. https://doi.org/10.1002/jps.3030460322

Durieux, P. F., Schiffmann, S. N., & de Kerchove d'Exaerde, A. (2012). Differential regulation of motor control and response to dopaminergic drugs by D1R and D2R neurons in distinct dorsal striatum subregions. *EMBO J*, *31*(3), 640-653. https://doi.org/10.1038/emboj.2011.400

Ebert, D. H., Gabel, H. W., Robinson, N. D., Kastan, N. R., Hu, L. S., Cohen, S., Navarro, A. J., Lyst, M. J., Ekiert, R., Bird, A. P., & Greenberg, M. E. (2013). Activity-dependent phosphorylation of MeCP2 threonine 308 regulates interaction with NCoR. *Nature*, *499*(7458), 341-345. https://doi.org/10.1038/nature12348

Echevarria-Cooper, D. M., Hawkins, N. A., Misra, S. N., Huffman, A. M., Thaxton, T., Thompson, C. H., Ben-Shalom, R., Nelson, A. D., Lipkin, A. M., George, A. L., Jr., Bender, K. J., & Kearney, J. A. (2022). Cellular and behavioral effects of altered NaV1.2 sodium channel ion permeability in Scn2aK1422E mice. *Hum Mol Genet*, *31*(17), 2964-2988. https://doi.org/10.1093/hmg/ddac087

Ecker, C., Suckling, J., Deoni, S. C., Lombardo, M. V., Bullmore, E. T., Baron-Cohen, S., Catani, M., Jezzard, P., Barnes, A., Bailey, A. J., Williams, S. C., Murphy, D. G., & Consortium, M. A. (2012). Brain anatomy and its relationship to behavior in adults with autism spectrum disorder: a multicenter magnetic resonance imaging study. *Arch Gen Psychiatry*, *69*(2), 195-209. https://doi.org/10.1001/archgenpsychiatry.2011.1251

Ellegood, J., & Crawley, J. N. (2015). Behavioral and Neuroanatomical Phenotypes in Mouse Models of Autism. *Neurotherapeutics*, *12*(3), 521-533. https://doi.org/10.1007/s13311-015-0360-z

Ellegood, J., Nakai, N., Nakatani, J., Henkelman, M., Takumi, T., & Lerch, J. (2015). Neuroanatomical Phenotypes Are Consistent With Autism-Like Behavioral Phenotypes in the 15q11-13 Duplication Mouse Model. *Autism Res*, *8*(5), 545-555. https://doi.org/10.1002/aur.1469

Ellenbroek, B., & Youn, J. (2016). Rodent models in neuroscience research: is it a rat race? *Dis Model Mech*, *9*(10), 1079-1087. https://doi.org/10.1242/dmm.026120

Enard, W., Gehre, S., Hammerschmidt, K., Holter, S. M., Blass, T., Somel, M., Bruckner, M. K., Schreiweis, C., Winter, C., Sohr, R., Becker, L., Wiebe, V., Nickel, B., Giger, T., Muller, U., Groszer, M., Adler, T., Aguilar, A., Bolle, I., . . . Paabo, S. (2009). A humanized version of Foxp2 affects cortico-basal ganglia circuits in mice. *Cell*, *137*(5), 961-971. https://doi.org/10.1016/j.cell.2009.03.041

Estes, A., Shaw, D. W., Sparks, B. F., Friedman, S., Giedd, J. N., Dawson, G., Bryan, M., & Dager, S. R. (2011). Basal ganglia morphometry and repetitive behavior in young children with autism spectrum disorder. *Autism Res*, *4*(3), 212-220. https://doi.org/10.1002/aur.193

Etherton, M. R., Blaiss, C. A., Powell, C. M., & Sudhof, T. C. (2009). Mouse neurexin-1alpha deletion causes correlated electrophysiological and behavioral changes consistent with cognitive impairments. *Proc Natl Acad Sci U S A*, *106*(42), 17998-18003. https://doi.org/10.1073/pnas.0910297106

Fadila, S., Quinn, S., Turchetti Maia, A., Yakubovich, D., Ovadia, M., Anderson, K. L., Giladi, M., & Rubinstein, M. (2020). Convulsive seizures and some behavioral comorbidities are uncoupled in the Scn1a(A1783V) Dravet syndrome mouse model. *Epilepsia*, *61*(10), 2289-2300. https://doi.org/10.1111/epi.16662

Feyder, M., Karlsson, R. M., Mathur, P., Lyman, M., Bock, R., Momenan, R., Munasinghe, J., Scattoni, M. L., Ihne, J., Camp, M., Graybeal, C., Strathdee, D., Begg, A., Alvarez, V. A., Kirsch, P., Rietschel, M., Cichon, S., Walter, H., Meyer-Lindenberg, A., . . . Holmes, A. (2010). Association of mouse Dlg4 (PSD-95) gene deletion and human DLG4 gene variation with phenotypes relevant to autism spectrum disorders and Williams' syndrome. *Am J Psychiatry*, *167*(12), 1508-1517. https://doi.org/10.1176/appi.ajp.2010.10040484

French, C. A., Jin, X., Campbell, T. G., Gerfen, E., Groszer, M., Fisher, S. E., & Costa, R. M. (2012). An aetiological Foxp2 mutation causes aberrant striatal activity and alters plasticity during skill learning. *Mol Psychiatry*, *17*(11), 1077-1085. https://doi.org/10.1038/mp.2011.105

Fu, M., Yu, X., Lu, J., & Zuo, Y. (2012). Repetitive motor learning induces coordinated formation of clustered dendritic spines in vivo. *Nature*, *483*(7387), 92-95. https://doi.org/10.1038/nature10844

Fuccillo, M. V. (2016). Striatal Circuits as a Common Node for Autism Pathophysiology. *Front Neurosci*, *10*, 27. https://doi.org/10.3389/fnins.2016.00027

Fuchs, C., Gennaccaro, L., Trazzi, S., Bastianini, S., Bettini, S., Lo Martire, V., Ren, E., Medici, G., Zoccoli, G., Rimondini, R., & Ciani, E. (2018). Heterozygous CDKL5 Knockout Female Mice Are a Valuable Animal Model for CDKL5 Disorder. *Neural Plast*, *2018*, 9726950. https://doi.org/10.1155/2018/9726950

Gandal, M. J., Edgar, J. C., Ehrlichman, R. S., Mehta, M., Roberts, T. P., & Siegel, S. J. (2010). Validating gamma oscillations and delayed auditory responses as translational biomarkers of autism. *Biol Psychiatry*, *68*(12), 1100-1106. https://doi.org/10.1016/j.biopsych.2010.09.031

Gandhi, T., & Lee, C. C. (2020). Neural Mechanisms Underlying Repetitive Behaviors in Rodent Models of Autism Spectrum Disorders. *Front Cell Neurosci*, *14*, 592710. https://doi.org/10.3389/fncel.2020.592710

Gao, Y., Irvine, E. E., Eleftheriadou, I., Naranjo, C. J., Hearn-Yeates, F., Bosch, L., Glegola, J. A., Murdoch, L., Czerniak, A., Meloni, I., Renieri, A., Kinali, M., &

Mazarakis, N. D. (2020). Gene replacement ameliorates deficits in mouse and human models of cyclin-dependent kinase-like 5 disorder. *Brain*, *143*(3), 811-832. https://doi.org/10.1093/brain/awaa028

Gerfen, C. R., & Surmeier, D. J. (2011). Modulation of striatal projection systems by dopamine. *Annu Rev Neurosci*, *34*, 441-466. https://doi.org/10.1146/annurev-neuro-061010-113641

Goffin, D., Allen, M., Zhang, L., Amorim, M., Wang, I. T., Reyes, A. R., Mercado-Berton, A., Ong, C., Cohen, S., Hu, L., Blendy, J. A., Carlson, G. C., Siegel, S. J., Greenberg, M. E., & Zhou, Z. (2011). Rett syndrome mutation MeCP2 T158A disrupts DNA binding, protein stability and ERP responses. *Nat Neurosci*, *15*(2), 274-283. https://doi.org/10.1038/nn.2997

Green, D., Charman, T., Pickles, A., Chandler, S., Loucas, T., Simonoff, E., & Baird, G. (2009). Impairment in movement skills of children with autistic spectrum disorders. *Dev Med Child Neurol*, *51*(4), 311-316. https://doi.org/10.1111/j.1469-8749.2008.03242.x

Groszer, M., Keays, D. A., Deacon, R. M., de Bono, J. P., Prasad-Mulcare, S., Gaub, S., Baum, M. G., French, C. A., Nicod, J., Coventry, J. A., Enard, W., Fray, M., Brown, S. D., Nolan, P. M., Paabo, S., Channon, K. M., Costa, R. M., Eilers, J., Ehret, G., . . . Fisher, S. E. (2008). Impaired synaptic plasticity and motor learning in mice with a point mutation implicated in human speech deficits. *Curr Biol*, *18*(5), 354-362. https://doi.org/10.1016/j.cub.2008.01.060

Haber, S. N., Fudge, J. L., & McFarland, N. R. (2000). Striatonigrostriatal pathways in primates form an ascending spiral from the shell to the dorsolateral striatum. *J Neurosci*, *20*(6), 2369-2382. https://doi.org/10.1523/JNEUROSCI.20-06-02369.2000

Hamilton, P. J., Campbell, N. G., Sharma, S., Erreger, K., Herborg Hansen, F., Saunders, C., Belovich, A. N., Consortium, N. A. A. S., Sahai, M. A., Cook, E. H., Gether, U., McHaourab, H. S., Matthies, H. J., Sutcliffe, J. S., & Galli, A. (2013). De novo mutation in the dopamine transporter gene associates dopamine dysfunction with autism spectrum disorder. *Mol Psychiatry*, *18*(12), 1315-1323. https://doi.org/10.1038/mp.2013.102

Hamm, R. J., Pike, B. R., O'Dell, D. M., Lyeth, B. G., & Jenkins, L. W. (1994). The rotarod test: an evaluation of its effectiveness in assessing motor deficits following traumatic brain injury. *J Neurotrauma*, *11*(2), 187-196. https://doi.org/10.1089/neu.1994.11.187

Hampson, D. R., & Blatt, G. J. (2015). Autism spectrum disorders and neuropathology of the cerebellum. *Front Neurosci*, *9*, 420. https://doi.org/10.3389/fnins.2015.00420

Harris, E., Myers, H., Saxena, K., Mitchell-Heggs, R., Kind, P., Chattarji, S., & Morris, R. G. M. (2021). Experiential modulation of social dominance in a SYNGAP1 rat model of Autism Spectrum Disorders. *Eur J Neurosci*, *54*(10), 7733-7748. https://doi.org/10.1111/ejn.15500

Hashiguchi, S., Doi, H., Kunii, M., Nakamura, Y., Shimuta, M., Suzuki, E., Koyano, S., Okubo, M., Kishida, H., Shiina, M., Ogata, K., Hirashima, F., Inoue, Y., Kubota, S., Hayashi, N., Nakamura, H., Takahashi, K., Katsumoto, A., Tada, M., . . . Tanaka, F. (2019). Ataxic phenotype with altered Ca(V)3.1 channel property in a

mouse model for spinocerebellar ataxia 42. *Neurobiol Dis*, *130*, 104516. https://doi.org/10.1016/j.nbd.2019.104516
Haswell, C. C., Izawa, J., Dowell, L. R., Mostofsky, S. H., & Shadmehr, R. (2009). Representation of internal models of action in the autistic brain. *Nat Neurosci*, *12*(8), 970-972. https://doi.org/10.1038/nn.2356
Hawes, S. L., Evans, R. C., Unruh, B. A., Benkert, E. E., Gillani, F., Dumas, T. C., & Blackwell, K. T. (2015). Multimodal Plasticity in Dorsal Striatum While Learning a Lateralized Navigation Task. *J Neurosci*, *35*(29), 10535-10549. https://doi.org/10.1523/JNEUROSCI.4415-14.2015
Heck, D. H., Zhao, Y., Roy, S., LeDoux, M. S., & Reiter, L. T. (2008). Analysis of cerebellar function in Ube3a-deficient mice reveals novel genotype-specific behaviors. *Hum Mol Genet*, *17*(14), 2181-2189. https://doi.org/10.1093/hmg/ddn117
Heng, M. Y., Detloff, P. J., & Albin, R. L. (2008). Rodent genetic models of Huntington disease. *Neurobiol Dis*, *32*(1), 1-9. https://doi.org/10.1016/j.nbd.2008.06.005
Hernandez, A., Delgado-Gonzalez, E., Durairaj, R. V., Reyes-Haro, D., Martinez-Torres, A., & Espinosa, F. (2023). Striatal synaptic changes and behavior in adult mouse upon prenatal exposure to valproic acid. *Brain Res*, *1815*, 148461. https://doi.org/10.1016/j.brainres.2023.148461
Hisaoka, T., Komori, T., Kitamura, T., & Morikawa, Y. (2018). Abnormal behaviours relevant to neurodevelopmental disorders in Kirrel3-knockout mice. *Sci Rep*, *8*(1), 1408. https://doi.org/10.1038/s41598-018-19844-7
Hollander, E., Anagnostou, E., Chaplin, W., Esposito, K., Haznedar, M. M., Licalzi, E., Wasserman, S., Soorya, L., & Buchsbaum, M. (2005). Striatal volume on magnetic resonance imaging and repetitive behaviors in autism. *Biol Psychiatry*, *58*(3), 226-232. https://doi.org/10.1016/j.biopsych.2005.03.040
Huang, H. S., Burns, A. J., Nonneman, R. J., Baker, L. K., Riddick, N. V., Nikolova, V. D., Riday, T. T., Yashiro, K., Philpot, B. D., & Moy, S. S. (2013). Behavioral deficits in an Angelman syndrome model: effects of genetic background and age. *Behav Brain Res*, *243*, 79-90. https://doi.org/10.1016/j.bbr.2012.12.052
Hulbert, S. W., Wang, X., Gbadegesin, S. O., Xu, Q., Xu, X., & Jiang, Y. H. (2020). A Novel Chd8 Mutant Mouse Displays Altered Ultrasonic Vocalizations and Enhanced Motor Coordination. *Autism Res*, *13*(10), 1685-1697. https://doi.org/10.1002/aur.2353
Hung, A. Y., Futai, K., Sala, C., Valtschanoff, J. G., Ryu, J., Woodworth, M. A., Kidd, F. L., Sung, C. C., Miyakawa, T., Bear, M. F., Weinberg, R. J., & Sheng, M. (2008). Smaller dendritic spines, weaker synaptic transmission, but enhanced spatial learning in mice lacking Shank1. *J Neurosci*, *28*(7), 1697-1708. https://doi.org/10.1523/JNEUROSCI.3032-07.2008
Ikeda, K., Satake, S., Onaka, T., Sugimoto, H., Takeda, N., Imoto, K., & Kawakami, K. (2013). Enhanced inhibitory neurotransmission in the cerebellar cortex of Atp1a3-deficient heterozygous mice. *J Physiol*, *591*(13), 3433-3449. https://doi.org/10.1113/jphysiol.2012.247817
Ito, S., Ogiwara, I., Yamada, K., Miyamoto, H., Hensch, T. K., Osawa, M., & Yamakawa, K. (2013). Mouse with Nav1.1 haploinsufficiency, a model for Dravet syndrome,

exhibits lowered sociability and learning impairment. *Neurobiol Dis*, *49*, 29-40. https://doi.org/10.1016/j.nbd.2012.08.003

Jaramillo, T. C., Speed, H. E., Xuan, Z., Reimers, J. M., Escamilla, C. O., Weaver, T. P., Liu, S., Filonova, I., & Powell, C. M. (2017). Novel Shank3 mutant exhibits behaviors with face validity for autism and altered striatal and hippocampal function. *Autism Res*, *10*(1), 42-65. https://doi.org/10.1002/aur.1664

Jhang, C. L., Huang, T. N., Hsueh, Y. P., & Liao, W. (2017). Mice lacking cyclin-dependent kinase-like 5 manifest autistic and ADHD-like behaviors. *Hum Mol Genet*, *26*(20), 3922-3934. https://doi.org/10.1093/hmg/ddx279

Jiang, Y. H., Armstrong, D., Albrecht, U., Atkins, C. M., Noebels, J. L., Eichele, G., Sweatt, J. D., & Beaudet, A. L. (1998). Mutation of the Angelman ubiquitin ligase in mice causes increased cytoplasmic p53 and deficits of contextual learning and long-term potentiation. *Neuron*, *21*(4), 799-811. https://doi.org/10.1016/s0896-6273(00)80596-6

Jin, P., & Warren, S. T. (2003). New insights into fragile X syndrome: from molecules to neurobehaviors. *Trends Biochem Sci*, *28*(3), 152-158. https://doi.org/10.1016/S0968-0004(03)00033-1

Jung, E. M., Moffat, J. J., Liu, J., Dravid, S. M., Gurumurthy, C. B., & Kim, W. Y. (2017). Arid1b haploinsufficiency disrupts cortical interneuron development and mouse behavior. *Nat Neurosci*, *20*(12), 1694-1707. https://doi.org/10.1038/s41593-017-0013-0

Jung, K. M., Sepers, M., Henstridge, C. M., Lassalle, O., Neuhofer, D., Martin, H., Ginger, M., Frick, A., DiPatrizio, N. V., Mackie, K., Katona, I., Piomelli, D., & Manzoni, O. J. (2012). Uncoupling of the endocannabinoid signalling complex in a mouse model of fragile X syndrome. *Nat Commun*, *3*, 1080. https://doi.org/10.1038/ncomms2045

Kaiser, F. M. P., Gruenbacher, S., Oyaga, M. R., Nio, E., Jaritz, M., Sun, Q., van der Zwaag, W., Kreidl, E., Zopf, L. M., Dalm, V., Pel, J., Gaiser, C., van der Vliet, R., Wahl, L., Rietman, A., Hill, L., Leca, I., Driessen, G., Laffeber, C., . . . Busslinger, M. (2022). Biallelic PAX5 mutations cause hypogammaglobulinemia, sensorimotor deficits, and autism spectrum disorder. *J Exp Med*, *219*(9). https://doi.org/10.1084/jem.20220498

Kao, F. C., Su, S. H., Carlson, G. C., & Liao, W. (2015). MeCP2-mediated alterations of striatal features accompany psychomotor deficits in a mouse model of Rett syndrome. *Brain Struct Funct*, *220*(1), 419-434. https://doi.org/10.1007/s00429-013-0664-x

Kawamura, A., Katayama, Y., Kakegawa, W., Ino, D., Nishiyama, M., Yuzaki, M., & Nakayama, K. I. (2021). The autism-associated protein CHD8 is required for cerebellar development and motor function. *Cell Rep*, *35*(1), 108932. https://doi.org/10.1016/j.celrep.2021.108932

Kosillo, P., & Bateup, H. S. (2021). Dopaminergic Dysregulation in Syndromic Autism Spectrum Disorders: Insights From Genetic Mouse Models. *Front Neural Circuits*, *15*, 700968. https://doi.org/10.3389/fncir.2021.700968

Kouser, M., Speed, H. E., Dewey, C. M., Reimers, J. M., Widman, A. J., Gupta, N., Liu, S., Jaramillo, T. C., Bangash, M., Xiao, B., Worley, P. F., & Powell, C. M. (2013). Loss of predominant Shank3 isoforms results in hippocampus-dependent

impairments in behavior and synaptic transmission. *J Neurosci*, *33*(47), 18448-18468. https://doi.org/10.1523/JNEUROSCI.3017-13.2013
Kravitz, A. V., Freeze, B. S., Parker, P. R., Kay, K., Thwin, M. T., Deisseroth, K., & Kreitzer, A. C. (2010). Regulation of parkinsonian motor behaviours by optogenetic control of basal ganglia circuitry. *Nature*, *466*(7306), 622-626. https://doi.org/10.1038/nature09159
Kreitzer, A. C., & Malenka, R. C. (2008). Striatal plasticity and basal ganglia circuit function. *Neuron*, *60*(4), 543-554. https://doi.org/10.1016/j.neuron.2008.11.005
Kupferschmidt, D. A., Augustin, S. M., Johnson, K. A., & Lovinger, D. M. (2019). Active Zone Proteins RIM1alphabeta Are Required for Normal Corticostriatal Transmission and Action Control. *J Neurosci*, *39*(8), 1457-1470. https://doi.org/10.1523/JNEUROSCI.1940-18.2018
Kwon, C. H., Luikart, B. W., Powell, C. M., Zhou, J., Matheny, S. A., Zhang, W., Li, Y., Baker, S. J., & Parada, L. F. (2006). Pten regulates neuronal arborization and social interaction in mice. *Neuron*, *50*(3), 377-388. https://doi.org/10.1016/j.neuron.2006.03.023
Lai, J. K., Lerch, J. P., Doering, L. C., Foster, J. A., & Ellegood, J. (2016). Regional brain volumes changes in adult male FMR1-KO mouse on the FVB strain. *Neuroscience*, *318*, 12-21. https://doi.org/10.1016/j.neuroscience.2016.01.021
Lalonde, R., Hayzoun, K., Derer, M., Mariani, J., & Strazielle, C. (2004). Neurobehavioral evaluation of Reln-rl-orl mutant mice and correlations with cytochrome oxidase activity. *Neurosci Res*, *49*(3), 297-305. https://doi.org/10.1016/j.neures.2004.03.012
Landi, S., Putignano, E., Boggio, E. M., Giustetto, M., Pizzorusso, T., & Ratto, G. M. (2011). The short-time structural plasticity of dendritic spines is altered in a model of Rett syndrome. *Sci Rep*, *1*, 45. https://doi.org/10.1038/srep00045
Le Duc, D., Giulivi, C., Hiatt, S. M., Napoli, E., Panoutsopoulos, A., Harlan De Crescenzo, A., Kotzaeridou, U., Syrbe, S., Anagnostou, E., Azage, M., Bend, R., Begtrup, A., Brown, N. J., Buttner, B., Cho, M. T., Cooper, G. M., Doering, J. H., Dubourg, C., Everman, D. B., . . . Jamra, R. (2019). Pathogenic WDFY3 variants cause neurodevelopmental disorders and opposing effects on brain size. *Brain*, *142*(9), 2617-2630. https://doi.org/10.1093/brain/awz198
Le Merrer, J., Detraux, B., Gandia, J., De Groote, A., Fonteneau, M., de Kerchove d'Exaerde, A., & Becker, J. A. J. (2023). Balance Between Projecting Neuronal Populations of the Nucleus Accumbens Controls Social Behavior in Mice. *Biol Psychiatry*. https://doi.org/10.1016/j.biopsych.2023.05.008
Leach, P. T., & Crawley, J. N. (2018). Touchscreen learning deficits in Ube3a, Ts65Dn and Mecp2 mouse models of neurodevelopmental disorders with intellectual disabilities. *Genes Brain Behav*, *17*(6), e12452. https://doi.org/10.1111/gbb.12452
Lena, I., & Mantegazza, M. (2019). Na(V)1.2 haploinsufficiency in Scn2a knock-out mice causes an autistic-like phenotype attenuated with age. *Sci Rep*, *9*(1), 12886. https://doi.org/10.1038/s41598-019-49392-7
Li, W., & Pozzo-Miller, L. (2020). Dysfunction of the corticostriatal pathway in autism spectrum disorders. *J Neurosci Res*, *98*(11), 2130-2147. https://doi.org/10.1002/jnr.24560

Li, Y. J., Zhang, K., Sun, T., Guo, Y. Y., Yang, Q., Liu, S. B., Wu, Y. M., & Zhao, M. G. (2023). Improvement of Learning and Memory by Elevating Brain D-Aspartate in a Mouse Model of Fragile X Syndrome. *Mol Neurobiol*. https://doi.org/10.1007/s12035-023-03438-0

Liu, D., Nanclares, C., Simbriger, K., Fang, K., Lorsung, E., Le, N., Amorim, I. S., Chalkiadaki, K., Pathak, S. S., Li, J., Gewirtz, J. C., Jin, V. X., Kofuji, P., Araque, A., Orr, H. T., Gkogkas, C. G., & Cao, R. (2022). Autistic-like behavior and cerebellar dysfunction in Bmal1 mutant mice ameliorated by mTORC1 inhibition. *Mol Psychiatry*. https://doi.org/10.1038/s41380-022-01499-6

Longo, F., & Klann, E. (2021). Reciprocal control of translation and transcription in autism spectrum disorder. *EMBO Rep*, *22*(6), e52110. https://doi.org/10.15252/embr.202052110

Lovinger, D. M. (2010). Neurotransmitter roles in synaptic modulation, plasticity and learning in the dorsal striatum. *Neuropharmacology*, *58*(7), 951-961. https://doi.org/10.1016/j.neuropharm.2010.01.008

Lubrich, C., Giesler, P., & Kipp, M. (2022). Motor Behavioral Deficits in the Cuprizone Model: Validity of the Rotarod Test Paradigm. *Int J Mol Sci*, *23*(19). https://doi.org/10.3390/ijms231911342

Luft, A. R., & Buitrago, M. M. (2005). Stages of Motor Skill Learning. *Molecular Neurobiology*, *32*(3), 205-216. https://doi.org/10.1385/mn:32:3:205

Lynch, J. F., 3rd, Ferri, S. L., Angelakos, C., Schoch, H., Nickl-Jockschat, T., Gonzalez, A., O'Brien, W. T., & Abel, T. (2020). Comprehensive Behavioral Phenotyping of a 16p11.2 Del Mouse Model for Neurodevelopmental Disorders. *Autism Res*, *13*(10), 1670-1684. https://doi.org/10.1002/aur.2357

Lyst, M. J., Ekiert, R., Ebert, D. H., Merusi, C., Nowak, J., Selfridge, J., Guy, J., Kastan, N. R., Robinson, N. D., de Lima Alves, F., Rappsilber, J., Greenberg, M. E., & Bird, A. (2013). Rett syndrome mutations abolish the interaction of MeCP2 with the NCoR/SMRT co-repressor. *Nat Neurosci*, *16*(7), 898-902. https://doi.org/10.1038/nn.3434

Ma, L., Day-Cooney, J., Benavides, O. J., Muniak, M. A., Qin, M., Ding, J. B., Mao, T., & Zhong, H. (2022). Locomotion activates PKA through dopamine and adenosine in striatal neurons. *Nature*, *611*(7937), 762-768. https://doi.org/10.1038/s41586-022-05407-4

Maccarrone, M., Rossi, S., Bari, M., De Chiara, V., Rapino, C., Musella, A., Bernardi, G., Bagni, C., & Centonze, D. (2010). Abnormal mGlu 5 receptor/endocannabinoid coupling in mice lacking FMRP and BC1 RNA. *Neuropsychopharmacology*, *35*(7), 1500-1509. https://doi.org/10.1038/npp.2010.19

Maenner, M. J., Warren, Z., Williams, A. R., Amoakohene, E., Bakian, A. V., Bilder, D. A., Durkin, M. S., Fitzgerald, R. T., Furnier, S. M., Hughes, M. M., Ladd-Acosta, C. M., McArthur, D., Pas, E. T., Salinas, A., Vehorn, A., Williams, S., Esler, A., Grzybowski, A., Hall-Lande, J., . . . Shaw, K. A. (2023). Prevalence and Characteristics of Autism Spectrum Disorder Among Children Aged 8 Years — Autism and Developmental Disabilities Monitoring Network, 11 Sites, United States, 2020. *MMWR. Surveillance Summaries*, *72*(2), 1-14. https://doi.org/10.15585/mmwr.ss7202a1

Mao, J. H., Langley, S. A., Huang, Y., Hang, M., Bouchard, K. E., Celniker, S. E., Brown, J. B., Jansson, J. K., Karpen, G. H., & Snijders, A. M. (2015). Identification of genetic factors that modify motor performance and body weight using Collaborative Cross mice. *Sci Rep*, *5*, 16247. https://doi.org/10.1038/srep16247

Marrone, M. C., Marinelli, S., Biamonte, F., Keller, F., Sgobio, C. A., Ammassari-Teule, M., Bernardi, G., & Mercuri, N. B. (2006). Altered cortico-striatal synaptic plasticity and related behavioural impairments in reeler mice. *Eur J Neurosci*, *24*(7), 2061-2070. https://doi.org/10.1111/j.1460-9568.2006.05083.x

Martella, G., Meringolo, M., Trobiani, L., De Jaco, A., Pisani, A., & Bonsi, P. (2018). The neurobiological bases of autism spectrum disorders: the R451C-neuroligin 3 mutation hampers the expression of long-term synaptic depression in the dorsal striatum. *Eur J Neurosci*, *47*(6), 701-708. https://doi.org/10.1111/ejn.13705

Martin, E. A., Muralidhar, S., Wang, Z., Cervantes, D. C., Basu, R., Taylor, M. R., Hunter, J., Cutforth, T., Wilke, S. A., Ghosh, A., & Williams, M. E. (2015). The intellectual disability gene Kirrel3 regulates target-specific mossy fiber synapse development in the hippocampus. *Elife*, *4*, e09395. https://doi.org/10.7554/eLife.09395

Mathis, A., Mamidanna, P., Cury, K. M., Abe, T., Murthy, V. N., Mathis, M. W., & Bethge, M. (2018). DeepLabCut: markerless pose estimation of user-defined body parts with deep learning. *Nat Neurosci*, *21*(9), 1281-1289. https://doi.org/10.1038/s41593-018-0209-y

Mei, Y., Monteiro, P., Zhou, Y., Kim, J. A., Gao, X., Fu, Z., & Feng, G. (2016). Adult restoration of Shank3 expression rescues selective autistic-like phenotypes. *Nature*, *530*(7591), 481-484. https://doi.org/10.1038/nature16971

Meltzer, A., & Van de Water, J. (2017). The Role of the Immune System in Autism Spectrum Disorder. *Neuropsychopharmacology*, *42*(1), 284-298. https://doi.org/10.1038/npp.2016.158

Miljanovic, N., Hauck, S. M., van Dijk, R. M., Di Liberto, V., Rezaei, A., & Potschka, H. (2021). Proteomic signature of the Dravet syndrome in the genetic Scn1a-A1783V mouse model. *Neurobiol Dis*, *157*, 105423. https://doi.org/10.1016/j.nbd.2021.105423

Minshew, N. J., Sung, K., Jones, B. L., & Furman, J. M. (2004). Underdevelopment of the postural control system in autism. *Neurology*, *63*(11), 2056-2061. https://doi.org/10.1212/01.wnl.0000145771.98657.62

Miura, K., Kishino, T., Li, E., Webber, H., Dikkes, P., Holmes, G. L., & Wagstaff, J. (2002). Neurobehavioral and electroencephalographic abnormalities in Ube3a maternal-deficient mice. *Neurobiol Dis*, *9*(2), 149-159. https://doi.org/10.1006/nbdi.2001.0463

Morello, N., Schina, R., Pilotto, F., Phillips, M., Melani, R., Plicato, O., Pizzorusso, T., Pozzo-Miller, L., & Giustetto, M. (2018). Loss of Mecp2 Causes Atypical Synaptic and Molecular Plasticity of Parvalbumin-Expressing Interneurons Reflecting Rett Syndrome-Like Sensorimotor Defects. *eNeuro*, *5*(5). https://doi.org/10.1523/ENEURO.0086-18.2018

Moy, S. S., Nadler, J. J., Young, N. B., Perez, A., Holloway, L. P., Barbaro, R. P., Barbaro, J. R., Wilson, L. M., Threadgill, D. W., Lauder, J. M., Magnuson, T. R., & Crawley, J. N. (2007). Mouse behavioral tasks relevant to autism: phenotypes of

10 inbred strains. *Behav Brain Res*, *176*(1), 4-20. https://doi.org/10.1016/j.bbr.2006.07.030
Muhia, M., Yee, B. K., Feldon, J., Markopoulos, F., & Knuesel, I. (2010). Disruption of hippocampus-regulated behavioural and cognitive processes by heterozygous constitutive deletion of SynGAP. *Eur J Neurosci*, *31*(3), 529-543. https://doi.org/10.1111/j.1460-9568.2010.07079.x
Mulherkar, S. A., & Jana, N. R. (2010). Loss of dopaminergic neurons and resulting behavioural deficits in mouse model of Angelman syndrome. *Neurobiol Dis*, *40*(3), 586-592. https://doi.org/10.1016/j.nbd.2010.08.002
Na, E. S., Nelson, E. D., Adachi, M., Autry, A. E., Mahgoub, M. A., Kavalali, E. T., & Monteggia, L. M. (2012). A mouse model for MeCP2 duplication syndrome: MeCP2 overexpression impairs learning and memory and synaptic transmission. *J Neurosci*, *32*(9), 3109-3117. https://doi.org/10.1523/JNEUROSCI.6000-11.2012
Nakajima, R., Takao, K., Hattori, S., Shoji, H., Komiyama, N. H., Grant, S. G. N., & Miyakawa, T. (2019). Comprehensive behavioral analysis of heterozygous Syngap1 knockout mice. *Neuropsychopharmacol Rep*, *39*(3), 223-237. https://doi.org/10.1002/npr2.12073
Nakamura, T., Arima-Yoshida, F., Sakaue, F., Nasu-Nishimura, Y., Takeda, Y., Matsuura, K., Akshoomoff, N., Mattson, S. N., Grossfeld, P. D., Manabe, T., & Akiyama, T. (2016). PX-RICS-deficient mice mimic autism spectrum disorder in Jacobsen syndrome through impaired GABAA receptor trafficking. *Nat Commun*, *7*, 10861. https://doi.org/10.1038/ncomms10861
Nakatani, J., Tamada, K., Hatanaka, F., Ise, S., Ohta, H., Inoue, K., Tomonaga, S., Watanabe, Y., Chung, Y. J., Banerjee, R., Iwamoto, K., Kato, T., Okazawa, M., Yamauchi, K., Tanda, K., Takao, K., Miyakawa, T., Bradley, A., & Takumi, T. (2009). Abnormal behavior in a chromosome-engineered mouse model for human 15q11-13 duplication seen in autism. *Cell*, *137*(7), 1235-1246. https://doi.org/10.1016/j.cell.2009.04.024
Naviaux, J. C., Schuchbauer, M. A., Li, K., Wang, L., Risbrough, V. B., Powell, S. B., & Naviaux, R. K. (2014). Reversal of autism-like behaviors and metabolism in adult mice with single-dose antipurinergic therapy. *Transl Psychiatry*, *4*(6), e400. https://doi.org/10.1038/tp.2014.33
Neale, B. M., Kou, Y., Liu, L., Ma'ayan, A., Samocha, K. E., Sabo, A., Lin, C. F., Stevens, C., Wang, L. S., Makarov, V., Polak, P., Yoon, S., Maguire, J., Crawford, E. L., Campbell, N. G., Geller, E. T., Valladares, O., Schafer, C., Liu, H., . . . Daly, M. J. (2012). Patterns and rates of exonic de novo mutations in autism spectrum disorders. *Nature*, *485*(7397), 242-245. https://doi.org/10.1038/nature11011
Nestler, E. J., & Hyman, S. E. (2010). Animal models of neuropsychiatric disorders. *Nat Neurosci*, *13*(10), 1161-1169. https://doi.org/10.1038/nn.2647
Niu, M., Zheng, N., Wang, Z., Gao, Y., Luo, X., Chen, Z., Fu, X., Wang, Y., Wang, T., Liu, M., Yao, T., Yao, P., Meng, J., Zhou, Y., Ge, Y., Wang, Z., Ma, Q., Xu, H., & Zhang, Y. W. (2020). RAB39B Deficiency Impairs Learning and Memory Partially Through Compromising Autophagy. *Front Cell Dev Biol*, *8*, 598622. https://doi.org/10.3389/fcell.2020.598622
Nolan, S. O., Reynolds, C. D., Smith, G. D., Holley, A. J., Escobar, B., Chandler, M. A., Volquardsen, M., Jefferson, T., Pandian, A., Smith, T., Huebschman, J., & Lugo,

J. N. (2017). Deletion of Fmr1 results in sex-specific changes in behavior. *Brain Behav*, *7*(10), e00800. https://doi.org/10.1002/brb3.800

Ouellette, J., Toussay, X., Comin, C. H., Costa, L. D. F., Ho, M., Lacalle-Aurioles, M., Freitas-Andrade, M., Liu, Q. Y., Leclerc, S., Pan, Y., Liu, Z., Thibodeau, J. F., Yin, M., Carrier, M., Morse, C. J., Dyken, P. V., Bergin, C. J., Baillet, S., Kennedy, C. R., . . . Lacoste, B. (2020). Vascular contributions to 16p11.2 deletion autism syndrome modeled in mice. *Nat Neurosci*, *23*(9), 1090-1101. https://doi.org/10.1038/s41593-020-0663-1

Packard, M. G., & Knowlton, B. J. (2002). Learning and memory functions of the Basal Ganglia. *Annu Rev Neurosci*, *25*, 563-593. https://doi.org/10.1146/annurev.neuro.25.112701.142937

Peixoto, R. T., Chantranupong, L., Hakim, R., Levasseur, J., Wang, W., Merchant, T., Gorman, K., Budnik, B., & Sabatini, B. L. (2019). Abnormal Striatal Development Underlies the Early Onset of Behavioral Deficits in Shank3B(-/-) Mice. *Cell Rep*, *29*(7), 2016-2027 e2014. https://doi.org/10.1016/j.celrep.2019.10.021

Pelka, G. J., Watson, C. M., Radziewic, T., Hayward, M., Lahooti, H., Christodoulou, J., & Tam, P. P. (2006). Mecp2 deficiency is associated with learning and cognitive deficits and altered gene activity in the hippocampal region of mice. *Brain*, *129*(Pt 4), 887-898. https://doi.org/10.1093/brain/awl022

Penagarikano, O., Abrahams, B. S., Herman, E. I., Winden, K. D., Gdalyahu, A., Dong, H., Sonnenblick, L. I., Gruver, R., Almajano, J., Bragin, A., Golshani, P., Trachtenberg, J. T., Peles, E., & Geschwind, D. H. (2011). Absence of CNTNAP2 leads to epilepsy, neuronal migration abnormalities, and core autism-related deficits. *Cell*, *147*(1), 235-246. https://doi.org/10.1016/j.cell.2011.08.040

Piochon, C., Kloth, A. D., Grasselli, G., Titley, H. K., Nakayama, H., Hashimoto, K., Wan, V., Simmons, D. H., Eissa, T., Nakatani, J., Cherskov, A., Miyazaki, T., Watanabe, M., Takumi, T., Kano, M., Wang, S. S., & Hansel, C. (2014). Cerebellar plasticity and motor learning deficits in a copy-number variation mouse model of autism. *Nat Commun*, *5*, 5586. https://doi.org/10.1038/ncomms6586

Pittenger, C., Fasano, S., Mazzocchi-Jones, D., Dunnett, S. B., Kandel, E. R., & Brambilla, R. (2006). Impaired bidirectional synaptic plasticity and procedural memory formation in striatum-specific cAMP response element-binding protein-deficient mice. *J Neurosci*, *26*(10), 2808-2813. https://doi.org/10.1523/JNEUROSCI.5406-05.2006

Platt, R. J., Zhou, Y., Slaymaker, I. M., Shetty, A. S., Weisbach, N. R., Kim, J. A., Sharma, J., Desai, M., Sood, S., Kempton, H. R., Crabtree, G. R., Feng, G., & Zhang, F. (2017). Chd8 Mutation Leads to Autistic-like Behaviors and Impaired Striatal Circuits. *Cell Rep*, *19*(2), 335-350. https://doi.org/10.1016/j.celrep.2017.03.052

Portmann, T., Yang, M., Mao, R., Panagiotakos, G., Ellegood, J., Dolen, G., Bader, P. L., Grueter, B. A., Goold, C., Fisher, E., Clifford, K., Rengarajan, P., Kalikhman, D., Loureiro, D., Saw, N. L., Zhengqui, Z., Miller, M. A., Lerch, J. P., Henkelman, M., . . . Dolmetsch, R. E. (2014). Behavioral abnormalities and circuit defects in the basal ganglia of a mouse model of 16p11.2 deletion syndrome. *Cell Rep*, *7*(4), 1077-1092. https://doi.org/10.1016/j.celrep.2014.03.036

Pratte, M., Panayotis, N., Ghata, A., Villard, L., & Roux, J. C. (2011). Progressive motor and respiratory metabolism deficits in post-weaning Mecp2-null male mice. *Behav Brain Res*, *216*(1), 313-320. https://doi.org/10.1016/j.bbr.2010.08.011

Price, M. G., Yoo, J. W., Burgess, D. L., Deng, F., Hrachovy, R. A., Frost, J. D., Jr., & Noebels, J. L. (2009). A triplet repeat expansion genetic mouse model of infantile spasms syndrome, Arx(GCG)10+7, with interneuronopathy, spasms in infancy, persistent seizures, and adult cognitive and behavioral impairment. *J Neurosci*, *29*(27), 8752-8763. https://doi.org/10.1523/JNEUROSCI.0915-09.2009

Punt, A. M., Judson, M. C., Sidorov, M. S., Williams, B. N., Johnson, N. S., Belder, S., den Hertog, D., Davis, C. R., Feygin, M. S., Lang, P. F., Jolfaei, M. A., Curran, P. J., van, I. W. F., Elgersma, Y., & Philpot, B. D. (2022). Molecular and behavioral consequences of Ube3a gene overdosage in mice. *JCI Insight*, *7*(18). https://doi.org/10.1172/jci.insight.158953

Qiu, Z. (2018). Deciphering MECP2-associated disorders: disrupted circuits and the hope for repair. *Curr Opin Neurobiol*, *48*, 30-36. https://doi.org/10.1016/j.conb.2017.09.004

Rahman, F. U., Kim, Y. R., Kim, E. K., Kim, H. R., Cho, S. M., Lee, C. S., Kim, S. J., Araki, K., Yamamura, K. I., Lee, M. N., Park, S. G., Yoon, W. K., Lee, K., Won, Y. S., Kim, H. C., Lee, Y., Lee, H. Y., & Nam, K. H. (2021). Topoisomerase IIIbeta Deficiency Induces Neuro-Behavioral Changes and Brain Connectivity Alterations in Mice. *Int J Mol Sci*, *22*(23). https://doi.org/10.3390/ijms222312806

Reith, R. M., McKenna, J., Wu, H., Hashmi, S. S., Cho, S. H., Dash, P. K., & Gambello, M. J. (2013). Loss of Tsc2 in Purkinje cells is associated with autistic-like behavior in a mouse model of tuberous sclerosis complex. *Neurobiol Dis*, *51*, 93-103. https://doi.org/10.1016/j.nbd.2012.10.014

Ricard, G., Molina, J., Chrast, J., Gu, W., Gheldof, N., Pradervand, S., Schutz, F., Young, J. I., Lupski, J. R., Reymond, A., & Walz, K. (2010). Phenotypic consequences of copy number variation: insights from Smith-Magenis and Potocki-Lupski syndrome mouse models. *PLoS Biol*, *8*(11), e1000543. https://doi.org/10.1371/journal.pbio.1000543

Ricobaraza, A., Mora-Jimenez, L., Puerta, E., Sanchez-Carpintero, R., Mingorance, A., Artieda, J., Nicolas, M. J., Besne, G., Bunuales, M., Gonzalez-Aparicio, M., Sola-Sevilla, N., Valencia, M., & Hernandez-Alcoceba, R. (2019). Epilepsy and neuropsychiatric comorbidities in mice carrying a recurrent Dravet syndrome SCN1A missense mutation. *Sci Rep*, *9*(1), 14172. https://doi.org/10.1038/s41598-019-50627-w

Rotaru, D. C., Mientjes, E. J., & Elgersma, Y. (2020). Angelman Syndrome: From Mouse Models to Therapy. *Neuroscience*, *445*, 172-189. https://doi.org/10.1016/j.neuroscience.2020.02.017

Rothwell, P. E., Fuccillo, M. V., Maxeiner, S., Hayton, S. J., Gokce, O., Lim, B. K., Fowler, S. C., Malenka, R. C., & Sudhof, T. C. (2014). Autism-associated neuroligin-3 mutations commonly impair striatal circuits to boost repetitive behaviors. *Cell*, *158*(1), 198-212. https://doi.org/10.1016/j.cell.2014.04.045

Roullet, F. I., Lai, J. K., & Foster, J. A. (2013). In utero exposure to valproic acid and autism--a current review of clinical and animal studies. *Neurotoxicol Teratol*, *36*, 47-56. https://doi.org/10.1016/j.ntt.2013.01.004

Roy, S., Zhao, Y., Allensworth, M., Farook, M. F., LeDoux, M. S., Reiter, L. T., & Heck, D. H. (2011). Comprehensive motor testing in Fmr1-KO mice exposes temporal defects in oromotor coordination. *Behav Neurosci*, *125*(6), 962-969. https://doi.org/10.1037/a0025920

Sakai, K., Shoji, H., Kohno, T., Miyakawa, T., & Hattori, M. (2016). Mice that lack the C-terminal region of Reelin exhibit behavioral abnormalities related to neuropsychiatric disorders. *Sci Rep*, *6*, 28636. https://doi.org/10.1038/srep28636

Sandin, S., Lichtenstein, P., Kuja-Halkola, R., Hultman, C., Larsson, H., & Reichenberg, A. (2017). The Heritability of Autism Spectrum Disorder. *JAMA*, *318*(12), 1182-1184. https://doi.org/10.1001/jama.2017.12141

Santos, F. J., Oliveira, R. F., Jin, X., & Costa, R. M. (2015). Corticostriatal dynamics encode the refinement of specific behavioral variability during skill learning. *Elife*, *4*, e09423. https://doi.org/10.7554/eLife.09423

Santos, M., Silva-Fernandes, A., Oliveira, P., Sousa, N., & Maciel, P. (2007). Evidence for abnormal early development in a mouse model of Rett syndrome. *Genes Brain Behav*, *6*(3), 277-286. https://doi.org/10.1111/j.1601-183X.2006.00258.x

Sathyamurthy, A., Barik, A., Dobrott, C. I., Matson, K. J. E., Stoica, S., Pursley, R., Chesler, A. T., & Levine, A. J. (2020). Cerebellospinal Neurons Regulate Motor Performance and Motor Learning. *Cell Rep*, *31*(6), 107595. https://doi.org/10.1016/j.celrep.2020.107595

Satterstrom, F. K., Kosmicki, J. A., Wang, J., Breen, M. S., De Rubeis, S., An, J.-Y., Peng, M., Collins, R., Grove, J., Klei, L., Stevens, C., Reichert, J., Mulhern, M. S., Artomov, M., Gerges, S., Sheppard, B., Xu, X., Bhaduri, A., Norman, U., . . . Walters, R. K. (2020). Large-Scale Exome Sequencing Study Implicates Both Developmental and Functional Changes in the Neurobiology of Autism. *Cell*, *180*(3), 568-584.e523. https://doi.org/10.1016/j.cell.2019.12.036

Saxton, R. A., & Sabatini, D. M. (2017). mTOR Signaling in Growth, Metabolism, and Disease. *Cell*, *168*(6), 960-976. https://doi.org/10.1016/j.cell.2017.02.004

Scandaglia, M., Lopez-Atalaya, J. P., Medrano-Fernandez, A., Lopez-Cascales, M. T., Del Blanco, B., Lipinski, M., Benito, E., Olivares, R., Iwase, S., Shi, Y., & Barco, A. (2017). Loss of Kdm5c Causes Spurious Transcription and Prevents the Fine-Tuning of Activity-Regulated Enhancers in Neurons. *Cell Rep*, *21*(1), 47-59. https://doi.org/10.1016/j.celrep.2017.09.014

Schaevitz, L. R., Gomez, N. B., Zhen, D. P., & Berger-Sweeney, J. E. (2013). MeCP2 R168X male and female mutant mice exhibit Rett-like behavioral deficits. *Genes Brain Behav*, *12*(7), 732-740. https://doi.org/10.1111/gbb.12070

Schiavi, S., Manduca, A., Carbone, E., Buzzelli, V., Rava, A., Feo, A., Ascone, F., Morena, M., Campolongo, P., Hill, M. N., & Trezza, V. (2023). Anandamide and 2-arachidonoylglycerol differentially modulate autistic-like traits in a genetic model of autism based on FMR1 deletion in rats. *Neuropsychopharmacology*, *48*(6), 897-907. https://doi.org/10.1038/s41386-022-01454-7

Schmitz, Y., Schmauss, C., & Sulzer, D. (2002). Altered dopamine release and uptake kinetics in mice lacking D2 receptors. *J Neurosci*, *22*(18), 8002-8009. https://doi.org/10.1523/JNEUROSCI.22-18-08002.2002

Schumann, C. M., & Nordahl, C. W. (2011). Bridging the gap between MRI and postmortem research in autism. *Brain Res*, *1380*, 175-186. https://doi.org/10.1016/j.brainres.2010.09.061
Shibutani, M., Horii, T., Shoji, H., Morita, S., Kimura, M., Terawaki, N., Miyakawa, T., & Hatada, I. (2017). Arid1b Haploinsufficiency Causes Abnormal Brain Gene Expression and Autism-Related Behaviors in Mice. *Int J Mol Sci*, *18*(9). https://doi.org/10.3390/ijms18091872
Shiflett, M. W., Gavin, M., & Tran, T. S. (2015). Altered hippocampal-dependent memory and motor function in neuropilin 2-deficient mice. *Transl Psychiatry*, *5*(3), e521. https://doi.org/10.1038/tp.2015.17
Shin, S., Santi, A., & Huang, S. (2021). Conditional Pten knockout in parvalbumin- or somatostatin-positive neurons sufficiently leads to autism-related behavioral phenotypes. *Mol Brain*, *14*(1), 24. https://doi.org/10.1186/s13041-021-00731-8
Shiotsuki, H., Yoshimi, K., Shimo, Y., Funayama, M., Takamatsu, Y., Ikeda, K., Takahashi, R., Kitazawa, S., & Hattori, N. (2010). A rotarod test for evaluation of motor skill learning. *J Neurosci Methods*, *189*(2), 180-185. https://doi.org/10.1016/j.jneumeth.2010.03.026
Silverman, J. L., Turner, S. M., Barkan, C. L., Tolu, S. S., Saxena, R., Hung, A. Y., Sheng, M., & Crawley, J. N. (2011). Sociability and motor functions in Shank1 mutant mice. *Brain Res*, *1380*, 120-137. https://doi.org/10.1016/j.brainres.2010.09.026
Simmons, D. H., Titley, H. K., Hansel, C., & Mason, P. (2021). Behavioral Tests for Mouse Models of Autism: An Argument for the Inclusion of Cerebellum-Controlled Motor Behaviors. *Neuroscience*, *462*, 303-319. https://doi.org/10.1016/j.neuroscience.2020.05.010
Sobue, A., Kushima, I., Nagai, T., Shan, W., Kohno, T., Aleksic, B., Aoyama, Y., Mori, D., Arioka, Y., Kawano, N., Yamamoto, M., Hattori, M., Nabeshima, T., Yamada, K., & Ozaki, N. (2018). Genetic and animal model analyses reveal the pathogenic role of a novel deletion of RELN in schizophrenia. *Sci Rep*, *8*(1), 13046. https://doi.org/10.1038/s41598-018-31390-w
Sonzogni, M., Wallaard, I., Santos, S. S., Kingma, J., du Mee, D., van Woerden, G. M., & Elgersma, Y. (2018). A behavioral test battery for mouse models of Angelman syndrome: a powerful tool for testing drugs and novel Ube3a mutants. *Mol Autism*, *9*, 47. https://doi.org/10.1186/s13229-018-0231-7
Souchet, B., Guedj, F., Sahun, I., Duchon, A., Daubigney, F., Badel, A., Yanagawa, Y., Barallobre, M. J., Dierssen, M., Yu, E., Herault, Y., Arbones, M., Janel, N., Creau, N., & Delabar, J. M. (2014). Excitation/inhibition balance and learning are modified by Dyrk1a gene dosage. *Neurobiol Dis*, *69*, 65-75. https://doi.org/10.1016/j.nbd.2014.04.016
Speed, H. E., Kouser, M., Xuan, Z., Reimers, J. M., Ochoa, C. F., Gupta, N., Liu, S., & Powell, C. M. (2015). Autism-Associated Insertion Mutation (InsG) of Shank3 Exon 21 Causes Impaired Synaptic Transmission and Behavioral Deficits. *J Neurosci*, *35*(26), 9648-9665. https://doi.org/10.1523/JNEUROSCI.3125-14.2015
Syding, L. A., Kubik-Zahorodna, A., Nickl, P., Novosadova, V., Kopkanova, J., Kasparek, P., Prochazka, J., & Sedlacek, R. (2022). Generation and Characterization of a

Novel Angelman Syndrome Mouse Model with a Full Deletion of the Ube3a Gene. *Cells*, *11*(18). https://doi.org/10.3390/cells11182815
Sztainberg, Y., Chen, H. M., Swann, J. W., Hao, S., Tang, B., Wu, Z., Tang, J., Wan, Y. W., Liu, Z., Rigo, F., & Zoghbi, H. Y. (2015). Reversal of phenotypes in MECP2 duplication mice using genetic rescue or antisense oligonucleotides. *Nature*, *528*(7580), 123-126. https://doi.org/10.1038/nature16159
Tai, L. H., Lee, A. M., Benavidez, N., Bonci, A., & Wilbrecht, L. (2012). Transient stimulation of distinct subpopulations of striatal neurons mimics changes in action value. *Nat Neurosci*, *15*(9), 1281-1289. https://doi.org/10.1038/nn.3188
Takayanagi, Y., Fujita, E., Yu, Z., Yamagata, T., Momoi, M. Y., Momoi, T., & Onaka, T. (2010). Impairment of social and emotional behaviors in Cadm1-knockout mice. *Biochem Biophys Res Commun*, *396*(3), 703-708. https://doi.org/10.1016/j.bbrc.2010.04.165
Takumi, T., & Tamada, K. (2018). CNV biology in neurodevelopmental disorders. *Curr Opin Neurobiol*, *48*, 183-192. https://doi.org/10.1016/j.conb.2017.12.004
Talantseva, O. I., Romanova, R. S., Shurdova, E. M., Dolgorukova, T. A., Sologub, P. S., Titova, O. S., Kleeva, D. F., & Grigorenko, E. L. (2023). The global prevalence of autism spectrum disorder: A three-level meta-analysis. *Front Psychiatry*, *14*, 1071181. https://doi.org/10.3389/fpsyt.2023.1071181
Tatsukawa, T., Raveau, M., Ogiwara, I., Hattori, S., Miyamoto, H., Mazaki, E., Itohara, S., Miyakawa, T., Montal, M., & Yamakawa, K. (2019). Scn2a haploinsufficient mice display a spectrum of phenotypes affecting anxiety, sociability, memory flexibility and ampakine CX516 rescues their hyperactivity. *Mol Autism*, *10*, 15. https://doi.org/10.1186/s13229-019-0265-5
Thomas, A. M., Schwartz, M. D., Saxe, M. D., & Kilduff, T. S. (2017). Sleep/Wake Physiology and Quantitative Electroencephalogram Analysis of the Neuroligin-3 Knockout Rat Model of Autism Spectrum Disorder. *Sleep*, *40*(10). https://doi.org/10.1093/sleep/zsx138
Till, S. M., Asiminas, A., Jackson, A. D., Katsanevaki, D., Barnes, S. A., Osterweil, E. K., Bear, M. F., Chattarji, S., Wood, E. R., Wyllie, D. J., & Kind, P. C. (2015). Conserved hippocampal cellular pathophysiology but distinct behavioural deficits in a new rat model of FXS. *Hum Mol Genet*, *24*(21), 5977-5984. https://doi.org/10.1093/hmg/ddv299
Tilot, A. K., Gaugler, M. K., Yu, Q., Romigh, T., Yu, W., Miller, R. H., Frazier, T. W., 2nd, & Eng, C. (2014). Germline disruption of Pten localization causes enhanced sex-dependent social motivation and increased glial production. *Hum Mol Genet*, *23*(12), 3212-3227. https://doi.org/10.1093/hmg/ddu031
Travers, B. G., Powell, P. S., Klinger, L. G., & Klinger, M. R. (2013). Motor difficulties in autism spectrum disorder: linking symptom severity and postural stability. *J Autism Dev Disord*, *43*(7), 1568-1583. https://doi.org/10.1007/s10803-012-1702-x
Tritsch, N. X., & Sabatini, B. L. (2012). Dopaminergic modulation of synaptic transmission in cortex and striatum. *Neuron*, *76*(1), 33-50. https://doi.org/10.1016/j.neuron.2012.09.023
Tropea, D., Giacometti, E., Wilson, N. R., Beard, C., McCurry, C., Fu, D. D., Flannery, R., Jaenisch, R., & Sur, M. (2009). Partial reversal of Rett Syndrome-like

symptoms in MeCP2 mutant mice. *Proc Natl Acad Sci U S A*, *106*(6), 2029-2034. https://doi.org/10.1073/pnas.0812394106

Troyb, E., Knoch, K., Herlihy, L., Stevens, M. C., Chen, C. M., Barton, M., Treadwell, K., & Fein, D. (2016). Restricted and Repetitive Behaviors as Predictors of Outcome in Autism Spectrum Disorders. *J Autism Dev Disord*, *46*(4), 1282-1296. https://doi.org/10.1007/s10803-015-2668-2

Tsai, P. T., Hull, C., Chu, Y., Greene-Colozzi, E., Sadowski, A. R., Leech, J. M., Steinberg, J., Crawley, J. N., Regehr, W. G., & Sahin, M. (2012). Autistic-like behaviour and cerebellar dysfunction in Purkinje cell Tsc1 mutant mice. *Nature*, *488*(7413), 647-651. https://doi.org/10.1038/nature11310

Tucci, V., Kleefstra, T., Hardy, A., Heise, I., Maggi, S., Willemsen, M. H., Hilton, H., Esapa, C., Simon, M., Buenavista, M. T., McGuffin, L. J., Vizor, L., Dodero, L., Tsaftaris, S., Romero, R., Nillesen, W. N., Vissers, L. E., Kempers, M. J., Vulto-van Silfhout, A. T., . . . Nolan, P. M. (2014). Dominant beta-catenin mutations cause intellectual disability with recognizable syndromic features. *J Clin Invest*, *124*(4), 1468-1482. https://doi.org/10.1172/JCI70372

Um, S. M., Ha, S., Lee, H., Kim, J., Kim, K., Shin, W., Cho, Y. S., Roh, J. D., Kang, J., Yoo, T., Noh, Y. W., Choi, Y., Bae, Y. C., & Kim, E. (2018). NGL-2 Deletion Leads to Autistic-like Behaviors Responsive to NMDAR Modulation. *Cell Rep*, *23*(13), 3839-3851. https://doi.org/10.1016/j.celrep.2018.05.087

Ung, D. C., Iacono, G., Meziane, H., Blanchard, E., Papon, M. A., Selten, M., van Rhijn, J. R., Montjean, R., Rucci, J., Martin, S., Fleet, A., Birling, M. C., Marouillat, S., Roepman, R., Selloum, M., Lux, A., Thepault, R. A., Hamel, P., Mittal, K., . . . Laumonnier, F. (2018). Ptchd1 deficiency induces excitatory synaptic and cognitive dysfunctions in mouse. *Mol Psychiatry*, *23*(5), 1356-1367. https://doi.org/10.1038/mp.2017.39

Uutela, M., Lindholm, J., Louhivuori, V., Wei, H., Louhivuori, L. M., Pertovaara, A., Akerman, K., Castren, E., & Castren, M. L. (2012). Reduction of BDNF expression in Fmr1 knockout mice worsens cognitive deficits but improves hyperactivity and sensorimotor deficits. *Genes Brain Behav*, *11*(5), 513-523. https://doi.org/10.1111/j.1601-183X.2012.00784.x

Van Dam, D., Errijgers, V., Kooy, R. F., Willemsen, R., Mientjes, E., Oostra, B. A., & De Deyn, P. P. (2005). Cognitive decline, neuromotor and behavioural disturbances in a mouse model for fragile-X-associated tremor/ataxia syndrome (FXTAS). *Behav Brain Res*, *162*(2), 233-239. https://doi.org/10.1016/j.bbr.2005.03.007

van der Vaart, T., van Woerden, G. M., Elgersma, Y., de Zeeuw, C. I., & Schonewille, M. (2011). Motor deficits in neurofibromatosis type 1 mice: the role of the cerebellum. *Genes Brain Behav*, *10*(4), 404-409. https://doi.org/10.1111/j.1601-183X.2011.00685.x

Vernazza-Martin, S., Martin, N., Vernazza, A., Lepellec-Muller, A., Rufo, M., Massion, J., & Assaiante, C. (2005). Goal directed locomotion and balance control in autistic children. *J Autism Dev Disord*, *35*(1), 91-102. https://doi.org/10.1007/s10803-004-1037-3

Vicidomini, C., Ponzoni, L., Lim, D., Schmeisser, M. J., Reim, D., Morello, N., Orellana, D., Tozzi, A., Durante, V., Scalmani, P., Mantegazza, M., Genazzani, A. A., Giustetto, M., Sala, M., Calabresi, P., Boeckers, T. M., Sala, C., & Verpelli, C.

(2017). Pharmacological enhancement of mGlu5 receptors rescues behavioral deficits in SHANK3 knock-out mice. *Mol Psychiatry*, *22*(5), 689-702. https://doi.org/10.1038/mp.2016.30

Vogel Ciernia, A., Pride, M. C., Durbin-Johnson, B., Noronha, A., Chang, A., Yasui, D. H., Crawley, J. N., & LaSalle, J. M. (2017). Early motor phenotype detection in a female mouse model of Rett syndrome is improved by cross-fostering. *Hum Mol Genet*, *26*(10), 1839-1854. https://doi.org/10.1093/hmg/ddx087

Voorn, P., Vanderschuren, L. J., Groenewegen, H. J., Robbins, T. W., & Pennartz, C. M. (2004). Putting a spin on the dorsal-ventral divide of the striatum. *Trends Neurosci*, *27*(8), 468-474. https://doi.org/10.1016/j.tins.2004.06.006

Wang, C., Geng, H., Liu, W., & Zhang, G. (2017). Prenatal, perinatal, and postnatal factors associated with autism: A meta-analysis. *Medicine (Baltimore)*, *96*(18), e6696. https://doi.org/10.1097/MD.0000000000006696

Wang, I. T., Allen, M., Goffin, D., Zhu, X., Fairless, A. H., Brodkin, E. S., Siegel, S. J., Marsh, E. D., Blendy, J. A., & Zhou, Z. (2012). Loss of CDKL5 disrupts kinome profile and event-related potentials leading to autistic-like phenotypes in mice. *Proc Natl Acad Sci U S A*, *109*(52), 21516-21521. https://doi.org/10.1073/pnas.1216988110

Wang, R., Tan, J., Guo, J., Zheng, Y., Han, Q., So, K. F., Yu, J., & Zhang, L. (2018). Aberrant Development and Synaptic Transmission of Cerebellar Cortex in a VPA Induced Mouse Autism Model. *Front Cell Neurosci*, *12*, 500. https://doi.org/10.3389/fncel.2018.00500

Wang, X., Bey, A. L., Katz, B. M., Badea, A., Kim, N., David, L. K., Duffney, L. J., Kumar, S., Mague, S. D., Hulbert, S. W., Dutta, N., Hayrapetyan, V., Yu, C., Gaidis, E., Zhao, S., Ding, J. D., Xu, Q., Chung, L., Rodriguiz, R. M., . . . Jiang, Y. H. (2016). Altered mGluR5-Homer scaffolds and corticostriatal connectivity in a Shank3 complete knockout model of autism. *Nat Commun*, *7*, 11459. https://doi.org/10.1038/ncomms11459

Wang, X., McCoy, P. A., Rodriguiz, R. M., Pan, Y., Je, H. S., Roberts, A. C., Kim, C. J., Berrios, J., Colvin, J. S., Bousquet-Moore, D., Lorenzo, I., Wu, G., Weinberg, R. J., Ehlers, M. D., Philpot, B. D., Beaudet, A. L., Wetsel, W. C., & Jiang, Y. H. (2011). Synaptic dysfunction and abnormal behaviors in mice lacking major isoforms of Shank3. *Hum Mol Genet*, *20*(15), 3093-3108. https://doi.org/10.1093/hmg/ddr212

Wang, Z., Yang, D., Jiang, Y., Wang, Y., Niu, M., Wang, C., Luo, H., Xu, H., Li, J., Zhang, Y. W., & Zhang, X. (2023). Loss of RAB39B does not alter MPTP-induced Parkinson's disease-like phenotypes in mice. *Front Aging Neurosci*, *15*, 1087823. https://doi.org/10.3389/fnagi.2023.1087823

Wei, H., Chadman, K. K., McCloskey, D. P., Sheikh, A. M., Malik, M., Brown, W. T., & Li, X. (2012). Brain IL-6 elevation causes neuronal circuitry imbalances and mediates autism-like behaviors. *Biochim Biophys Acta*, *1822*(6), 831-842. https://doi.org/10.1016/j.bbadis.2012.01.011

Weiss, L. A., Shen, Y., Korn, J. M., Arking, D. E., Miller, D. T., Fossdal, R., Saemundsen, E., Stefansson, H., Ferreira, M. A., Green, T., Platt, O. S., Ruderfer, D. M., Walsh, C. A., Altshuler, D., Chakravarti, A., Tanzi, R. E., Stefansson, K., Santangelo, S. L., Gusella, J. F., . . . Autism, C. (2008). Association between microdeletion and

microduplication at 16p11.2 and autism. *N Engl J Med*, *358*(7), 667-675. https://doi.org/10.1056/NEJMoa075974
Weiss, M. J., Moran, M. F., Parker, M. E., & Foley, J. T. (2013). Gait analysis of teenagers and young adults diagnosed with autism and severe verbal communication disorders. *Front Integr Neurosci*, *7*, 33. https://doi.org/10.3389/fnint.2013.00033
Weissberg, O., & Elliott, E. (2021). The Mechanisms of CHD8 in Neurodevelopment and Autism Spectrum Disorders. *Genes (Basel)*, *12*(8). https://doi.org/10.3390/genes12081133
Wiltschko, A. B., Tsukahara, T., Zeine, A., Anyoha, R., Gillis, W. F., Markowitz, J. E., Peterson, R. E., Katon, J., Johnson, M. J., & Datta, S. R. (2020). Revealing the structure of pharmacobehavioral space through motion sequencing. *Nat Neurosci*, *23*(11), 1433-1443. https://doi.org/10.1038/s41593-020-00706-3
Winden, K. D., Ebrahimi-Fakhari, D., & Sahin, M. (2018). Abnormal mTOR Activation in Autism. *Annu Rev Neurosci*, *41*, 1-23. https://doi.org/10.1146/annurev-neuro-080317-061747
Wohr, M., Fong, W. M., Janas, J. A., Mall, M., Thome, C., Vangipuram, M., Meng, L., Sudhof, T. C., & Wernig, M. (2022). Myt1l haploinsufficiency leads to obesity and multifaceted behavioral alterations in mice. *Mol Autism*, *13*(1), 19. https://doi.org/10.1186/s13229-022-00497-3
Wohr, M., Silverman, J. L., Scattoni, M. L., Turner, S. M., Harris, M. J., Saxena, R., & Crawley, J. N. (2013). Developmental delays and reduced pup ultrasonic vocalizations but normal sociability in mice lacking the postsynaptic cell adhesion protein neuroligin2. *Behav Brain Res*, *251*, 50-64. https://doi.org/10.1016/j.bbr.2012.07.024
Xing, L., Simon, J. M., Ptacek, T. S., Yi, J. J., Loo, L., Mao, H., Wolter, J. M., McCoy, E. S., Paranjape, S. R., Taylor-Blake, B., & Zylka, M. J. (2023). Autism-linked UBE3A gain-of-function mutation causes interneuron and behavioral phenotypes when inherited maternally or paternally in mice. *Cell Rep*, *42*(7), 112706. https://doi.org/10.1016/j.celrep.2023.112706
Xiong, Q., Oviedo, H. V., Trotman, L. C., & Zador, A. M. (2012). PTEN regulation of local and long-range connections in mouse auditory cortex. *J Neurosci*, *32*(5), 1643-1652. https://doi.org/10.1523/JNEUROSCI.4480-11.2012
Xu, B., Ho, Y., Fasolino, M., Medina, J., O'Brien, W. T., Lamonica, J. M., Nugent, E., Brodkin, E. S., Fuccillo, M. V., Bucan, M., & Zhou, Z. (2023). Allelic contribution of Nrxn1α to autism-relevant behavioral phenotypes in mice. *PLOS Genetics*, *19*(2), e1010659. https://doi.org/10.1371/journal.pgen.1010659
Xu, M., Song, P., Huang, W., He, R., He, Y., Zhou, X., Gu, Y., Pan, S., & Hu, Y. (2018). Disruption of AT-hook 1 domain in MeCP2 protein caused behavioral abnormality in mice. *Biochim Biophys Acta Mol Basis Dis*, *1864*(2), 347-358. https://doi.org/10.1016/j.bbadis.2017.10.022
Xu, Y., Ye, H., Shen, Y., Xu, Q., Zhu, L., Liu, J., & Wu, J. Y. (2011). Dscam mutation leads to hydrocephalus and decreased motor function. *Protein Cell*, *2*(8), 647-655. https://doi.org/10.1007/s13238-011-1072-8

Yang, G., Pan, F., & Gan, W. B. (2009). Stably maintained dendritic spines are associated with lifelong memories. *Nature*, *462*(7275), 920-924. https://doi.org/10.1038/nature08577

Yang, M., Bozdagi, O., Scattoni, M. L., Wöhr, M., Roullet, F. I., Katz, A. M., Abrams, D. N., Kalikhman, D., Simon, H., Woldeyohannes, L., Zhang, J. Y., Harris, M. J., Saxena, R., Silverman, J. L., Buxbaum, J. D., & Crawley, J. N. (2012). Reduced Excitatory Neurotransmission and Mild Autism-Relevant Phenotypes in Adolescent Shank3 Null Mutant Mice. *The Journal of Neuroscience*, *32*(19), 6525-6541. https://doi.org/10.1523/jneurosci.6107-11.2012

Yasumura, M., Yoshida, T., Yamazaki, M., Abe, M., Natsume, R., Kanno, K., Uemura, T., Takao, K., Sakimura, K., Kikusui, T., Miyakawa, T., & Mishina, M. (2014). IL1RAPL1 knockout mice show spine density decrease, learning deficiency, hyperactivity and reduced anxiety-like behaviours. *Sci Rep*, *4*, 6613. https://doi.org/10.1038/srep06613

Yin, H. H., Knowlton, B. J., & Balleine, B. W. (2005). Blockade of NMDA receptors in the dorsomedial striatum prevents action-outcome learning in instrumental conditioning. *Eur J Neurosci*, *22*(2), 505-512. https://doi.org/10.1111/j.1460-9568.2005.04219.x

Yin, H. H., Knowlton, B. J., & Balleine, B. W. (2006). Inactivation of dorsolateral striatum enhances sensitivity to changes in the action-outcome contingency in instrumental conditioning. *Behav Brain Res*, *166*(2), 189-196. https://doi.org/10.1016/j.bbr.2005.07.012

Yin, H. H., Mulcare, S. P., Hilário, M. R. F., Clouse, E., Holloway, T., Davis, M. I., Hansson, A. C., Lovinger, D. M., & Costa, R. M. (2009). Dynamic reorganization of striatal circuits during the acquisition and consolidation of a skill. *Nature Neuroscience*, *12*(3), 333-341. https://doi.org/10.1038/nn.2261

Yin, J., Chen, W., Chao, E. S., Soriano, S., Wang, L., Wang, W., Cummock, S. E., Tao, H., Pang, K., Liu, Z., Pereira, F. A., Samaco, R. C., Zoghbi, H. Y., Xue, M., & Schaaf, C. P. (2018). Otud7a Knockout Mice Recapitulate Many Neurological Features of 15q13.3 Microdeletion Syndrome. *Am J Hum Genet*, *102*(2), 296-308. https://doi.org/10.1016/j.ajhg.2018.01.005

Yin, X., Jones, N., Yang, J., Asraoui, N., Mathieu, M. E., Cai, L., & Chen, S. X. (2021). Delayed motor learning in a 16p11.2 deletion mouse model of autism is rescued by locus coeruleus activation. *Nat Neurosci*, *24*(5), 646-657. https://doi.org/10.1038/s41593-021-00815-7

Yoshida, T., Yamagata, A., Imai, A., Kim, J., Izumi, H., Nakashima, S., Shiroshima, T., Maeda, A., Iwasawa-Okamoto, S., Azechi, K., Osaka, F., Saitoh, T., Maenaka, K., Shimada, T., Fukata, Y., Fukata, M., Matsumoto, J., Nishijo, H., Takao, K., . . . Fukai, S. (2021). Canonical versus non-canonical transsynaptic signaling of neuroligin 3 tunes development of sociality in mice. *Nat Commun*, *12*(1), 1848. https://doi.org/10.1038/s41467-021-22059-6

Zampella, C. J., Wang, L. A. L., Haley, M., Hutchinson, A. G., & de Marchena, A. (2021). Motor Skill Differences in Autism Spectrum Disorder: a Clinically Focused Review. *Curr Psychiatry Rep*, *23*(10), 64. https://doi.org/10.1007/s11920-021-01280-6

Zeidan, J., Fombonne, E., Scorah, J., Ibrahim, A., Durkin, M. S., Saxena, S., Yusuf, A., Shih, A., & Elsabbagh, M. (2022). Global prevalence of autism: A systematic review update. *Autism Research*, *15*(5), 778-790. https://doi.org/10.1002/aur.2696

Zhang, Q., Goto, H., Akiyoshi-Nishimura, S., Prosselkov, P., Sano, C., Matsukawa, H., Yaguchi, K., Nakashiba, T., & Itohara, S. (2016). Diversification of behavior and postsynaptic properties by netrin-G presynaptic adhesion family proteins. *Mol Brain*, *9*, 6. https://doi.org/10.1186/s13041-016-0187-5

Zhang, W., Ma, L., Yang, M., Shao, Q., Xu, J., Lu, Z., Zhao, Z., Chen, R., Chai, Y., & Chen, J. F. (2020). Cerebral organoid and mouse models reveal a RAB39b-PI3K-mTOR pathway-dependent dysregulation of cortical development leading to macrocephaly/autism phenotypes. *Genes Dev*, *34*(7-8), 580-597. https://doi.org/10.1101/gad.332494.119

Zhou, Y., Kaiser, T., Monteiro, P., Zhang, X., Van der Goes, M. S., Wang, D., Barak, B., Zeng, M., Li, C., Lu, C., Wells, M., Amaya, A., Nguyen, S., Lewis, M., Sanjana, N., Zhou, Y., Zhang, M., Zhang, F., Fu, Z., & Feng, G. (2016). Mice with Shank3 Mutations Associated with ASD and Schizophrenia Display Both Shared and Distinct Defects. *Neuron*, *89*(1), 147-162. https://doi.org/10.1016/j.neuron.2015.11.023

# Chapter 3: Loss of Tsc1 from striatal direct pathway neurons impairs endocannabinoid-LTD and enhances motor routine learning*

Katherine Cording

Helen Wills Neuroscience Institute
University of California, Berkeley

*The following chapter includes previously published work:
Benthall, K. N.[#], Cording, K. R.[#], Agopyan-Miu, A., Wong, C. D., Chen, E. Y., & Bateup, H.S. (2021). Loss of Tsc1 from striatal direct pathway neurons impairs endocannabinoid-LTD and enhances motor routine learning. *Cell Rep*, *36*(6), 109511. https://doi.org/10.1016/j.celrep.2021.109511 [#]equal contribution

## Introduction

Autism spectrum disorder (ASD) is characterized by social and communication deficits, as well as the presence of restricted and repetitive behaviors (RRBs). Over a hundred genes have been associated with ASD risk (Satterstrom et al., 2020), including genes that cause syndromic disorders, which are associated with a constellation of neurological, psychiatric and medical conditions (Sztainberg & Zoghbi, 2016). One such disorder is Tuberous Sclerosis Complex (TSC), which is caused by mutations in either *TSC1* or *TSC2*. Up to 50% of individuals with TSC are diagnosed with ASD and most have epilepsy and other behavioral or cognitive disorders (Curatolo et al., 2015; Davis et al., 2015). The TSC1 and TSC2 proteins form a complex that negatively regulates the mTORC1 signaling pathway, a central signaling hub controlling cellular metabolic processes such as protein and lipid synthesis and autophagy (Saxton & Sabatini, 2017). When the TSC1/2 complex is disrupted, mTORC1 signaling is constitutively active, leading to excessive cell growth and altered cellular metabolism (Huang & Manning, 2008). Dysregulation of mTORC1 signaling is not limited to TSC but may occur commonly in ASD (de Vries, 2010; Kelleher & Bear, 2008; Tang et al., 2014; Winden et al., 2018).

While epilepsy in TSC likely arises from altered excitability in forebrain circuits, the brain regions and cell types important for ASD-related behaviors are less well understood. We hypothesized that alterations in striatal circuits, which mediate motor learning, action selection, and habit formation, might contribute to the RRBs observed in TSC patients with ASD. Indeed, striatal alterations have been implicated in ASD by structural and functional MRI studies (Di Martino et al., 2011; Qiu et al., 2010; Turner et al., 2006). Further, in a study of TSC children with and without ASD, striatal metabolism was found to differ specifically in those children with ASD and was correlated with the presence of RRBs (Asano et al., 2001).

Mouse studies support the link between striatal alterations and ASD-related behaviors (Fuccillo, 2016; Li & Pozzo-Miller, 2020; Rothwell et al., 2014), showing that mutations in ASD-risk genes can endow the striatum with an enhanced ability to acquire fixed motor routines (Hisaoka et al., 2018; Kwon et al., 2006; Nakatani et al., 2009; Penagarikano et al., 2011; Platt et al., 2017; Rothwell et al., 2014). Changes in striatal synaptic properties have been reported in multiple mouse models with mutations in ASD-risk genes (Fuccillo, 2016; Li & Pozzo-Miller, 2020; Peca et al., 2011; Peixoto et al., 2016). Our group has previously shown input- and cell type-specific changes in synaptic transmission in striatal neurons with postnatal deletion of *Tsc1* (Benthall et al., 2018). Therefore, the goal of this study was to determine whether loss of Tsc1 selectively in striatal neurons is sufficient to alter motor behaviors relevant to ASD.

Striatal function depends on the coordinated activity of two subpopulations of GABAergic principal cells: direct pathway spiny projection neurons (dSPNs) and indirect pathway spiny projection neurons (iSPNs). dSPNs preferentially express D1-type dopamine receptors, while iSPNs express D2-type dopamine receptors and A2A-type adenosine receptors (Gerfen & Surmeier, 2011). dSPNs and iSPNs are distinct in their projection targets, diverging as they leave the striatum to innervate the globus pallidus internal segment (GPi) and substantia nigra pars reticulata (SNr), or the globus pallidus external segment (GPe), respectively (Gerfen & Surmeier, 2011). At the simplest level, bulk activation of dSPNs increases locomotor behavior and action selection while

stimulation of iSPNs inhibits movement (Kravitz et al., 2010; Tai et al., 2012). Coordinated activity between dSPNs and iSPNs allows for the selection of appropriate actions to be performed in a given context, while inappropriate actions are suppressed. Cortical and thalamic inputs make the primary glutamatergic synapses onto dSPNs and iSPNs (Ding et al., 2008; Doig et al., 2010), and modification of the strength of this excitatory drive by long-term synaptic plasticity mediates motor learning and habit formation (Graybiel & Grafton, 2015; Gremel & Lovinger, 2017).

To determine how developmental loss of Tsc1 affects striatal synapses and whether this is sufficient to alter striatal-dependent motor behaviors, we generated mice in which *Tsc1* was selectively deleted from either dSPNs or iSPNs. We find that motor routine learning is selectively enhanced in dSPN-Tsc1 KO mice, which also occurs in mice with global haploinsufficiency of *Tsc2*. Further, we find that *Tsc1* deletion causes a non-cell autonomous enhancement of corticostriatal drive of dSPNs but not iSPNs, which is associated with loss of endocannabinoid-mediated long-term depression (eCB-LTD). Together, these findings demonstrate that increased cortical drive of dSPNs resulting from Tsc1 loss is sufficient to enhance the learning of a fixed motor routine.

**Results**

*Upregulation of mTORC1 and somatic hypertrophy in SPNs with Tsc1 deletion*

To test whether striatal-specific disruption of the Tsc1/2 complex is sufficient to alter motor behaviors, we generated mice with conditional deletion of *Tsc1* from dSPNs or iSPNs (Fig. 1A,B). We used the EY217 *Drd1-Cre* founder line from GENSAT to disrupt *Tsc1* in dSPNs as it has a more striatal-restricted expression profile than the commonly used EY262 line when bred to a Cre-dependent tdTomato reporter (Ai9) (Fig. S1A,B). In preliminary studies, we found that *Tsc1$^{fl/fl}$;Drd1-Cre$^{+}$*(EY262) mice died prematurely, around postnatal day 15. The premature mortality may have been caused by seizures due to cortical Cre expression in this line (Fig. S1B), as loss of Tsc1 from a relatively small percent of cortical neurons is sufficient to induce seizures (Lim et al., 2017). *Tsc1$^{fl/fl}$;Drd1-Cre$^{+}$*(EY217)*;Ai9$^{+/-}$* mice (referred to as dSPN-Tsc1 KO), did not exhibit premature mortality and had only very sparse tdTomato expression in the cortex (Fig. S1C,D), as well as in a small number of cells in the cerebellum (Fig. S1E,F). Notably, Cre expression in *Drd1-Cre*(EY217)*;Ai9* mice was highest in the dorsal striatum, with 40-45% of neurons exhibiting Cre-dependent recombination, whereas less than 8% of neurons in the ventral striatum exhibited Cre recombinase activity (Fig. S2A-E).

To target iSPNs, we used the *Adora2a-Cre* (KG139) GENSAT mouse line as A2A receptors are enriched in iSPNs and exhibit selective expression in the striatum compared to other brain regions (Schiffmann & Vanderhaeghen, 1993). We found that *Adora2a-Cre* induced uniform tdTomato expression throughout the dorsal and ventral striatum in approximately 45% of neurons (Fig. S2F-J). No seizures were observed in *Tsc1$^{fl/fl}$;Adora2a-Cre$^{+}$;Ai9$^{+/-}$* mice (referred to as iSPN-Tsc1 KO).

To confirm that Tsc1 deletion upregulated mTORC1 signaling in dSPNs and iSPNs, we quantified the phosphorylation of ribosomal protein S6, which is a commonly used read-out of mTORC1 activity. Loss of Tsc1 caused a gene dose-sensitive increase in p-S6 levels in dorsal striatal dSPNs and iSPNs, indicating mTORC1 pathway hyperactivity in both cell types (Fig. 1C-G and J-N). Prior studies have demonstrated

pronounced somatic hypertrophy in Tsc1 KO neurons in various brain regions, consistent with the known role of mTORC1 in regulating cell size (Bateup et al., 2011; Feliciano et al., 2011; Kosillo et al., 2019; Malik et al., 2019; Normand et al., 2013; Tavazoie et al., 2005; Tsai et al., 2012). However, in the striatum, we observed a relatively modest increase in soma volume in dSPN- and iSPN-Tsc1 KO mice (Fig. 1H,I and O,P). dSPN-Tsc1 Het neurons had a small increase in soma volume compared to wild-type (WT) while iSPN-Tsc1 Het neurons had slightly reduced soma volume (Fig. 1H,O). Together these results show that complete loss of Tsc1 from SPNs results in robust activation of mTORC1 signaling leading to moderate somatic hypertrophy. Heterozygous loss of Tsc1 mildly increases mTORC1 activity in dSPNs and iSPNs but does not strongly affect soma size.

*Loss of Tsc1 from dSPNs but not iSPNs enhances motor routine learning*

To determine whether SPN-specific loss of Tsc1 was sufficient to alter motor behaviors, we investigated general locomotor activity and self-grooming behavior in the open field. We found no significant differences in the total distance traveled, number of rears, or grooming bouts in dSPN- or iSPN-Tsc1 Het or KO mice compared to controls (Fig. S3A-F). These results suggest that loss of Tsc1 from a single SPN subtype is not sufficient to alter gross motor behaviors or induce spontaneous stereotypies. A summary of the behavior test results by genotype and sex are shown in Supplemental Table 1.

The accelerating rotarod is a striatal-dependent motor learning assay (Yin et al., 2009) is altered in multiple mouse models with mutations in ASD-risk genes (Fuccillo, 2016). In this test, mice learn to run on a rod revolving at increasing speed over four days of training with three trials performed each day (Rothwell et al., 2014). Over the course of training, mice develop a stereotyped motor routine to stay on the apparatus for increasing amounts of time and thus reach higher terminal velocities on later trials. We found that dSPN-Tsc1 Het and KO mice had similar initial rotarod performance as WT littermates on the first trial, reflecting normal baseline motor coordination (Fig. 2A,B). However, dSPN-Tsc1 KO mice exhibited significantly enhanced motor learning measured by the slope of performance from the first to last trial for each mouse, compared to littermate controls (Fig. 2C). dSPN-Tsc1 Het animals also displayed a mild enhancement of motor learning consistent with a gene dose-dependent effect (Fig. 2A). The enhancement in rotarod performance was most pronounced for the more challenging 10-80 rpm acceleration trials. Across these trials (trials #7-12), 72% and 70% of dSPN-Tsc1 Het and KO mice, respectively, displayed continued improvement indicated by a positive slope of their learning curve (Fig. 2D). This contrasted with the ~ 50% of dSPN-Tsc1 WT mice that showed improvement across trials 7-12, reflecting a near ceiling level of performance by trial 7 (Fig. 2D). These results were unlikely to be driven by changes in weight as this was not significantly different between genotypes (dSPN-Tsc1 WT male = 34.55 +/- 2.42g, Het male = 33.11 +/- 1.65g, KO male = 29.20 +/- 1.35g, p=0.3453, Kruskal-Wallis test; dSPN-Tsc1 WT female = 31.30 +/- 1.99g, Het female = 26.50 +/- 1.22g, KO female = 25.44 +/- 1.77g; p=0.0910, Kruskal- Wallis test). Further, we found that weight was not strongly correlated with rotarod learning rate for either sex (Fig. S3G,H). We examined rotarod performance in mice with loss of Tsc1 in iSPNs and strikingly we found no difference in either initial motor performance, learning

rate, or performance on the 10-80 rpm trials between genotypes (Fig. 2E-H). Together these results show that loss of Tsc1 from dSPNs, but not iSPNs, leads to enhanced motor routine learning.

To rule out that the motor learning phenotype in dSPN-Tsc1 KO mice was an anomaly due to cell type-specific loss of Tsc1, we tested mice that were heterozygous for a germline loss-of-function mutation in *Tsc2* (Onda et al., 1999). Heterozygous mice were used as germline homozygous deletion of *Tsc2* is embryonic lethal (Onda et al., 1999). Similar to dSPN-Tsc1 KO mice, *Tsc2*$^{+/-}$ mice had normal initial motor performance but exhibited a significant increase in learning rate compared to WT littermates that became apparent in the more challenging trials of the test (Fig. 2I-L). Again, this was not likely due to a change in weight as this was not significantly different between genotypes (Tsc2 WT male = 27.41 +/- 0.63g vs Tsc2 Het male = 25.45 +/- 0.47g, p=0.0637, Mann-Whitney test; Tsc2 WT female = 19.53 +/- 0.55g vs Tsc2 Het female = 19.53 +/- 0.65g; p=0.9989, unpaired t-test). These findings demonstrate that increased motor learning can be induced by even partial disruption of the Tsc1/2 complex and that loss of Tsc1 from dSPNs alone is sufficient to drive this change.

*Loss of Tsc1 increases cortical drive of dSPNs*

Motor learning relies on corticostriatal transmission, therefore, changes in SPN response to cortical activity could account for enhanced motor routine acquisition in dSPN-Tsc1 KO mice. To test this, we crossed the *Tsc1;Drd1-Cre;Ai9* and *Tsc1;Adora2a-Cre;Ai9* mice to the *Thy1-ChR2-YFP* mouse line, which expresses channelrhodopsin (ChR2-YFP) in a subset of cortical layer V pyramidal cells (Arenkiel et al., 2007) (Fig. 3A). To simulate a train of cortical inputs, we applied ten light pulses over the recording site in dorsolateral striatum and recorded responses in SPNs in the absence of any synaptic blockers (Fig. 3B). By varying the intensity of cortical stimulation, either subthreshold depolarizations or action potentials (APs) could be elicited with a given probability. We quantified the percentage of stimuli that evoked APs at different light intensities and found that cortical terminal stimulation resulted in significantly increased spike probability in dSPN-Tsc1 KO cells compared to WT (Fig. 3C,D and Fig. S4). Notably, loss of one copy of Tsc1 in dSPNs was sufficient to increase corticostriatal drive as dSPN-Tsc1 Het neurons also showed enhanced cortically-driven spiking (Fig. 3C,D).

We performed the cortical stimulation experiment in iSPNs and found that WT iSPNs were more readily driven to spike than dSPNs, consistent with their increased intrinsic excitability (Benthall et al., 2018; Gertler et al., 2008). Therefore, we reduced the length of the light pulse to avoid saturating the response. Interestingly, the number of cortically-driven APs in iSPNs was not different between genotypes at any light intensity (Fig. 3E,F). These results are consistent with the behavioral results and demonstrate that deletion of *Tsc1* has a selective impact on dSPNs, while iSPNs are remarkably unaffected.

*Increased cortico-dSPN excitability results from enhanced synaptic transmission*

Given that dSPN-Tsc1 Het and KO neurons exhibited a clear enhancement of corticostriatal excitability that was not observed in iSPNs, we further analyzed dSPNs to investigate the potential mechanism for this change. Enhanced cortical drive of dSPN-

Tsc1 Het and KO neurons could result from increased intrinsic membrane excitability, increased synaptic excitation, or both. To test if changes in intrinsic excitability occurred in dSPN-Tsc1 KO neurons, we injected positive current and measured the number of APs fired as a function of current step amplitude. The input-output curve for dSPN-Tsc1 KO cells was shifted slightly to the right relative to dSPN-Tsc1 WT and Het neurons, indicating a small decrease in intrinsic membrane excitability (Fig. 3G,H).

Intrinsic hypoexcitability has been observed in other neuron types with Tsc1 loss (Bateup et al., 2013; Kosillo et al., 2019; Normand et al., 2013; Tsai et al., 2012; Yang et al., 2012) and may result from changes in cell size, which impact passive membrane properties. However, we did not observe significant changes in membrane resistance or capacitance in dSPN-Tsc1 Het or KO cells (Fig. S5A,B), which may reflect the relatively small changes in soma size in SPNs (see Fig. 1). Since changes in intrinsic properties could not account for the enhanced corticostriatal excitability observed in dSPNs, we measured synaptic excitability by recording AMPA receptor (AMPAR)-mediated excitatory post-synaptic currents (EPSCs) evoked by optical stimulation of cortical terminals. We observed significantly larger EPSCs in dSPN- Tsc1 Het and KO cells compared to WT, particularly at higher light intensities (Fig. 3I,J). When we measured the ratio of AMPAR currents recorded at -70 mV to NMDAR currents recorded at +40 mV (with 5% light power), we found no significant differences among genotypes (Fig. 3K,L). These results suggest a general enhancement of excitatory synaptic transmission onto Tsc1 KO dSPNs rather than a selective potentiation of AMPAR-mediated responses.

To investigate the specific synaptic properties that were altered in dSPN-Tsc1 KO and Het neurons, we recorded miniature excitatory post-synaptic currents (mEPSCs) at six weeks of age and found a small increase in the amplitude and large increase in the frequency of mEPSCs onto dSPN-Tsc1 KO cells compared to WT (Fig. 4A-C). A significant increase in mEPSC frequency was also observed in dSPN-Tsc1 Het cells (Fig. 4C). To determine the developmental timing of these changes, we recorded mEPSCs in dSPN-Tsc1 WT and KO neurons at 2, 3 and 4 weeks of age. We found that the increased mEPSC amplitude and frequency in dSPN-Tsc1 KO neurons did not emerge until 4 weeks of age, a time when corticostriatal circuits are maturing and becoming refined (Kuo & Liu, 2019; Peixoto et al., 2016) (Fig. S5C,D). Thus, loss of Tsc1 may not affect the initial development of excitatory synapses but could affect their activity-dependent refinement. Consistent with a lack of cortico- iSPN excitability change, no significant changes in mEPSC amplitude or frequency were observed in iSPN-Tsc1 Het or KO cells at six weeks of age (Fig. 4D-F).

While changes in mEPSC amplitude usually reflect increased post-synaptic AMPAR content, increased mEPSC frequency can result from a greater number of synaptic contacts or a change in presynaptic release probability. To measure synapse number, we sparsely labeled dSPNs in the dorsal striatum using an AAV expressing Cre-dependent tdTomato. We imaged and reconstructed individual dSPNs and quantified the density of dendritic spines, which are the sites of corticostriatal synapses onto SPNs. We found that dSPN-Tsc1 KO neurons had equivalent spine density to dSPN-Tsc1 WT cells (Fig. 4G-K), suggesting that the increased mEPSC frequency was due to a change in presynaptic release probability. To investigate this, we measured the paired pulse ratio (PPR) of AMPAR currents evoked by two electrical stimuli delivered

50 ms apart. The stimulating electrode was placed in or just above the corpus callosum to preferentially activate cortical inputs (Assous et al., 2019; Ding et al., 2008). We found a significant decrease in PPR in dSPN-Tsc1 KO cells compared to WT, consistent with increased presynaptic release probability of cortical inputs onto dSPNs (Fig. 4L).

*Endocannabinoid-mediated long-term depression is impaired in dSPN-Tsc1 KO neurons*

One mechanism that could explain enhanced presynaptic corticostriatal transmission onto dSPN-Tsc1 KO neurons is a loss of long-term depression (LTD), which would render cells unable to depress excitatory inputs. Corticostriatal terminals express CB1 receptors that mediate endocannabinoid-LTD (eCB-LTD), a prominent form of striatal synaptic depression (Kreitzer & Malenka, 2008; Lovinger, 2010). Upon coincident activation of group 1 metabotropic glutamate receptors (mGluR1/5) and L-type calcium channels, SPNs release the endocannabinoids anandamide (AEA) or 2-arachidonoylglycerol (2-AG), which act as retrograde signals that activate presynaptic CB1Rs to decrease corticostriatal release probability (Luscher & Huber, 2010). It was previously thought that eCB-LTD occurs primarily in iSPNs (Kreitzer & Malenka, 2007), but recent studies using selective stimulation of corticostriatal terminals have revealed eCB-LTD in both SPN subtypes (Wu et al., 2015). Since another form of mGluR-dependent LTD expressed in the hippocampus is impaired in multiple TSC mouse models (Auerbach et al., 2011; Bateup et al., 2011; Chevere-Torres et al., 2012; Potter et al., 2013), and selective disruption of 2-AG release from dSPNs causes increased glutamatergic transmission (Shonesy et al., 2018), we reasoned that loss of eCB-LTD could occur in dSPNs with *Tsc1* deletion.

We induced eCB-LTD in dSPNs with wash-on of the group 1 mGluR agonist DHPG and monitored the amplitude of EPSCs in response to optogenetic stimulation of cortical terminals in the dorsolateral striatum. Stimulation strength was adjusted for each cell to evoke 500-700 pA currents during the baseline period. While dSPN-Tsc1 WT neurons showed a long-lasting synaptic depression to ~79% of baseline levels, eCB-LTD did not consistently occur in dSPN- Tsc1 KO neurons, which exhibited only a small initial reduction in EPSC amplitude during DHPG application that was not maintained (Fig. 5A). dSPN-Tsc1 Het cells exhibited an intermediate level of eCB-LTD (Fig. S6A), consistent with their intermediate increase in mEPSC frequency and corticostriatal drive (see Figs. 3 and 4). To ensure that the protocol was inducing eCB-dependent LTD, we washed on DHPG in the presence of AM-251, a CB1R antagonist, and found that LTD was blocked in control dSPNs (Fig. S6B). The deficit in eCB-LTD in Tsc1-KO dSPNs could not be explained by a difference in presynaptic CB1R function, as direct activation of CB1Rs with the agonist WIN-2 depressed corticostriatal EPSCs to a similar extent in Tsc1 KO and WT dSPNs (Fig. 5B).

To investigate a potential molecular basis for the loss of eCB-LTD in Tsc1 KO dSPNs, we performed translating ribosome affinity purification (TRAP) to assess the translational status of mRNAs encoding key proteins involved in eCB-LTD. To do this, we engineered an AAV to express a Cre-dependent GFP-tagged ribosomal protein (EGFP-L10a) and injected this into the dorsal striatum of *Drd1-Cre*$^{+}$ mice that were WT or homozygous floxed for Tsc1 (Fig. 6A,B). This approach enabled selective expression of EGFP-L10a in dSPNs (Fig. 6C) and isolation of ribosome-bound mRNAs from dSPNs using TRAP (Heiman et al., 2014; Heiman et al., 2008). We verified the specificity of this

approach using qPCR to quantify the relative levels of *Drd1* (D1 receptor) and *Drd2* (D2 receptor) mRNA in the TRAP samples compared to the unbound samples, which include RNA from all striatal cell types. As expected, *Drd1* mRNA was significantly enriched in the TRAP samples from both dSPN-Tsc1 WT and dSPN-Tsc1 KO mice compared to the unbound samples (Fig. 6D). Accordingly, *Drd2* mRNA was depleted from the TRAP samples, demonstrating preferential isolation of mRNA from dSPNs (Fig. 6E).

We compared the relative expression levels of mRNAs encoding proteins required for eCB-LTD including the two types of group 1 mGluRs (*Grm1* and *Grm5*), the requisite mGluR scaffold protein Homer 1 (*Homer1*), and phospholipase C beta (*Plcb1*), which promotes the formation of diacylglycerol that is subsequently converted to 2-AG by diacylglycerol lipase (Ohno-Shosaku & Kano, 2014). We also compared the levels of ribosome-bound *Drd1* as a control. We found that dSPN-Tsc1 KO mice had increased amounts of total ribosome-bound mRNA (0.0518 +/- 0.0077 vs 0.0313 +/- 0.0031 ratio of TRAP-isolated mRNA to unbound RNA in dSPN KO vs WT mice, p=0.0138, unpaired t-test), consistent with a global increase in protein synthesis resulting from high mTORC1 activity. However, all four components of the eCB-LTD pathway showed a relative reduction in ribosome-bound mRNA levels in dSPN-Tsc1 KO mice compared to WT when normalized to *Actb* (B-Actin) (Fig. 6F-I). Notably, levels of *Drd1* mRNA were not significantly different between genotypes (Fig. 6J). The amount of ribosome-bound mRNA is generally thought to reflect translation efficiency (Gobet & Naef, 2017), therefore these results suggest a relative downregulation in the translation of multiple mRNAs encoding proteins required for eCB-LTD. Such decreased expression may contribute to the lack of functional eCB-LTD in Tsc1 KO dSPNs.

## Figures

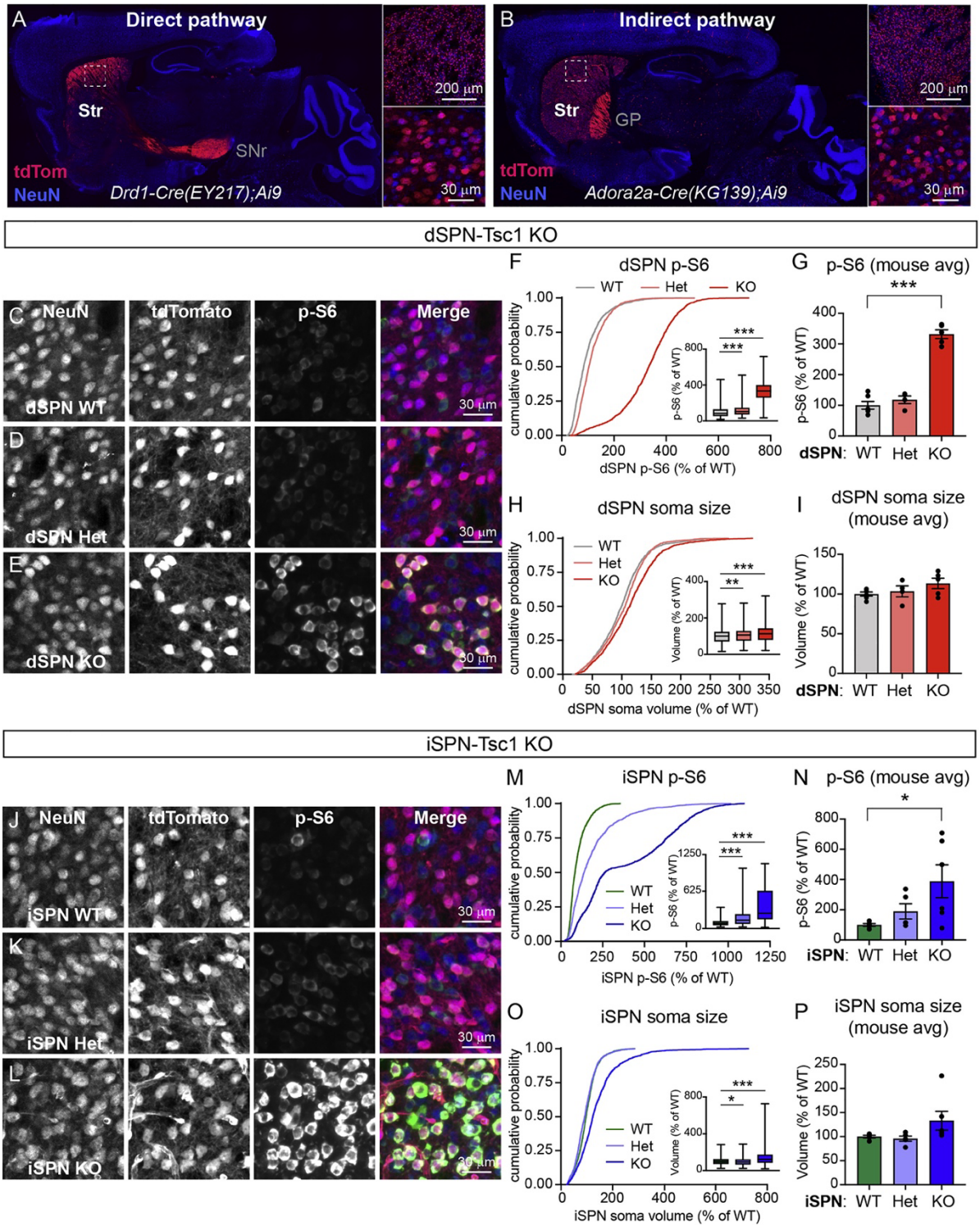


**Figure 1. Developmental loss of Tsc1 from striatal projection neurons induces mTORC1 activation.**

(A-B) Images of sagittal brain sections showing the expression patterns of a tdTomato Cre reporter (red) in a *Drd1-Cre*$^{+}$*;Ai9*$^{+/-}$ mouse (EY217 GENSAT founder line, A) and an

*Adora2a-Cre*$^{+}$*;Ai9*$^{+/-}$ mouse (KG139 GENSAT founder line, B). Right panels show higher magnification images of the dorsal striatum (boxed regions). Neurons are labeled in blue using an anti-NeuN antibody. Str=striatum, SNr=substantia nigra pars reticulata, GP=globus pallidus

(C-E) Confocal images of dorsolateral striatum from a dSPN-Tsc1 WT (C), Tsc1 Het (D), and Tsc1 KO (E) mouse labeled with antibodies against phosphorylated S6 (p-S6, Ser240/244, green in the merged image) and NeuN (blue in the merged image). TdTomato (red in the merged imaged) is expressed in dSPNs.

(F) Cumulative distributions of dSPN p-S6 fluorescence intensity per cell, expressed as a percentage of wild-type (WT). 1800 cells from 6 dSPN-Tsc1 WT mice, 1200 cells from 4 dSPN- Tsc1 Het mice, and 1500 cells from 5 dSPN-Tsc1 KO mice were analyzed. Inset box plots display the 25-75%-ile p-S6 per cell by genotype (line at the median, whiskers = min to max). $p<0.0001$, Kruskal-Wallis test; WT vs Het, ***, $p<0.0001$; WT vs KO, ***, $p<0.0001$, Dunn's multiple comparisons test.

(G) Bar graphs display the mean +/- SEM p-S6 level per mouse for each genotype (calculated from the data in F). Dots represent values for individual mice. $p<0.0001$, $F(2, 12)=0.1553$, one- way ANOVA; WT vs Het, $p=0.3701$; WT vs KO, ***, $p<0.0001$, Holm-Sidak's multiple comparisons test.

(H) Cumulative distributions of dSPN soma volume per cell, measured from the same cells as in panel F, expressed as a percentage of wild-type (WT). Inset box plots display the 25-75%-ile soma volume per cell by genotype (line at the median, whiskers = min to max). $p<0.0001$, Kruskal- Wallis test; WT vs Het, **, $p=0.0071$; WT vs KO, ***, $p<0.0001$, Dunn's multiple comparisons test.

(I) Bar graphs display the mean +/- SEM soma volume per mouse for each genotype (calculated from the data in H). Dots represent values for individual mice. $p=0.1927$, $F(2,12)=1.030$, one-way ANOVA.

(J-L) Confocal images of dorsolateral striatum from an iSPN-Tsc1 WT (J), Tsc1 Het (K), and Tsc1 KO (L) mouse labeled with antibodies against phosphorylated S6 (p-S6, Ser240/244, green in the merged image) and NeuN (blue in the merged image). TdTomato (red in the merged imaged) is expressed in iSPNs.

(M) Cumulative distributions of iSPN p-S6 fluorescence intensity per cell, expressed as a percentage of wild-type (WT). 1500 cells from 5 iSPN-Tsc1 WT mice, 1500 cells from 5 iSPN- Tsc1 Het mice, and 1800 cells from 6 iSPN-Tsc1 KO mice were analyzed. Inset box plots display the 25-75%-ile p-S6 per cell by genotype (line at the median, whiskers = min to max). $p<0.0001$, Kruskal-Wallis test; WT vs Het, ***, $p<0.0001$; WT vs KO, ***, $p<0.0001$, Dunn's multiple comparisons test.

(N) Bar graphs display the mean +/- SEM p-S6 level per mouse for each genotype (calculated from the data in M). Dots represent values for individual mice. $p=0.0481$, $F(2, 13)=10.59$, one- way ANOVA; WT vs Het, $p=0.4393$; WT vs KO, *, $p=0.0368$, Holm-Sidak's multiple comparisons test.

(O) Cumulative distributions of iSPN soma volume per cell, measured from the same cells as in panel M, expressed as a percentage of wild-type (WT). Inset box plots display the 25-75%-ile soma volume per cell by genotype (line at the median, whiskers = min to max). $p<0.0001$, Kruskal-Wallis test; WT vs Het, *, $p=0.0142$; WT vs KO, ***, $p<0.0001$, Dunn's multiple comparisons test.

(P) Bar graphs display the mean +/- SEM soma volume per mouse for each genotype (calculated from the data in O). Dots represent values for individual mice. p=0.0242, Kruskal- Wallis test; WT vs Het, p>0.9999; WT vs KO, p=0.0687, Dunn's multiple comparisons test. See also Figures S1 and S2.

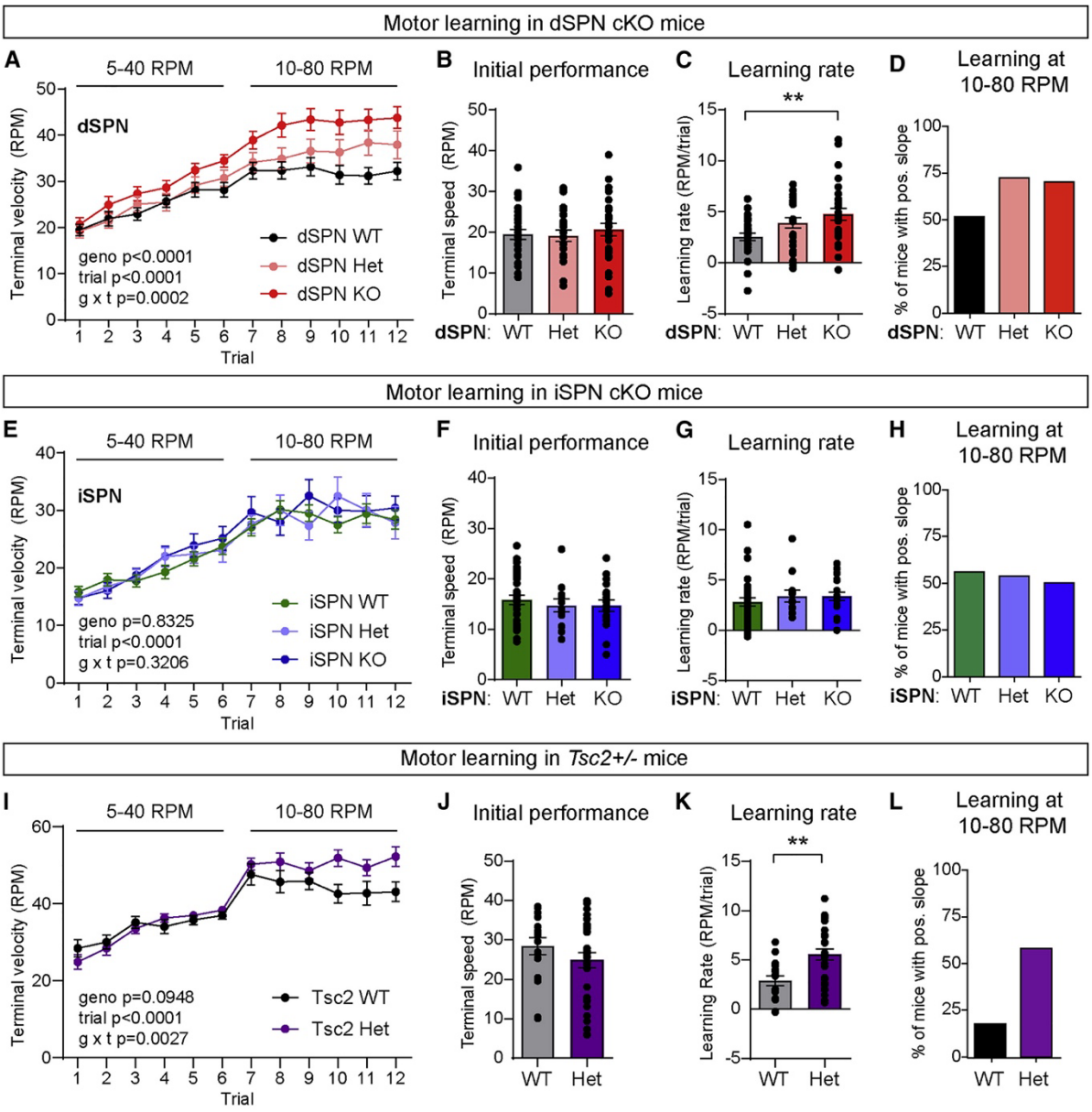


**Figure 2. Mutations in Tsc1 or Tsc2 enhance motor routine learning.**
(A) Accelerating rotarod learning curve across 12 trials (4 days) in dSPN-Tsc1 WT (n=30), Het (n=25), and KO (n=29) mice. Circles represent mean +/- SEM. Repeated measures two-way ANOVA p values are shown; geno F (4, 110)=7.034, trial F (5.092, 560.1)=105.8, g x t F (44, 120)=1.987. RPM = revolutions per minute.
(B) Rotarod performance on trial 1 for dSPN-Tsc1 WT, Het and KO mice quantified as terminal speed. Bars represent mean +/- SEM. Dots represent values for individual mice (n is the same as in panel A). p=0.7233, Kruskal-Wallis test.
(C) Overall learning rate of dSPN-Tsc1 WT, Het and KO mice calculated as the slope of the line of performance on the first trial (1) to the last trial (12) for each mouse (RPM/day). Bars represent mean +/- SEM. Dots represent values for individual mice (n is the same as in panel A). p=0.0120, Kruskal-Wallis test; dSPN WT vs KO, **, p=0.0071; dSPN WT vs Het, p=0.1170, Dunn's multiple comparisons test.

(D) Percentage of dSPN-Tsc1 WT, Het, and KO mice with a positive learning curve (slope of performance) from trial 7 to trial 12 (10-80 RPM acceleration).
(E) Accelerating rotarod learning curve across 12 trials (4 days) in iSPN-Tsc1 WT (n=34), Het (n=13), and KO (n=18) mice. Dots represent mean +/- SEM. Repeated measures two-way ANOVA p values are shown; geno F (2, 62)=0.1839, trial F (4.935, 306)=52.73, g x t F (22, 682)=1.118.
(F) Rotarod performance on trial 1 for iSPN-Tsc1 WT, Het, and KO mice quantified as terminal speed. Bars represent mean +/- SEM. Dots represent individual mice (n is the same as in panel E). p=0.6737, Kruskal-Wallis test.
(G) Overall learning rate of iSPN-Tsc1 WT, Het and KO mice calculated as the slope of the line of performance on the first trial to the last trial for individual mice (RPM/day). Bars represent mean +/- SEM. Dots represent individual mice (n is the same as in panel E). p=0.2761, Kruskal- Wallis test.
(H) Percentage of iSPN-Tsc1 WT, Het, and KO mice with a positive learning curve (slope of performance) from trial 7 to trial 12 (10-80 RPM acceleration).
(I) Accelerating rotarod learning curve across 12 trials (4 days) in global *Tsc2* WT (n=17) and *Tsc2* Het (n=31) mice. Circles represent mean +/- SEM. Repeated measures two-way ANOVA p values are shown; geno F (1, 46)=2.910, trial F (5.997, 275.9)=40.22, g x t F (11, 506)=2.639.
(J) Rotarod performance on trial 1 for *Tsc2* WT and Het mice quantified as terminal speed. Bars represent mean +/- SEM. Dots represent individual mice (n is the same as in panel I). p=0.2533, two-tailed unpaired t-test.
(K) Overall learning rate of *Tsc2* WT and Het mice calculated as the slope of the line of performance on the first trial to the last trial for individual mice (RPM/day). Bars represent mean
+/- SEM. Dots represent individual mice (n is the same as in panel I). **, p=0.0057, Mann- Whitney test.
(L) Percentage of *Tsc2* WT and Het mice with a positive learning curve (slope of performance) from trial 7 to trial 12 (10-80 RPM acceleration).
See also Figure S3 and Table S1.

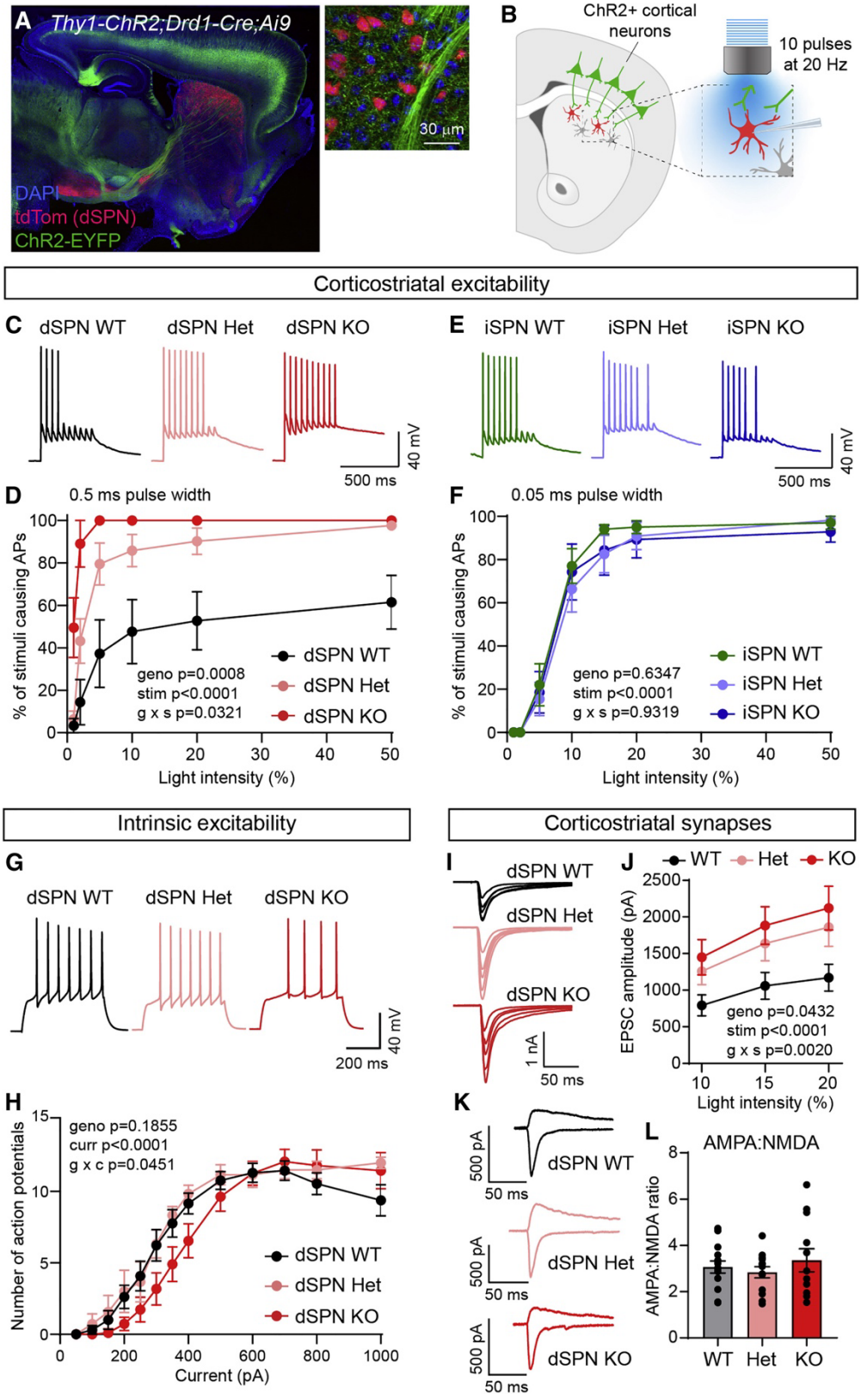
A
Thy1-ChR2;Drd1-Cre;Ai9
30 μm
DAPI
tdTom (dSPN)
ChR2-EYFP
B
ChR2+ cortical neurons
10 pulses at 20 Hz
Corticostriatal excitability
C
dSPN WT
dSPN Het
dSPN KO
40 mV
500 ms
D
0.5 ms pulse width
% of stimuli causing APs
geno p=0.0008
stim p<0.0001
g x s p=0.0321
dSPN WT
dSPN Het
dSPN KO
Light intensity (%)
E
iSPN WT
iSPN Het
iSPN KO
40 mV
500 ms
F
0.05 ms pulse width
% of stimuli causing APs
geno p=0.6347
stim p<0.0001
g x s p=0.9319
iSPN WT
iSPN Het
iSPN KO
Light intensity (%)
Intrinsic excitability
G
dSPN WT
dSPN Het
dSPN KO
40 mV
200 ms
H
Number of action potentials
geno p=0.1855
curr p<0.0001
g x c p=0.0451
dSPN WT
dSPN Het
dSPN KO
Current (pA)
Corticostriatal synapses
I
dSPN WT
dSPN Het
dSPN KO
1 nA
50 ms
J
WT
Het
KO
EPSC amplitude (pA)
geno p=0.0432
stim p<0.0001
g x s p=0.0020
Light intensity (%)
K
500 pA
50 ms
dSPN WT
dSPN Het
dSPN KO
L
AMPA:NMDA
AMPA:NMDA ratio
WT
Het
KO

**Figure 3. Tsc1 loss selectively increases cortico-dSPN synaptic drive.**
(A) Confocal image of a sagittal brain section from a *Tsc1$^{wt/fl}$;Thy1-ChR2-EYFP$^{+}$;Drd1-Cre$^{+}$;Ai9$^{+/-}$* mouse. Right image shows cortical terminals expressing ChR2-EYFP (green) in the dorsal striatum. tdTomato (red) labels dSPNs. DAPI stained nuclei are in blue.
(B) Schematic of the experiment. Cortical terminals expressing ChR2 were stimulated with 10 pulses of blue light at 20 Hz and responses were recorded from dSPNs in dorsolateral striatum.
(C) Example traces of action potentials (AP) in dSPNs evoked by cortical terminal stimulation at 10% light intensity for the indicated genotypes.
(D) Quantification (mean +/- SEM) of the percentage of cortical terminal stimuli that evoked APs in dSPNs. dSPN-Tsc1 WT n=5 neurons from 2 mice, dSPN Het n=7 neurons from 2 mice, dSPN KO n=5 neurons from 2 mice. Mixed-effects model (REML) p values are shown; geno F (2, 14)=12.25, stim F (2.125, 26.35)=45.79, g x s (10, 62)=2.164.
(E) Example traces of APs in iSPNs evoked by cortical terminal stimulation at 10% light intensity for the indicated genotypes.
(F) Quantification (mean +/- SEM) of the percentage of cortical terminal stimuli that evoked APs in iSPNs. iSPN-Tsc1 WT n=10 neurons from 3 mice, iSPN Het n=10 neurons from 3 mice, iSPN KO n=7 neurons from 3 mice. Repeated measures two-way ANOVA p values are shown; geno F (2, 24)=0.4633, stim F (2.464, 59.13)=198.6, g x s F (12, 144)=0.4655.
(G) Example traces of APs in dSPNs evoked by a 350 pA current step for the indicated genotypes.
(H) Quantification of the number of APs induced by depolarizing current steps in dSPN-Tsc1 WT, Het and KO neurons. Circles represent mean +/- SEM. dSPN WT n=13 neurons from 3 mice, dSPN Het n=6 neurons from 2 mice, dSPN KO n=11 neurons from 3 mice. Mixed-effects model (REML) p values are shown; geno F (2, 27)=1.794, curr F (2.2127, 57.08)=95.26, g x c F (24, 322)=1.572.
(I) Example traces show EPSCs induced by optogenetic corticostriatal stimulation at different light intensities (5-20%) in dSPN-Tsc1 WT, Het and KO neurons.
(J) Quantification (mean +/- SEM) of corticostriatal EPSC amplitude in dSPN-Tsc1 WT, Het and KO neurons induced by different light intensities (0.5 ms pulse width). dSPN-Tsc1 WT n=18 neurons from 8 mice, dSPN Het n=7 neurons from 3 mice, dSPN KO n=22 neurons from 10 mice. Repeated measures two-way ANOVA p values are shown; geno F (2, 44)=3.376, stim F (1.590, 69.98)=119.4, g x s F (4, 88)=4.597.
(K) Example traces show pairs of EPSCs evoked by optogenetic corticostriatal stimulation (5% light intensity) recorded at +40 mV (top traces) and -70 mV (bottom traces) from dSPN-Tsc1 WT, Het and KO neurons.
(L) Quantification of AMPA:NMDA ratio per cell in dSPN-Tsc1 WT, Het and KO neurons evoked by 5% light stimulation. Bars represent mean +/- SEM. Dots represent values for individual neurons. dSPN-Tsc1 WT n=14 neurons from 8 mice, dSPN Het n=13 neurons from 5 mice, dSPN KO n=12 neurons from 8 mice. p=0.5765, F (2, 36)= 2.759, one-way ANOVA. See also Figure S4 and S5.

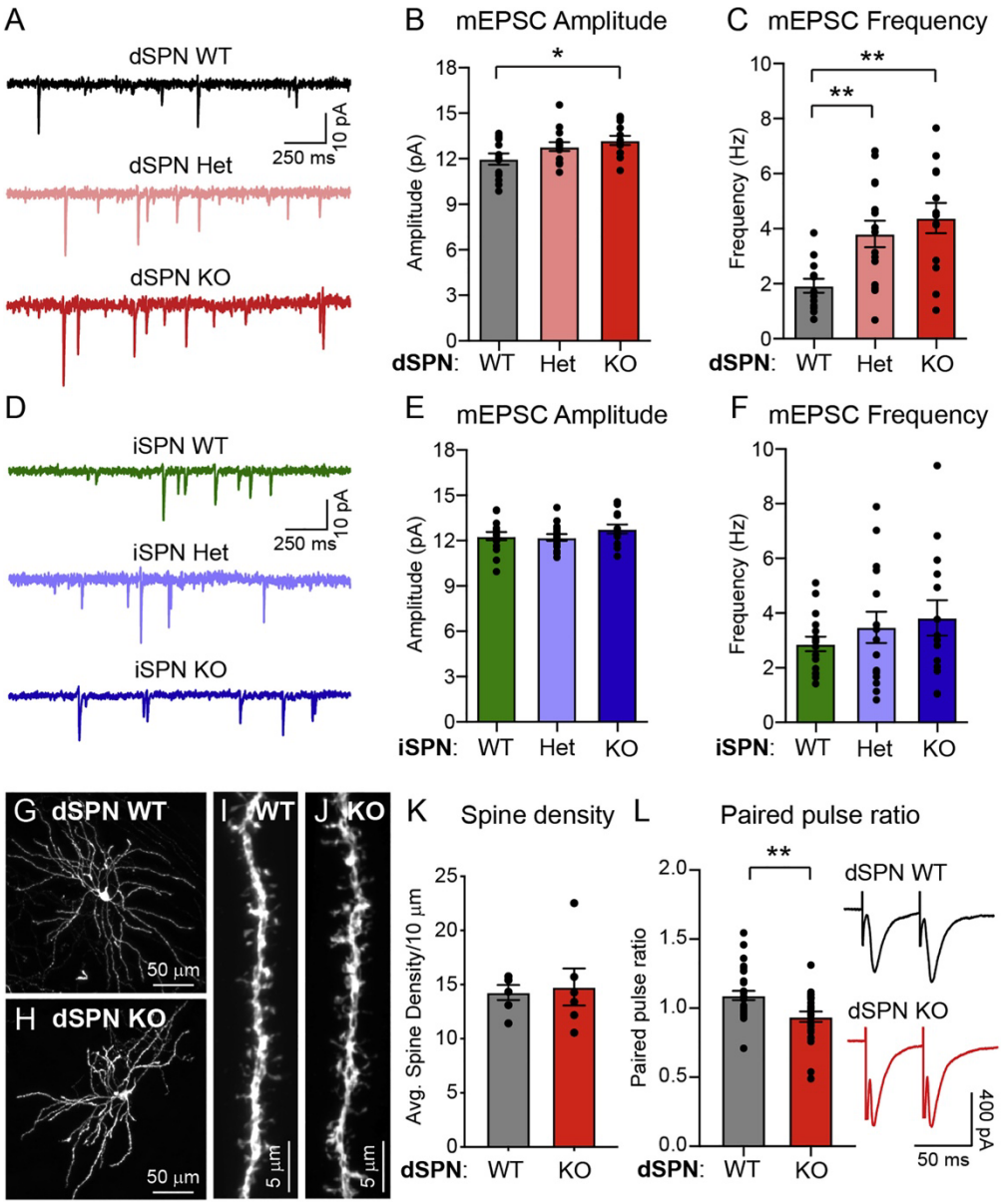


**Figure 4. Loss of Tsc1 increases excitatory synaptic transmission onto dSPNs.**
(A) Example traces of miniature excitatory post-synaptic currents (mEPSCs) recorded from dSPN-Tsc1 WT, Het and KO neurons.
(B-C) Mean +/- SEM mEPSC amplitude (B) and frequency (C) recorded from dSPN-Tsc1 WT, Het and KO neurons. Dots represent individual neurons. For panel B, p=0.0337, F (2, 38)=3.712, one-way ANOVA; p=0.0766 (dSPN WT vs Het), *, p=0.0217 (dSPN WT vs KO), Holm-Sidak's multiple comparisons tests. For panel C, p=0.0014, F (2, 38)=7.822, one-way ANOVA; **, p=0.0049 (dSPN WT vs Het), **, p=0.0011 (dSPN WT vs KO), Holm-Sidak's multiple comparisons tests. For both B and C, dSPN WT n=13 neurons from 3 mice, dSPN Het n=15 neurons from 3 mice, dSPN KO n=13 neurons from 3 mice.
(D) Example traces of mEPSCs recorded from iSPN-Tsc1 WT, Het and KO neurons.

(E-F) Mean +/- SEM mEPSC amplitude (E) and frequency (F) recorded from iSPN-Tsc1 WT, Het and KO neurons. Dots represent individual neurons. For panel E, p=0.2942, F (2, 42)=1.260, one-way ANOVA. For panel F, p=0.4083, F (2, 42)=0.9151, one-way ANOVA. For both E and F, iSPN WT n=16 neurons from 3 mice, iSPN Het n=15 neurons from 3 mice, iSPN KO n=14 neurons from 3 mice.
(G-H) Confocal images of individual Tsc1 WT (G) and KO (H) dSPNs labeled with tdTomato. (I-J) Representative images of dendritic spines from a Tsc1 WT (I) and KO (J) dSPN.
(K) Quantification (mean +/- SEM) of dendritic spine density per 10 μm of dendrite in Tsc1 WT and KO dSPNs. Dots represent the average spine density for individual neurons. dSPN WT n=6 neurons (12 dendrites) from 3 mice, dSPN KO n=6 neurons (13 dendrites) from 3 mice. p=0.8182, Mann-Whitney test.
(L) Electrical stimulation (50 ms ISI) was used to evoke pairs of excitatory synaptic currents in Tsc1 WT and KO dSPNs. Paired pulse ratio (PPR) was measured as the amplitude of the second response divided by the first response. Bars represent mean +/- SEM, dots represent individual neurons. dSPN WT n=28 neurons from 10 mice, dSPN KO n=24 neurons from 9 mice. **, p=0.0038, two-tailed unpaired t test. See also Figure S5.

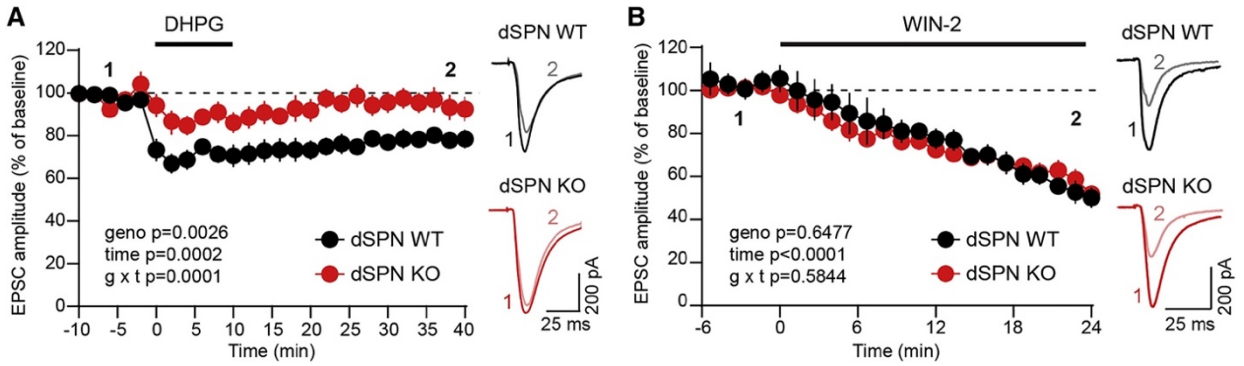


**Figure 5. dSPN-Tsc1 KO neurons have impaired eCB-LTD.**

(A) Corticostriatal terminals in the dorsolateral striatum were stimulated with blue light to evoke EPSCs in dSPN-Tsc1 WT and KO neurons DHPG (100 μM) was washed on for 10 minutes to induce eCB-LTD. Data are presented as mean +/- SEM percent of baseline (dashed line). Repeated measures two-way ANOVA p values are shown; geno $F(1, 10)=15.93$, time $F(3.479, 34.79)=7.993$, g x t $F(25, 250)=2.563$. dSPN WT n=7 neurons from 3 mice, dSPN KO n=5 neurons from 4 mice. Example traces on the right show the average EPSCs from the baseline period ("1") and 35-40 minutes after DHPG application ("2") for each genotype.

(B) Corticostriatal terminals were stimulated with blue light to evoke EPSCs in dSPN-Tsc1 WT and KO neurons. WIN-2 (2 μM) was applied at time 0 to activate CB1 receptors. Data are presented as mean +/- SEM percent of baseline (dashed line). Mixed-effects model (REML) p values are shown; geno $F(1, 4)=0.2433$, time $F(2.410, 9.641)=29.36$, g x t $F(1.551, 4.329)=0.5214$. dSPN WT n=5 neurons from 4 mice, dSPN KO n=4 neurons from 3 mice. Example traces on the right show the average EPSC from the last 5 minutes of the baseline period ("1") and 19-24 minutes after WIN-2 application ("2"). See also Figure S6.

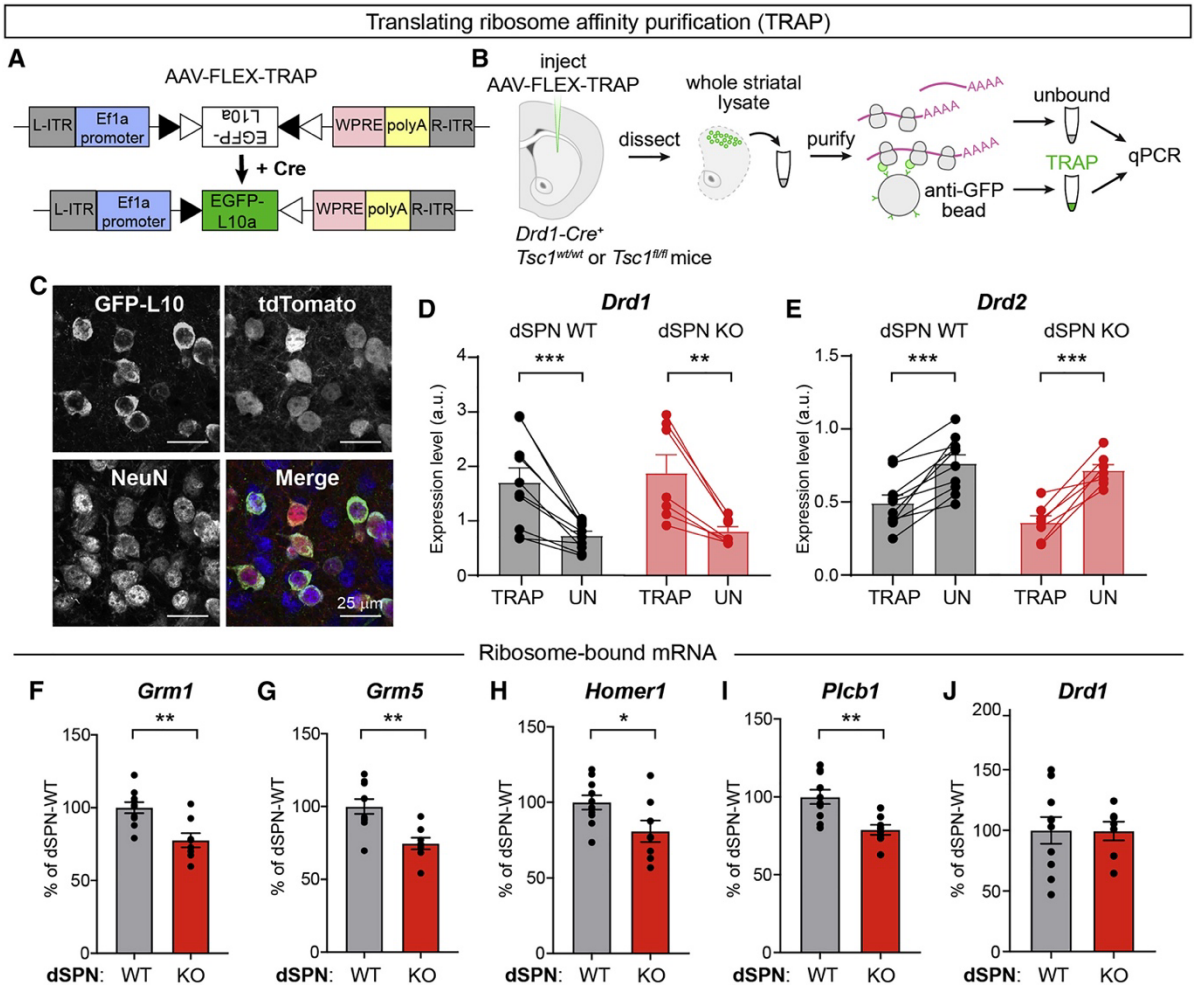


**Figure 6. dSPN Tsc1 KO cells exhibit reduced ribosome engagement of mRNAs involved in mGluR-eCB signaling.**

(A) Schematic of the design of AAV-FLEX-TRAP, which allows Cre-dependent expression of a GFP-tagged ribosomal subunit (EGFP-L10a).

(B) Schematic of the workflow for the Translational Ribosome Affinity Purification (TRAP) experiment.

(C) Images of EGFP-L10a expression from an AAV5-hSyn-DIO-EGFP-L10a injection into the dorsolateral striatum of a *Tsc1*$^{wt/wt}$*;Drd1-Cre*$^{+}$*;Ai9*$^{+/-}$ mouse showing expression in tdTomato$^{+}$ dSPNs. In the merged image, EGFP-L10 is in green, tdTomato is in red, and anti-NeuN is in blue to label neurons.

(D-E) Quantification of relative *Drd1* (D) and *Drd2* (E) mRNA levels in TRAP samples (ribosome bound mRNA isolated from dSPNs) versus the unbound ("UN", all striatal tissue) from the same mouse measured by qPCR. Bars represent mean +/- SEM. Dots represent individual samples, taken from one mouse. For panel D, ***, p=0.0009 (dSPN WT); **, p=0.0053 (dSPN KO), paired t-tests. For panel E, ***, p=0.0003 (dSPN WT); ***, p=0.0007 (dSPN KO), paired t-tests. For panels D and E, dSPN-Tsc1 WT n=10 and dSPN-Tsc1 KO n=7 mice.

(F-J) Quantification of *Grm1* (F), *Grm5* (G), *Homer1* (H), *Plcb1* (I), and *Drd1* (J) mRNA levels in TRAP samples (ribosome bound mRNA isolated from dSPNs) relative to *Actb*

from dSPN-Tsc1 WT and KO mice measured by qPCR. Bars represent mean +/- SEM and dots represent individual mice. For panel F, **, p=0.0022; panel G, **, p=0.0018; panel H, *, p=0.0346; panel I, **, p=0.0025; panel J, p=0.9702; two-tailed unpaired t-tests. For all panels, dSPN-Tsc1 WT n=10 and dSPN-Tsc1 KO n=8 mice (except for Drd1, dSPN KO n=7 mice).

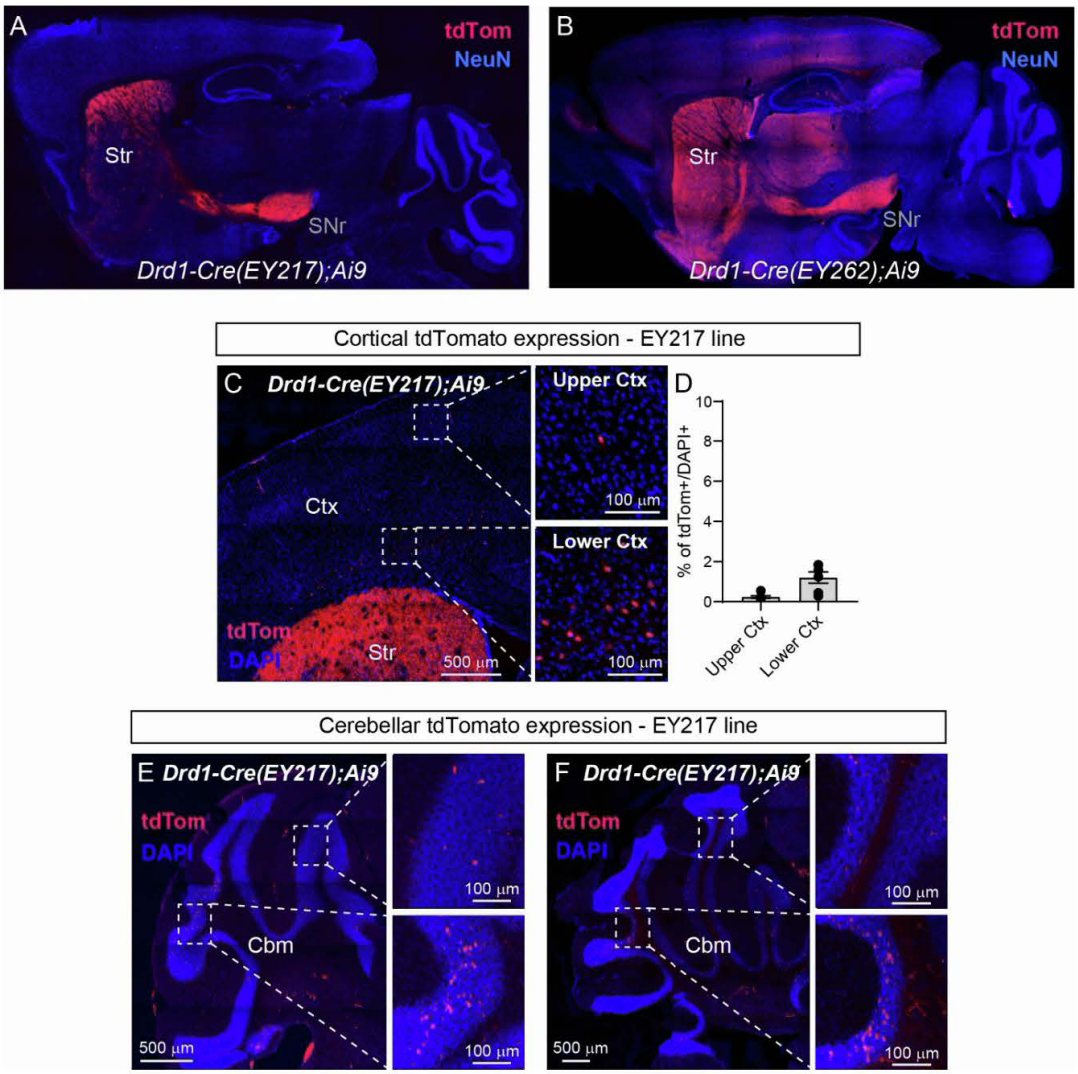


**Supplementary figure 1. Cre-mediated recombination in *Drd1-Cre;Ai9* mice. Related to Figure 1.**

(A-B) Images of sagittal brain sections showing the Cre-dependent tdTomato (red) expression pattern of a *Drd1-Cre(EY217);Ai9* mouse (A) and a *Drd1-Cre(EY262);Ai9* mouse (B). NeuN immunostaining (blue) labels neurons. Note the striatal-restricted tdTomato expression in the EY217 line with axon terminals in the SNr. Str=striatum, SNr=substantia nigra pars reticulata.

(C) Left panel shows an image of the motor cortex (Ctx) and dorsal striatum (Str) with tdTomato (red) expression in a sparse population of cortical cells. DAPI labeled nuclei are in blue. Right panels show higher magnification images of the boxed regions in the left panel.

(D) Quantification (mean +/- SEM) of the percentage of tdTomato+ cells/DAPI+ cells in the upper and lower layers of the cortex in *Drd1-Cre(EY217);Ai9* mice (n=2 sections from 3 mice).

(E,F) Images of tdTomato expression in a sparse population of cells in the cerebellar granule cell layer. Examples from two different mice are shown. Cbm=cerebellum. Right panels show higher magnification images of the boxed regions.

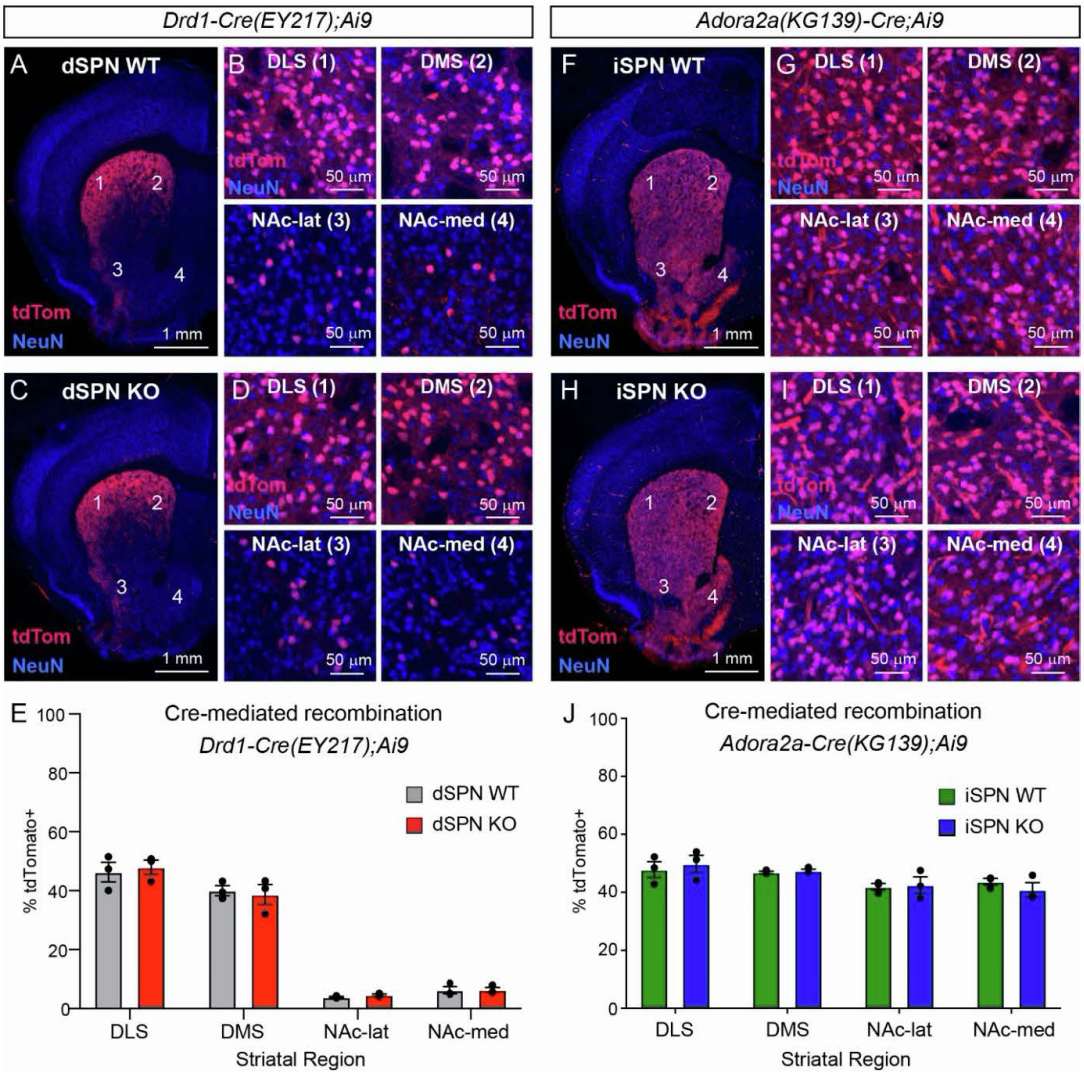


**Supplementary figure 2. Cre-mediated recombination in the striatum of *Drd1-Cre;Ai9* and *Adora2a-Cre;Ai9* mice. Related to Figure 1.**

(A-D) Confocal images of coronal brain sections showing Cre-dependent tdTomato expression (red) in a *Tsc1*$^{wt/wt}$*;Drd1-Cre*$^{+}$*;Ai9*$^{+}$ mouse (A,B) and a *Tsc1*$^{fl/fl}$*;Drd1-Cre*$^{+}$*;Ai9*$^{+}$ mouse (C,D). NeuN immunostaining is in blue. Higher magnification images (B,D) show region-specific expression patterns in the dorsolateral striatum (DLS, site #1), dorsomedial striatum (DMS, site #2), nucleus accumbens lateral shell (NAc-lat, site #3), and nucleus accumbens medial shell (NAc-med, site #4).

(E) Quantification of tdTomato regional expression patterns in *Tsc1*$^{wt/wt}$*;Drd1-Cre*$^{+}$*;Ai9*$^{+}$ and *Tsc1*$^{fl/fl}$*;Drd1-Cre*$^{+}$*;Ai9*$^{+}$ mice. Bars represent mean +/- SEM and dots represent individual mice. Shown is the percentage of NeuN+ cells that are tdTomato+ in a given striatal region. n=3 mice per genotype.

(F-I) Confocal images of coronal brain sections showing Cre-dependent tdTomato expression (red) in a *Tsc1*$^{wt/wt}$*;Adora2a-Cre*$^{+}$*;Ai9*$^{+}$ mouse (F,G) and a *Tsc1*$^{fl/fl}$*;Adora2a-Cre*$^{+}$*;Ai9*$^{+}$ mouse (H,I). Higher magnification images (G,I) show region- specific expression patterns.

(J) Quantification of tdTomato regional expression patterns in *Tsc1*$^{wt/wt}$*;Adora2a-Cre*$^{+}$*;Ai9*$^{+}$ and *Tsc1*$^{fl/fl}$*;Adora2a-Cre*$^{+}$*;Ai9*$^{+}$ mice. Bars represent mean +/- SEM and dots represent individual mice. Shown is the percentage of NeuN+ cells that are tdTomato+ in a given striatal region. n=3 mice per genotype.

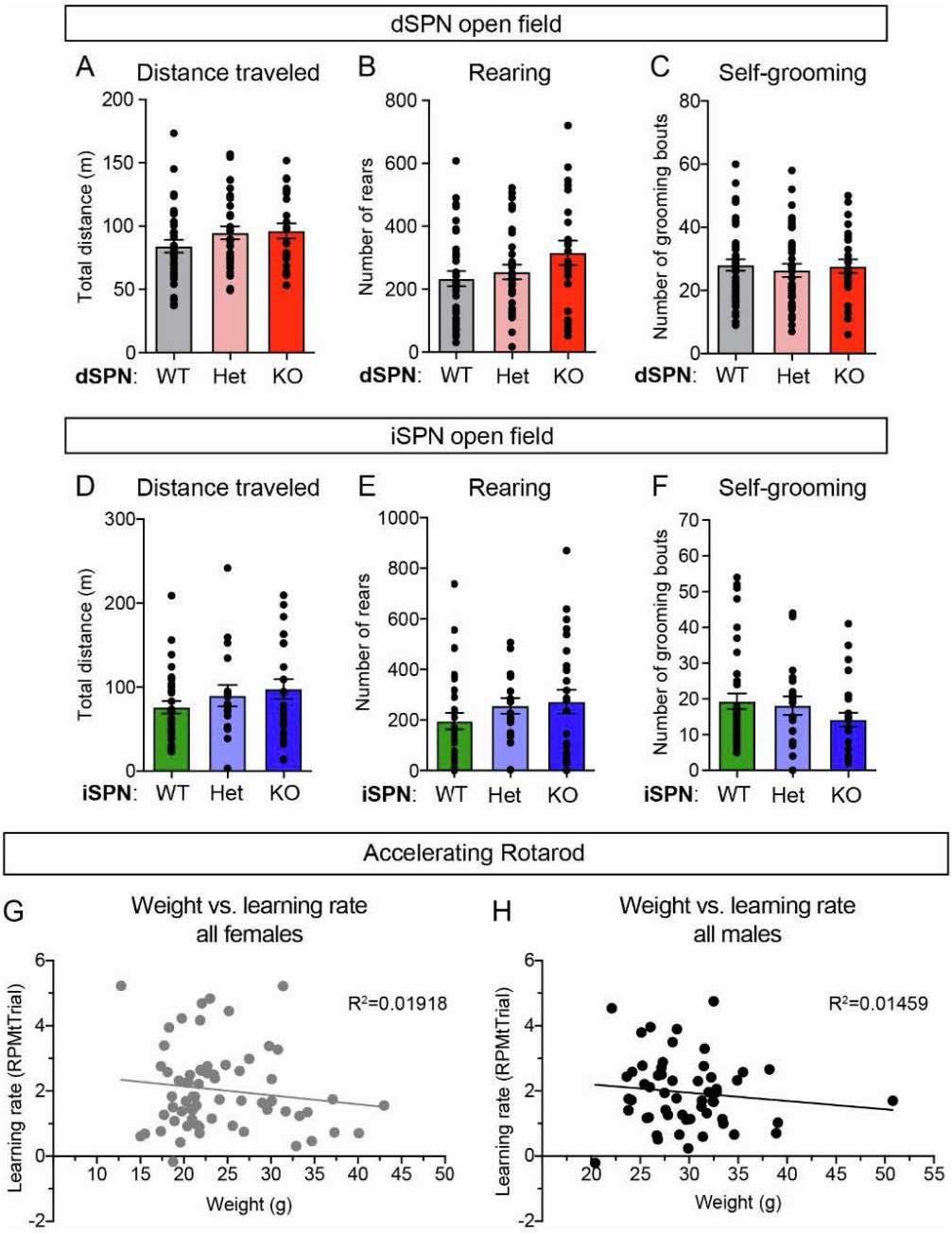


**Supplementary figure 3. Open field behavior results and additional rotarod analysis. Related to Figure 2.**

(A-C) Quantification of open field parameters in dSPN Tsc1-WT, Het, and KO mice. Distance traveled (A) is the total distance traveled in the open field over 60 minutes. Rearing (B) is the number of rears in 60 minutes. Self-grooming (C) is the number of grooming bouts in the first 20 minutes of the open field test. Bars represent mean +/- SEM. Dots represent individual mice. For panels A and B, n=36 dSPN-WT, 32 dSPN-Het, and 23 dSPN-KO mice. For panel C, n=44 dSPN-WT, 37 dSPN-Het, and 26 dSPN-KO mice. For panel A, p=0.2006, Kruskal-Wallis test; panel B, p=0.1252, F (2, 88)=2.128, one-way ANOVA; panel C, p=0.8112, F (2, 104)=0.2097, one-way ANOVA.

(D-F) Quantification of open field parameters in iSPN Tsc1-WT, Het, and KO mice. Bars represent mean +/- SEM. Dots represent individual mice. For panels D and E, n=32 iSPN-WT, 18 iSPN-Het, and 25 iSPN-KO mice. For panel F, n=40 iSPN-WT, 20 iSPN-Het, and 29 iSPN-KO mice. For panel D, p=0.4028, Kruskal-Wallis test; panel E, p=0.2367, Kruskal-Wallis test; panel F, p=0.2497, Kruskal-Wallis test.
(G-H) Graphs show the relationship between weight in grams (g) and overall learning rate on the rotarod test for individual female (G) and male (H) mice of all genotypes. Learning rate was calculated as the slope of the line of performance from trial 1 to trial 12. There was not a significant relationship between weight and rotarod learning rate for females (Linear regression analysis, p=0.2674, F (1, 64)=1.252, n=66 mice) or males (Linear regression analysis, p=0.3796, F (1, 53)=0.7849, n=55 mice). Mice from all strains (dSPN-Tsc1, iSPN-Tsc1, and Tsc2) and genotypes were pooled for this analysis.

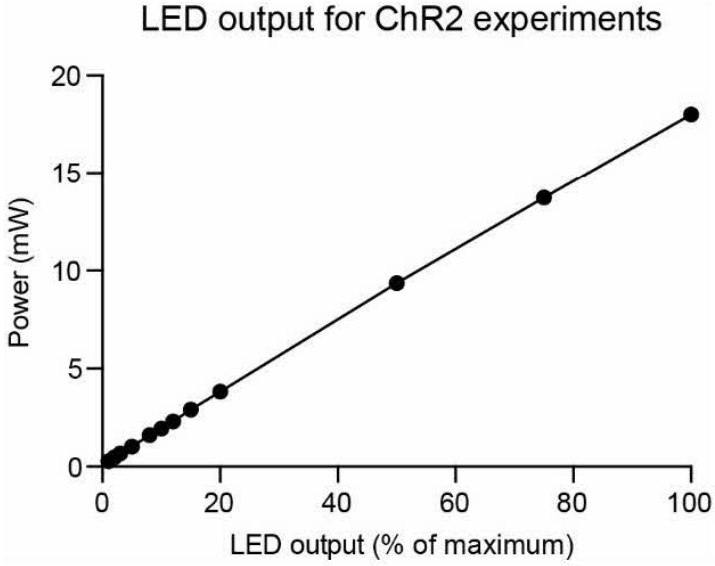


**Supplementary figure 4. Light power plotted as a function of LED output. Related to Figure 3.**
470 nm light power measured under the microscope objective showed a linear relationship with LED output.

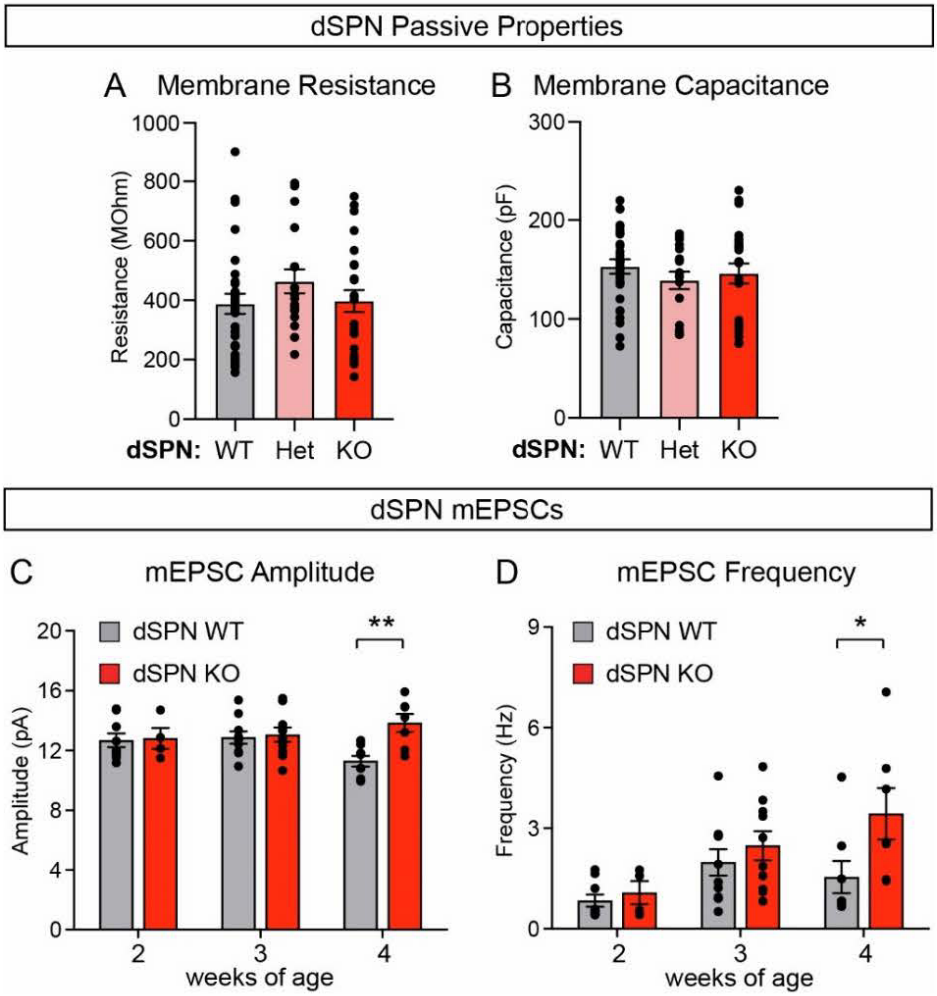


**Supplementary figure 5. dSPN passive membrane properties and mEPSCs across early postnatal development. Related to Figures 3 and 4.**

(A-B) Mean +/- SEM membrane resistance (Rm, A) and capacitance (Cm, B) of Tsc1-WT, Het and KO dSPNs from voltage clamp recordings. Dots represent values for individual neurons. dSPN WT n=29 neurons from 10 mice, dSPN Het n=18 neurons from 6 mice, dSPN KO n=24 neurons from 9 mice. Rm, p=0.2585, Kruskal-Wallis test; Cm, p=0.6018, Kruskal-Wallis test.

(C-D) Mean +/- SEM mEPSC amplitude (C) and frequency (D) recorded from dSPN Tsc1-WT and KO neurons at 2, 3 or 4 weeks of age. Dots represent values for individual neurons. Two weeks: n=9 dSPN WT neurons from 1 mouse and 4 dSPN KO neurons from 1 mouse. Three weeks: n=10 dSPN WT neurons from 2 mice and 10 dSPN KO neurons from 2 mice. Four weeks: n=8 dSPN WT neurons from 2 mice and 7 dSPN KO neurons from 2 mice. Comparisons were made between dSPN-WT and KO neurons at each developmental age. For panel C, 2 weeks, p=0.8252, Mann-Whitney test, 3 weeks, p=0.7741, unpaired t-test; 4 weeks, **, p=0.0093, Mann-Whitney test. For panel D; 2 weeks, p=0.7105, Mann-Whitney test; 3 weeks, p=0.4045, unpaired t-test; 4 weeks, *, p=0.0289, Mann-Whitney test.

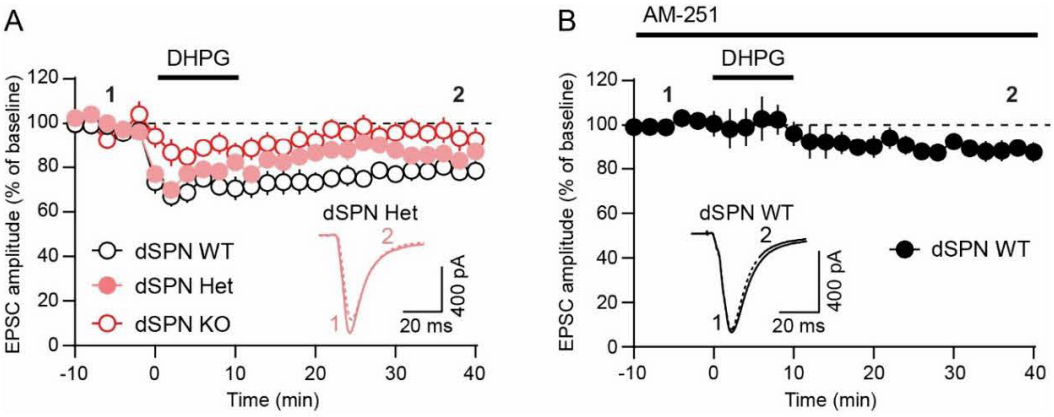


**Supplementary figure 6. eCB-LTD in dSPNs. Related to Figure 5.**
(A) Cortical terminals were stimulated with blue light (30s ISI) in striatal slices from *Tsc1*$^{wt/fl}$*;D1-Cre*$^{+}$*;Thy1-ChR2*$^{+}$*;Ai9*$^{+/-}$ mice to evoke EPSCs in dSPNs. eCB-LTD was induced by 10-minute bath application of the mGluR1/5 agonist DHPG (100 μM). EPSC amplitude was monitored and expressed as a percent of baseline levels and plotted versus time (mean +/- SEM). n=9 dSPN Tsc1-Het neurons from 7 mice. For reference, the dSPN WT and KO data are replotted from the analysis in Fig. 5A (open circles). Dashed line indicates 100% of baseline. Example traces show the average EPSC from the baseline period ("1", solid line) and 35-40 minutes after DHPG application ("2", dashed line) for a representative dSPN Tsc1-Het neuron.
(B) Cortical terminals were stimulated with blue light (30s ISI) in striatal slices from *Tsc1*$^{wt/wt}$*;D1-Cre*$^{+}$*;Thy1-ChR2*$^{+}$*;Ai9*$^{+/-}$ mice to evoke EPSCs in Tsc1 WT dSPNs. The CB1 receptor antagonist AM-251 (10 μM) was bath applied throughout the recording. Following a 10-minute baseline period, DHPG (100 μM) was washed on for 10 minutes. EPSC amplitude was monitored and expressed as a percent of baseline levels and plotted versus time (mean +/- SEM). n=5 neurons from 5 mice. Example traces show the average EPSC from the baseline period ("1", solid line) and 35-40 minutes after DHPG application ("2", dashed line) for a representative dSPN Tsc1-WT neuron.

## Discussion

In this study we tested whether cell type-specific deletion of *Tsc1* from striatal neurons was sufficient to alter synaptic function and motor behaviors. We found that in both direct and indirect pathway SPNs, developmental loss of *Tsc1* upregulated mTORC1 signaling and modestly increased soma size. However, we found that mTORC1 activation in dSPNs, but not iSPNs, enhanced motor routine learning in the absence of spontaneous stereotypies or locomotor hyperactivity. Further, we found that loss of Tsc1 from dSPNs was associated with increased corticostriatal synaptic excitability and an impairment in eCB-LTD. Notably, loss of one copy of *Tsc1* was sufficient to increase cortical drive of dSPNs and enhance motor learning. These findings implicate the striatal direct pathway as a possible driver of altered motor behaviors in TSC.

It has been shown that loss of Tsc1 in either the cerebellum or thalamus is sufficient to cause social behavior deficits and spontaneous RRBs including repetitive self-grooming (Normand et al., 2013; Tsai et al., 2012). Given the central role of the striatum in action selection and motor learning, we hypothesized that alterations in striatal circuits might also contribute to altered motor behaviors in mouse models of TSC. Indeed, siRNA-mediated knock-down of *Tsc1* in the dorsal striatum has been shown to induce behavioral changes (Lee et al., 2018). Here we found that mice with loss of Tsc1 in dorsal striatal dSPNs, but not iSPNs, had enhanced performance on the accelerating rotarod, a motor learning task that relies on corticostriatal transmission (Kupferschmidt et al., 2019; Yin et al., 2009). Previous work has shown that striatal mTORC1 signaling is required for motor learning on the accelerating rotarod, as both pharmacological and genetic intrastriatal inhibition of mTOR signaling impairs rotarod learning (Bergeron et al., 2014). Our results are congruent with these findings and show that increasing mTORC1 activity in dSPNs enhances rotarod performance. Notably, an extended accelerating rotarod task may be necessary to reveal motor learning phenotypes, as *Tsc1* and *Tsc2* heterozygous mice were reported to have no changes in rotarod performance when an abbreviated version of the task was used (Sato et al., 2012).

Performance in the accelerating rotarod task is commonly affected in mice with mutations in ASD-risk genes, as several other genetic ASD mouse models exhibit enhanced rotarod performance (Ahmed et al., 2023; Chadman et al., 2008; Hisaoka et al., 2018; Kwon et al., 2006; Nakatani et al., 2009; Penagarikano et al., 2011; Platt et al., 2017; Rothwell et al., 2014). However, this is not the case for all ASD-risk genes (Portmann et al., 2014; Wang et al., 2016; Yin et al., 2021). Most of the aforementioned mouse models have global gene deletions in which brain regions and circuits outside of the striatum could contribute to the phenotype. However, two studies showed that selectively disrupting *Nlgn3* or *Chd8* in striatal neurons was sufficient to increase rotarod learning (Platt et al., 2017; Rothwell et al., 2014). Moreover, similar to what was observed here, loss of *Nlgn3* from dSPNs alone led to enhanced motor learning, implicating the direct pathway as a key driver of this phenotype (Rothwell et al., 2014). Interestingly, in these studies, ventral striatal disruption of the gene was responsible for the motor learning improvement. Here, deletion of *Tsc1* from dSPNs was largely restricted to the dorsal striatum, and our findings are consistent with literature establishing the dorsal striatum's role in motor learning (Yin et al., 2009). Further studies

will be needed to define the contributions of dorsal versus ventral striatal circuits to motor learning and elucidate the contributions of specific striatal subregions to behavioral changes in TSC mouse models.

While enhanced motor routine learning may be a shared phenotype across multiple mouse models of ASD, the synaptic and cellular mechanisms driving this phenotype may be distinct depending on the specific gene that is altered. dSPN-Nlgn3 KO mice displayed normal excitatory synaptic transmission and eCB-LTD but had a deficit in inhibition (Rothwell et al., 2014). In *Chd8*$^{+/-}$ mice, there was increased spontaneous excitatory transmission onto SPNs; however, the SPN sub-type was not defined (Platt et al., 2017). We found that dSPN-Tsc1 Het and KO cells had strongly enhanced corticostriatal excitation that was due to increased synaptic, but not intrinsic, excitability. The enhanced cortical drive was likely driven by changes in presynaptic function as we found increased release probability and mEPSC frequency in dSPN-Tsc1 KO neurons, consistent with our prior study (Benthall et al., 2018). Given that the cortical inputs were wild-type in our model, a potential explanation for increased release probability is a change in retrograde signaling from dSPNs to cortical terminals. Indeed, we found that eCB-LTD was disrupted in Tsc1 KO dSPNs despite normal presynaptic CB1 receptor function. This suggests that loss of Tsc1 and upregulation of mTORC1 signaling in dSPNs interferes with one or more post-synaptic processes required for this form of plasticity: 1) expression of group 1 mGluRs, 2) signaling downstream of mGluRs, and/or 3) synthesis and release of eCBs. We found that multiple mRNAs encoding proteins required for eCB-LTD exhibited relatively reduced ribosome engagement in dSPN-Tsc1 KO cells compared to WT. Together, this suggests that loss of Tsc1 and deregulation of mTORC1 signaling in dSPNs impairs post-synaptic mGluR signaling via altered expression of key components of this pathway. Notably, striatal eCB-LTD is also disrupted in a mouse model of the neurodevelopmental disorder Fragile X Syndrome and in mice with an ASD-linked R451C *Nlgn3* mutation (Jung et al., 2012; Martella et al., 2018). In both of these mouse models, the phenotypes could be improved by pharmacologically enhancing cannabinoid signaling.

A chronic impairment of eCB-LTD in Tsc1 KO dSPNs may lead to increased glutamatergic transmission over time. In support of this idea, disruption of endocannabinoid synthesis in dSPNs via cell type-specific loss of DAGL$\alpha$, the enzyme required for 2-AG production, is sufficient to cause glutamatergic hyperactivity (Shonesy et al., 2018). Therefore, loss of eCB-LTD may be the primary driving mechanism that leads to increased cortical activation of Tsc1 KO dSPNs. This is consistent with our observation that changes in mEPSC properties in dSPN-Tsc1 KO neurons do not arise until four weeks of age and later. While initial synapse formation may occur normally in Tsc1 KO dSPNs, activity-dependent refinement of cortical synapses, which occurs over the first few weeks of postnatal life (Kuo & Liu, 2019), may be impaired by an inability to depress cortical inputs. Interestingly, the study by Shonesy et al, showed that while disruption of 2-AG signaling in dSPNs led to synaptic and behavioral consequences, loss of DAGL$\alpha$ from iSPNs had no measurable effects on behavior (Shonesy et al., 2018), consistent with the lack of behavior changes reported here for iSPN-Tsc1 KO mice.

Taken together, our results support a model whereby developmental loss of Tsc1 from dSPNs impairs eCB-LTD resulting in unchecked corticostriatal drive. While further

work will be needed to establish a causal link between enhanced cortico-dSPN activity and increased rotarod learning, it is possible that perturbed presynaptic plasticity in Tsc1 KO dSPNs may alter corticostriatal coupling during rotarod training, leading to atypical learning in this paradigm (Kupferschmidt et al., 2019). In terms of autistic behaviors in individuals with TSC, our findings suggest that striatal synaptic and circuit changes, which in mice increases the ability to learn a stereotyped motor routine, could be a contributor to the emergence of restricted, repetitive patterns of behavior.

**Experimental procedures**

Mice

To generate conditional deletion of *Tsc1* in dSPNs, *Tsc1*$^{fl/fl}$ mice (Jackson Laboratory strain #005680 (Kwiatkowski et al., 2002)) of mixed background were crossed with *Drd1a-Cre* (EY217) mice (GENSAT (MMRRC #030778-UCD) (Gong et al., 2007)). To delete *Tsc1* from iSPNs, *Tsc1*$^{fl/fl}$ mice were crossed with *Adora2a-Cre* (KG139) mice (GENSAT (MMRRC #031168-UCD) (Gong et al., 2007)). To identify Cre-expressing neurons, dSPN-Tsc1 KO and iSPN-Tsc1 KO mice were bred to the tdTomato Cre reporter Ai9 mouse line (Jackson Laboratory strain #007909 (Madisen et al., 2010)). To express YFP-tagged ChR2 in a subset of Layer V cortical pyramidal cells, the Thy1-ChR2-YFP mouse line (Jackson Laboratories strain #007612 (Arenkiel et al., 2007)) was bred into each line. *Tsc2*$^{+/-}$ mice (Jackson Laboratory strain #004686 (Onda et al., 1999)) were used for the rotarod experiments.

Mice were group housed on a 12 h light/dark cycle and given ad libitum access to standard rodent chow and water. Both male and female animals were used for experimentation. The ages, sexes, and numbers of mice used for each experiment are indicated in the respective method details and figure legends. All mice used for experiments were heterozygous or hemizygous for the Ai9, Drd1-Cre, Adora2a-Cre, or Thy1-ChR2-YFP transgenes to avoid potential physiological or behavioral alterations.

All animal procedures were conducted in accordance with protocols approved by the University of California, Berkeley Institutional Animal Care and Use Committee (IACUC) and Office of Laboratory Animal Care (OLAC).

Brain sectioning and immunohistochemistry

Adult mice were anesthetized with isoflurane and transcardial perfusion was performed with 10 ml of 1x PBS followed by 10 ml of ice cold 4% PFA in 1x PBS (EMS, 15710-S) and post-fixed in 4% PFA in 1x PBS overnight at 4˚C. 30 µm coronal sections were made using a freezing microtome (American Optical, AO 860) and stored in 1x PBS at 4˚C.

For immunohistochemistry, individual wells of sections were washed with 1x PBS, then blocked for 1 hour at RT with BlockAid blocking solution (Life Tech, B10710). Primary antibodies diluted in PBS-Tx (1x PBS with 0.25% Triton-X-100 (Sigma, T8787)) were added and tissue was incubated for 48 h with gentle shaking at 4˚C. Sections were then washed 3 x 10 min with PBS- Tx. Secondary antibodies diluted 1:500 in PBS-Tx were added and incubated with shaking for 1 h at room temperature. Sections were then washed 3 x 10 min in 1x PB. Sections were mounted onto SuperFrost slides (VWR, 48311-703) and coverslipped with VECTASHIELD HardSet with DAPI (VWR, 101098-050). The following antibodies were used: anti- phosphorylated S6 ribosomal protein (Ser240/244, 1:800, Cell Signaling Technology, 5364S), anti-GFP (1:1000, Abcam, ab13970), anti-NeuN (1:800, Millipore, MAB377), Alexa Fluor 488 and Alexa Fluor 633 conjugated secondary antibodies (1:500, Invitrogen, A-21070 and A- 31553).

Confocal microscopy and image analysis

To analyze p-S6 levels and soma volume, Z-stack images of striatal sections were taken on a confocal microscope (Zeiss LSM 780 AxioExaminer or Olympus FLUOVIEW FV3000) with a 20x objective using the same acquisition settings for each

section. For quantification, cellular regions of interest (ROIs) were automatically created based on the tdTomato signal with the Surfaces module in Imaris software (Oxford Instruments). The mean p-S6 fluorescence intensity per ROI and average soma volume were calculated using Imaris. Values for Tsc1 Het and KO cells were normalized to the average of all wild-type cells imaged in the same batch. To generate cumulative probability plots, 300 cells from each mouse were used (100 or 150 cells per section, 2-3 sections per mouse).

To analyze Cre-mediated recombination patterns in Drd1- and Adora2a-Cre;Ai9 mice, Z-stack images of cortex, cerebellum, dorsolateral striatum, dorsomedial striatum, nucleus accumbens lateral shell, and nucleus accumbens medial shell were taken on a confocal microscope (Olympus FLUOVIEW FV3000) with a 20x objective. For quantification, ROIs were manually defined in ImageJ for all NeuN positive cells (for striatum and nucleus accumbens) or automatically created based on the DAPI signal with the Surfaces module in Imaris software (for cortex) and used to determine co-localization with the Cre-dependent tdTomato signal.

To analyze AAV-FLEX-TRAP (EGFP-L10a) expression, Z-stack images of dorsal striatum were taken on a confocal microscope (Olympus FLUOVIEW FV3000) with a 20x objective. For quantification, ROIs were manually defined in ImageJ for all GFP positive cells and used to verify co-localization with the Cre-dependent tdTomato signal. 85-93% of EGFP-L10a positive cells in the dorsal striatum were tdTomato positive.

Dendritic imaging and spine analysis

Neonatal (P1-4) dSPN-Tsc1 KO mice were cryoanesthetized and injected bilaterally with 200 nL AAV9.CAG.Flex.tdTomato.WPRE.bGH (Penn Vector Core, AllenInstitute864), diluted 1:500 to achieve sparse transduction. Injections were targeted to the dorsal striatum, with coordinates approximately 1.2 mm lateral to midline, 2.0 mm posterior to bregma, and 1.5 mm ventral to the head surface. At age P40-50, mice were perfused and brains were post-fixed with 4% paraformaldehyde, then sectioned at 80 µm. Sections were blocked for 1 hr at RT in BlockAid (ThermoFisher, B10710) and incubated for 48 hr at 4°C with an antibody against RFP (1:1000, Rockland (VWR), RL600-401-379). Sections were washed 3 x 10 min in PBS-Tx and incubated for 1 hr at RT with Alexa Fluor 546 secondary antibody (1:500, Invitrogen, A-11035). Sections were washed 3 x 10 min in PBS and mounted onto slides using VECTASHIELD HardSet with DAPI (VWR, 101098-050). Z-stack images of individual dendrites were taken on a confocal microscope (Zeiss LSM 880 NLO AxioExaminer) with a 63x objective using Airyscan. To quantify spine density, dendrites and spines were reconstructed using the FilamentTracer module in Imaris software (Oxford Instruments). The spine density of each dendrite was calculated using Imaris. Spine density analysis was initially separated into the first 40 µm of the dendrite (proximal) and the final 40 µm of the dendrite (distal). There was no significant difference between proximal and distal spine density within cells or across genotypes. These values were therefore combined and spine density of the entire 80 µm length of dendrite is reported.

Behavioral analysis

Behavior studies were carried out in the dark phase of the light cycle under red lights (open field) or white lights (rotarod). Mice were habituated to the behavior testing room for at least 30 min prior to testing and covered by a black-out curtain. Mice were given at least one day between different tests. All behavior equipment was cleaned between each trial and mouse with 70% ethanol, and additionally rinsed in diluted soap followed by water at the end of the day. If male and female mice were to be tested on the same day, male mice were run first then returned to the husbandry room, after which all equipment was thoroughly cleaned prior to bringing in female mice for habituation. All animals to be tested from a given cage were run in each behavior test in the same day. Behavioral tests were performed with young adult male and female mice (6-10 weeks old). Mice had access to a running wheel in their home cage. The experimenter was blind to genotype throughout the testing and scoring procedures.

*Open field*

Exploratory behavior in a novel environment and general locomotor activity were assessed by a 60 min session in an open field chamber (40 cm L x 40 cm W x 34 cm H) made of transparent plexiglass. Horizontal infrared photobeams were positioned to detect rearing. The mouse was placed in the bottom right hand corner of the arena and behavior was recorded using an overhead camera and analyzed using the ANY-maze (Stoelting Co.) behavior tracking software. An observer manually scored self-grooming behavior during the first 20 minutes of the test. A grooming bout was defined as an unbroken series of grooming movements, including licking of body, paws, or tail, as well as licking of forepaws followed by rubbing of face with paws.

*Rotarod*

The accelerating rotarod test was used to examine motor learning. Mice were trained on a rotarod apparatus (Ugo Basile, 47650) for four consecutive days. Three trials were completed per day with a 5 min break between trials. The rotarod was accelerated from 5-40 revolutions per minute (rpm) over 300 s for trials 1-6 (days 1 and 2), and from 10-80 rpm over 300 s for trials 7-12 (days 3 and 4). On the first testing day, mice were first acclimated to the apparatus by being placed on the rotarod rotating at a constant 5 rpm for 60 s and returned to their home cage for 5 minutes prior to starting trial 1. Latency to fall, or to rotate off the top of the rotarod barrel, was measured by the rotarod stop-trigger timer.

<u>Electrophysiology</u>

Mice (P40-50) were perfused transcardially with ice-cold ACSF (pH=7.4) containing (in mM): 127 NaCl, 25 $NaHCO_3$, 1.25 $NaH_2PO_4$, 2.5 KCl, 1$MgCl_2$, 2 $CaCl_2$, and 25 glucose, bubbled continuously with carbogen (95% $O_2$ and 5% $CO_2$). Brains were rapidly removed and coronal slices (275 μm) were cut on a VT1000S vibratome (Leica) in oxygenated ice-cold choline-based external solution (pH=7.8) containing (in mM): 110 choline chloride, 25 $NaHCO_3$, 1.25 $NaHPO_4$, 2.5 KCl, 7 $MgCl_2$, 0.5 $CaCl_2$, 25 glucose, 11.6 sodium ascorbate, and 3.1 sodium pyruvate. Slices were recovered in ACSF at 34°C for 15 min and then kept at RT before recording.

Recordings were made with a MultiClamp 700B amplifier (Molecular Devices) at RT using 3-5 MOhm glass patch electrodes (Sutter, BF150-86-7.5). Data was acquired

using ScanImage software, written and maintained by Dr. Bernardo Sabatini (https://github.com/bernardosabatini/ SabalabAcq). Traces were analyzed in Igor Pro (Wavemetrics). Recordings with a series resistance >25 MOhms or holding current above -200 pA were rejected.

*Current-clamp recordings*

Current clamp recordings were made using a potassium-based internal solution (pH=7.4) containing (in mM): 135 KMeSO4, 5 KCl, 5 HEPES, 4 Mg-ATP, 0.3 Na-GTP, 10 phosphocreatine, and 1 ETGA. For corticostriatal excitability experiments, optogenetic stimulation consisted of a full-field pulse of blue light (470 nm, 0.15 ms for iSPNs or 0.5 ms for dSPNs, CoolLED) through a 63x objective. Light power was linear over the range of intensities tested (see Fig. S4). No synaptic blockers were included. For intrinsic excitability experiments, NBQX (10 μM, Tocris, 1044), CPP (10 μM, Tocris, 0247) and picrotoxin (50 μM, Abcam, 120315) were added to the external solution to block synaptic transmission. 500 ms depolarizing current steps were applied to induce action potentials. No holding current was applied to the membrane.

*Voltage-clamp recordings*

Voltage-clamp recordings were made using a cesium-based internal solution (pH=7.4) containing (in mM): 120 CsMeSO4, 15 CsCl, 10 TEA-Cl, 8 NaCl, 10 HEPES, 1 EGTA, 5 QX-314, 4 Mg-ATP, and 0.3 Na-GTP. Recordings were acquired with the amplifier Bessel filter set at 3 kHz. Miniature excitatory synaptic currents (mEPSCs) were recorded in the presence of TTX (1 μM, Abcam, 120055) to prevent action potential-mediated release. Picrotoxin (50 μM) and CPP (10 μM) were included for mEPSC experiments to isolate AMPAR-mediated events. Corticostriatal synaptic stimulation experiments to measure evoked AMPA-mediated EPSCs were performed in picrotoxin (50 μM) and CPP (10 μM), and optogenetic stimulation consisted of a full-field pulse of blue light (470 nm, 0.15 ms) through a 63x objective. To measure AMPA/NMDA ratio, experiments were performed in 50 μM picrotoxin and the membrane was held at different potentials to isolate primarily AMPAR (-70 mV) or compound AMPAR and NMDAR (+40 mV) currents. The current amplitude at +40 mV was measured 50 ms after stimulation, by which time the AMPAR-mediated current has decayed. To measure paired pulse ratio, experiments were performed in 50 μM picrotoxin and the membrane was held at -70 mV. To preferentially excite cortical inputs, a concentric bipolar stimulating electrode (FHC) was placed in the corpus callosum dorsomedial to the recording site in dorsolateral striatum. A 0.2 ms stimulus was applied with a 50 ms interstimulus-interval.

*eCB-LTD*

Endocannabinoid-mediated long-term depression (eCB-LTD) was induced in *Tsc1;Drd1- Cre;Ai9;Thy1-ChR2-YFP* mice by bath application of the group 1 mGluR agonist DHPG (100 μM, Sigma, D3689) for 10 min, following a 10 min baseline measurement of EPSC amplitude with single full field light pulses (3-15% light intensity, 0.15 ms) delivered every 30 seconds to stimulate corticostriatal terminals. Light intensity was adjusted for each cell to evoke 500-700 pA currents during the baseline period. DHPG was subsequently washed off and EPSC amplitude was monitored every 30 sec

for an additional 40 min. Picrotoxin (50 μM) was added to the bath during eCB-LTD experiments to isolate excitatory events, and perfusion flow rate was set to 5 mL/min. Cells were held at -50 mV to facilitate opening of L-type calcium channels. The CB1R antagonist AM 251 (10 μM, Tocris, 1117) was added to the bath during a subset of eCB-LTD experiments with dSPN-Tsc1 WT cells to verify that the LTD observed during these experiments was dependent upon CB1R activation. For CB1R agonism experiments, WIN-2 (2 μM, EMD Millipore, 504344) was applied to the bath throughout the recording.

AAV-FLEX-TRAP plasmid and virus construction

The AAV-hSyn-DIO-EGFP-L10a-WPRE-hGH and AAV-Ef1a-DIO-EGFP-L10a-WPRE-hGH plasmids were assembled from pAAV-hSyn-DIO-mCherry (Addgene plasmid #50459) and pAAV-EF1A-DIO-mCherry (Addgene plasmid #50462), which were gifts from Dr. Bryan Roth, and an EGFP-L10a construct, which was a gift from Dr. Anne Schaefer. AAV serotype 5 viruses were prepared by the University of Pennsylvania Vector Core with a titer of 5.97 x 1012 for AAV5-hSyn-DIO-EGFP-L10a-WPRE-hGH and 3.22 x 1012 for AAV5-Ef1a-DIO-EGFP-L10a- WPRE-hGH.

Stereotaxic intracranial injections

Mice were anesthetized with isoflurane and mounted on a stereotaxic frame equipped with ear cups. 800 nl of an AAV serotype 5 Ef1a or hSyn promoter-driven DIO-EGFP-L10a virus (AAV- FLEX-TRAP) was bilaterally injected into the dorsal striatum of 3-8 week old *Tsc1;Drd1-Cre* mice of both sexes. Coordinates for injection were +/-1.6 M/L, +0.6 A/P, -1.3 D/V. Mice were used for experiments 11-14 days after AAV-FLEX-TRAP virus injection.

Translating ribosome affinity purification (TRAP)

*Anti-GFP magnetic bead preparation*

Each TRAP experiment was performed on 6 samples in parallel, with dSPN-Tsc1-WT and Tsc1- KO mice processed together. For 6 mice, two batches of beads were prepped in parallel in separate tubes. TRAP was performed according to published methods (Heiman et al., 2014; Heiman et al., 2008). All steps were performed on ice unless otherwise noted. 450 μL of Dynabeads MyOne Streptavidin T1 (ThermoFisher, 65601) were washed using a magnetic tube rack in RNase-free PBS and then incubated in Protein L solution (850 μL PBS + 150 μg Protein L, ThermoFisher, 29997) for 35 min at room temperature (RT). Beads were washed 5x with 3% IgG Protease-free BSA to block, then incubated with 150 μg of two different anti-GFP antibodies (19C8 and 19F7, Memorial Sloan Kettering Antibody and Bioresource Core), diluted in 900 μL PBS, for 1 hr at RT. Beads were then washed 3x in 0.15 M KCl buffer without cyclohexamide (- CHX), then resuspended in 630 μL of 0.15 M KCl (+CHX).

*Immunoprecipitation*

Mice were anesthetized, and brains were dissected and blocked to contain mainly striatum. Bilateral striata from each animal were placed into glass homogenization tubes on ice, and pestles were inserted. Homogenization took place at 4°C (3 strokes at 300 RPM, 12 strokes at 900 RPM, Yamato Lab Stirrer, LT400), care was taken to avoid generating bubbles. Lysates were poured into pre-chilled Eppendorf

tubes and centrifuged for 10 min at 2,000 x g at 4 °C to precipitate large organelles. Samples were then transferred to a new pre-chilled tube and volumes were measured. 10% NP-40 (1/9 sample volume, ~70-80 µL) was added, then DHPC (1/9 new sample volume) was added, and samples were incubated on ice for 5 min. 200 mg DHPC stock (Avanti Polar Lipids, 850306P) was dissolved in 1.38 mL ddH2O. Samples were then centrifuged for 10 min at 16,000 x g at 4 °C to precipitate mitochondria. Antibody-bound beads were resuspended by inversion, and 200 µL of beads were added to 6 separate tubes. Supernatants from samples were then transferred into tubes with beads and incubated on rotators at 4 °C overnight.

*Isolation and purification of RNA*

Samples were spun down briefly and placed on magnets pre-chilled on ice. Supernatants were collected and transferred to pre-chilled “unbound” tubes. Beads were washed 4x with 0.35 M KCl buffer, with samples sitting on ice for 1 min between washes to reduce background binding. Beads were resuspended in 350 µL RLT-beta-ME from an RNeasy kit (Qiagen, 74004). 100 µL of unbound samples were added separately to 350 µL RLT-beta-ME. Samples (bound and unbound) were then rotated for 10 min at RT. Samples were placed on the magnet and supernatants were removed and added into fresh tubes containing 350 µL of 80% EtOH, mixed, and then all 700 µL of sample + EtOH was added to an RNeasy kit pre-chilled column. 350 µL of unbound sample was also mixed with 350 µL of EtOH and added to an RNeasy column. At this point there were 12 columns, one bound and one unbound sample for each mouse. Samples were centrifuged for 30 sec at 8000 x g at RT. Flow-through was passed through the column twice more to repeat binding. Flow-through was then discarded and 500 µL of RPE buffer was added to each column and spun for 30 sec at 8000 x g. Flow-through was discarded and 500 µL of 80% EtOH was added to the column. Columns were spun for 2 min at 8000 x g at RT. Flow-through was discarded, and columns were dried by spinning for 5 min at full speed with the cap open. Dried columns were placed into new collection tubes (not pre-chilled) and 28 µL RNase-free water was added directly to the column membrane. Columns were incubated for 5 min at RT with the caps closed, then spun for 1 min at max speed at RT. RNA concentration and quality was determined by NanoDrop and Bioanalyzer at the UC Berkeley Functional Genomics Laboratory core facility.

*Quantitative PCR*

Reverse transcription was performed using random hexamer primers and Superscript III reverse transcriptase (ThermoFisher, 18080051). Real-time PCR was performed in triplicate with 1 uL cDNA using a Bio-Rad CFX384 thermal cycler with TaqMan Universal PCR Master Mix, no AmpErase UNG (Lifetech, 4324018) and TaqMan probes. The following TaqMan probes were used: *Grm1* (Mm01187086_m1), *Grm5* (Mm00690332_m1), *Homer1* (Mm00516275), *Plcb1* (Mm00479998), *Drd1* (Mm01353211_m1), *Drd2* (Mm00438545_m1), and *Actb* (Mm02619580_g1). Values for all mRNAs were normalized to *Actb* for each sample.

Quantification and Statistical Analysis

Experiments were designed to compare the main effect of genotype within each mouse line. The sample sizes were based on prior studies and are indicated in the figure legend for each experiment. Whenever possible, quantification and analyses were performed blind to genotype. GraphPad Prism version 9 was used to perform statistical analyses. The statistical tests and outcomes for each experiment are indicated in the respective figure legend. Two-tailed paired or unpaired t-tests were used for comparisons between two groups. For data that did not pass the D'Agostino & Pearson normality test, a Mann-Whitney test was used. A one-way ANOVA with Holm-Sidak's post-hoc tests was used to compare the means of three or more groups. For data that did not pass the D'Agostino and Pearson normality test, the Kruskal-Wallis test with Dunn's post-hoc tests was used. Repeated measures (RM) two-way ANOVAs were used to compare differences between groups for experiments with two independent variables. For data sets that had values randomly missing, mixed-effects model analysis was performed in place of a RM two-way ANOVA. P-values were corrected for multiple comparisons. Statistical significance was defined in the figure panels as follows: *$p<0.05$, **$p<0.01$, ***$p<0.001$.

**References**


Ahmed, N. Y., Knowles, R., Liu, L., Yan, Y., Li, X., Schumann, U., Wang, Y., Sontani, Y., Reynolds, N., Natoli, R., Wen, J., Del Pino, I., Mi, D., & Dehorter, N. (2023). Developmental deficits of MGE-derived interneurons in the Cntnap2 knockout mouse model of autism spectrum disorder. *Front Cell Dev Biol*, *11*, 1112062. https://doi.org/10.3389/fcell.2023.1112062

Arenkiel, B. R., Peca, J., Davison, I. G., Feliciano, C., Deisseroth, K., Augustine, G. J., Ehlers, M. D., & Feng, G. (2007). In vivo light-induced activation of neural circuitry in transgenic mice expressing channelrhodopsin-2. *Neuron*, *54*(2), 205-218. https://doi.org/10.1016/j.neuron.2007.03.005

Asano, E., Chugani, D. C., Muzik, O., Behen, M., Janisse, J., Rothermel, R., Mangner, T. J., Chakraborty, P. K., & Chugani, H. T. (2001). Autism in tuberous sclerosis complex is related to both cortical and subcortical dysfunction. *Neurology*, *57*(7), 1269-1277. https://doi.org/10.1212/wnl.57.7.1269

Assous, M., Martinez, E., Eisenberg, C., Shah, F., Kosc, A., Varghese, K., Espinoza, D., Bhimani, S., Tepper, J. M., Shiflett, M. W., & Tran, T. S. (2019). Neuropilin 2 Signaling Mediates Corticostriatal Transmission, Spine Maintenance, and Goal-Directed Learning in Mice. *J Neurosci*, *39*(45), 8845-8859. https://doi.org/10.1523/JNEUROSCI.1006-19.2019

Auerbach, B. D., Osterweil, E. K., & Bear, M. F. (2011). Mutations causing syndromic autism define an axis of synaptic pathophysiology. *Nature*, *480*(7375), 63-68. https://doi.org/10.1038/nature10658

Bateup, H. S., Johnson, C. A., Denefrio, C. L., Saulnier, J. L., Kornacker, K., & Sabatini, B. L. (2013). Excitatory/inhibitory synaptic imbalance leads to hippocampal hyperexcitability in mouse models of tuberous sclerosis. *Neuron*, *78*(3), 510-522. https://doi.org/10.1016/j.neuron.2013.03.017

Bateup, H. S., Takasaki, K. T., Saulnier, J. L., Denefrio, C. L., & Sabatini, B. L. (2011). Loss of Tsc1 in vivo impairs hippocampal mGluR-LTD and increases excitatory synaptic function. *J Neurosci*, *31*(24), 8862-8869. https://doi.org/10.1523/JNEUROSCI.1617-11.2011

Benthall, K. N., Ong, S. L., & Bateup, H. S. (2018). Corticostriatal Transmission Is Selectively Enhanced in Striatonigral Neurons with Postnatal Loss of Tsc1. *Cell Rep*, *23*(11), 3197-3208. https://doi.org/10.1016/j.celrep.2018.05.037

Bergeron, Y., Chagniel, L., Bureau, G., Massicotte, G., & Cyr, M. (2014). mTOR signaling contributes to motor skill learning in mice. *Front Mol Neurosci*, *7*, 26. https://doi.org/10.3389/fnmol.2014.00026

Chadman, K. K., Gong, S., Scattoni, M. L., Boltuck, S. E., Gandhy, S. U., Heintz, N., & Crawley, J. N. (2008). Minimal aberrant behavioral phenotypes of neuroligin-3 R451C knockin mice. *Autism Res*, *1*(3), 147-158. https://doi.org/10.1002/aur.22

Chevere-Torres, I., Maki, J. M., Santini, E., & Klann, E. (2012). Impaired social interactions and motor learning skills in tuberous sclerosis complex model mice expressing a dominant/negative form of tuberin. *Neurobiol Dis*, *45*(1), 156-164. https://doi.org/10.1016/j.nbd.2011.07.018

Curatolo, P., Moavero, R., & de Vries, P. J. (2015). Neurological and neuropsychiatric aspects of tuberous sclerosis complex. *Lancet Neurol*, *14*(7), 733-745. https://doi.org/10.1016/S1474-4422(15)00069-1

Davis, P. E., Peters, J. M., Krueger, D. A., & Sahin, M. (2015). Tuberous Sclerosis: A New Frontier in Targeted Treatment of Autism. *Neurotherapeutics*, *12*(3), 572-583. https://doi.org/10.1007/s13311-015-0359-5
de Vries, P. J. (2010). Targeted treatments for cognitive and neurodevelopmental disorders in tuberous sclerosis complex. *Neurotherapeutics*, *7*(3), 275-282. https://doi.org/10.1016/j.nurt.2010.05.001
Di Martino, A., Kelly, C., Grzadzinski, R., Zuo, X. N., Mennes, M., Mairena, M. A., Lord, C., Castellanos, F. X., & Milham, M. P. (2011). Aberrant striatal functional connectivity in children with autism. *Biol Psychiatry*, *69*(9), 847-856. https://doi.org/10.1016/j.biopsych.2010.10.029
Ding, J., Peterson, J. D., & Surmeier, D. J. (2008). Corticostriatal and thalamostriatal synapses have distinctive properties. *J Neurosci*, *28*(25), 6483-6492. https://doi.org/10.1523/JNEUROSCI.0435-08.2008
Doig, N. M., Moss, J., & Bolam, J. P. (2010). Cortical and thalamic innervation of direct and indirect pathway medium-sized spiny neurons in mouse striatum. *J Neurosci*, *30*(44), 14610-14618. https://doi.org/10.1523/JNEUROSCI.1623-10.2010
Feliciano, D. M., Su, T., Lopez, J., Platel, J. C., & Bordey, A. (2011). Single-cell Tsc1 knockout during corticogenesis generates tuber-like lesions and reduces seizure threshold in mice. *J Clin Invest*, *121*(4), 1596-1607. https://doi.org/10.1172/JCI44909
Fuccillo, M. V. (2016). Striatal Circuits as a Common Node for Autism Pathophysiology. *Front Neurosci*, *10*, 27. https://doi.org/10.3389/fnins.2016.00027
Gerfen, C. R., & Surmeier, D. J. (2011). Modulation of striatal projection systems by dopamine. *Annu Rev Neurosci*, *34*, 441-466. https://doi.org/10.1146/annurev-neuro-061010-113641
Gertler, T. S., Chan, C. S., & Surmeier, D. J. (2008). Dichotomous anatomical properties of adult striatal medium spiny neurons. *J Neurosci*, *28*(43), 10814-10824. https://doi.org/10.1523/JNEUROSCI.2660-08.2008
Gobet, C., & Naef, F. (2017). Ribosome profiling and dynamic regulation of translation in mammals. *Curr Opin Genet Dev*, *43*, 120-127. https://doi.org/10.1016/j.gde.2017.03.005
Gong, S., Doughty, M., Harbaugh, C. R., Cummins, A., Hatten, M. E., Heintz, N., & Gerfen, C. R. (2007). Targeting Cre recombinase to specific neuron populations with bacterial artificial chromosome constructs. *J Neurosci*, *27*(37), 9817-9823. https://doi.org/10.1523/JNEUROSCI.2707-07.2007
Graybiel, A. M., & Grafton, S. T. (2015). The striatum: where skills and habits meet. *Cold Spring Harb Perspect Biol*, *7*(8), a021691. https://doi.org/10.1101/cshperspect.a021691
Gremel, C. M., & Lovinger, D. M. (2017). Associative and sensorimotor cortico-basal ganglia circuit roles in effects of abused drugs. *Genes Brain Behav*, *16*(1), 71-85. https://doi.org/10.1111/gbb.12309
Heiman, M., Kulicke, R., Fenster, R. J., Greengard, P., & Heintz, N. (2014). Cell type-specific mRNA purification by translating ribosome affinity purification (TRAP). *Nat Protoc*, *9*(6), 1282-1291. https://doi.org/10.1038/nprot.2014.085
Heiman, M., Schaefer, A., Gong, S., Peterson, J. D., Day, M., Ramsey, K. E., Suarez-Farinas, M., Schwarz, C., Stephan, D. A., Surmeier, D. J., Greengard, P., &

Heintz, N. (2008). A translational profiling approach for the molecular characterization of CNS cell types. *Cell*, *135*(4), 738-748. https://doi.org/10.1016/j.cell.2008.10.028
Hisaoka, T., Komori, T., Kitamura, T., & Morikawa, Y. (2018). Abnormal behaviours relevant to neurodevelopmental disorders in Kirrel3-knockout mice. *Sci Rep*, *8*(1), 1408. https://doi.org/10.1038/s41598-018-19844-7
Huang, J., & Manning, B. D. (2008). The TSC1-TSC2 complex: a molecular switchboard controlling cell growth. *Biochem J*, *412*(2), 179-190. https://doi.org/10.1042/BJ20080281
Jung, K. M., Sepers, M., Henstridge, C. M., Lassalle, O., Neuhofer, D., Martin, H., Ginger, M., Frick, A., DiPatrizio, N. V., Mackie, K., Katona, I., Piomelli, D., & Manzoni, O. J. (2012). Uncoupling of the endocannabinoid signalling complex in a mouse model of fragile X syndrome. *Nat Commun*, *3*, 1080. https://doi.org/10.1038/ncomms2045
Kelleher, R. J., 3rd, & Bear, M. F. (2008). The autistic neuron: troubled translation? *Cell*, *135*(3), 401-406. https://doi.org/10.1016/j.cell.2008.10.017
Kosillo, P., Doig, N. M., Ahmed, K. M., Agopyan-Miu, A., Wong, C. D., Conyers, L., Threlfell, S., Magill, P. J., & Bateup, H. S. (2019). Tsc1-mTORC1 signaling controls striatal dopamine release and cognitive flexibility. *Nat Commun*, *10*(1), 5426. https://doi.org/10.1038/s41467-019-13396-8
Kravitz, A. V., Freeze, B. S., Parker, P. R., Kay, K., Thwin, M. T., Deisseroth, K., & Kreitzer, A. C. (2010). Regulation of parkinsonian motor behaviours by optogenetic control of basal ganglia circuitry. *Nature*, *466*(7306), 622-626. https://doi.org/10.1038/nature09159
Kreitzer, A. C., & Malenka, R. C. (2007). Endocannabinoid-mediated rescue of striatal LTD and motor deficits in Parkinson's disease models. *Nature*, *445*(7128), 643-647. https://doi.org/10.1038/nature05506
Kreitzer, A. C., & Malenka, R. C. (2008). Striatal plasticity and basal ganglia circuit function. *Neuron*, *60*(4), 543-554. https://doi.org/10.1016/j.neuron.2008.11.005
Kuo, H. Y., & Liu, F. C. (2019). Synaptic Wiring of Corticostriatal Circuits in Basal Ganglia: Insights into the Pathogenesis of Neuropsychiatric Disorders. *eNeuro*, *6*(3). https://doi.org/10.1523/ENEURO.0076-19.2019
Kupferschmidt, D. A., Augustin, S. M., Johnson, K. A., & Lovinger, D. M. (2019). Active Zone Proteins RIM1alphabeta Are Required for Normal Corticostriatal Transmission and Action Control. *J Neurosci*, *39*(8), 1457-1470. https://doi.org/10.1523/JNEUROSCI.1940-18.2018
Kwiatkowski, D. J., Zhang, H., Bandura, J. L., Heiberger, K. M., Glogauer, M., el-Hashemite, N., & Onda, H. (2002). A mouse model of TSC1 reveals sex-dependent lethality from liver hemangiomas, and up-regulation of p70S6 kinase activity in Tsc1 null cells. *Hum Mol Genet*, *11*(5), 525-534. https://doi.org/10.1093/hmg/11.5.525
Kwon, C. H., Luikart, B. W., Powell, C. M., Zhou, J., Matheny, S. A., Zhang, W., Li, Y., Baker, S. J., & Parada, L. F. (2006). Pten regulates neuronal arborization and social interaction in mice. *Neuron*, *50*(3), 377-388. https://doi.org/10.1016/j.neuron.2006.03.023

Lee, Y., Kim, H., & Han, P. L. (2018). Striatal Inhibition of MeCP2 or TSC1 Produces Sociability Deficits and Repetitive Behaviors. *Exp Neurobiol*, *27*(6), 539-549. https://doi.org/10.5607/en.2018.27.6.539
Li, W., & Pozzo-Miller, L. (2020). Dysfunction of the corticostriatal pathway in autism spectrum disorders. *J Neurosci Res*, *98*(11), 2130-2147. https://doi.org/10.1002/jnr.24560
Lim, J. S., Gopalappa, R., Kim, S. H., Ramakrishna, S., Lee, M., Kim, W. I., Kim, J., Park, S. M., Lee, J., Oh, J. H., Kim, H. D., Park, C. H., Lee, J. S., Kim, S., Kim, D. S., Han, J. M., Kang, H. C., Kim, H. H., & Lee, J. H. (2017). Somatic Mutations in TSC1 and TSC2 Cause Focal Cortical Dysplasia. *Am J Hum Genet*, *100*(3), 454-472. https://doi.org/10.1016/j.ajhg.2017.01.030
Lovinger, D. M. (2010). Neurotransmitter roles in synaptic modulation, plasticity and learning in the dorsal striatum. *Neuropharmacology*, *58*(7), 951-961. https://doi.org/10.1016/j.neuropharm.2010.01.008
Luscher, C., & Huber, K. M. (2010). Group 1 mGluR-dependent synaptic long-term depression: mechanisms and implications for circuitry and disease. *Neuron*, *65*(4), 445-459. https://doi.org/10.1016/j.neuron.2010.01.016
Madisen, L., Zwingman, T. A., Sunkin, S. M., Oh, S. W., Zariwala, H. A., Gu, H., Ng, L. L., Palmiter, R. D., Hawrylycz, M. J., Jones, A. R., Lein, E. S., & Zeng, H. (2010). A robust and high-throughput Cre reporting and characterization system for the whole mouse brain. *Nat Neurosci*, *13*(1), 133-140. https://doi.org/10.1038/nn.2467
Malik, R., Pai, E. L., Rubin, A. N., Stafford, A. M., Angara, K., Minasi, P., Rubenstein, J. L., Sohal, V. S., & Vogt, D. (2019). Tsc1 represses parvalbumin expression and fast-spiking properties in somatostatin lineage cortical interneurons. *Nat Commun*, *10*(1), 4994. https://doi.org/10.1038/s41467-019-12962-4
Martella, G., Meringolo, M., Trobiani, L., De Jaco, A., Pisani, A., & Bonsi, P. (2018). The neurobiological bases of autism spectrum disorders: the R451C-neuroligin 3 mutation hampers the expression of long-term synaptic depression in the dorsal striatum. *Eur J Neurosci*, *47*(6), 701-708. https://doi.org/10.1111/ejn.13705
Nakatani, J., Tamada, K., Hatanaka, F., Ise, S., Ohta, H., Inoue, K., Tomonaga, S., Watanabe, Y., Chung, Y. J., Banerjee, R., Iwamoto, K., Kato, T., Okazawa, M., Yamauchi, K., Tanda, K., Takao, K., Miyakawa, T., Bradley, A., & Takumi, T. (2009). Abnormal behavior in a chromosome-engineered mouse model for human 15q11-13 duplication seen in autism. *Cell*, *137*(7), 1235-1246. https://doi.org/10.1016/j.cell.2009.04.024
Normand, E. A., Crandall, S. R., Thorn, C. A., Murphy, E. M., Voelcker, B., Browning, C., Machan, J. T., Moore, C. I., Connors, B. W., & Zervas, M. (2013). Temporal and mosaic Tsc1 deletion in the developing thalamus disrupts thalamocortical circuitry, neural function, and behavior. *Neuron*, *78*(5), 895-909. https://doi.org/10.1016/j.neuron.2013.03.030
Ohno-Shosaku, T., & Kano, M. (2014). Endocannabinoid-mediated retrograde modulation of synaptic transmission. *Curr Opin Neurobiol*, *29*, 1-8. https://doi.org/10.1016/j.conb.2014.03.017
Onda, H., Lueck, A., Marks, P. W., Warren, H. B., & Kwiatkowski, D. J. (1999). Tsc2(+/-) mice develop tumors in multiple sites that express gelsolin and are influenced by

genetic background. *J Clin Invest*, *104*(6), 687-695. https://doi.org/10.1172/JCI7319

Peca, J., Feliciano, C., Ting, J. T., Wang, W., Wells, M. F., Venkatraman, T. N., Lascola, C. D., Fu, Z., & Feng, G. (2011). Shank3 mutant mice display autistic-like behaviours and striatal dysfunction. *Nature*, *472*(7344), 437-442. https://doi.org/10.1038/nature09965

Peixoto, R. T., Wang, W., Croney, D. M., Kozorovitskiy, Y., & Sabatini, B. L. (2016). Early hyperactivity and precocious maturation of corticostriatal circuits in Shank3B(-/-) mice. *Nat Neurosci*, *19*(5), 716-724. https://doi.org/10.1038/nn.4260

Penagarikano, O., Abrahams, B. S., Herman, E. I., Winden, K. D., Gdalyahu, A., Dong, H., Sonnenblick, L. I., Gruver, R., Almajano, J., Bragin, A., Golshani, P., Trachtenberg, J. T., Peles, E., & Geschwind, D. H. (2011). Absence of CNTNAP2 leads to epilepsy, neuronal migration abnormalities, and core autism-related deficits. *Cell*, *147*(1), 235-246. https://doi.org/10.1016/j.cell.2011.08.040

Platt, R. J., Zhou, Y., Slaymaker, I. M., Shetty, A. S., Weisbach, N. R., Kim, J. A., Sharma, J., Desai, M., Sood, S., Kempton, H. R., Crabtree, G. R., Feng, G., & Zhang, F. (2017). Chd8 Mutation Leads to Autistic-like Behaviors and Impaired Striatal Circuits. *Cell Rep*, *19*(2), 335-350. https://doi.org/10.1016/j.celrep.2017.03.052

Portmann, T., Yang, M., Mao, R., Panagiotakos, G., Ellegood, J., Dolen, G., Bader, P. L., Grueter, B. A., Goold, C., Fisher, E., Clifford, K., Rengarajan, P., Kalikhman, D., Loureiro, D., Saw, N. L., Zhengqui, Z., Miller, M. A., Lerch, J. P., Henkelman, M., . . . Dolmetsch, R. E. (2014). Behavioral abnormalities and circuit defects in the basal ganglia of a mouse model of 16p11.2 deletion syndrome. *Cell Rep*, *7*(4), 1077-1092. https://doi.org/10.1016/j.celrep.2014.03.036

Potter, W. B., Basu, T., O'Riordan, K. J., Kirchner, A., Rutecki, P., Burger, C., & Roopra, A. (2013). Reduced juvenile long-term depression in tuberous sclerosis complex is mitigated in adults by compensatory recruitment of mGluR5 and Erk signaling. *PLoS Biol*, *11*(8), e1001627. https://doi.org/10.1371/journal.pbio.1001627

Qiu, A., Adler, M., Crocetti, D., Miller, M. I., & Mostofsky, S. H. (2010). Basal ganglia shapes predict social, communication, and motor dysfunctions in boys with autism spectrum disorder. *J Am Acad Child Adolesc Psychiatry*, *49*(6), 539-551, 551 e531-534. https://doi.org/10.1016/j.jaac.2010.02.012

Rothwell, P. E., Fuccillo, M. V., Maxeiner, S., Hayton, S. J., Gokce, O., Lim, B. K., Fowler, S. C., Malenka, R. C., & Sudhof, T. C. (2014). Autism-associated neuroligin-3 mutations commonly impair striatal circuits to boost repetitive behaviors. *Cell*, *158*(1), 198-212. https://doi.org/10.1016/j.cell.2014.04.045

Sato, A., Kasai, S., Kobayashi, T., Takamatsu, Y., Hino, O., Ikeda, K., & Mizuguchi, M. (2012). Rapamycin reverses impaired social interaction in mouse models of tuberous sclerosis complex. *Nat Commun*, *3*, 1292. https://doi.org/10.1038/ncomms2295

Satterstrom, F. K., Kosmicki, J. A., Wang, J., Breen, M. S., De Rubeis, S., An, J.-Y., Peng, M., Collins, R., Grove, J., Klei, L., Stevens, C., Reichert, J., Mulhern, M. S., Artomov, M., Gerges, S., Sheppard, B., Xu, X., Bhaduri, A., Norman, U., . . . Walters, R. K. (2020). Large-Scale Exome Sequencing Study Implicates Both

Developmental and Functional Changes in the Neurobiology of Autism. *Cell*, *180*(3), 568-584.e523. https://doi.org/10.1016/j.cell.2019.12.036
Saxton, R. A., & Sabatini, D. M. (2017). mTOR Signaling in Growth, Metabolism, and Disease. *Cell*, *168*(6), 960-976. https://doi.org/10.1016/j.cell.2017.02.004
Schiffmann, S. N., & Vanderhaeghen, J. J. (1993). Adenosine A2 receptors regulate the gene expression of striatopallidal and striatonigral neurons. *J Neurosci*, *13*(3), 1080-1087. https://doi.org/10.1523/JNEUROSCI.13-03-01080.1993
Shonesy, B. C., Parrish, W. P., Haddad, H. K., Stephenson, J. R., Baldi, R., Bluett, R. J., Marks, C. R., Centanni, S. W., Folkes, O. M., Spiess, K., Augustin, S. M., Mackie, K., Lovinger, D. M., Winder, D. G., Patel, S., & Colbran, R. J. (2018). Role of Striatal Direct Pathway 2-Arachidonoylglycerol Signaling in Sociability and Repetitive Behavior. *Biol Psychiatry*, *84*(4), 304-315. https://doi.org/10.1016/j.biopsych.2017.11.036
Sztainberg, Y., & Zoghbi, H. Y. (2016). Lessons learned from studying syndromic autism spectrum disorders. *Nat Neurosci*, *19*(11), 1408-1417. https://doi.org/10.1038/nn.4420
Tai, L. H., Lee, A. M., Benavidez, N., Bonci, A., & Wilbrecht, L. (2012). Transient stimulation of distinct subpopulations of striatal neurons mimics changes in action value. *Nat Neurosci*, *15*(9), 1281-1289. https://doi.org/10.1038/nn.3188
Tang, G., Gudsnuk, K., Kuo, S. H., Cotrina, M. L., Rosoklija, G., Sosunov, A., Sonders, M. S., Kanter, E., Castagna, C., Yamamoto, A., Yue, Z., Arancio, O., Peterson, B. S., Champagne, F., Dwork, A. J., Goldman, J., & Sulzer, D. (2014). Loss of mTOR-dependent macroautophagy causes autistic-like synaptic pruning deficits. *Neuron*, *83*(5), 1131-1143. https://doi.org/10.1016/j.neuron.2014.07.040
Tavazoie, S. F., Alvarez, V. A., Ridenour, D. A., Kwiatkowski, D. J., & Sabatini, B. L. (2005). Regulation of neuronal morphology and function by the tumor suppressors Tsc1 and Tsc2. *Nat Neurosci*, *8*(12), 1727-1734. https://doi.org/10.1038/nn1566
Tsai, P. T., Hull, C., Chu, Y., Greene-Colozzi, E., Sadowski, A. R., Leech, J. M., Steinberg, J., Crawley, J. N., Regehr, W. G., & Sahin, M. (2012). Autistic-like behaviour and cerebellar dysfunction in Purkinje cell Tsc1 mutant mice. *Nature*, *488*(7413), 647-651. https://doi.org/10.1038/nature11310
Turner, K. C., Frost, L., Linsenbardt, D., McIlroy, J. R., & Muller, R. A. (2006). Atypically diffuse functional connectivity between caudate nuclei and cerebral cortex in autism. *Behav Brain Funct*, *2*, 34. https://doi.org/10.1186/1744-9081-2-34
Wang, X., Bey, A. L., Katz, B. M., Badea, A., Kim, N., David, L. K., Duffney, L. J., Kumar, S., Mague, S. D., Hulbert, S. W., Dutta, N., Hayrapetyan, V., Yu, C., Gaidis, E., Zhao, S., Ding, J. D., Xu, Q., Chung, L., Rodriguiz, R. M., . . . Jiang, Y. H. (2016). Altered mGluR5-Homer scaffolds and corticostriatal connectivity in a Shank3 complete knockout model of autism. *Nat Commun*, *7*, 11459. https://doi.org/10.1038/ncomms11459
Winden, K. D., Ebrahimi-Fakhari, D., & Sahin, M. (2018). Abnormal mTOR Activation in Autism. *Annu Rev Neurosci*, *41*, 1-23. https://doi.org/10.1146/annurev-neuro-080317-061747

Wu, Y. W., Kim, J. I., Tawfik, V. L., Lalchandani, R. R., Scherrer, G., & Ding, J. B. (2015). Input- and cell-type-specific endocannabinoid-dependent LTD in the striatum. *Cell Rep*, *10*(1), 75-87. https://doi.org/10.1016/j.celrep.2014.12.005

Yang, S. B., Tien, A. C., Boddupalli, G., Xu, A. W., Jan, Y. N., & Jan, L. Y. (2012). Rapamycin ameliorates age-dependent obesity associated with increased mTOR signaling in hypothalamic POMC neurons. *Neuron*, *75*(3), 425-436. https://doi.org/10.1016/j.neuron.2012.03.043

Yin, H. H., Mulcare, S. P., Hilário, M. R. F., Clouse, E., Holloway, T., Davis, M. I., Hansson, A. C., Lovinger, D. M., & Costa, R. M. (2009). Dynamic reorganization of striatal circuits during the acquisition and consolidation of a skill. *Nature Neuroscience*, *12*(3), 333-341. https://doi.org/10.1038/nn.2261

Yin, X., Jones, N., Yang, J., Asraoui, N., Mathieu, M. E., Cai, L., & Chen, S. X. (2021). Delayed motor learning in a 16p11.2 deletion mouse model of autism is rescued by locus coeruleus activation. *Nat Neurosci*, *24*(5), 646-657. https://doi.org/10.1038/s41593-021-00815-7

# Chapter 4: Loss of Cntnap2 alters striatal neuron excitability and drives repetitive, inflexible behaviors in mice

Katherine Cording

Helen Wills Neuroscience Institute
University of California, Berkeley

## Introduction

Autism spectrum disorder (ASD) is a neurodevelopmental disorder characterized by alterations in social communication and interaction, as well as the presentation of restricted, repetitive behaviors (APA, 2022). Given that ASD has high heritability (Sandin et al., 2017), much work has been done in the last 30 years to identify genes that confer risk of developing ASD (De Rubeis et al., 2014; Iossifov et al., 2014; Sanders et al., 2015). Through this, hundreds of high-confidence or strong candidate risk genes have been identified, varying greatly in the protein products for which they code, from transcriptional and translational regulators to ion channels, receptors and cell adhesion molecules (Satterstrom et al., 2020). Given the wide genetic and functional heterogeneity of the genes implicated in ASD, more recent work has focused on identifying brain regions that may be common sites of alteration across a range of ASD risk gene mutations. The basal ganglia, in particular the striatum, the primary input center of the basal ganglia, represents one such commonly altered brain region in ASD (Fuccillo, 2016). Indeed, work from our lab and others have identified changes in striatal circuit function and striatum-associated behaviors in the context of mutations in ASD risk genes (Benthall et al., 2021; Platt et al., 2017; Rothwell et al., 2014). However, whether basal ganglia circuits are convergently altered by mutations in all ASD risk genes is an open question. Here we investigated whether loss of function of the syndromic ASD risk gene *Cntnap2,* in mice, alters striatal physiology and basal ganglia-dependent behaviors.

*CNTNAP2* codes for a neurexin-like cell adhesion molecule called Caspr2 (Contactin associated protein-like 2) (Poliak et al., 1999; Poliak et al., 2003). Caspr2 is primarily localized at the juxtaparanodes of myelinated axons and is involved in the clustering of potassium channels (Poliak et al., 2003; Scott et al., 2019). In mice, *in vitro* work suggests that Caspr2 may also play a role in AMPAR trafficking and cell morphology (Anderson et al., 2012; Gdalyahu et al., 2015; Varea et al., 2015), and *ex vivo* studies indicate that it can control cell excitability and circuit synchronicity (Martin-de-Saavedra et al., 2022). Caspr2 is expressed throughout cortical and subcortical regions from early stages of development onward (Penagarikano et al., 2011). Given this, Caspr2 has also been shown to be important for proper neurodevelopment, playing a role in neuronal migration (Penagarikano et al., 2011), the maturation and function of parvalbumin-positive GABAergic interneurons (Penagarikano et al., 2011; Scott et al., 2019; Vogt et al., 2018), and the timing of myelination (Scott et al., 2019). When mutated, *CNTNAP2* results in a neurodevelopmental syndrome that can include language disorders, epilepsy, obsessive compulsive disorder, as well as ASD (Penagarikano & Geschwind, 2012; Rodenas-Cuadrado et al., 2014). A mouse model of this syndrome, *Cntnap2*$^{-/-}$, has been shown to exhibit good face validity for ASD-relevant social and motor behavior alterations (Brunner et al., 2015; Dawes et al., 2018; Penagarikano et al., 2011; Scott et al., 2019). However, the impact of *Cntnap2* loss on

striatal synaptic physiology and excitability and corticostriatal-dependent behaviors has not been comprehensively assessed.

The striatum is primarily composed of GABAergic spiny projection neurons, which make up two functionally distinct output pathways: the D1-receptor expressing cells of the direct pathway (dSPNs), which project to substantia nigra pars reticulata (SNr) and are generally thought to promote movement when activated in bulk, and the D2-receptor expressing cells of the indirect pathway (iSPNs), which project to external globus pallidus (GPe) and are generally thought to inhibit competing movement when activated in bulk (Calabresi et al., 2014; Gerfen & Surmeier, 2011; Kravitz et al., 2010; Tai et al., 2012). SPNs are intermixed throughout the striatum and receive excitatory glutamatergic inputs from cortex and thalamus, as well as dopaminergic input from the midbrain (Ding et al., 2008; Doig et al., 2010; Gerfen & Surmeier, 2011). Modification of the excitatory drive onto SPNs, and in turn the coordinated activity between the pathways, mediates action selection, motor learning and habit formation (Hawes et al., 2015; Santos et al., 2015; Yin et al., 2005, 2006), functional roles relevant to the manifestation of RRBs. Although SPNs compromise over 95% of the cells in striatum, there are a wide range of distinct interneurons, primarily GABAergic, that contribute significantly to the inhibitory circuitry of the striatum. Parvalbumin (PV) interneurons, which make up ~2% of the cells in striatum, provide the largest feedforward inhibition onto SPNs (Burke et al., 2017). Changes in the number and/or function of PV interneurons have been identified in a number of diverse ASD mouse models, including *Cntnap2*$^{-/-}$, implicating PV circuitry as a potential common alteration across ASD mouse models (Filice et al., 2020; Juarez & Martinez Cerdeno, 2022)..

To determine how loss of *Cntnap2* affects striatal function, we assessed intrinsic and synaptic physiology of SPNs and striatal PV-interneurons in the dorsolateral striatum and utilized a range of assays to assess striatum-associated behaviors in *Cntnap2*$^{-/-}$ mice. We find that SPNs of both the direct and indirect pathways exhibit increased corticostriatal drive, despite unchanged excitatory cortical input onto these cells. Although decreased inhibitory function has been identified in other brain regions in *Cntnap2*$^{-/-}$ mice, we find no deficit in broad or PV-specific inhibitory input onto SPNs in the case of *Cntnap2* loss. Instead, we identify a significant increase in the intrinsic excitability of SPNs in *Cntnap2*$^{-/-}$ mice, in particular in dSPNs, which likely underlies the increased corticostriatal drive exhibited by these cells. Behaviorally, we find that *Cntnap2*$^{-/-}$ mice exhibit RRB-like behaviors including increased grooming, marble burying and nosepoking in the holeboard assay. *Cntnap2*$^{-/-}$ mice also exhibit significant changes in assays of motor learning and cognitive flexibility, exhibiting significantly increased motor routine learning in the accelerating rotarod, and cognitive inflexibility in an odor-based reversal learning task. Taken together, these findings identify increased corticostriatal drive in *Cntnap2*$^{-/-}$ mice, likely caused by increased SPN intrinsic

excitability, in particular in dSPNs. This enhanced direct pathway drive may play a role in the increased spontaneous and learned repetitive behaviors exhibited by these mice.

## Results

### *Cntnap2*$^{-/-}$ SPNs exhibit increased cortical drive

Emerging evidence suggests that corticostriatal synapses are a common site of alteration in ASD (Li & Pozzo-Miller, 2020). To test whether mice with loss of Cntnap2 exhibit changes in corticostriatal drive, we crossed *Cntnap2*$^{-/-}$;Drd1a-tdTomato (D1tdT) mice to Thy1-ChR2-YFP mice, which express channelrhodopsin in a subset of layer V pyramidal neurons (Fig. 1A) (Ade et al., 2011; Arenkiel et al., 2007; Poliak et al., 2003). Offspring were bred to yield *Cntnap2*$^{-/-}$;D1tdT;Thy1-ChR2-YFP mice and *Cntnap2*$^{+/+}$;D1tdT;Thy1-ChR2 littermate controls. We recorded from SPNs in the dorsolateral striatum (DLS), as this sensorimotor striatal subregion is implicated in the acquisition of habitual or procedural behaviors (Packard & Knowlton, 2002). Changes in physiological function in this area may be connected to the acquisition of repetitive motor behaviors in ASD (Evans et al., 2024; Fuccillo, 2016). To simulate a train of cortical inputs, we applied ten pulses of blue light over the recording site in DLS and measured the number of action potentials (APs) fired by SPNs in the absence of synaptic blockers (Fig. 1A). We altered the light intensity to vary the probability of eliciting subthreshold depolarizations or AP firing. Direct pathway SPNs (dSPNs) were identified using tdTomato fluorescence, and tdTomato negative neurons were designated putative indirect pathway SPNs (iSPNs).

We quantified the number of evoked APs at different light intensities and found that both dSPNs and iSPNs in *Cntnap2*$^{-/-}$ mice exhibited significantly increased spike probability compared to wild-type (WT) SPNs (Fig. 1B-E). This suggests increased corticostriatal drive, consistent with findings in another mouse model with ASD risk gene mutation (Benthall et al., 2021). To test whether the enhanced spiking probability was due to a change in the synaptic strength of *Cntnap2*$^{-/-}$ SPNs, we applied blue LED light of varying intensity over the recording site in DLS to evoke AMPAR-driven excitatory postsynaptic currents (EPSCs) (Fig. 1F). We found that the average optically-evoked EPSC amplitude was not significantly different across a range of light intensities in *Cntnap2*$^{-/-}$ dSPNs or iSPNs compared to WT SPNs (Fig. 1G-J).

As an additional measure of synaptic input, we measured the number of dendritic spines in *Cntnap2*$^{-/-}$ and WT SPNs, which are typically the sites of cortical synaptic innervation (Bouyer et al., 1984; Xu et al., 1989). To visualize spines, we injected neonate *Cntnap2*;Drd1a-tdTomato (D1-tdT) mice with AAV5-Synapsin-GFP virus to sparsely label dSPNs and iSPNs in the DLS (Fig. S1) (Keaveney et al., 2018). We found that *Cntnap2*$^{-/-}$ SPNs in adult mice had similar spine density as WT SPNs (Fig. S1), suggesting no overall change in synapse number. Together, these results show that dSPNs and iSPNs in *Cntnap2*$^{-/-}$ mice exhibit enhanced cortically-driven spiking.

However, this is not due to a change in corticostriatal synaptic strength or overall synapse density.

*Cntnap2$^{-/-}$ mice do not exhibit reduced inhibition*

Previous work on *Cntnap2$^{-/-}$* mice has indicated a reduction in the number and/or function of fast-spiking parvalbumin (PV) interneurons across multiple brain regions (Ahmed et al., 2023; Antoine et al., 2019; Jurgensen & Castillo, 2015; Paterno et al., 2021; Penagarikano et al., 2011; Vogt et al., 2018). While inhibitory deficits have been identified in the cortex and hippocampus (Antoine et al., 2019; Jurgensen & Castillo, 2015), and the number of PV interneurons has been reported to be decreased in striatum (Penagarikano et al., 2011), a comprehensive assessment of inhibitory synaptic function has yet to be completed in the striatum of *Cntnap2$^{-/-}$* mice. To determine if there are broad deficits in inhibition onto SPNs in *Cntnap2$^{-/-}$* mice, we used intrastriatal electrical stimulation to evoke inhibitory postsynaptic currents (IPSCs) in dSPNs and iSPNs (Fig. 2A). We found that in *Cntnap2$^{-/-}$* dSPNs, the average electrically-evoked IPSCs across a range of stimulation intensities were not different from WT dSPNs (Fig. 2B,C). However, in *Cntnap2$^{-/-}$* iSPNs, IPSCs were, on average, significantly larger than those in WT iSPNs, although we note that the responses were variable across cells (Fig. 2D,E).

There are many sources of inhibition in the striatum (Burke et al., 2017), which can all be activated with electrical stimulation. To assess whether inhibition from PV interneurons specifically is altered in *Cntnap2$^{-/-}$* mice, we crossed *Cntnap2$^{-/-}$*;D1tdT mice to PV-Cre;RCL-ChR2-H134R-EYFP (Ai32) mice to express channelrhodopsin in PV interneurons (Fig. 2F) (Hippenmeyer et al., 2005; Madisen et al., 2010). We applied a blue light pulse of varying intensity over the recording site to evoke PV interneuron-specific IPSCs in SPNs, in the presence of excitatory synaptic blockers (Fig. 2F). We found that the average optically-driven IPSC did not differ in amplitude in *Cntnap2$^{-/-}$* dSPNs or iSPNs compared to WT controls (Fig. 2G-J).

To directly measure PV neuron function, we assessed the intrinsic excitability of PV interneurons in *Cntnap2$^{-/-}$* mice. To visualize PV interneurons for recordings, we crossed *Cntnap2$^{-/-}$* mice to PV-Cre;RCL-tdT (Ai9) mice (Fig. S2A). Plotting the number of APs fired as a function of current step size indicated that there were no significant differences in the intrinsic excitability of PV interneurons in *Cntnap2$^{-/-}$* mice compared to WT mice (Fig. S2B,C). There were also no changes in intrinsic cell properties such as membrane resistance, capacitance, or aspects of AP shape in PV interneurons in *Cntnap2$^{-/-}$* mice compared to controls (Fig. S2D-K).

Finally, given prior reports of altered PV cell number in *Cntnap2$^{-/-}$* mice (Paterno et al., 2021; Penagarikano et al., 2011; Vogt et al., 2018), we counted PV expressing cells in the striatum, using immunohistochemistry and *in situ* hybridization. We found no significant difference in the number of PV-positive cells in the dorsal striatum of

*Cntnap2*$^{-/-}$ mice compared to WT (Fig. S3A-F). Analysis of PV immunoreactivity per cell (Fig. S3H), *Pvalb* mRNA expression per cell (Fig. S3I-L), or total PV protein levels in the striatum (Fig. S3M,N) also showed no significant differences due to loss of Cntnap2. Overall, we did not observe significant changes in either PV interneuron number, PV expression, or PV interneuron-mediated inhibition in the adult *Cntnap2*$^{-/-}$ striatum compared to WT controls.

*SPN intrinsic excitability is increased in Cntnap2*$^{-/-}$ *mice*

Given that the increased cortical drive onto *Cntnap2*$^{-/-}$ SPNs is not explained by a gain of function of excitatory or loss of function of inhibitory synaptic function, we tested whether it could be due to a change in the intrinsic excitability of SPNs. To measure this, we recorded from *Cntnap2*$^{-/-}$ dSPNs and iSPNs in *Cntnap2*$^{-/-}$;D1tdT mice and injected current steps of increasing amplitude. We found that SPNs in *Cntnap2*$^{-/-}$ mice exhibited significantly increased intrinsic excitability compared to WT SPNs, which was most pronounced for dSPNs (Fig. 3A-L). *Cntnap2*$^{-/-}$ dSPNs, but not iSPNs, also had reduced rheobase current (Fig. 3C), the minimum current required to evoke an AP, as well as increased membrane resistance (Fig. 3D). Membrane capacitance (Fig. 3E,K), resting membrane potential (Fig. 3F,L), and AP shape (Fig. S4) were not significantly changed in *Cntnap2-/-* SPNs. Given the lack of synaptic changes observed in *Cntnap2*$^{-/-}$ SPNs, the increase in SPN intrinsic excitability likely underlies their enhanced corticostriatal drive (see Fig. 1).

*Cntnap2*$^{-/-}$ *mice exhibit increased spontaneous repetitive behaviors*

Restricted, repetitive behaviors (RRBs) comprise one of the primary symptom domains of ASD (APA, 2022). Alterations in striatal circuits are thought to be involved in the manifestation of RRBs, given the striatum's role in action selection and motor control (Estes et al., 2011; Fuccillo, 2016; Hollander et al., 2005; Langen et al., 2014). To determine whether the altered striatal physiology in *Cntnap2*$^{-/-}$ mice accompanied changes in motor behavior, we first assessed general locomotor activity and self-grooming in the open field assay (Fig. 4A,B). We found no significant differences in the total distance traveled, average speed, or number of rears in *Cntnap2*$^{-/-}$ mice compared to WT controls (Fig. 4E-G). We did find that *Cntnap2*$^{-/-}$ mice made significantly more entries into the center of the open field arena than WT mice, which may reflect a reduction in avoidance behavior in these mice (Fig. 4H). Manually scored grooming behavior (Fig. 4B) revealed that *Cntnap2*$^{-/-}$ mice initiated more grooming bouts than WT controls (Fig. 4I).

To further assess spontaneous motor behaviors in *Cntnap2*$^{-/-}$ mice, we utilized the marble burying assay (Fig. 4C). This test takes advantage of a mouse's natural tendency to dig or bury, and the number of marbles buried is used as a measure of persistent or repetitive behavior (Angoa-Perez et al., 2013). We found that *Cntnap2*$^{-/-}$

mice buried significantly more marbles on average than WT controls (Fig. 4J). Another measure of spontaneous repetitive behavior that takes advantage of exploratory behavior in mice is the holeboard assay (Fig. 4D). In this task, the number of nose pokes made into unbaited holes is recorded. We found that *Cntnap2*$^{-/-}$ mice made significantly more nosepokes within a 10-minute period than WT mice (Fig. 4K). This was largely due to increased poking during the last 5 minutes of the test (Fig. 4L-M), indicating persistent poking behavior in *Cntnap2*$^{-/-}$ mice. Together with the increased grooming identified in the open field, increased marble burying and nose poking indicate an increase in RRBs in *Cntnap2*$^{-/-}$ mice.

To gain further insight into the spontaneous behavior profile of *Cntnap2*$^{-/-}$ mice, we utilized a combination of DeepLabCut and MoSeq to perform unbiased, machine learning-based assessment of general locomotion and behavior in an additional cohort of *Cntnap2*$^{-/-}$ mice (Fig. S5) (Mathis et al., 2018; Wiltschko et al., 2020). Again, we found that *Cntnap2*$^{-/-}$ mice did not exhibit major changes in basic locomotor activity compared to WT littermates (Fig. S5A). Analysis of movement "syllables" using MoSeq revealed that across the 25 most frequently performed syllables, two syllables associated with grooming were performed with increased frequency in *Cntnap2*$^{-/-}$ mice (Fig. S5B). *Cntnap2*$^{-/-}$ mice also had an increased number of grooming bouts as well as increased total grooming time (Fig. S5C-D), replicating the findings in the manually scored cohort (see Fig. 4I). While syllable usage was generally similar between WT and *Cntnap2*$^{-/-}$ mice, transitions between syllables differed between the groups (Fig. S5E). A measure of the entropy of transitions revealed that *Cntnap2*$^{-/-}$ mice exhibited significantly less entropy, suggesting less variability in the transition from one movement syllable to the next (Fig. S5F). This rigidity in motor sequence may be indicative of more restricted motor behavior overall. Finally, we tested whether a trained decoder could accurately distinguish WT and *Cntnap2*$^{-/-}$ mice using information about syllable usage, transitions, and movement. The decoding models performed significantly better than chance at identifying WT and *Cntnap2*$^{-/-}$ mice based on their syllable usage and transitions, but not general locomotor activity (Fig. S5G). Together, this analysis demonstrates that while overall locomotor activity is not strongly affected in *Cnantp2*$^{-/-}$ mice, the behavior patterns of these mice are distinct from WT, reflecting enhanced presence of RRBs.

*Cntnap2*$^{-/-}$ *mice exhibit enhanced motor learning*

The accelerating rotarod is a striatal-dependent measure of motor coordination and learning that has been used across a range of ASD mouse models (Cording & Bateup, 2023). Changes in corticostriatal circuits have been identified in mouse models of ASD with altered performance in the task. Given the altered corticostriatal drive in *Cntnap2*$^{-/-}$ mice, we tested whether motor coordination and learning were affected in these mice. In the rotarod test, mice learn to walk and then run to stay on a rotating rod as it increases in speed over the course of five minutes. Mice perform three trials a day

for four days. In trials one through six, the rod increases in speed from five to 40 revolutions per minute (RPM), while in trials seven through 12 the rod increases from 10 to 80 RPM (Fig. 5A). Learning occurs over trials within a day, as well as across days, as the mouse develops and hones a stereotyped motor pattern to stay on the rod for increasing amounts of time (Rothwell et al., 2014; Yin et al., 2009). We found that *Cntnap2*$^{-/-}$ mice performed significantly better than WT mice in this task, in particular in the later trials when the rod is rotating at the faster 10 to 80 RPM speed (Fig. 5B). Initial performance (terminal velocity on trial one) was not different between WT and *Cntnap2*$^{-/-}$ mice (Fig. 5C), but the rate of learning from trial one to trial 12 was significantly increased in *Cntnap2*$^{-/-}$ mice (Fig. 5D). These findings expand upon previous work indicating increased performance on both steady-state and accelerating rotarod tasks utilizing slower speeds in *Cntnap2*$^{-/-}$ mice (Dawes et al., 2018; Penagarikano et al., 2011). These results also align with the increased rotarod performance seen in other ASD mouse models exhibiting increased corticostriatal drive (Benthall et al., 2021; Cording & Bateup, 2023).

*Cntnap2*$^{-/-}$ *mice exhibit cognitive inflexibility*

RRBs include not just stereotyped movements, but also insistence on sameness and perseverative interests (APA, 2022). Cognitive inflexibility, a deficit in the ability to flexibly adapt and update behavior, is a manifestation of ASD and some other psychiatric disorders that, like RRBs, is associated with striatal dysfunction (Fuccillo, 2016). Indeed, in individuals with ASD, the severity of RRBs is associated with measures of cognitive inflexibility, and imaging evidence suggests that altered corticostriatal connectivity may be present in the case of both repetitive behaviors and cognitive inflexibility (Uddin, 2021). To assess cognitive flexibility in *Cntnap2*$^{-/-}$ mice, we utilized a four-choice odor-based reversal learning assay (Lin et al., 2022). Briefly, mice are trained to dig for a reward in one of four pots containing scented wood shavings (Fig. 6A). On the first day of the task (acquisition), the rewarded pot is scented with odor one (O1). Mice reach criterion when they have chosen O1 for at least eight of 10 consecutive trials. On day two, mice are given a test of recall where the rewarded pot is again scented with O1. After reaching criterion, reversal trials begin, and the rewarded pot is now scented with the previously unrewarded odor two (O2). To reach criterion, mice must learn the new association of O2 and reward and choose O2 for eight of 10 consecutive trials.

During acquisition, *Cntnap2*$^{-/-}$ mice performed similarly to WT controls, not differing in the average number of trials needed to reach criterion, the number of quadrant entries made before choosing a pot to dig in, or the latency to choose a pot (Fig. 6B-D). On day two, *Cntnap2*$^{-/-}$ mice performed similarly to controls during recall, demonstrating successful consolidation of the odor-reward pairing (Fig. 6E). However, we found that *Cntnap2*$^{-/-}$ mice exhibited a significant deficit in reversal learning, requiring

significantly more trials on average than WTs to reach criterion once the odor-reward pairing was changed (Fig. 6F). Interestingly, *Cntnap2*$^{-/-}$ mice made fewer quadrant entries before making a digging choice and exhibited significantly decreased latency to make a choice compared to controls during reversal (Fig. 6G,H). Even after the first correct choice of O2 during reversal, *Cntnap2*$^{-/-}$ mice took significantly more trials to reach criterion than WTs (Fig. 6I). In terms of errors, *Cntnap2*$^{-/-}$ mice made significantly more reversal errors than WT mice (Fig. 6J), in particular perseverative (continuing to choose O1) and regressive (choosing O1 after correctly choosing O2 once) errors (Fig. 6K). *Cntnap2*$^{-/-}$ mice did not differ from WT controls in choices of the novel (newly introduced during reversal) or irrelevant (never rewarded) odors, or in number of omitted trials (timing out without making a choice) (Fig. 6K). Instead, the persistence in choosing O1, even after at least one correct choice of O2, drove the cognitive inflexibility in these mice (Fig. 6L). This persistence in choice, and the speed at which it was done, may be reflective of the broader scope of RRBs in *Cntnap2*$^{-/-}$ mice.

## Figures

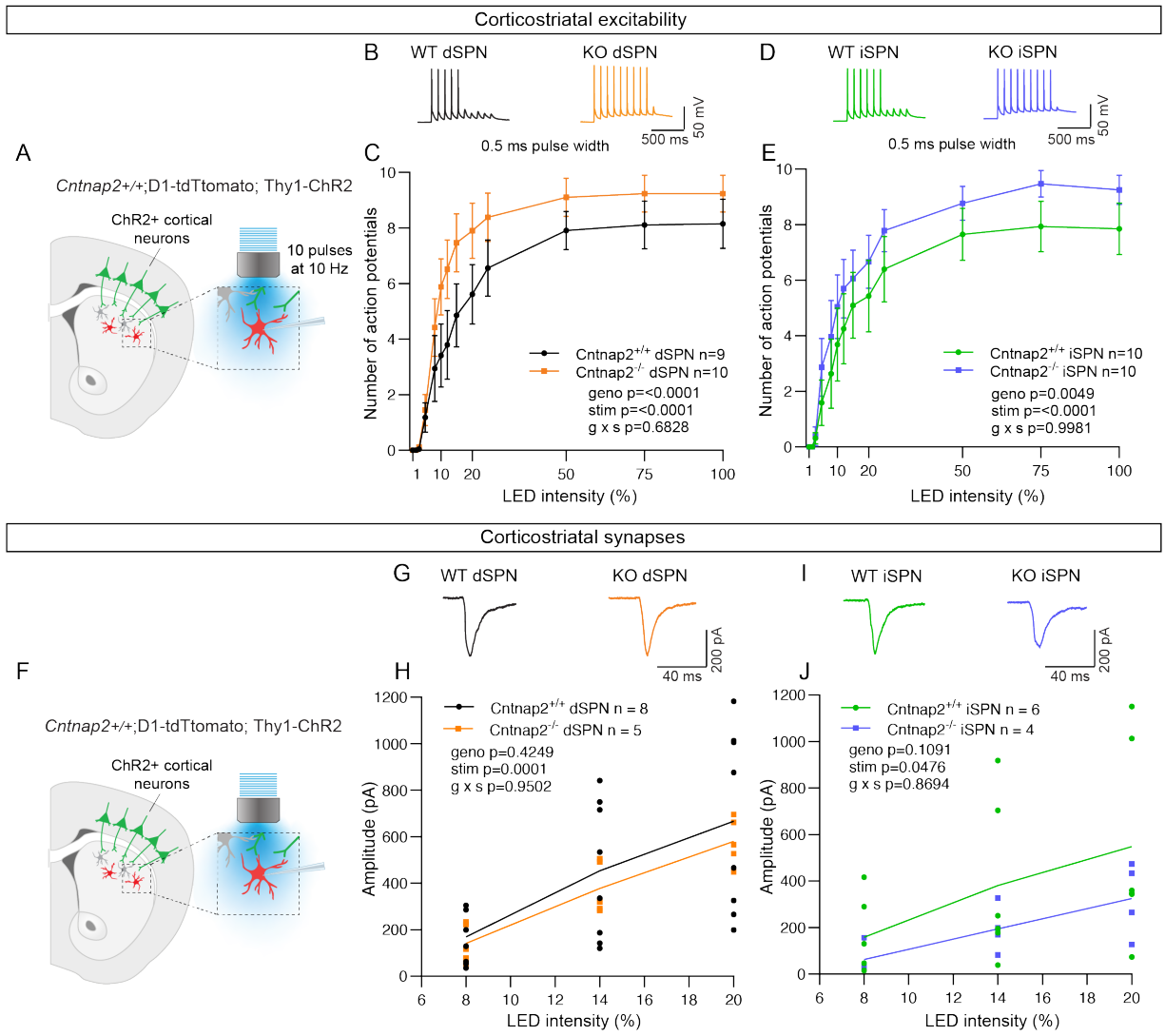


**Figure 1. *Cntnap2*$^{-/-}$ SPNs exhibit increased cortical drive**

(A) Schematic of the corticostriatal excitability experiment. Cortical terminals expressing ChR2 were stimulated with 10 pulses of blue light at 10 Hz and responses were recorded from dSPNs (red) and iSPNs (grey) in dorsolateral striatum.

(B) Example single traces of action potentials (APs) in dSPNs evoked by cortical terminal stimulation at 20% light intensity for the indicated genotypes.

(C) Quantification (mean ± SEM) of the number of APs evoked in dSPNs at different light intensities. *Cntnap2*$^{+/+}$ n = 9 mice, 24 cells, *Cntnap2*$^{-/-}$ n = 10 mice, 22 cells. Two-way ANOVA p values are shown; geno F (1, 221) = 16.75, stim F (12, 221) = 34.19, g x s F (12, 221) = 0.7682.

(D) Example single traces of action potentials (APs) in iSPNs evoked by cortical terminal stimulation at 20% light intensity for the indicated genotypes.

(E) Quantification (mean ± SEM) of the number of APs evoked in iSPNs at different light intensities. *Cntnap2*$^{+/+}$ n = 9 mice, 23 cells, *Cntnap2*$^{-/-}$ n = 10 mice, 21 cells. Two-way ANOVA p values are shown; geno F (1, 234) = 8.067, stim F (12, 234) = 24.88, g x s F (12, 234) = 0.2057.
(F) Schematic of the corticostriatal synaptic function experiment. Cortical terminals expressing ChR2 were stimulated with blue light at increasing intensity and responses were recorded from dSPNs (red) and iSPNs (grey) in dorsolateral striatum.
(G) Average trace from an example neuron of EPSCs induced by ChR2$^{+}$ cortical terminal stimulation at 14% light intensity in dSPNs for the indicated genotypes.
(H) Quantification of EPSC amplitude evoked in dSPNs at different light intensities (line represents the mean, dots/squares represent average EPSC amplitude for each mouse). *Cntnap2*$^{+/+}$ n = 8 mice, 17 cells, *Cntnap2*$^{-/-}$ n = 5 mice, 13 cells. Two-way ANOVA p values are shown; geno F (1, 33) = 0.6527, stim F (2, 33) = 11.80, g x s F (2, 33) = 0.05117.
(I) Average trace from an example neuron of EPSCs induced by ChR2+ cortical terminal stimulation at 14% light intensity in iSPNs for the indicated genotypes.
(J) Quantification EPSC amplitude evoked in iSPNs at different light intensities (line represents mean, dots/squares represent average for mouse). *Cntnap2*$^{+/+}$ n = 6 mice, 13 cells, *Cntnap2*$^{-/-}$ n = 4 mice, 11 cells. Two-way ANOVA p values are shown; geno F (1, 24) = 2.770, stim F (2, 24) = 3.466, g x s F (2, 24) = 0.1408.

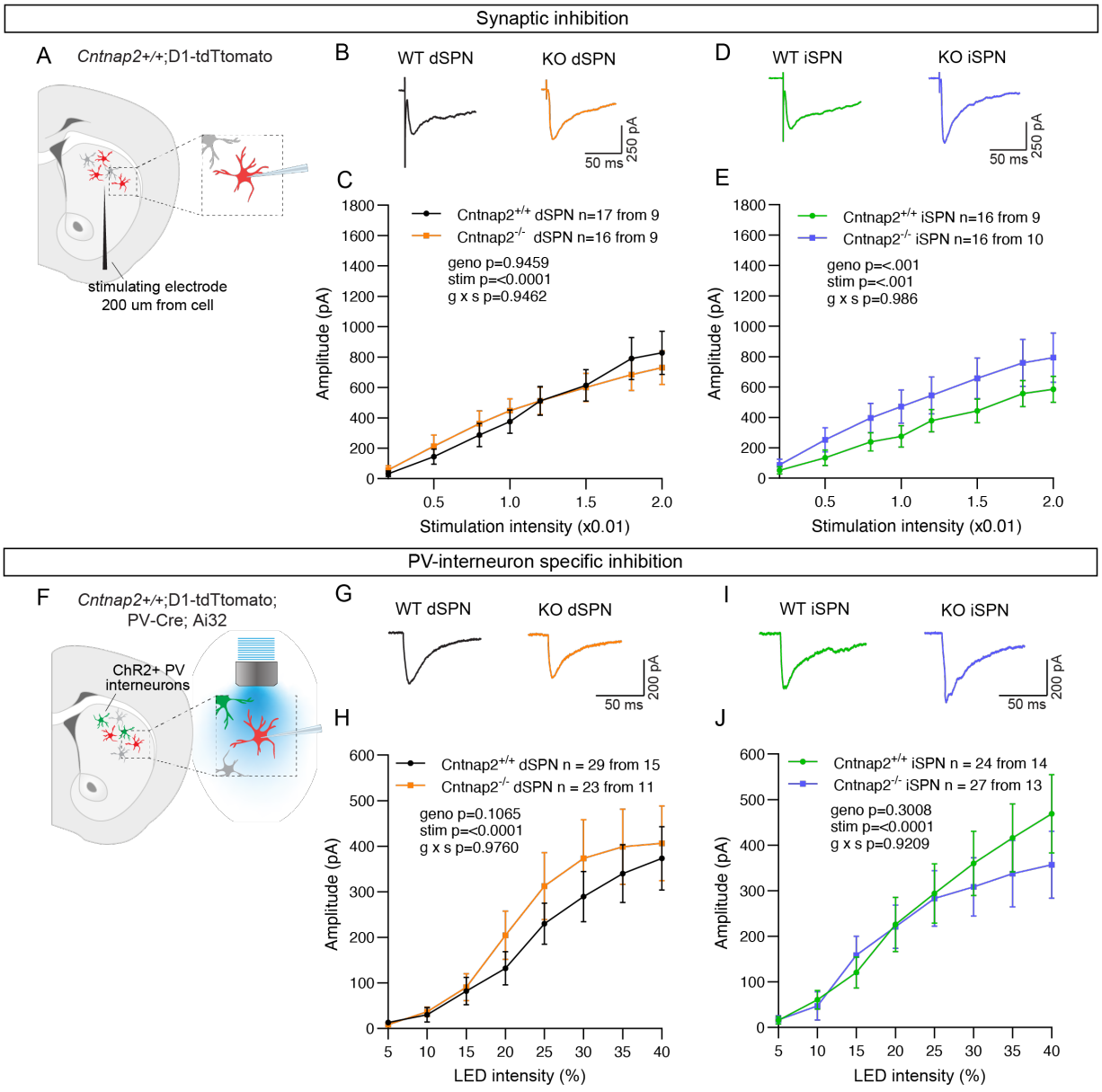


**Figure 2. *Cntnap2*$^{-/-}$ mice do not exhibit reduced inhibition**

(A) Schematic of the experiment. A bipolar stimulating electrode was placed roughly 200 mm from the recording site. A range of electrical stimulation intensities were applied to the tissue while IPSCs were recorded from dSPNs (red) and iSPNs (grey) in dorsolateral striatum.

(B) Average trace from an example neuron of IPSCs in dSPNs evoked by electrical stimulation at 1.5 (x0.01 mA) intensity for the indicated genotypes.

(C) Quantification (mean ± SEM) of the amplitude of IPSCs evoked in dSPNs at different stimulation intensities. *Cntnap2*$^{+/+}$ n = 17 cells from 9 mice, *Cntnap2*$^{-/-}$ n = 16 cells from 9 mice. Two-way ANOVA p values are shown; geno F (1, 248) = 0.004612, stim F (7, 248) = 16.09, g x s F (7, 249) = 0.3164.

(D) Average trace from an example neuron of IPSCs in iSPNs evoked by electrical stimulation at 1.5 (x0.01) intensity for the indicated genotypes.
(E) Quantification (mean ± SEM) of the amplitude of IPSCs evoked in iSPNs at different stimulation intensities. *Cntnap2*$^{+/+}$ n = 16 cells from 9 mice, *Cntnap2*$^{-/-}$ n = 16 cells from 10 mice. Two-way ANOVA p values are shown; geno F (1, 240) = 11.25, stim F (7, 240) = 10.17, g x s F (7, 240) = 0.1947.
(F) Schematic of the experiment. PV interneuron terminals expressing ChR2 were stimulated with blue light at a range of intensities and optically-evoked IPSCs were recorded from dSPNs (red) and iSPNs (grey) in dorsolateral striatum.
indicated genotypes.
(G) Average trace from an example neuron of IPSCs in dSPNs evoked by optogenetic PV interneuron stimulation at 30% light intensity for the indicated genotypes.
(H) Quantification (mean ± SEM) of the amplitude of IPSCs evoked in dSPNs at different light intensities. *Cntnap2*$^{+/+}$ n = 29 cells from 15 mice, *Cntnap2*$^{-/-}$ n = 23 cells from 11 mice. Two-way ANOVA p values are shown; geno F (1, 504) = 0.006524, stim F (7, 504) = 14.26, g x s F (7, 504) = 0.1124.
(I) Average trace from an example neuron of IPSCs in iSPNs evoked by optogenetic PV interneuron stimulation at 30% light intensity for the indicated genotypes.
(J) Quantification (mean ± SEM) of the amplitude of IPSCs evoked in iSPNs at different light intensities. *Cntnap2*$^{+/+}$ n = 24 cells from 14 mice, *Cntnap2*$^{-/-}$ n = 27 cells from 13 mice. Two-way ANOVA p values are shown; geno F (1, 392) = 2.638, stim F (7, 392) = 13.59, g x s F (7, 392) = 0.5088.

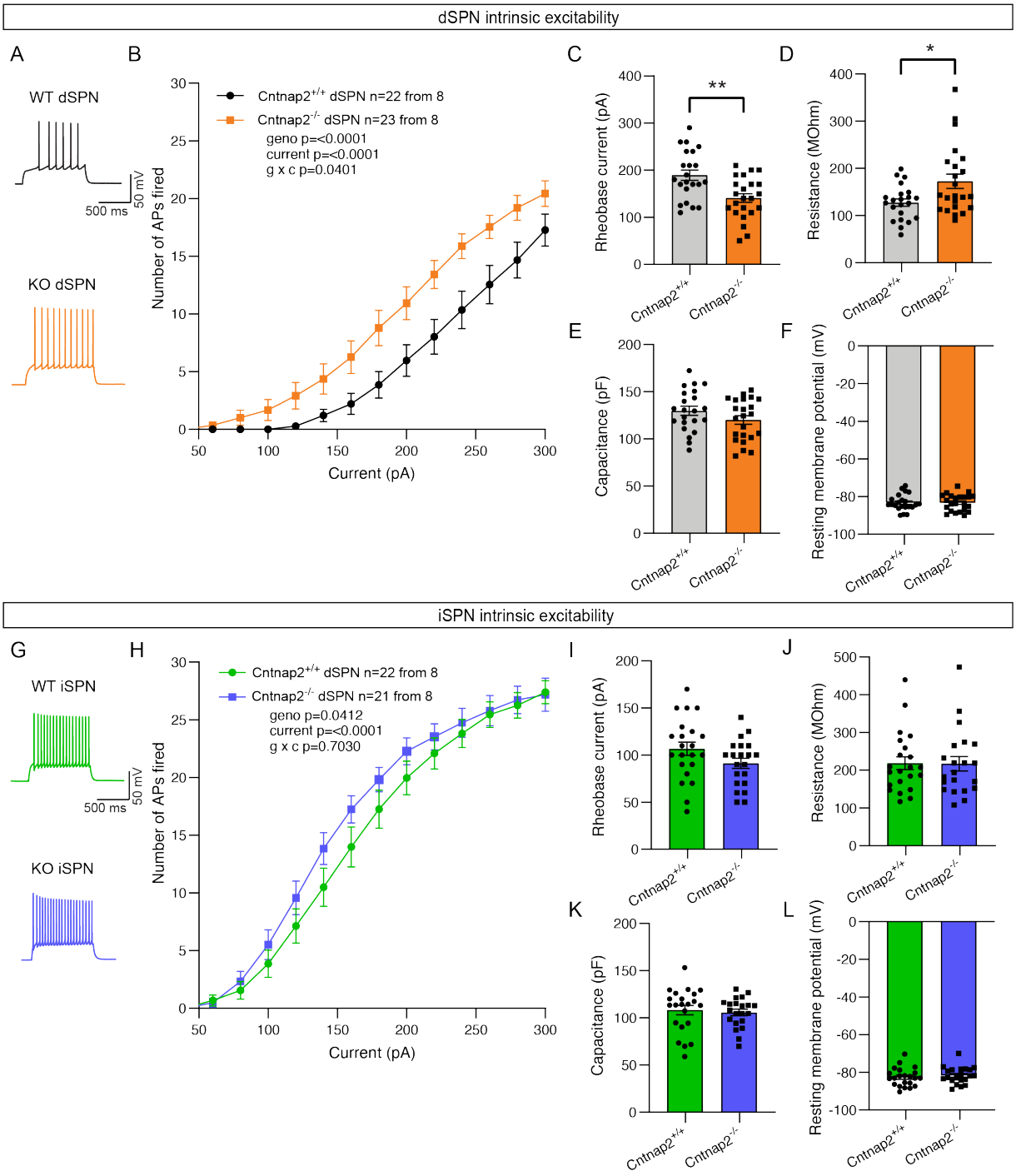


**Figure 3. SPN intrinsic excitability is increased in *Cntnap2*$^{-/-}$ mice**

(A) Example traces of APs in dSPNs evoked by a 200 pA current step for the indicated genotypes.

(B) Quantification (mean ± SEM) of the number of APs evoked in dSPNs at different current step amplitudes. *Cntnap2*$^{+/+}$ n = 22 cells from 8 mice, *Cntnap2*$^{-/-}$ n = 23 cells

from 8 mice. Two-way ANOVA p values are shown; geno F (1, 688) = 48.80, stim F (15, 688) = 107.5, g x s F (15, 688) = 1.737.
(C) Quantification (mean ± SEM) of the rheobase current. Dots/squares represent the rheobase current for each neuron. n is the same as in panel B. p = 0.0016, two-tailed unpaired t test.
(D-F) Quantification (mean ± SEM) of the membrane resistance (D), p = 0.0328, Mann-Whitney test; membrane capacitance (E), p = 0.2182, Mann-Whitney test; and resting membrane potential (F), p = 0.9914, two-tailed unpaired t test. Dots/squares represent the average value for each neuron. n is the same as in panel B.
(G) Example traces of APs in iSPNs evoked by a 200 pA current step for the indicated genotypes.
(H) Quantification (mean ± SEM) of the number of APs evoked in iSPNs at different current step amplitudes. *Cntnap2*$^{+/+}$ n = 22 cells from 8 mice, *Cntnap2*$^{-/-}$ n = 21 cells from 8 mice. Two-way ANOVA p values are shown; geno F (1, 656) = 4.186, stim F (15, 656) = 118.7, g x s F (15, 656) = 0.7780.
(I) Quantification (mean ± SEM) of the rheobase current. Dots/squares represent the rheobase current for each neuron. n is the same as in panel H. p = 0.0923, two-tailed unpaired t test.
(J-K) Quantification (mean ± SEM) of the membrane resistance (J), p = 0.8193, Mann-Whitney test; membrane capacitance (K), p = 0.6886, two-tailed unpaired t test; and resting membrane potential (L), p = 0.4859, two-tailed unpaired t test. Dots/squares represent the average value for each neuron. n is the same as in panel H.

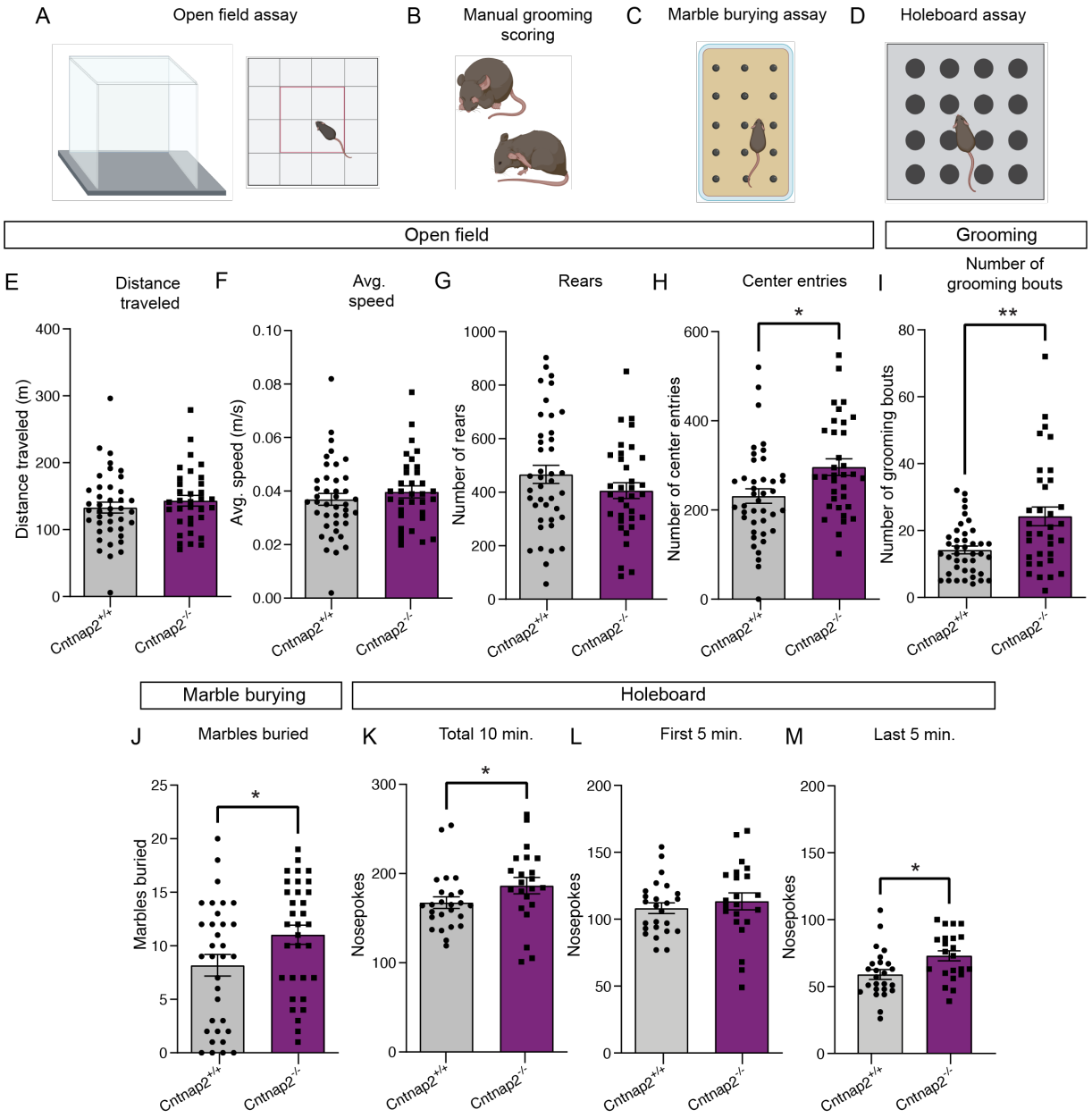


**Figure 4. *Cntnap2*$^{-/-}$ mice exhibit increased spontaneous repetitive behaviors**
(A-D) Schematics of the behavioral assays used to measure spontaneous repetitive behaviors in *Cntnap2*$^{+/+}$ and *Cntnap2*$^{-/-}$ mice, created with BioRender.com.
(E-H) Quantification (mean ± SEM) of open field performance. (E) total distance traveled, p = 0.3538, Mann-Whitney test; (F) average speed, p = 0.3832, Mann-Whitney test; (G) number of rears, p = 0.1892, two-tailed unpaired t test; (H) number of center entries, p = 0.0101, two-tailed unpaired t test. *Cntnap2*$^{+/+}$ n = 41 mice, *Cntnap2*$^{-/-}$ n = 34 mice.

(I) Quantification (mean ± SEM) of the total number of grooming bouts in the first 20 minutes of the open field test, p = 0.0034, Mann-Whitney test, *Cntnap2*$^{+/+}$ n = 41 mice, *Cntnap2*$^{-/-}$ n = 34 mice.
(J) Quantification (mean ± SEM) of the number of total marbles buried in the marble burying assay. *Cntnap2*$^{+/+}$ n = 33 mice and *Cntnap2*$^{-/-}$ n = 33 mice, p = 0.0396, two-tailed unpaired t test.
(K-M) Quantification (mean ± SEM) of performance in the holeboard assay. (K) Total number of nose pokes made in 10 minutes, p = 0.0212, Mann-Whitney test; (L) nose pokes made in the first five minutes, p = 0.4811, two-tailed unpaired t test; and (M) nose pokes made in the last five minutes, p = 0.0116, two-tailed unpaired t test. *Cntnap2*$^{+/+}$ n = 25 mice, *Cntnap2*$^{-/-}$ n = 22 mice.
For panels E-M, dots/squares represent the value for each mouse.

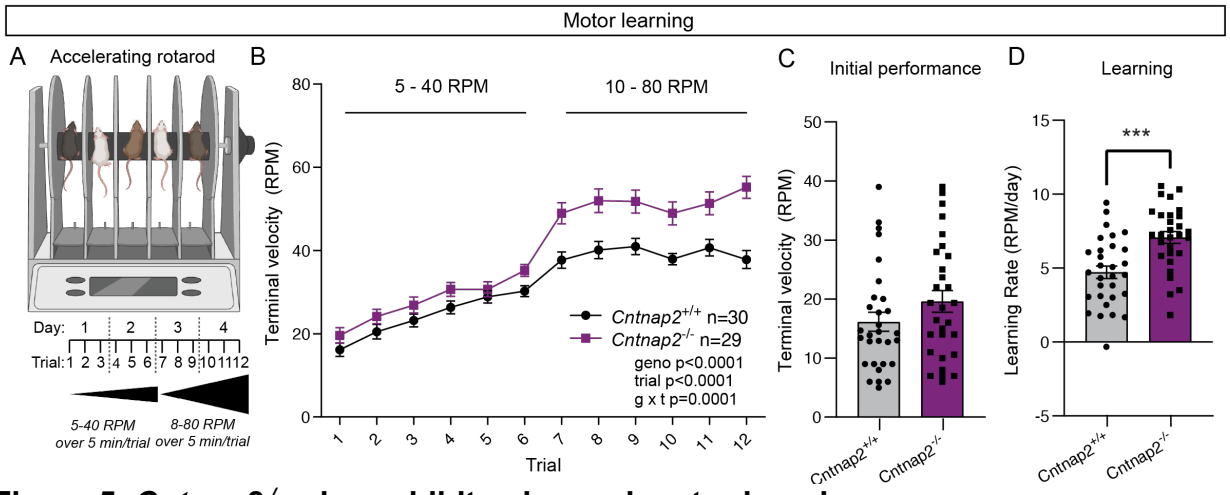


**Figure 5. *Cntnap2*$^{-/-}$ mice exhibit enhanced motor learning**

(A) Schematic of the accelerating rotarod assay (top), and structure of the task over days (bottom). Mice walk to stay on the rotating rod for three 5-minute trials a day for two days at 5-40 RPM acceleration, followed by three trials a day for two days at 10-80 RPM.

(B) Quantification (mean ± SEM) of accelerating rotarod performance across 12 trials (4 days) for the indicated genotypes. *Cntnap2*$^{+/+}$ n = 30 mice, *Cntnap2*$^{-/-}$ n = 29 mice. Two-way ANOVA p values are shown; geno F (1, 683) = 91.86, stim F (11, 683) = 56.53, g x s F (11, 683) = 2.859.

(C) Quantification (mean ± SEM) of rotarod performance on trial 1 quantified as terminal speed. Dots/squares represent the performance of individual mice. n is same as in panel B, p = 0.0994, Mann-Whitney test.

(D) Quantification (mean ± SEM) of overall learning calculated as the slope of the line of performance on the first trial (1) to the last trial (12) for each mouse (RPM/day). Dots/squares represent the learning rate for individual mice. n is same as in panel B, p = 0.0002, two-tailed unpaired t test.

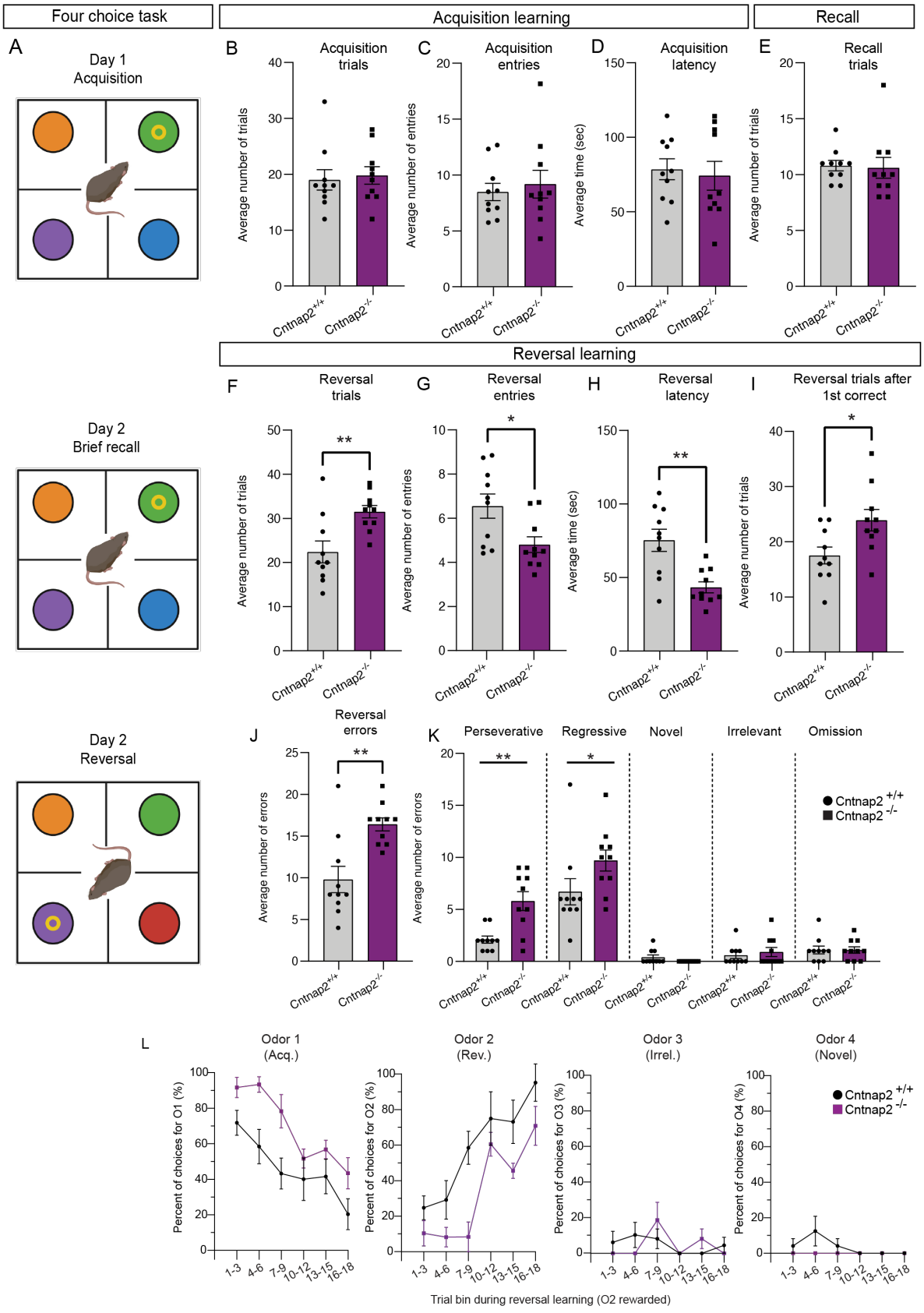
Four choice task
Acquisition learning
Recall
A
Day 1
Acquisition
B
Acquisition
trials
Average number of trials
C
Acquisition
entries
Average number of entries
D
Acquisition
latency
Average time (sec)
E
Recall
trials
Average number of trials
Cntnap2+/+
Cntnap2-/-
Reversal learning
Day 2
Brief recall
F
Reversal
trials
G
Reversal
entries
H
Reversal
latency
I
Reversal trials after
1st correct
Day 2
Reversal
J
Reversal
errors
Average number of errors
K
Perseverative
Regressive
Novel
Irrelevant
Omission
Cntnap2 +/+
Cntnap2 -/-
L
Odor 1
(Acq.)
Odor 2
(Rev.)
Odor 3
(Irrel.)
Odor 4
(Novel)
Percent of choices for O1 (%)
Percent of choices for O2 (%)
Percent of choices for O3 (%)
Percent of choices for O4 (%)
1-3
4-6
7-9
10-12
13-15
16-18
Trial bin during reversal learning (O2 rewarded)

**Figure 6. *Cntnap2*$^{-/-}$ mice exhibit cognitive inflexibility**

(A) Schematic of the four-choice odor-based reversal learning task. Yellow ring represents the location of the food reward. Red circle in the Day 2 Reversal panel indicates a novel odor.

(B-D) Quantification of parameters during acquisition learning. Mean ± SEM number of trials to reach criterion (at least 8 out of last 10 trials correct) (B), p = 0.5397, Mann-Whitney test; number of quadrant entries before making a choice (C), p = 0.9118, Mann-Whitney test; and latency to make a choice (D), p = 0.7224, two-tailed unpaired t test. Dots/squares represent the value for each mouse.

(E) Quantification (mean ± SEM) of the number of trials to reach criterion (at least 8 out of last 10 trials correct) during the recall test on day 2, p = 0.3737, Mann-Whitney test.

(F-I) Quantification of parameters during reversal learning. Mean ± SEM number of trials to reach criterion (at least 8 out of last 10 trials correct) (F), p = 0.0048, two-tailed unpaired t test; number of quadrant entries before making a choice (G), p = 0.0158, two-tailed unpaired t test; latency to make a choice (H), p = 0.0013, two-tailed unpaired t test; and number of trials to reach criterion after the first correct choice (I), p = 0.0183, two-tailed unpaired t test.

(J) Quantification (mean ± SEM) of the total number of errors made during reversal learning, p = 0.0034, Mann-Whitney test.

(K) Quantification (mean ± SEM) of the different error types made during reversal learning, Perseverative errors, p = 0.0013, two-tailed unpaired t test; regressive errors p = 0.0284, Mann-Whitney test; novel errors, p = 0.2105, Mann-Whitney test; irrelevant errors p = 0.7628, Mann-Whitney test, omissions, p = 0.9201, Mann-Whitney test.

(L) Quantification (mean ± SEM) of the percent of choices made for the given odor labeled in each subpanel, binned across three trials, during reversal learning. Odor 1 was rewarded during acquisition learning and odor 2 was rewarded during reversal learning.

For panels B-L, n = 10 *Cntnap2*$^{+/+}$ mice and 10 *Cntnap2*$^{-/-}$ mice.

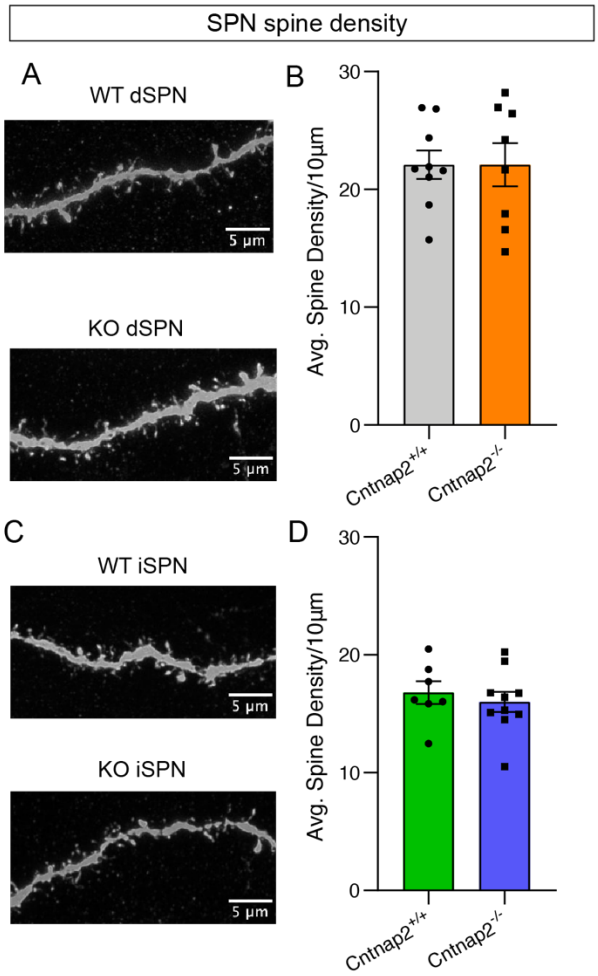


**Supplementary Figure 1. *Cntnap2*$^{-/-}$ SPNs do no exhibit altered spine density**
(A) Representative images of dendritic spines from dSPNs for the indicated genotypes. (B) Quantification (mean ± SEM) of dendritic spine density per 10 um of dendrite in *Cntnap2*$^{+/+}$ and *Cntnap2*$^{-/-}$ dSPNs. Dots/squares represent the average spine density per neuron. *Cntnap2*$^{+/+}$ n = 9 neurons (15 dendrites) from 6 mice, *Cntnap2*$^{-/-}$ n = 8 neurons (15 dendrites) from 6 mice. p = 0.9964, two-tailed unpaired t test.
(C) Representative images of dendritic spines from iSPNs for the indicated genotypes. (D) Quantification (mean ± SEM) of dendritic spine density per 10 um of dendrite in *Cntnap2*$^{+/+}$ and *Cntnap2*$^{-/-}$ iSPNs. Dots/squares represent the average spine density per neuron. *Cntnap2*$^{+/+}$ n = 7 neurons (15 dendrites) from 4 mice, *Cntnap2*$^{-/-}$ n = 10 neurons (15 dendrites) from 7 mice. p = 0.5362, Mann-Whitney test.

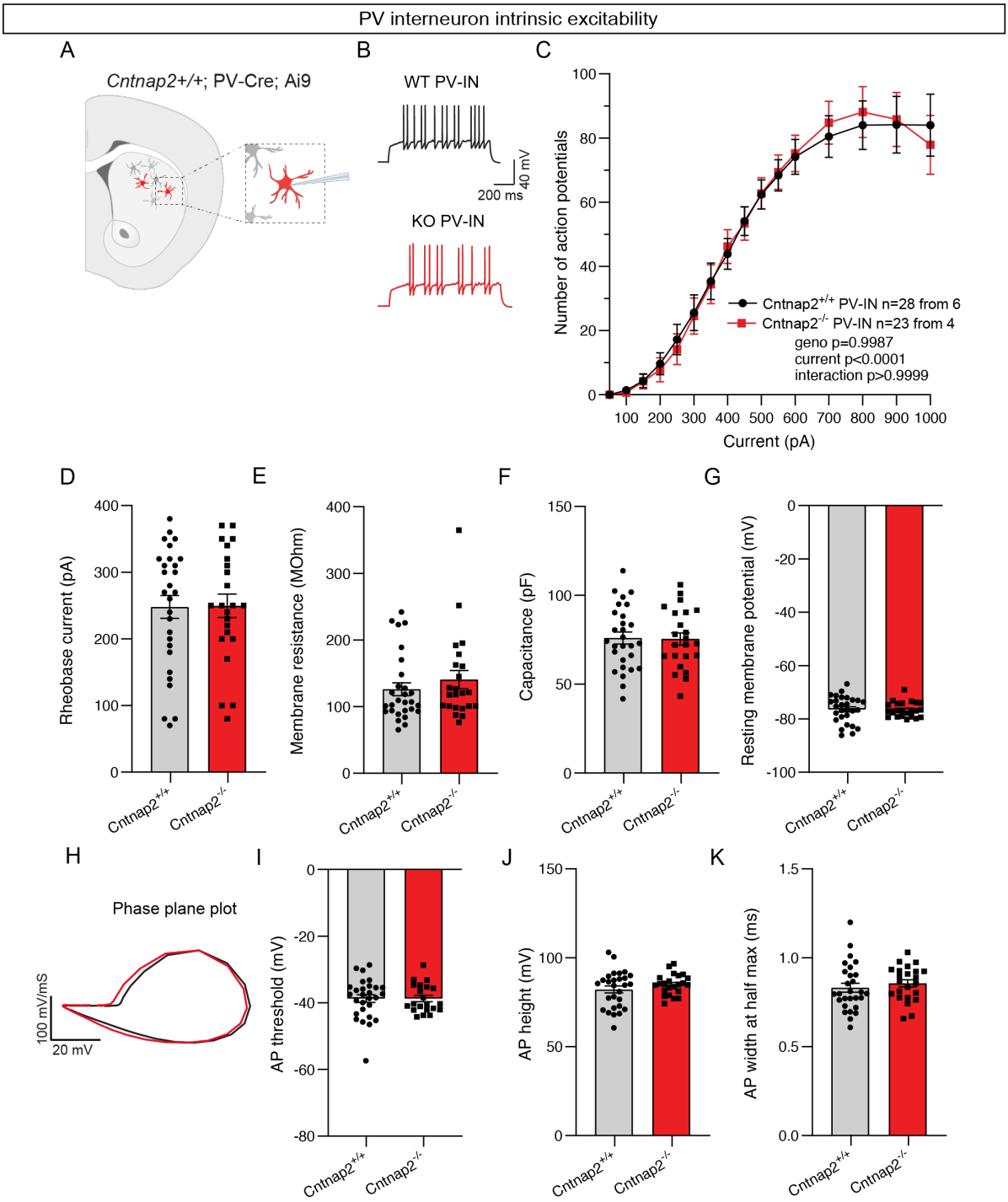


**Supplementary Figure 2. *Cntnap2*$^{-/-}$ PV interneurons do not exhibit changes in intrinsic excitability**

(A) Schematic of the experiment. tdTomato-expressing PV interneurons were recorded in the dorsolateral striatum and injected with current steps of varying magnitude to evoke firing.

(B) Example traces of APs in PV interneurons evoked by a 200 pA current step for the indicated genotypes.
(C) Quantification (mean ± SEM) of the number of APs evoked in PV interneurons at different current step amplitudes. *Cntnap2*$^{+/+}$ n = 28 cells from 6 mice, *Cntnap2*$^{-/-}$ n = 23 cells from 4 mice. Two-way ANOVA p values are shown; geno F (1, 784) = 2.728e-006, stim F (15, 784) = 67.25, g x s F (15, 784) = 0.1039.
(D) Quantification (mean ± SEM) of the rheobase current. Dots/squares represent the rheobase current for each neuron. n is the same as in panel D. p = 0.8852, two-tailed unpaired t test.
(E-G) Quantification (mean ± SEM) of the membrane resistance (E), p = 0.3422, Mann-Whitney test; membrane capacitance (F), p = 0.9055, two-tailed unpaired t test; and resting membrane potential (G), p = 0.3141, two-tailed unpaired t test. Dots/squares represent the average value for each neuron. n is the same as in panel D.
(H) Phase plane plot of a single AP evoked in PV interneurons in *Cntnap2*$^{+/+}$ (black) and *Cntnap2*$^{-/-}$ (red) mice.
(I-K) Quantification (mean ± SEM) of the AP threshold (I), p = 0.6025, two-tailed unpaired t test; AP height (J), p = 0.2850, two-tailed unpaired t test; and AP width at half max (K), p = 0.2561, two-tailed unpaired t test. Dots/squares represent the value for the first spike evoked at rheobase for each neuron. N is the same as in panel D.

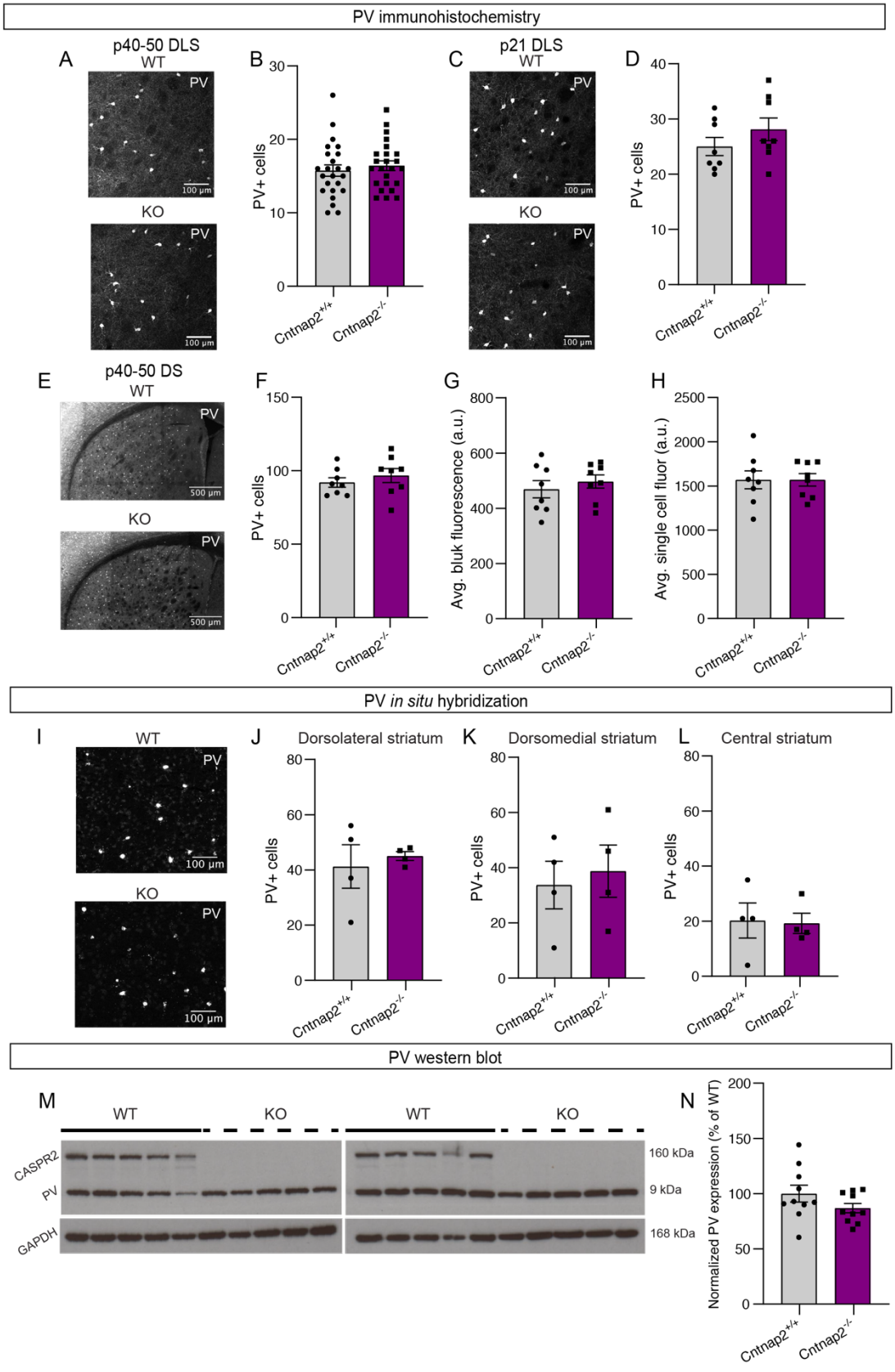
PV immunohistochemistry
A
p40-50 DLS
WT
PV
100 µm
KO
PV
100 µm
B
PV+ cells
30
20
10
0
Cntnap2+/+
Cntnap2-/-
C
p21 DLS
WT
PV
100 µm
KO
PV
100 µm
D
PV+ cells
40
30
20
10
0
Cntnap2+/+
Cntnap2-/-
E
p40-50 DS
WT
PV
500 µm
KO
PV
500 µm
F
PV+ cells
150
100
50
0
Cntnap2+/+
Cntnap2-/-
G
Avg. bluk fluorescence (a.u.)
800
600
400
200
0
Cntnap2+/+
Cntnap2-/-
H
Avg. single cell fluor (a.u.)
2500
2000
1500
1000
500
0
Cntnap2+/+
Cntnap2-/-
PV in situ hybridization
I
WT
PV
100 µm
KO
PV
100 µm
J
Dorsolateral striatum
PV+ cells
80
60
40
20
0
Cntnap2+/+
Cntnap2-/-
K
Dorsomedial striatum
PV+ cells
80
60
40
20
0
Cntnap2+/+
Cntnap2-/-
L
Central striatum
PV+ cells
80
60
40
20
0
Cntnap2+/+
Cntnap2-/-
PV western blot
M
WT
KO
WT
KO
CASPR2
PV
GAPDH
160 kDa
9 kDa
168 kDa
N
Normalized PV expression (% of WT)
200
150
100
50
0
Cntnap2+/+
Cntnap2-/-

**Supplementary Figure 3. *Cntnap2*$^{-/-}$ mice do not exhibit changes in PV cell number or expression**

(A) Representative confocal images of dorsolateral striatum labeled with an antibody against parvalbumin (PV) protein (grey) for the indicated genotypes, mice aged p40-50.
(B) Quantification (mean ± SEM) of the number of parvalbumin positive cells per ROI, p = 0.5144, two-tailed unpaired t test. *Cntnap2*$^{+/+}$ n = 24 sections from 12 mice (2 sections imaged per mouse), *Cntnap2*$^{-/-}$ n = 24 sections from 12 mice (2 sections imaged per mouse).
(C) Representative confocal images of dorsolateral striatum labeled with an antibody against PV protein (grey) for the indicated genotypes, mice aged p21.
(D) Quantification (mean ± SEM) of the number of parvalbumin positive cells per ROI, p = 0.2554, two-tailed unpaired t test. *Cntnap2*$^{+/+}$ n = 8 sections from 4 mice (2 sections imaged per mouse), *Cntnap2*$^{-/-}$ n = 8 sections from 4 mice (2 sections imaged per mouse).
(E) Representative confocal images of dorsal striatum labeled with an antibody against parvalbumin protein (grey) for the indicated genotypes, mice aged p40-50.
(F) Quantification (mean ± SEM) of the number of parvalbumin positive cells in the whole dorsal striatum, p = 0.4201, two-tailed unpaired t test. *Cntnap2*$^{+/+}$ n = 8 sections from 4 mice (2 sections imaged per mouse), *Cntnap2*$^{-/-}$ n = 8 sections from 4 mice (2 sections imaged per mouse).
(G) Quantification (mean ± SEM) of the average bulk fluorescence of parvalbumin antibody staining in dorsal striatum, p = 0.4878, two-tailed unpaired t test. *Cntnap2*$^{+/+}$ n = 8 sections from 4 mice (2 sections imaged per mouse), *Cntnap2*$^{-/-}$ n = 8 sections from 4 mice (2 sections imaged per mouse).
(H) Quantification (mean ± SEM) of the average single cell fluorescence of parvalbumin antibody staining in dorsal striatum, p = 0.9996, two-tailed unpaired t test. *Cntnap2*$^{+/+}$ n = 8 sections from 4 mice (2 sections imaged per mouse), *Cntnap2*$^{-/-}$ n = 8 sections from 4 mice (2 sections imaged per mouse).
(I) Representative confocal images of *in situ* hybridization for *Pvalb* in dorsolateral striatum (grey) for the indicated genotypes, mice aged p40-50.
(J-L) Quantification (mean ± SEM) of the number of *Pvalb* positive cells in the dorsolateral striatum (J), p = >0.9999, Mann-Whitney test; dorsomedial striatum (K), p = 0.7429, Mann-Whitney test; and central striatum (L), p = 0.6286, Mann-Whitney test. *Cntnap2*$^{+/+}$ n = 4 sections from 2 mice (2 sections imaged per mouse), *Cntnap2*$^{-/-}$ n = 4 sections from 2 mice (2 sections imaged per mouse).
(M) Representative western blots for CASPR2, PV, and GAPDH in dorsal striatal tissue punches.

(N) Quantification (mean ± SEM) of PV protein expression normalized to GAPDH. Data are presented as a percentage of *Cntnap2*$^{+/+}$ levels, p = 0.1485, two-tailed unpaired t test. *Cntnap2*$^{+/+}$ n = 10 samples from 10 mice, *Cntnap2*$^{-/-}$ n = 10 samples from 10 mice.

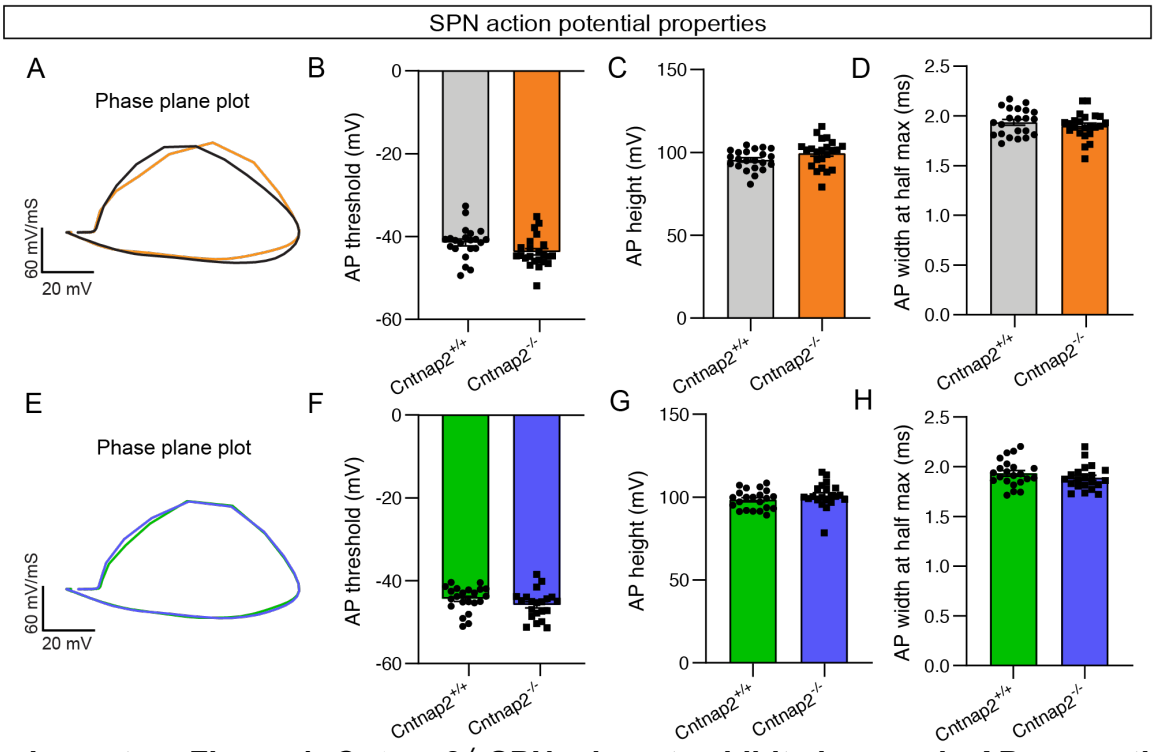


**Supplementary Figure 4. *Cntnap2*$^{-/-}$ SPNs do not exhibit changes in AP properties**

(A) Phase plane plot of a single AP evoked in dSPNs in *Cntnap2*$^{+/+}$ (black) and *Cntnap2*$^{-/-}$ (orange) mice.

(B-D) Quantification (mean ± SEM) of the AP threshold (B), p = 0.0516, two-tailed unpaired t test; AP height (C), p = 0.0833, two-tailed unpaired t test; and AP width at half max (D), p = 0.3792, two-tailed unpaired t test. Dots/squares represent the value for the first spike evoked at rheobase for each neuron. *Cntnap2*$^{+/+}$ n = 22 cells from 8 mice, *Cntnap2*$^{-/-}$ n = 23 cells from 8 mice.

(E) Phase plane plot of a single AP evoked in iSPNs in *Cntnap2*$^{+/+}$ (green) and *Cntnap2*$^{-/-}$ (blue) mice.

(F-H) Quantification (mean ± SEM) of the AP threshold (F), p = 0.1495, two-tailed unpaired t test; AP height (G), p = 0.1794, Mann-Whitney test; and AP width at half max (H), p = 0.2409, two-tailed unpaired t test. Dots/squares represent the value for the first spike evoked at rheobase for each neuron. *Cntnap2*$^{+/+}$ n = 22 cells from 8 mice, *Cntnap2*$^{-/-}$ n = 21 cells from 8 mice.

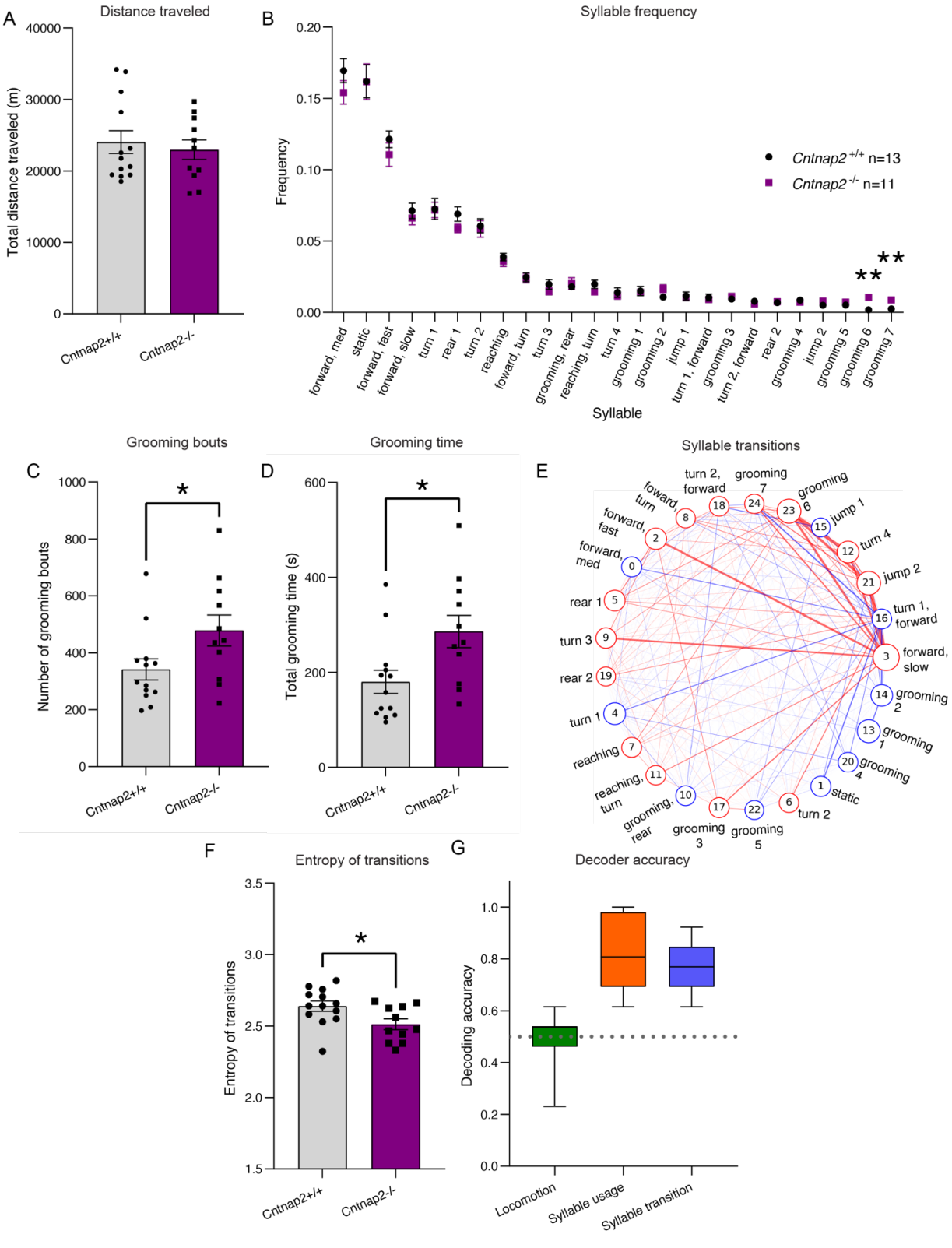
A
Distance traveled
Total distance traveled (m)
40000
30000
20000
10000
0
Cntnap2+/+
Cntnap2-/-
B
Syllable frequency
Frequency
0.20
0.15
0.10
0.05
0.00
Cntnap2 +/+ n=13
Cntnap2 -/- n=11
**
**
forward, med
static
forward, fast
forward, slow
turn 1
rear 1
turn 2
reaching
foward, turn
turn 3
grooming, rear
reaching, turn
turn 4
grooming 1
grooming 2
jump 1
turn 1, forward
grooming 3
turn 2, forward
rear 2
grooming 4
jump 2
grooming 5
grooming 6
grooming 7
Syllable
C
Grooming bouts
Number of grooming bouts
1000
800
600
400
200
0
*
Cntnap2+/+
Cntnap2-/-
D
Grooming time
Total grooming time (s)
600
400
200
0
*
Cntnap2+/+
Cntnap2-/-
E
Syllable transitions
turn 2, forward
grooming 7
grooming 6
foward, turn
forward, fast
forward, med
jump 1
turn 4
jump 2
turn 1, forward
forward, slow
grooming 2
grooming 1
grooming 4
static
turn 2
grooming 5
grooming 3
grooming, rear
reaching, turn
reaching
turn 1
rear 2
turn 3
rear 1
F
Entropy of transitions
Entropy of transitions
3.5
3.0
2.5
2.0
1.5
*
Cntnap2+/+
Cntnap2-/-
G
Decoder accuracy
Decoding accuracy
1.0
0.8
0.6
0.4
0.2
0.0
Locomotion
Syllable usage
Syllable transition

**Supplementary Figure 5. DeepLabCut, MoSeq identify increased grooming, decreased movement entropy in *Cntnap2*$^{-/-}$ mice**

(A) Quantification (mean ± SEM) of the total distance traveled in the open field assay, p = 0.8201, Mann-Whitney test; *Cntnap2*$^{+/+}$ n = 13 mice and *Cntnap2*$^{-/-}$ n = 11 mice,

(B) Quantification (mean ± SEM) of the frequency of movement syllables in the open field assay. *Cntnap2*$^{+/+}$ n = 13 mice and *Cntnap2*$^{-/-}$ n = 11 mice, p = 0.00125 for grooming 6, p = 0.00125 for grooming 7, Kruskal-Wallis test with Dunn's correction for multiple comparisons.

(C) Quantification (mean ± SEM) of the number of grooming bouts performed in the open field assay. *Cntnap2*$^{+/+}$ n = 13 mice and *Cntnap2*$^{-/-}$ n = 11 mice, p = 0.0352, Mann-Whitney test.

(D) Quantification (mean ± SEM) of the total time spent grooming in the open field assay. *Cntnap2*$^{+/+}$ n = 13 mice and *Cntnap2*$^{-/-}$ n = 11 mice, p = 0.0129, Mann-Whitney test.

(E) Map depicting the difference in transitions between syllables for *Cntnap2*$^{+/+}$ and *Cntnap2*$^{-/-}$ mice (*Cntnap2*$^{-/-}$ - *Cntnap2*$^{+/+}$). A red circle around a syllable name indicates increased usage of that syllable in *Cntnap2*$^{-/-}$ mice, a blue circle around a syllable name indicates decreased usage of that syllable in *Cntnap2*$^{-/-}$ mice. A red line between syllable names indicates increased usage of that syllable transition in *Cntnap2*$^{-/-}$ mice, a blue line between syllable names indicates decreased usage of that syllable transition in *Cntnap2*$^{-/-}$ mice. The thickness of lines scale with size of difference.

(F) Quantification (mean ± SEM) of the entropy of all syllable transitions in the open field assay. *Cntnap2*$^{+/+}$ n = 13 mice and *Cntnap2*$^{-/-}$ n = 11 mice, p = 0.0236, two-tailed unpaired t test.

(G) Accuracy of a Random Forest decoder trained on DeepLabCut basic locomotor data (green), MoSeq syllable usage data (orange), or MoSeq syllable transition data (blue) in distinguishing between *Cntnap2*$^{+/+}$ and *Cntnap2*$^{-/-}$ mice. Dotted line represents chance performance.

## Discussion

In this study we tested whether loss of the ASD risk gene *Cntnap2* results in altered striatal function and the manifestation of altered motor behaviors. We found that both direct and indirect pathway SPNs exhibit significantly increased cortical drive in *Cntnap2*$^{-/-}$ mice. This change was likely not due to a change in excitatory or inhibitory input, as excitatory cortical input onto SPNs was unchanged and there were no significant deficits in inhibition onto SPNs in these mice. Instead, loss of Cntnap2 resulted in a significant increase in intrinsic excitability in SPNs, in particular in dSPNs. This increase in excitability is likely what underlies the increased corticostriatal drive seen in *Cntnap2*$^{-/-}$ mice. *Cntnap2*$^{-/-}$ mice exhibited significant increases in repetitive motor behaviors, spending more time grooming in the open field assay, burying more marbles in the marble burying assay, and performing more nosepokes in the holeboard assay. These mice also exhibited enhanced motor learning, performing significantly better than controls in the accelerating rotarod task. Finally, *Cntnap2*$^{-/-}$ mice exhibited increased cognitive inflexibility in the four choice reversal learning task.

The loss of Caspr2 has a variable impact on intrinsic excitability across brain regions and cell types. The increased intrinsic excitability that we identified in SPNs is a cellular phenotype that has been reported in Purkinje cells of the cerebellum (Fernandez et al., 2021), and pyramidal cells of the cortex (Antoine et al., 2019; Cifuentes-Diaz et al., 2023) (however we note hypoactivity (Brumback et al., 2018) or unchanged excitability (Lazaro et al., 2019) of pyramidal cells in some cortical regions in *Cntnap2*$^{-/-}$ mice). Caspr2 has been shown to be involved in the clustering of voltage-gated potassium channels, in particular at the juxtaparanodes of myelinated axons (Poliak et al., 1999; Poliak et al., 2003) and axon initial segment (Inda et al., 2006) (although subcellular distribution assay reveals that Caspr2 is present throughout the neuron (Varea et al., 2015)). Indeed there are profound deficits in the clustering of Kv1-family channels in *Cntnap2*$^{-/-}$ mice, particularly Kv1.2 channels (Scott et al., 2019). These channels play an important role in regulating the intrinsic excitability of SPNs (Nisenbaum et al., 1994), and when blocked, result in decreased rheobase and increased firing in SPNs (Shen et al., 2004). The loss of Caspr2 in *Cntnap2*$^{-/-}$ mice that results in the improper localization of these channels may contribute to the decreased rheobase and increased SPN excitability seen in these mice. While Caspr2 has most often been discussed for this interaction with Kv1-family channels, recent work has shown that it can also play a role in calcium signaling. The extracellular domain of Caspr2, after undergoing cleavage through proteolytic processing, can interact with the calcium extrusion pump PMCA2, promoting calcium export and likely decreasing cell excitability (Martin-de-Saavedra et al., 2022). That this process, which increases with neuronal activity, is missing in *Cntnap2*$^{-/-}$ mice may also contribute to the increased intrinsic excitability that we found in SPNs.

Prior studies of *Cntnap2*$^{-/-}$ mice have identified changes in the number of parvalbumin (PV) interneurons in cortex (Penagarikano et al., 2011; Vogt et al., 2018), hippocampus (Paterno et al., 2021; Penagarikano et al., 2011) and striatum (Penagarikano et al., 2011). However, this finding is inconsistent across *Cntnap2*$^{-/-}$ mouse studies, as others have reported no change in the number of PV interneurons in these regions (Ahmed et al., 2023; Lauber et al., 2018; Scott et al., 2019). One possible explanation for this disparity is altered PV protein expression in *Cntnap2*$^{-/-}$ mice such that immunoreactivity varies in cell counting assessments. This is supported by the finding that the number of Vicia Villosa Agglutinin-positive (VVA+) perineuronal nets (PNN) that preferentially surround PV cells is unchanged in *Cntnap2*$^{-/-}$ mice, even when PV immunoreactivity varies (Hartig et al., 1992; Haunso et al., 2000; Lauber et al., 2018). Parvalbumin, a $Ca^{2+}$ buffer, plays an important role in the intrinsic fast-spiking properties of PV interneurons, such that a reduction in PV protein expression is known to change PV intrinsic function (Orduz et al., 2013). However, altered intrinsic function of PV interneurons has also been variably reported across brain regions and studies of *Cntnap2*$^{-/-}$ mice, with subtle changes in PV firing properties reported in developing striatum (Ahmed et al., 2023) and adult cortex (Vogt et al., 2018), but unchanged intrinsic function of PV cells reported in hippocampus (Paterno et al., 2021) and medial prefrontal cortex (Lazaro et al., 2019). In this study, we find no significant change in the number of PV interneurons or the striatal expression of PV protein in *Cntnap2*$^{-/-}$ mice. Following from this, we find no significant deficit in PV-specific inhibition onto SPNs nor do we find any differences in PV interneuron intrinsic excitability in these mice. Interestingly, we find that broad inhibition measured through intrastriatal stimulation is enhanced specifically onto iSPNs in *Cntnap2*$^{-/-}$ mice. This change is likely driven by altered function or connectivity of one of a number of non-PV interneurons, or other SPNs, that provide lateral inhibition onto iSPNs, as PV-specific inhibition onto these cells was unchanged. It is possible that this gain of function in inhibition onto *Cntnap2*$^{-/-}$ iSPNs results in increased disinhibition of nearby connected dSPNs, further increasing direct pathway activity. However, inhibitory connectivity between SPNs in the striatum is relatively weak and sparse compared to the inhibitory connectivity between GABAergic interneurons and SPNs (Burke et al., 2017).

The striatum can be separated into functionally distinct subregions. We focused on the dorsal striatum in this study because of its role in controlling motor and cognitive functions (Voorn et al., 2004). While the ventral striatum, implicated in mediating limbic functions like appetitive behavior and reward, likely also plays a role in ASD-associated behaviors (Fuccillo, 2016; Subramanian et al., 2017), our interest in the motor behavior symptom domain drew our focus to dorsal striatum. Further parsing, based primarily on differences in cortical inputs, separates the dorsomedial striatum (DMS) from dorsolateral striatum (DLS), with the former considered an associative region involved in goal-directed learning of action-outcome pairs and the latter implicated in the acquisition

of habitual or procedural behaviors (Packard & Knowlton, 2002). We focused on cell function in DLS in this study because we believe that this subregion plays a role in the repetitive behaviors seen in ASD, as stereotyped, perseverative or persistent behaviors likely recruit DLS circuitry (Evans et al., 2024; Fuccillo, 2016). In the accelerating rotarod assay, learning and performance in the task has been associated with changes in DLS. Positive modulation of the firing rate of neurons in DLS occurs during rotarod training, in particular in later trials of the task, and synaptic potentiation of DLS SPNs into late training is necessary for intact performance. Following from this, lesions of DLS impair both early and late learning (Yin et al., 2009). However, we note that in some mouse models, deletion of an ASD risk gene specifically from nucleus accumbens (NAc) was sufficient to increase rotarod performance, supporting a potential role for the ventral striatum in the performance of this task (Platt et al., 2017; Rothwell et al., 2014). We found that *Cntnap2*$^{-/-}$ mice exhibit increased performance in the accelerating rotarod task, in particular at the later stages of the task where DLS function has been most implicated. Functionally, we also found increased cortical drive of SPNs in DLS in these mice, in particular in direct pathway dSPNs, a change that resulted in increased rotarod performance in another mouse model of ASD (Benthall et al., 2021). Together this supports a connection between the functional change observed in DLS SPN physiology and the increased motor routine learning in *Cntnap2*$^{-/-}$ mice.

We identified a range of other altered basal ganglia-associated behaviors in *Cntnap2*$^{-/-}$ mice in this study, some of which are likely to implicate altered function of other striatal subregions. We observed increased spontaneous grooming in *Cntnap2*$^{-/-}$ mice, a phenotype that has been previously reported (Penagarikano et al., 2011). Early evidence implicates the striatum in the control of the syntax or sequence of movements in a rodent grooming bout, such that very small lesions of DLS are capable of disrupting grooming (Cromwell & Berridge, 1996). However, recent work has also outlined roles for cellular modulation in DMS and ventral striatal Islands of Calleja in the control of grooming behavior (Ramirez-Armenta et al., 2022; Zhang et al., 2021). *Cntnap2*$^{-/-}$ mice also exhibited increases in marble burying and nosepoking in the holeboard assay. The precise neurobiological substrates of these behaviors are yet unclear, but evidence linking increases in these behaviors to changes in cortico-striatal and amygdala-striatal function supports the notion that these behaviors may fit into a broader basal ganglia-associated RRB-like domain (Albelda & Joel, 2012; Lee et al., 2024). In the four choice reversal learning task, *Cntnap2*$^{-/-}$ mice exhibited no differences in acquisition learning, suggesting that these mice have no broad deficit in learning (supported as well by the enhanced learning seen in the rotarod task). However, in the reversal stage of the task, *Cntnap2*$^{-/-}$ mice took significant more trials to learn a new odor-reward pairing, owing primarily to continued choice of the previously rewarded odor. The DMS and nucleus accumbens (NAc, ventral striatum), in particular dopaminergic release and modulation in these regions, have been shown to play an important role in reversal learning

(Izquierdo et al., 2017), and in the four choice task in particular (Delevich et al., 2022). Although, we note that in one study utilizing the assay, decreased dopamine release solely in DLS coincided with a similar deficit in reversal learning to that seen in *Cntnap2*$^{-/-}$ mice in this study (Lin et al., 2022). Although potentially due to altered cellular function in different striatal regions, taken together, the learning phenotypes seen in *Cntnap2*$^{-/-}$ mice in the accelerating rotarod and reversal learning assay share an underlying rigidity in behavioral choice. In both cases, changes in striatal circuits likely underlie the repetitive, stereotyped motor procedures, as may be the case for the inflexible behaviors seen in ASD etiology as a whole.

Changes in striatal function have been implicated in both human and animal studies as playing a potential role in some of the behavioral manifestations of ASD (Fuccillo, 2016; Hollander et al., 2005; Langen et al., 2014). In more recent years, changes at the corticostriatal synapse in particular have been increasingly identified across a diverse genetic range of ASD mouse models (Li & Pozzo-Miller, 2020). In some cases, there are convergent behavioral changes observed across models that share in altered corticostriatal circuits. In the case of the accelerating rotarod for example, a number of ASD mouse models that exhibit synaptic changes expected to enhance striatal activation, in particular increasing corticostriatal drive and/or excitability of the direct pathway, also exhibit enhanced performance on the task (Benthall et al., 2021; Platt et al., 2017; Rothwell et al., 2014). However, the cellular changes that likely underlie the shared change in striatal output are divergent, resulting from a reduction in inhibition onto SPNs (Rothwell et al., 2014), enhanced excitatory input onto SPNs (Benthall et al., 2021), or a combination of the two (Platt et al., 2017). In this study we found that *Cntnap2*$^{-/-}$ mice also exhibit altered corticostriatal function through increased corticostriatal drive, and enhanced rotarod performance. In this model, this is likely due to the increased intrinsic excitability of SPNs, in particular dSPNs, as neither enhanced excitatory nor decreased inhibitory signaling onto SPNs were identified in *Cntnap2*$^{-/-}$ mice. Together, our results fit into a model where divergent cellular changes in the striatum across a genetically diverse group of ASD mouse models similarly enhance corticostriatal drive, in particular in the direct pathway, and in turn imbue the striatum with enhanced motor routine learning. It's possible that this shared gain-of-function in striatal circuits plays a role in the formation of perseverative or repetitive behaviors in ASD-like motor behaviors more broadly.

**Acknowledgements**
We thank Emilie Tu for carrying out the holeboard and four-choice odor-based reversal learning task, and Hongli Wang, PhD for carrying out the DeepLabCut and MoSeq analysis.

**Experimental procedures**

Mice

*Cntnap2*$^{-/-}$ mice (Jackson Laboratory strain #017482; (Poliak et al., 2003)) of a mixed 129/SvEv and C57BL/6J background were used to study Cntnap2 loss. To identify SPNs of the direct pathway (dSPNs), *Cntnap2*$^{-/-}$ mice were crossed to Drd1a-tdTomato (D1-tdT) mice (Jackson Laboratory strain #016204; (Ade et al., 2011)). To express YFP-tagged ChR2 in a subset of Layer V cortical pyramidal cells, the Thy1-ChR2-YFP mouse line (Jackson Laboratories strain #007612; (Arenkiel et al., 2007)) was bred to *Cntnap2*$^{-/-}$;D1-tdT mice. To express YFP-tagged ChR2 in parvalbumin (PV) interneurons, the PV-Cre mouse line (Jackson Laboratories strain #017320; (Hippenmeyer et al., 2005)) was bred to the Ai32 mouse line (Jackson Laboratories strain #017320; (Madisen et al., 2012)), leading to expression of ChR2-YFP in PV positive cells. These mice were crossed to *Cntnap2*$^{-/-}$;D1-tdT mice to assess PV interneuron inhibition onto SPNs in *Cntnap2*$^{-/-}$ mice. To identify PV interneurons, PV-Cre mice were bred to the tdTomato Cre reporter Ai9 mouse line (Jackson Laboratory strain #007909; (Madisen et al., 2010)). These mice were crossed to *Cntnap2*$^{-/-}$ mice to assess PV interneuron intrinsic excitability in *Cntnap2*$^{-/-}$ mice.

Mice were group housed on a 12 h light/dark cycle (dark cycle 9:00 AM – 9:00 PM) and given ad libitum access to standard rodent chow and water. Both male and female animals were used for experimentation. The ages, sexes, and numbers of mice used for each experiment are indicated in the respective method details and figure legends. All mice used for experiments were heterozygous or hemizygous for the Drd1a-tdTomato, Thy1-ChR2-YFP, PV-Cre, Ai32, or Ai9 transgenes to avoid potential physiological or behavioral alterations. All animal procedures were conducted in accordance with protocols approved by the University of California, Berkeley Institutional Animal Care and Use Committee (IACUC) and Office of Laboratory Animal Care (OLAC).

Electrophysiology

Mice (P50-60) were quickly anesthetized with isoflurane and perfused transcardially with ice-cold ACSF (pH = 7.4) containing (in mM): 127 NaCl, 25 NaHCO3, 1.25 NaH2PO4, 2.5 KCl, 1 MgCl2, 2 CaCl2, and 25 glucose, bubbled continuously with carbogen (95% O2 and 5% CO2). Brains were rapidly removed and coronal slices (275 um) were cut on a VT1000S vibratome (Leica) in oxygenated ice-cold choline-based external solution (pH = 7.8) containing (in mM): 110 choline chloride, 25 NaHCO3, 1.25 NaHPO4, 2.5 KCl, 7 MgCl2, 0.5 CaCl2, 25 glucose, 11.6 sodium ascorbate, and 3.1

sodium pyruvate. Slices were recovered in ACSF at 36°C for 15 min and then kept at RT before recording. Recordings were made with a MultiClamp 700B amplifier (Molecular Devices) at RT using 3-5 MOhm glass patch electrodes (Sutter, BF150-86-7.5). Data were acquired using ScanImage software, written and maintained by Dr. Bernardo Sabatini (https://github. com/bernardosabatini/ SabalabAcq). Traces were analyzed in Igor Pro (Wavemetrics). Recordings with a series resistance > 25 MOhms or holding current above 200 pA were rejected.

*Current-clamp recordings*

Current clamp recordings were made using a potassium-based internal solution (pH = 7.4) containing (in mM): 135 KMeSO4, 5 KCl, 5 HEPES, 4 Mg-ATP, 0.3 Na-GTP, 10 phosphocreatine, and 1 EGTA. For corticostriatal excitability experiments, optogenetic stimulation consisted of a full-field pulse of blue light (470 nm, 0.5 ms, CoolLED) through a 63x objective. Light power was linear over the range of intensities tested. No synaptic blockers were included. For intrinsic excitability experiments (both SPN and PV interneuron), NBQX (10 mM, Tocris, 1044), CPP (10 mM, Tocris, 0247) and picrotoxin (50 mM, Abcam, 120315) were added to the external solution to block synaptic transmission. One second depolarizing current steps were applied to induce action potentials. No holding current was applied to the membrane.

*Voltage-clamp recordings*

Voltage-clamp recordings were made using a cesium-based internal solution (pH = 7.4) containing (in mM): 120 CsMeSO4, 15 CsCl, 10 TEA-Cl, 8 NaCl, 10 HEPES, 1 EGTA, 5 QX-314, 4 Mg-ATP, and 0.3 Na-GTP. Recordings were acquired with the amplifier Bessel filter set at 3 kHz. Corticostriatal synaptic stimulation experiments to measure evoked AMPA-mediated EPSCs were performed in picrotoxin (50 mM), and optogenetic stimulation consisted of a full-field pulse of blue light (470 nm, 0.15 ms) through a 63x objective. Synaptic stimulation experiments to measure evoked IPSCs were performed in NBQX (10 mM, Tocris, 1044) and CPP (10 mM, Tocris, 0247). For electrically evoked IPSCs, a concentric bipolar stimulating electrode (FHC #30214) was placed in dorsal striatum, roughly 200 um medial to the recording site in dorsolateral striatum, and a 0.15 ms stimulus was applied. For PV-interneuron optically evoked IPSCs, a full-field pulse of blue light (470 nm, 0.15 ms) was applied through a 63x objective at the recording site.

<u>Dendritic imaging and spine analysis</u>

Neonatal (P1-3) *Cntnap2*$^{-/-}$;D1-tdT and *Cntnap2*$^{+/+}$;D1-tdT mice were cryoanesthetized and injected bilaterally with 200 nL AAV1.hSyn.eGFP.WPRE.bGH (Penn Vector Core, p1696 (Keaveney et al., 2018)), diluted 1:75 in saline to achieve sparse transduction. Injections were targeted to the dorsal striatum, with coordinates

approximately 1.3 mm lateral to midline, 2.0 mm posterior to bregma, and 1.5 mm ventral to the head surface. At age P50-60, mice were anesthetized with isoflurane and transcardial perfusion was performed with 10 mL of 1x PBS followed by 10 mL of ice cold 4% PFA (EMS, 15710-S) in 1x PBS. Brains were post-fixed in 4% PFA in 1x PBS overnight at 4°C. 80 µm coronal sections were made using a freezing microtome (American Optical, AO 860) and stored in 1x PBS at 4°C. Sections were blocked for 1 hour at RT in BlockAid (ThermoFisher, B10710) and incubated for 48 hours with gentle shaking at 4°C with antibodies against GFP (1:2500, Abcam, 13970) and RFP (1:1000, Rockland (VWR), 600-401-379) diluted in PBS-Tx (1x PBS with 0.25% Triton X-100 (Sigma, T8787)). Sections were washed 3 x 10 min in PBS-Tx and incubated with gentle shaking for 1 hour at RT with Alexa Fluor 488 and 546 secondary antibodies (1:500, Invitrogen, A11039, A11035). Sections were washed 3 x 10 min in 1x PBS and mounted onto SuperFrost slides (VWR, 48311- 703) using VECTASHIELD HardSet Antifade Mounting Medium (Vector Laboratories, H-1400-10). Z stack images of individual dendrites were taken on a confocal microscope (Olympus FLUOVIEW FV3000) with a 60x oil immersion objective (Olympus #1-U2B832) at 2.5x zoom with a step size of 0.4 µm. To quantify spine density, dendrites and spines were reconstructed using the FilamentTracer module in Imaris software (Oxford Instruments). The spine density of each dendrite was calculated using Imaris. Dendrites analyzed varied in total length, but excluded the most proximal and distal portions of the dendrite.

Brain sectioning and immunohistochemistry

Adult mice were perfused as above and brains were post-fixed with 4% paraformaldehyde overnight, then sectioned coronally at 30 µm. For immunohistochemistry, individual wells of sections were washed with 3 x 5 min with 1x PBS, then blocked for 1 hour at RT with BlockAid blocking solution. Primary antibodies diluted in PBS-Tx were added and tissue was incubated for 48 hours with gentle shaking at 4°C. Sections were then washed 3 x 10 min with PBS-Tx. Secondary antibodies diluted 1:500 in PBS-Tx were added and incubated with gentle shaking for 1 hour at room temperature. Sections were washed 3 x 10 min in 1x PBS. Sections were mounted onto SuperFrost slides (VWR, 48311- 703) and coverslipped with VECTASHIELD HardSet with DAPI (Vector Laboratories, H-1500-10) or VECTASHIELD HardSet Antifade Mounting Medium (Vector Laboratories, H-1400-10). The following antibodies were used: mouse anti-PV (1:1000, Sigma, P3088), rabbit anti-PV (1:1000, Abcam, 11427), anti-RFP (1:500, Rockland, 600-401-379), Alexa Fluor 405, 488 and 546 conjugated secondary antibodies (1:500, Invitrogen, A-31553, A-11001, A-11003, and A-11035).

*PV cell counting*

To count PV interneurons, Z-stack images of immunostained striatal sections were taken on a confocal microscope (Olympus FLUOVIEW FV3000) with a 10x or 20x objective (Olympus # 1-U2B824 or Olympus # 1-U2B825) and step size of 2 µm. For quantification, image stacks were Z-projected to maximum intensity using Fiji (ImageJ) and cropped to a 400um X 400um image in anatomically matched sections of the DLS using a blank channel to minimize bias. All positive cells were then counted in the PV channel using the ROI manager tool. To quantify bulk and individual cell PV fluorescence, ROIs were manually defined in ImageJ using the Freehand tool (whole dorsolateral striatum area (DLS) or all individual PV positive cells within DLS ROI) and mean fluorescence intensity was measured.

Western Blot

Adult mice (P48-55) were deeply anesthetized with isoflurane and decapitated. Brains were rapidly dissected on ice, and 1.5 mm dorsal striatum punches (Biopunch, Ted Pella, 15111-15) were collected from both hemispheres, flash-frozen in liquid nitrogen, and stored at −80°C. On the day of analysis, frozen samples were sonicated (QSonica Q55) until homogenized in 200 µl lysis buffer containing 1% SDS in 1x PBS with Halt phosphatase inhibitor cocktail (Fisher Scientific, PI78420) and Complete mini EDTA-free protease inhibitor cocktail (Roche, 4693159001). Sample homogenates were then boiled on a heat block at 95°C for 5 min and allowd to cool to RT. Total protein content was determined using a BCA assay (ThermoScientific #23227). Following the BCA assay, protein homogenates were mixed with 4x Laemmli sample buffer (BioRad, 161-0747). Proteins (12.5µg) were then loaded onto 12% Criterion TGX gels (BioRad, 5671044) and run at 65 V. Proteins were then transferred to a PVDF membrane (BioRad, 1620177) at 11 V for 14 hours at 4°C using the BioRad Criterion Blotter. Membranes were briefly reactivated in methanol and rinsed in water 3x. After rinsing, membranes were blocked in 5% milk in 1x TBS with 1% Tween (TBS-Tween) for 1 hour at RT before being incubated with primary antibodies diluted in 5% milk in TBS-Tween overnight at 4°C. The following day, after 3 x 10 min washes with TBS-Tween, membranes were incubated with secondary antibodies for 1 hour at RT. Following 6 × 10 min washes, membranes were incubated with chemiluminescence substrate (PerkinElmer #NEL105001EA) for 1 min and exposed to Amersham Hyperfilm ECL (VWR, 95017-661). Bands were quantified by densitometry using ImageJ software. GAPDH was used to normalize protein content and data is expressed as a percentage of control within a given experiment. The following antibodies were used: anti-Cntnap2 (1:5000, Abcam, 153856), anti-PV (1:2500, Abcam, 11427), anti-GAPDH (1:5000, Cell Signaling, 51745S), and anti-rabbit goat HRP conjugate (1:5000, BioRad, 1705046).

*In situ* hybridization

Fluorescent in situ hybridization was performed to quantify *Pvalb* mRNA expression in the striatum of *Cntnap2*$^{+/+}$ and *Cntnap2*$^{-/-}$ mice. Brains were harvested, flash-frozen in OCT mounting medium (Fisher Scientific #23-730-571) on dry ice and stored at -80°C for up to 6 months. 12-18 µm sections were collected using a cryostat, mounted directly onto Superfrost Plus glass slides (VWR #48311-703) and stored at -80°C for up to 6 months. In situ hybridization was performed according to the protocols provided with the RNAscope Multiplex Fluorescent Reagent Kit (ACD #323100). *Drd1a* mRNA was visualized with a probe in channel 2 (ACD #406491-C2) and *Pvalb* mRNA in channel 3 (ACD #421931-C3). After incubation, sections were secured on slides using VectaShield HardSet mounting medium with DAPI (Vector Laboratories, H-1500-10) and 60 x 24 mm rectangular glass coverslips (VWR #16004-096). Sections were imaged on an Olympus FluoView 3000 confocal microscope using a 10x objective with 1.5x zoom and a step size of 2 µm. *Pvalb* positive cells were quantified across the entire striatum using the ROI manager tool in ImageJ.

Behavioral analysis

All behavior studies were carried out in the dark phase of the light cycle under red lights (open field) or white lights (marble burying, holeboard, rotarod). Mice were habituated to the behavior testing room for at least 30 min prior to testing and covered by a black-out curtain. Mice were given at least one day between different tests. All behavior equipment was cleaned between each trial and mouse with 70% ethanol, and rinsed in diluted soap followed by water at the end of the day. If male and female mice were to be tested on the same day, male mice were run first then returned to the husbandry room, after which all equipment was thoroughly cleaned prior to bringing in female mice for habituation. Behavioral tests were performed with young adult male and female mice (7-11 weeks old). The experimenter was blind to genotype throughout the testing and scoring procedures.

*Open field assay*

Exploratory behavior in a novel environment and general locomotor activity were assessed by a 60 min session in an open field chamber (40 cm L x 40 cm W x 34 cm H) made of transparent plexiglass. Horizontal infrared photobeams were positioned to detect rearing. The mouse was placed in the bottom right-hand corner of the arena and behavior was recorded using an overhead camera and analyzed using the ANY-maze (Stoelting Co.) behavior tracking software. An observer manually scored self-grooming behavior during the first 20 minutes of the test. A grooming bout was defined as an unbroken series of grooming movements, including licking of body, paws, or tail, as well as licking of forepaws followed by rubbing of face with paws.

*Open field assay with DeepLabCut/MoSeq analysis*

60 min video for each animal was recorded with a monochrome camera (GS3-U3-41C6NIR-C) and a 16 mm wide angle lens (LM16HC) placed on top of the open field arena from a height of 50 cm. To extract the body part (keypoint) coordinates from the video recordings, DeepLabCut (DLC) 2.3.4 (Mathis, et al. 2018; Nath, et al. 2019) was used. Fourteen body parts including nose, head, left ear, right ear, left forelimb, right forelimb, spine 1, spine 2, spine 3, left hindlimb, right hindlimb, tail 1, tail 2, and tail 3 were manually labelled on a small subset of the video frames. A DLC model was then trained using the annotated frames to label those 14 body parts for all videos recorded. The total distance travelled, and number of center entries were calculated using the coordinate of bodypart tail 1. Discrete behavior syllables were extracted using Keypoint-MoSeq 0.4.4 (Weinreb, et al. 2023). Syllable usage and transition data were obtained using built-in functions of the Keypoint-MoSeq package. Decoding analysis was performed using customized Python 3.9 script. Code available upon request/Github.

*Marble burying assay*

The marble burying assay was used to test for repetitive stereotyped behaviors. 20 black marbles were arranged in an orderly 4 x 5 fashion on top of 5 cm of clean corncob bedding in a standard mouse cage. Overhead room lights were on and white noise was played to induce mild stress. Mice were placed in the cage with the marbles for 30 minutes. The number of unburied marbles (>50% exposed) was recorded after the session.

*Holeboard assay*

The holeboard assay was used to measure exploratory and repetitive behavior. The holeboard apparatus consisted of a smooth, flat opaque gray plastic platform, suspended 10 cm from the base by four plastic pegs in each corner. The board contained 16 evenly spaced 2 cm diameter holes and was surrounded by a 30 cm high clear plastic square encasing. During testing, mice were placed into the center of the holeboard. Mice explored the board for 10 minutes while video was recorded from both an above and side-view camera. Videos were used post-hoc to manually count and map the number of nosepokes made during the task. Nosepokes were defined as the mouse's nose passing through the board barrier when viewed through the side-view camera angle.

*Accelerating rotarod assay*

The accelerating rotarod test was used to examine motor coordination learning. Mice were trained on a rotarod apparatus (Ugo Basile, 47650) for four consecutive days. Three trials were completed per day with a 5 min break between trials. The rotarod was accelerated from 5-40 revolutions per minute (rpm) over 300 s for trials 1-6 (days 1 and 2), and from 10-80 rpm over 300 s for trials 7-12 (days 3 and 4). On the first

testing day, mice were first acclimated to the apparatus by being placed on the rotarod rotating at a constant 5 rpm for 60 s and returned to their home cage for 5 min prior to starting trial 1. Latency to fall, or to rotate off the top of the rotarod barrel, was measured by the rotarod stop-trigger timer.

*Four choice odor-based reversal learning test*

The four-choice odor-based reversal test was used to assess learning and cognitive flexibility. Animals were food restricted for 6 days in total, with unrestricted access to drinking water, and maintained at 90-95% of ad lib feeding body weight. Food was given at the end of the day once testing was completed. Food restriction and introduction to Froot Loop pieces began 48 hours before pre-training. The four-choice test was performed in a custom-made square box (30.5 cm L × 30.5 cm W × 23 cm H) constructed of clear acrylic. Four internal walls 7.6 cm wide partially divided the arena into four quadrants. A 15.2 cm diameter removable cylinder fit in the center of the maze and was lowered between trials (after a digging response) to isolate the mouse from the rest of the maze. Odor stimuli were presented mixed with wood shavings in white ceramic pots measuring 7.3 cm in diameter and 4.5 cm deep. Pots were sham baited with a piece of Fruit Loop cereal (Kellogg's, Battle Creek, MI) secured underneath a mesh screen at the bottom of the pot. The apparatus was cleaned with 2.5% acetic acid followed by water and the pots were cleaned with 70% ethanol followed by water between mice. The apparatus was cleaned with diluted soap and water at the end of each testing day.

On the first habituation day of pre-training (day 1), animals were allowed to freely explore the testing arena for 30 min and consume small pieces of Froot Loops placed inside empty pots positioned in each of the four corners. On the second shaping day of pre-training (day 2), mice learned to dig to find cereal pieces buried in unscented coarse pine wood shavings (Harts Mountain Corporation, Secaucus, NJ). A single pot was used and increasing amounts of unscented wood shavings were used to cover each subsequent cereal reward. The quadrant containing the pot was alternated on each trial and all quadrants were rewarded equally. Trials were untimed and consisted of (in order): two trials with no shavings, two trials with a dusting of shavings, two trials with the pot a quarter full, two trials with the pot half full, and four trials with the cereal piece completely buried by shavings. The mouse was manually returned to the center cylinder between trials.

On the days for odor discrimination (day 3, acquisition) and reversal (day 4), wood shavings were freshly scented on the day of testing. Anise extract (McCormick, Hunt Valley, MD) was used undiluted at 0.02 ml/g of shavings. Clove, litsea, and eucalyptus oils (San Francisco Massage Supply Co., San Francisco, CA) were diluted 1:10 in mineral oil and mixed at 0.02 ml/g of shavings. Thymol (thyme; Alfa Aesar) was diluted 1:20 in 50% ethanol and mixed at 0.01 ml/g of shavings. During the

discrimination phase (day 3), mice had to discriminate between four pots with four different odors and learn which one contained a buried food reward. Each trial began with the mouse confined to the start cylinder, once the cylinder was lifted, timing began and the mouse could freely explore the arena until it chose to dig in a pot. Digging was defined as purposefully moving the shavings with both front paws. A trial was terminated if no choice was made within 3 min and recorded as omission. Criterion was met when the animal completed eight out of ten consecutive trials correctly. The rewarded odor during acquisition was anise.

The first four odor choices made during acquisition were analyzed to determine innate odor preference by the percentage of choices for a given odor: *Cntnap2*$^{+/+}$ 60% thyme, 25% anise, 12.5 clove, 2.5% litsea and *Cntnap2*$^{-/-}$ 47.5% thyme, 45% anise, 7.5% clove, 0% litsea. We note that both *Cntnap2*$^{+/+}$ and *Cntnap2*$^{-/-}$ mice exhibited the strongest innate preference for thyme, an unrewarded odor.

The reversal phase of the task was carried out on day 4. Mice first performed the task with the same rewarded odor as the discrimination day to ensure they learned and remembered the task. After reaching criterion on recall (eight out of ten consecutive trials correct), the rewarded odor was switched and mice underwent a reversal learning test in which a previously unrewarded odor (clove) was rewarded. A novel odor (eucalyptus) was also introduced, which replaced thyme. Perseverative errors were choices to dig in the previously rewarded odor that was no longer rewarded. Regressive errors were choosing the previously rewarded odor after the first correct choice of the newly rewarded odor. Novel errors were choices to dig in the pot with the newly introduced odor for reversal testing. Irrelevant errors were choices to dig in the pot that had never been rewarded (litsea). Omissions were trials in which the mouse failed to make a digging choice within 3 min from the start of the trial. Total errors were the sum of perseverative, regressive, irrelevant, novel, and omission errors. Criterion was met when the mouse completed eight out of ten consecutive trials correctly. The spatial location of the odors was shuffled on each trial.

Quantification and statistical analysis

Experiments were designed to compare the main effect of genotype. The sample sizes were based on prior studies and are indicated in the figure legend for each experiment. Whenever possible, quantification and analyses were performed blind to genotype. GraphPad Prism version 10 was used to perform statistical analyses. The statistical tests and outcomes for each experiment are indicated in the respective figure legend. Two-tailed unpaired t tests were used for comparisons between two groups. For data that did not pass the D'Agostino & Pearson normality test, a Mann-Whitney test was used. Two-way ANOVAs were used to compare differences between groups for experiments with two independent variables. Statistical significance was defined in the figure panels as follows: *$p < 0.05$, **$p < 0.01$, ***$p < 0.001$

**References**


Ade, K. K., Wan, Y., Chen, M., Gloss, B., & Calakos, N. (2011). An Improved BAC Transgenic Fluorescent Reporter Line for Sensitive and Specific Identification of Striatonigral Medium Spiny Neurons. *Front Syst Neurosci*, *5*, 32. https://doi.org/10.3389/fnsys.2011.00032

Ahmed, N. Y., Knowles, R., Liu, L., Yan, Y., Li, X., Schumann, U., Wang, Y., Sontani, Y., Reynolds, N., Natoli, R., Wen, J., Del Pino, I., Mi, D., & Dehorter, N. (2023). Developmental deficits of MGE-derived interneurons in the Cntnap2 knockout mouse model of autism spectrum disorder. *Front Cell Dev Biol*, *11*, 1112062. https://doi.org/10.3389/fcell.2023.1112062

Albelda, N., & Joel, D. (2012). Animal models of obsessive-compulsive disorder: exploring pharmacology and neural substrates. *Neurosci Biobehav Rev*, *36*(1), 47-63. https://doi.org/10.1016/j.neubiorev.2011.04.006

Anderson, G. R., Galfin, T., Xu, W., Aoto, J., Malenka, R. C., & Sudhof, T. C. (2012). Candidate autism gene screen identifies critical role for cell-adhesion molecule CASPR2 in dendritic arborization and spine development. *Proc Natl Acad Sci U S A*, *109*(44), 18120-18125. https://doi.org/10.1073/pnas.1216398109

Angoa-Perez, M., Kane, M. J., Briggs, D. I., Francescutti, D. M., & Kuhn, D. M. (2013). Marble burying and nestlet shredding as tests of repetitive, compulsive-like behaviors in mice. *J Vis Exp*(82), 50978. https://doi.org/10.3791/50978

Antoine, M. W., Langberg, T., Schnepel, P., & Feldman, D. E. (2019). Increased Excitation-Inhibition Ratio Stabilizes Synapse and Circuit Excitability in Four Autism Mouse Models. *Neuron*, *101*(4), 648-661 e644. https://doi.org/10.1016/j.neuron.2018.12.026

APA. (2022). *Diagnostic and Statistical Manual of Mental Disorders* (5th ed., text rev. ed.). https://doi.org/https://doi.org/10.1176/appi.books.9780890425787

Arenkiel, B. R., Peca, J., Davison, I. G., Feliciano, C., Deisseroth, K., Augustine, G. J., Ehlers, M. D., & Feng, G. (2007). In vivo light-induced activation of neural circuitry in transgenic mice expressing channelrhodopsin-2. *Neuron*, *54*(2), 205-218. https://doi.org/10.1016/j.neuron.2007.03.005

Benthall, K. N., Cording, K. R., Agopyan-Miu, A., Wong, C. D., Chen, E. Y., & Bateup, H. S. (2021). Loss of Tsc1 from striatal direct pathway neurons impairs endocannabinoid-LTD and enhances motor routine learning. *Cell Rep*, *36*(6), 109511. https://doi.org/10.1016/j.celrep.2021.109511

Bouyer, J. J., Park, D. H., Joh, T. H., & Pickel, V. M. (1984). Chemical and structural analysis of the relation between cortical inputs and tyrosine hydroxylase-containing terminals in rat neostriatum. *Brain Res*, *302*(2), 267-275. https://doi.org/10.1016/0006-8993(84)90239-7

Brumback, A. C., Ellwood, I. T., Kjaerby, C., Iafrati, J., Robinson, S., Lee, A. T., Patel, T., Nagaraj, S., Davatolhagh, F., & Sohal, V. S. (2018). Identifying specific prefrontal neurons that contribute to autism-associated abnormalities in physiology and social behavior. *Mol Psychiatry*, *23*(10), 2078-2089. https://doi.org/10.1038/mp.2017.213

Brunner, D., Kabitzke, P., He, D., Cox, K., Thiede, L., Hanania, T., Sabath, E., Alexandrov, V., Saxe, M., Peles, E., Mills, A., Spooren, W., Ghosh, A., Feliciano, P., Benedetti, M., Luo Clayton, A., & Biemans, B. (2015). Comprehensive

Analysis of the 16p11.2 Deletion and Null Cntnap2 Mouse Models of Autism Spectrum Disorder. *PLoS One*, *10*(8), e0134572. https://doi.org/10.1371/journal.pone.0134572

Burke, D. A., Rotstein, H. G., & Alvarez, V. A. (2017). Striatal Local Circuitry: A New Framework for Lateral Inhibition. *Neuron*, *96*(2), 267-284. https://doi.org/10.1016/j.neuron.2017.09.019

Calabresi, P., Picconi, B., Tozzi, A., Ghiglieri, V., & Di Filippo, M. (2014). Direct and indirect pathways of basal ganglia: a critical reappraisal. *Nat Neurosci*, *17*(8), 1022-1030. https://doi.org/10.1038/nn.3743

Cifuentes-Diaz, C., Canali, G., Garcia, M., Druart, M., Manett, T., Savariradjane, M., Guillaume, C., Le Magueresse, C., & Goutebroze, L. (2023). Differential impacts of Cntnap2 heterozygosity and Cntnap2 null homozygosity on axon and myelinated fiber development in mouse. *Front Neurosci*, *17*, 1100121. https://doi.org/10.3389/fnins.2023.1100121

Cording, K. R., & Bateup, H. S. (2023). Altered motor learning and coordination in mouse models of autism spectrum disorder. *Front Cell Neurosci*, *17*, 1270489. https://doi.org/10.3389/fncel.2023.1270489

Cromwell, H. C., & Berridge, K. C. (1996). Implementation of action sequences by a neostriatal site: a lesion mapping study of grooming syntax. *J Neurosci*, *16*(10), 3444-3458. https://doi.org/10.1523/JNEUROSCI.16-10-03444.1996

Dawes, J. M., Weir, G. A., Middleton, S. J., Patel, R., Chisholm, K. I., Pettingill, P., Peck, L. J., Sheridan, J., Shakir, A., Jacobson, L., Gutierrez-Mecinas, M., Galino, J., Walcher, J., Kuhnemund, J., Kuehn, H., Sanna, M. D., Lang, B., Clark, A. J., Themistocleous, A. C., . . . Bennett, D. L. (2018). Immune or Genetic-Mediated Disruption of CASPR2 Causes Pain Hypersensitivity Due to Enhanced Primary Afferent Excitability. *Neuron*, *97*(4), 806-822 e810. https://doi.org/10.1016/j.neuron.2018.01.033

De Rubeis, S., He, X., Goldberg, A. P., Poultney, C. S., Samocha, K., Cicek, A. E., Kou, Y., Liu, L., Fromer, M., Walker, S., Singh, T., Klei, L., Kosmicki, J., Shih-Chen, F., Aleksic, B., Biscaldi, M., Bolton, P. F., Brownfeld, J. M., Cai, J., . . . Buxbaum, J. D. (2014). Synaptic, transcriptional and chromatin genes disrupted in autism. *Nature*, *515*(7526), 209-215. https://doi.org/10.1038/nature13772

Delevich, K., Hoshal, B., Zhou, L. Z., Zhang, Y., Vedula, S., Lin, W. C., Chase, J., Collins, A. G. E., & Wilbrecht, L. (2022). Activation, but not inhibition, of the indirect pathway disrupts choice rejection in a freely moving, multiple-choice foraging task. *Cell Rep*, *40*(4), 111129. https://doi.org/10.1016/j.celrep.2022.111129

Ding, J., Peterson, J. D., & Surmeier, D. J. (2008). Corticostriatal and thalamostriatal synapses have distinctive properties. *J Neurosci*, *28*(25), 6483-6492. https://doi.org/10.1523/JNEUROSCI.0435-08.2008

Doig, N. M., Moss, J., & Bolam, J. P. (2010). Cortical and thalamic innervation of direct and indirect pathway medium-sized spiny neurons in mouse striatum. *J Neurosci*, *30*(44), 14610-14618. https://doi.org/10.1523/JNEUROSCI.1623-10.2010

Estes, A., Shaw, D. W., Sparks, B. F., Friedman, S., Giedd, J. N., Dawson, G., Bryan, M., & Dager, S. R. (2011). Basal ganglia morphometry and repetitive behavior in

young children with autism spectrum disorder. *Autism Res*, *4*(3), 212-220. https://doi.org/10.1002/aur.193
Evans, M. M., Kim, J., Abel, T., Nickl-Jockschat, T., & Stevens, H. E. (2024). Developmental Disruptions of the Dorsal Striatum in Autism Spectrum Disorder. *Biol Psychiatry*, *95*(2), 102-111. https://doi.org/10.1016/j.biopsych.2023.08.015
Fernandez, M., Sanchez-Leon, C. A., Llorente, J., Sierra-Arregui, T., Knafo, S., Marquez-Ruiz, J., & Penagarikano, O. (2021). Altered Cerebellar Response to Somatosensory Stimuli in the Cntnap2 Mouse Model of Autism. *eNeuro*, *8*(5). https://doi.org/10.1523/ENEURO.0333-21.2021
Filice, F., Janickova, L., Henzi, T., Bilella, A., & Schwaller, B. (2020). The Parvalbumin Hypothesis of Autism Spectrum Disorder. *Front Cell Neurosci*, *14*, 577525. https://doi.org/10.3389/fncel.2020.577525
Fuccillo, M. V. (2016). Striatal Circuits as a Common Node for Autism Pathophysiology. *Front Neurosci*, *10*, 27. https://doi.org/10.3389/fnins.2016.00027
Gdalyahu, A., Lazaro, M., Penagarikano, O., Golshani, P., Trachtenberg, J. T., & Geschwind, D. H. (2015). Correction: The Autism Related Protein Contactin-Associated Protein-Like 2 (CNTNAP2) Stabilizes New Spines: An In Vivo Mouse Study. *PLoS One*, *10*(5), e0129638. https://doi.org/10.1371/journal.pone.0129638
Gerfen, C. R., & Surmeier, D. J. (2011). Modulation of striatal projection systems by dopamine. *Annu Rev Neurosci*, *34*, 441-466. https://doi.org/10.1146/annurev-neuro-061010-113641
Hartig, W., Brauer, K., & Bruckner, G. (1992). Wisteria floribunda agglutinin-labelled nets surround parvalbumin-containing neurons. *Neuroreport*, *3*(10), 869-872. https://doi.org/10.1097/00001756-199210000-00012
Haunso, A., Ibrahim, M., Bartsch, U., Letiembre, M., Celio, M. R., & Menoud, P. (2000). Morphology of perineuronal nets in tenascin-R and parvalbumin single and double knockout mice. *Brain Res*, *864*(1), 142-145. https://doi.org/10.1016/s0006-8993(00)02173-9
Hawes, S. L., Evans, R. C., Unruh, B. A., Benkert, E. E., Gillani, F., Dumas, T. C., & Blackwell, K. T. (2015). Multimodal Plasticity in Dorsal Striatum While Learning a Lateralized Navigation Task. *J Neurosci*, *35*(29), 10535-10549. https://doi.org/10.1523/JNEUROSCI.4415-14.2015
Hippenmeyer, S., Vrieseling, E., Sigrist, M., Portmann, T., Laengle, C., Ladle, D. R., & Arber, S. (2005). A developmental switch in the response of DRG neurons to ETS transcription factor signaling. *PLoS Biol*, *3*(5), e159. https://doi.org/10.1371/journal.pbio.0030159
Hollander, E., Anagnostou, E., Chaplin, W., Esposito, K., Haznedar, M. M., Licalzi, E., Wasserman, S., Soorya, L., & Buchsbaum, M. (2005). Striatal volume on magnetic resonance imaging and repetitive behaviors in autism. *Biol Psychiatry*, *58*(3), 226-232. https://doi.org/10.1016/j.biopsych.2005.03.040
Inda, M. C., DeFelipe, J., & Munoz, A. (2006). Voltage-gated ion channels in the axon initial segment of human cortical pyramidal cells and their relationship with chandelier cells. *Proc Natl Acad Sci U S A*, *103*(8), 2920-2925. https://doi.org/10.1073/pnas.0511197103

Iossifov, I., O'Roak, B. J., Sanders, S. J., Ronemus, M., Krumm, N., Levy, D., Stessman, H. A., Witherspoon, K. T., Vives, L., Patterson, K. E., Smith, J. D., Paeper, B., Nickerson, D. A., Dea, J., Dong, S., Gonzalez, L. E., Mandell, J. D., Mane, S. M., Murtha, M. T., . . . Wigler, M. (2014). The contribution of de novo coding mutations to autism spectrum disorder. *Nature*, *515*(7526), 216-221. https://doi.org/10.1038/nature13908

Izquierdo, A., Brigman, J. L., Radke, A. K., Rudebeck, P. H., & Holmes, A. (2017). The neural basis of reversal learning: An updated perspective. *Neuroscience*, *345*, 12-26. https://doi.org/10.1016/j.neuroscience.2016.03.021

Juarez, P., & Martinez Cerdeno, V. (2022). Parvalbumin and parvalbumin chandelier interneurons in autism and other psychiatric disorders. *Front Psychiatry*, *13*, 913550. https://doi.org/10.3389/fpsyt.2022.913550

Jurgensen, S., & Castillo, P. E. (2015). Selective Dysregulation of Hippocampal Inhibition in the Mouse Lacking Autism Candidate Gene CNTNAP2. *J Neurosci*, *35*(43), 14681-14687. https://doi.org/10.1523/JNEUROSCI.1666-15.2015

Keaveney, M. K., Tseng, H. A., Ta, T. L., Gritton, H. J., Man, H. Y., & Han, X. (2018). A MicroRNA-Based Gene-Targeting Tool for Virally Labeling Interneurons in the Rodent Cortex. *Cell Rep*, *24*(2), 294-303. https://doi.org/10.1016/j.celrep.2018.06.049

Kravitz, A. V., Freeze, B. S., Parker, P. R., Kay, K., Thwin, M. T., Deisseroth, K., & Kreitzer, A. C. (2010). Regulation of parkinsonian motor behaviours by optogenetic control of basal ganglia circuitry. *Nature*, *466*(7306), 622-626. https://doi.org/10.1038/nature09159

Langen, M., Bos, D., Noordermeer, S. D., Nederveen, H., van Engeland, H., & Durston, S. (2014). Changes in the development of striatum are involved in repetitive behavior in autism. *Biol Psychiatry*, *76*(5), 405-411. https://doi.org/10.1016/j.biopsych.2013.08.013

Lauber, E., Filice, F., & Schwaller, B. (2018). Dysregulation of Parvalbumin Expression in the Cntnap2-/- Mouse Model of Autism Spectrum Disorder. *Front Mol Neurosci*, *11*, 262. https://doi.org/10.3389/fnmol.2018.00262

Lazaro, M. T., Taxidis, J., Shuman, T., Bachmutsky, I., Ikrar, T., Santos, R., Marcello, G. M., Mylavarapu, A., Chandra, S., Foreman, A., Goli, R., Tran, D., Sharma, N., Azhdam, M., Dong, H., Choe, K. Y., Penagarikano, O., Masmanidis, S. C., Racz, B., . . . Golshani, P. (2019). Reduced Prefrontal Synaptic Connectivity and Disturbed Oscillatory Population Dynamics in the CNTNAP2 Model of Autism. *Cell Rep*, *27*(9), 2567-2578 e2566. https://doi.org/10.1016/j.celrep.2019.05.006

Lee, I. B., Lee, E., Han, N. E., Slavuj, M., Hwang, J. W., Lee, A., Sun, T., Jeong, Y., Baik, J. H., Park, J. Y., Choi, S. Y., Kwag, J., & Yoon, B. J. (2024). Persistent enhancement of basolateral amygdala-dorsomedial striatum synapses causes compulsive-like behaviors in mice. *Nat Commun*, *15*(1), 219. https://doi.org/10.1038/s41467-023-44322-8

Li, W., & Pozzo-Miller, L. (2020). Dysfunction of the corticostriatal pathway in autism spectrum disorders. *J Neurosci Res*, *98*(11), 2130-2147. https://doi.org/10.1002/jnr.24560

Lin, W. C., Liu, C., Kosillo, P., Tai, L. H., Galarce, E., Bateup, H. S., Lammel, S., & Wilbrecht, L. (2022). Transient food insecurity during the juvenile-adolescent

period affects adult weight, cognitive flexibility, and dopamine neurobiology. *Curr Biol*, *32*(17), 3690-3703 e3695. https://doi.org/10.1016/j.cub.2022.06.089

Madisen, L., Mao, T., Koch, H., Zhuo, J. M., Berenyi, A., Fujisawa, S., Hsu, Y. W., Garcia, A. J., 3rd, Gu, X., Zanella, S., Kidney, J., Gu, H., Mao, Y., Hooks, B. M., Boyden, E. S., Buzsaki, G., Ramirez, J. M., Jones, A. R., Svoboda, K., . . . Zeng, H. (2012). A toolbox of Cre-dependent optogenetic transgenic mice for light-induced activation and silencing. *Nat Neurosci*, *15*(5), 793-802. https://doi.org/10.1038/nn.3078

Madisen, L., Zwingman, T. A., Sunkin, S. M., Oh, S. W., Zariwala, H. A., Gu, H., Ng, L. L., Palmiter, R. D., Hawrylycz, M. J., Jones, A. R., Lein, E. S., & Zeng, H. (2010). A robust and high-throughput Cre reporting and characterization system for the whole mouse brain. *Nat Neurosci*, *13*(1), 133-140. https://doi.org/10.1038/nn.2467

Martin-de-Saavedra, M. D., Dos Santos, M., Culotta, L., Varea, O., Spielman, B. P., Parnell, E., Forrest, M. P., Gao, R., Yoon, S., McCoig, E., Jalloul, H. A., Myczek, K., Khalatyan, N., Hall, E. A., Turk, L. S., Sanz-Clemente, A., Comoletti, D., Lichtenthaler, S. F., Burgdorf, J. S., . . . Penzes, P. (2022). Shed CNTNAP2 ectodomain is detectable in CSF and regulates Ca(2+) homeostasis and network synchrony via PMCA2/ATP2B2. *Neuron*, *110*(4), 627-643 e629. https://doi.org/10.1016/j.neuron.2021.11.025

Mathis, A., Mamidanna, P., Cury, K. M., Abe, T., Murthy, V. N., Mathis, M. W., & Bethge, M. (2018). DeepLabCut: markerless pose estimation of user-defined body parts with deep learning. *Nat Neurosci*, *21*(9), 1281-1289. https://doi.org/10.1038/s41593-018-0209-y

Nisenbaum, E. S., Xu, Z. C., & Wilson, C. J. (1994). Contribution of a slowly inactivating potassium current to the transition to firing of neostriatal spiny projection neurons. *J Neurophysiol*, *71*(3), 1174-1189. https://doi.org/10.1152/jn.1994.71.3.1174

Orduz, D., Bischop, D. P., Schwaller, B., Schiffmann, S. N., & Gall, D. (2013). Parvalbumin tunes spike-timing and efferent short-term plasticity in striatal fast spiking interneurons. *J Physiol*, *591*(13), 3215-3232. https://doi.org/10.1113/jphysiol.2012.250795

Packard, M. G., & Knowlton, B. J. (2002). Learning and memory functions of the Basal Ganglia. *Annu Rev Neurosci*, *25*, 563-593. https://doi.org/10.1146/annurev.neuro.25.112701.142937

Paterno, R., Marafiga, J. R., Ramsay, H., Li, T., Salvati, K. A., & Baraban, S. C. (2021). Hippocampal gamma and sharp-wave ripple oscillations are altered in a Cntnap2 mouse model of autism spectrum disorder. *Cell Rep*, *37*(6), 109970. https://doi.org/10.1016/j.celrep.2021.109970

Penagarikano, O., Abrahams, B. S., Herman, E. I., Winden, K. D., Gdalyahu, A., Dong, H., Sonnenblick, L. I., Gruver, R., Almajano, J., Bragin, A., Golshani, P., Trachtenberg, J. T., Peles, E., & Geschwind, D. H. (2011). Absence of CNTNAP2 leads to epilepsy, neuronal migration abnormalities, and core autism-related deficits. *Cell*, *147*(1), 235-246. https://doi.org/10.1016/j.cell.2011.08.040

Penagarikano, O., & Geschwind, D. H. (2012). What does CNTNAP2 reveal about autism spectrum disorder? *Trends Mol Med*, *18*(3), 156-163. https://doi.org/10.1016/j.molmed.2012.01.003

Platt, R. J., Zhou, Y., Slaymaker, I. M., Shetty, A. S., Weisbach, N. R., Kim, J. A., Sharma, J., Desai, M., Sood, S., Kempton, H. R., Crabtree, G. R., Feng, G., & Zhang, F. (2017). Chd8 Mutation Leads to Autistic-like Behaviors and Impaired Striatal Circuits. *Cell Rep*, *19*(2), 335-350. https://doi.org/10.1016/j.celrep.2017.03.052

Poliak, S., Gollan, L., Martinez, R., Custer, A., Einheber, S., Salzer, J. L., Trimmer, J. S., Shrager, P., & Peles, E. (1999). Caspr2, a new member of the neurexin superfamily, is localized at the juxtaparanodes of myelinated axons and associates with K+ channels. *Neuron*, *24*(4), 1037-1047. https://doi.org/10.1016/s0896-6273(00)81049-1

Poliak, S., Salomon, D., Elhanany, H., Sabanay, H., Kiernan, B., Pevny, L., Stewart, C. L., Xu, X., Chiu, S. Y., Shrager, P., Furley, A. J., & Peles, E. (2003). Juxtaparanodal clustering of Shaker-like K+ channels in myelinated axons depends on Caspr2 and TAG-1. *J Cell Biol*, *162*(6), 1149-1160. https://doi.org/10.1083/jcb.200305018

Ramirez-Armenta, K. I., Alatriste-Leon, H., Verma-Rodriguez, A. K., Llanos-Moreno, A., Ramirez-Jarquin, J. O., & Tecuapetla, F. (2022). Optogenetic inhibition of indirect pathway neurons in the dorsomedial striatum reduces excessive grooming in Sapap3-knockout mice. *Neuropsychopharmacology*, *47*(2), 477-487. https://doi.org/10.1038/s41386-021-01161-9

Rodenas-Cuadrado, P., Ho, J., & Vernes, S. C. (2014). Shining a light on CNTNAP2: complex functions to complex disorders. *Eur J Hum Genet*, *22*(2), 171-178. https://doi.org/10.1038/ejhg.2013.100

Rothwell, P. E., Fuccillo, M. V., Maxeiner, S., Hayton, S. J., Gokce, O., Lim, B. K., Fowler, S. C., Malenka, R. C., & Sudhof, T. C. (2014). Autism-associated neuroligin-3 mutations commonly impair striatal circuits to boost repetitive behaviors. *Cell*, *158*(1), 198-212. https://doi.org/10.1016/j.cell.2014.04.045

Sanders, S. J., He, X., Willsey, A. J., Ercan-Sencicek, A. G., Samocha, K. E., Cicek, A. E., Murtha, M. T., Bal, V. H., Bishop, S. L., Dong, S., Goldberg, A. P., Jinlu, C., Keaney, J. F., 3rd, Klei, L., Mandell, J. D., Moreno-De-Luca, D., Poultney, C. S., Robinson, E. B., Smith, L., . . . State, M. W. (2015). Insights into Autism Spectrum Disorder Genomic Architecture and Biology from 71 Risk Loci. *Neuron*, *87*(6), 1215-1233. https://doi.org/10.1016/j.neuron.2015.09.016

Sandin, S., Lichtenstein, P., Kuja-Halkola, R., Hultman, C., Larsson, H., & Reichenberg, A. (2017). The Heritability of Autism Spectrum Disorder. *JAMA*, *318*(12), 1182-1184. https://doi.org/10.1001/jama.2017.12141

Santos, F. J., Oliveira, R. F., Jin, X., & Costa, R. M. (2015). Corticostriatal dynamics encode the refinement of specific behavioral variability during skill learning. *Elife*, *4*, e09423. https://doi.org/10.7554/eLife.09423

Satterstrom, F. K., Kosmicki, J. A., Wang, J., Breen, M. S., De Rubeis, S., An, J.-Y., Peng, M., Collins, R., Grove, J., Klei, L., Stevens, C., Reichert, J., Mulhern, M. S., Artomov, M., Gerges, S., Sheppard, B., Xu, X., Bhaduri, A., Norman, U., . . . Walters, R. K. (2020). Large-Scale Exome Sequencing Study Implicates Both

Developmental and Functional Changes in the Neurobiology of Autism. *Cell*, *180*(3), 568-584.e523. https://doi.org/10.1016/j.cell.2019.12.036
Scott, R., Sanchez-Aguilera, A., van Elst, K., Lim, L., Dehorter, N., Bae, S. E., Bartolini, G., Peles, E., Kas, M. J. H., Bruining, H., & Marin, O. (2019). Loss of Cntnap2 Causes Axonal Excitability Deficits, Developmental Delay in Cortical Myelination, and Abnormal Stereotyped Motor Behavior. *Cereb Cortex*, *29*(2), 586-597. https://doi.org/10.1093/cercor/bhx341
Shen, W., Hernandez-Lopez, S., Tkatch, T., Held, J. E., & Surmeier, D. J. (2004). Kv1.2-containing K+ channels regulate subthreshold excitability of striatal medium spiny neurons. *J Neurophysiol*, *91*(3), 1337-1349. https://doi.org/10.1152/jn.00414.2003
Subramanian, K., Brandenburg, C., Orsati, F., Soghomonian, J. J., Hussman, J. P., & Blatt, G. J. (2017). Basal ganglia and autism - a translational perspective. *Autism Res*, *10*(11), 1751-1775. https://doi.org/10.1002/aur.1837
Tai, L. H., Lee, A. M., Benavidez, N., Bonci, A., & Wilbrecht, L. (2012). Transient stimulation of distinct subpopulations of striatal neurons mimics changes in action value. *Nat Neurosci*, *15*(9), 1281-1289. https://doi.org/10.1038/nn.3188
Uddin, L. Q. (2021). Cognitive and behavioural flexibility: neural mechanisms and clinical considerations. *Nat Rev Neurosci*, *22*(3), 167-179. https://doi.org/10.1038/s41583-021-00428-w
Varea, O., Martin-de-Saavedra, M. D., Kopeikina, K. J., Schurmann, B., Fleming, H. J., Fawcett-Patel, J. M., Bach, A., Jang, S., Peles, E., Kim, E., & Penzes, P. (2015). Synaptic abnormalities and cytoplasmic glutamate receptor aggregates in contactin associated protein-like 2/Caspr2 knockout neurons. *Proc Natl Acad Sci U S A*, *112*(19), 6176-6181. https://doi.org/10.1073/pnas.1423205112
Vogt, D., Cho, K. K. A., Shelton, S. M., Paul, A., Huang, Z. J., Sohal, V. S., & Rubenstein, J. L. R. (2018). Mouse Cntnap2 and Human CNTNAP2 ASD Alleles Cell Autonomously Regulate PV+ Cortical Interneurons. *Cereb Cortex*, *28*(11), 3868-3879. https://doi.org/10.1093/cercor/bhx248
Voorn, P., Vanderschuren, L. J., Groenewegen, H. J., Robbins, T. W., & Pennartz, C. M. (2004). Putting a spin on the dorsal-ventral divide of the striatum. *Trends Neurosci*, *27*(8), 468-474. https://doi.org/10.1016/j.tins.2004.06.006
Wiltschko, A. B., Tsukahara, T., Zeine, A., Anyoha, R., Gillis, W. F., Markowitz, J. E., Peterson, R. E., Katon, J., Johnson, M. J., & Datta, S. R. (2020). Revealing the structure of pharmacobehavioral space through motion sequencing. *Nat Neurosci*, *23*(11), 1433-1443. https://doi.org/10.1038/s41593-020-00706-3
Xu, Z. C., Wilson, C. J., & Emson, P. C. (1989). Restoration of the corticostriatal projection in rat neostriatal grafts: electron microscopic analysis. *Neuroscience*, *29*(3), 539-550. https://doi.org/10.1016/0306-4522(89)90129-2
Yin, H. H., Knowlton, B. J., & Balleine, B. W. (2005). Blockade of NMDA receptors in the dorsomedial striatum prevents action-outcome learning in instrumental conditioning. *Eur J Neurosci*, *22*(2), 505-512. https://doi.org/10.1111/j.1460-9568.2005.04219.x
Yin, H. H., Knowlton, B. J., & Balleine, B. W. (2006). Inactivation of dorsolateral striatum enhances sensitivity to changes in the action-outcome contingency in

instrumental conditioning. *Behav Brain Res*, *166*(2), 189-196. https://doi.org/10.1016/j.bbr.2005.07.012

Yin, H. H., Mulcare, S. P., Hilário, M. R. F., Clouse, E., Holloway, T., Davis, M. I., Hansson, A. C., Lovinger, D. M., & Costa, R. M. (2009). Dynamic reorganization of striatal circuits during the acquisition and consolidation of a skill. *Nature Neuroscience*, *12*(3), 333-341. https://doi.org/10.1038/nn.2261

Zhang, Y. F., Vargas Cifuentes, L., Wright, K. N., Bhattarai, J. P., Mohrhardt, J., Fleck, D., Janke, E., Jiang, C., Cranfill, S. L., Goldstein, N., Schreck, M., Moberly, A. H., Yu, Y., Arenkiel, B. R., Betley, J. N., Luo, W., Stegmaier, J., Wesson, D. W., Spehr, M., . . . Ma, M. (2021). Ventral striatal islands of Calleja neurons control grooming in mice. *Nat Neurosci*, *24*(12), 1699-1710. https://doi.org/10.1038/s41593-021-00952-z

**Dissertation summary**

Autism spectrum disorder (ASD) is a neurodevelopmental disorder with an estimated global prevalence of 1 in 100 (Zeidan et al., 2022). Genetic sequencing has led to the identification of over 100 strong candidate or high confidence ASD risk genes, which vary greatly in the types of proteins for which they code (Satterstrom et al., 2020). With this increase in identification of ASD risk genes, many mouse models of the disorder have been developed that exhibit good construct validity, harboring mutations in risk genes that have been identified in the human ASD population (Bey & Jiang, 2014; Nestler & Hyman, 2010). Despite the genetic heterogeneity of risk genes, ASD is diagnosed primarily through the identification of behaviors that fall into two domains: persistent deficits in social communication and interaction, and the presentation of restricted, repetitive patterns of behavior (APA, 2022). Given this shared symptomology, much work has been done to identify brain regions that may be commonly altered in ASD. The basal ganglia, in particular the striatum, the main input center of the basal ganglia, has been identified as one such brain region (Fuccillo, 2016; Li & Pozzo-Miller, 2020). Indeed, studies in both humans and animal models have shown that the striatum plays a functional role in both social and motor behaviors (Baez-Mendoza & Schultz, 2013; Graybiel & Grafton, 2015; Gunaydin & Deisseroth, 2014; Hassler, 1978). While evidence from a genetically diverse number of ASD mouse models have identified changes in striatal function (Cording & Bateup, 2023; Fuccillo, 2016; Li & Pozzo-Miller, 2020), a comprehensive assessment of the striatum as a convergently altered region in ASD has yet to be done. This dissertation, through literature review and the results of two studies, details convergent striatal changes in the context of ASD-associated motor behaviors in particular.

The second chapter of this dissertation provides a comprehensive literature review of the relationship between striatal circuit function, and changes in performance in the accelerating rotarod motor learning assay, a behavioral test used commonly to assess motor function in ASD mouse models. Corticostriatal changes, which have been identified across a range of ASD mouse models, are likely to drive alterations in this behavior, as it relies on proper corticostriatal synaptic plasticity and function. Here I collated rotarod behavior findings across more than 50 genetically distinct ASD mouse models, highlighting the studies that identified increased rotarod performance in the model. While in many of these models assessment of striatal circuit function was not pursued, a few mouse models that exhibit increased performance in the rotarod also exhibit increased cortical drive of striatal cells. Given that cortical, in particular sensorimotor, input into the striatum is necessary for motor sequence learning, it is possible that increased drive at this synapse imbues the striatum with the ability to more efficiently carry out these sequences. This may underlie the increased rotarod performance seen in the ASD mouse models covered in this review, and may factor in to the stereotyped, repetitive motor behaviors seen in ASD more broadly.

To determine the cell autonomous impact of ASD-related mutations, I first worked with a mouse model that utilized striatal cell type-specific developmental deletion of the ASD risk gene *Tsc1*. We found that mice with *Tsc1* deletion in striatal projection neurons of the direct pathway (dSPNs), but not the indirect pathway (iSPNs), exhibit increased

performance in the accelerating rotarod. Electrophysiological assessment determined that *Tsc1* KO dSPNs also exhibit increased cortical drive, which was not the case for *Tsc1* KO iSPNs. This is likely due to increased glutamatergic release from cortical inputs onto these cells, as *Tsc1* KO dSPN paired-pulse ratio is decreased compared to wildtype (WT) dSPNs. Measuring endocannabinoid-mediated long-term depression, the most common form of synaptic depression utilized by SPNs of the dorsal striatum, revealed a deficit in this form of LTD in *Tsc1* KO dSPNs. The lack of this brake on corticostriatal plasticity is likely what underlies the increase in cortical drive of these cells, and potentially the resultant change in rotarod performance.

To assess striatal function and striatum-related behaviors in an ASD mouse model with whole-brain loss of a risk gene, I next worked with mice lacking the ASD risk gene *Cntnap2*. I found that in the dorsal striatum of *Cntnap2*$^{-/-}$ mice, both dSPNs and iSPNs exhibit increased cortical drive. This change is not likely due to enhanced synaptic excitation or decreased inhibition onto these cells, as cortical excitatory input was normal, and there were no deficits in broad or PV-interneuron specific inhibitory input onto SPNs in *Cntnap2*$^{-/-}$ mice. Instead, the intrinsic excitability of SPNs in *Cntnap2*$^{-/-}$ mice was significantly increased, in particular in dSPNs. This increase in excitability likely underlies the increased cortical drive in these cells, whereby an equivalent strength of cortical input is sufficient to drive more downstream striatal activation. Behaviorally, *Cntnap2*$^{-/-}$ mice perform significantly better in the accelerating rotarod task, exhibit increased spontaneous repetitive motor behaviors, and have decreased cognitive flexibility in a reversal learning task. Taken together, *Cntnap2*$^{-/-}$ mice exhibit increased cortical drive, in particular of the striatal direct pathway, which coincides with increased motor routine learning, and other inflexible repetitive behaviors.

In summary, this dissertation has shown through review of the literature and the study of two genetically distinct mouse models that striatal circuits are a site of convergent dysfunction in ASD mouse models. More specifically, changes in corticostriatal drive, in particular in the movement-initiating direct pathway, occur in a number of these models. While the cellular physiological phenotypes that occur in these models differ, just as their ASD risk gene underpinnings do, the cumulative impact on striatal output is the same. In the case of the *Tsc1* model, a deficit in eCB-LTD onto dSPNs is likely driving the increased cortical input onto these cells, while in the *Cntnap2* model, increased intrinsic excitability of dSPNs likely underlies the increased cortical drive. Ultimately, increased excitability of the direct pathway occurs in both models. This change in drive coincides with increased performance on the accelerating rotarod assay of motor learning in both models, as it does in other ASD mouse models discussed in Chapter 2. As rotarod learning is a corticostriatal-dependent behavior, increased activation of the direct pathway may imbue mice with an increased ability to learn and execute the motor sequence required to stay on the rod for longer. Further study is needed to directly connect the physiological changes observed in the models discussed with the behavioral changes that they share, but it is possible that the increased motor routine learning observed these mice contributes to the emergence of restricted, repetitive behaviors in ASD more broadly.

**Future directions**

The experiments of this dissertation identify changes in striatal circuit physiology and striatum-associated behaviors in two distinct ASD mouse models. However, more direct functional relationships both between 1) the mutated gene and the physiological change that occurs, and 2) the physiological change and the behavioral alterations observed remain to be defined. Potential future pursuits in both avenues are described below.

*Connecting gene mutation to cellular function*

In the *Tsc1* model, deletion of *Tsc1* from dSPNs but not iSPNs led to changes in physiology and rotarod behavior. Specifically, dSPNs exhibited increased cortical drive, likely due to increased glutamate release probability onto these cells. This release change may occur due to a developmental deficit in eCB-LTD: Tsc1 KO dSPNs exhibited impaired eCB-LTD, and significant decreases in ribosome bound mRNA encoding proteins involved in eCB-LTD signaling (e.g. Type 1 metabotropic glutamate receptors - *Grm1* and *Grm5*, mGluR scaffolding protein Homer1 - *Homer1*, and the endocannabinoid precursor phospholipase C beta 1 - *Plcb1*). Since it is unclear whether this change in ribosome-bound mRNA reflects a change in protein expression, a western blot assay of striatal tissue would more clearly indicate which stage of endocannabinoid production and/or release is specifically impacted. From these results, a clearer understanding of the particular molecular impact that *Tsc1* deletion has on dSPNs would arise, as would a target for potential rescue of the eCB-LTD deficit.

In the *Cntnap2* model, whole brain loss of *Cntnap2* resulted in significantly increased intrinsic excitability of both dSPNs and iSPNs. *Cntnap2* has been implicated in a number of neuronal processes (Anderson et al., 2012; Martin-de-Saavedra et al., 2022; Varea et al., 2015), but most classically it is thought to be involved in the clustering of voltage-gated potassium channels (Inda et al., 2006; Poliak et al., 1999; Poliak et al., 2003). In cortical culture work, Caspr2, the protein that *Cntnap2* encodes, was most associated with Kv1.1 and Kv1.2 channels (Scott et al., 2019). As these channels, in particular Kv1.2, play a direct and important role in SPN intrinsic excitability, it is likely that either the proper organization or function of these channels is altered in *Cntnap2*$^{-/-}$ SPNs (Nisenbaum et al., 1994; Shen et al., 2004). Physiological experiments that isolate and assess the Kv1.2-dependent slowly-inactivating A-type current in *Cntnap2*$^{-/-}$ SPNs would identify altered Kv1.2 function downstream of Caspr2 loss, and may mechanistically explain the intrinsic excitability change in these cells.

*Connecting cellular function to behavioral phenotype*

In both the *Tsc1* and *Cntnap2* models assessed, we identified increased corticostriatal drive as well as enhanced performance in the rotarod task, a corticostriatal-dependent behavior (Dang et al., 2006; Kupferschmidt et al., 2019; Yin et al., 2009). However, it is unclear whether the increased direct pathway drive in these mice is the mechanism that drives increased performance in the accelerating rotarod task. In the case of the *Tsc1* KO dSPN model, where the eCB-LTD deficit likely underlies the increased drive of dSPNs, we found reduction in the ribosome binding of mRNA transcripts for protein machinery involved in the production and release of eCBs. This suggests that this deficit in eCB-LTD may be due to a lack of availability/release of eCBs, as cannabinoid receptors were shown to be functional in these mice.

Administering a positive allosteric modulator of an eCB precursor like diacylglycerol lipase (DAGL$\alpha$) in the *Tsc1* KO dSPN mice, or inhibiting eCB-LTD machinery in a WT mouse and assessing rotarod behavior would more clearly illuminate the functional relationship between eCB-LTD at dSPNs and rotarod behavior.

In the case of the *Cntap2* model, increased intrinsic excitability, in particular in dSPNs, likely underlies the increased cortical drive of these cells and in turn may increase rotarod performance. Expression of the inward-rectifying potassium channel Kir in dSPNs of *Cntnap2*$^{-/-}$ mice would decrease their intrinsic excitability, and thus may eliminate the increased motor learning phenotype seen in these mice. Indeed, it has been shown that decreasing dSPN intrinsic excitability in the dorsal striatum in WT mice is sufficient to decrease performance in the rotarod (Rothwell et al., 2014). In our study, *Cntnap2*$^{-/-}$ mice exhibited a number of other altered motor behaviors in addition to increased motor learning. For these behaviors, the involvement of the dorsolateral striatum, the region in which we performed recordings, is less defined. For this reason, assessment of circuits in *Cntnap2*$^{-/-}$ mice in the other implicated striatal subregions might better illuminate a potential functional relationship with behavior: Islands of Calleja and dorsomedial striatum (DMS) for self-grooming behavior (Ramirez-Armenta et al., 2022; Zhang et al., 2021) and DMS and nucleus accumbens (NAc) for four-choice reversal learning behavior (Delevich et al., 2022; Izquierdo et al., 2017). However, we note that for the four-choice reversal learning assay utilized, one study found that decreased dopamine release solely in the DLS coincided with a similar cognitive inflexibility phenotype in the task to that observed in our *Cntnap2* study (Lin et al., 2022). Preliminary evidence in the lab suggests that *Cntnap2*$^{-/-}$ mice also exhibit decreased dopamine release specifically in the DLS (data not shown), as measured by fast-scan cyclic voltammetry. Further analysis of dopaminergic circuits in *Cntnap2-/-* mice should be pursued to investigate this potential functional connection.

In conclusion, the literature summarized in chapters one and two, and the study findings described in chapters three and four of this dissertation support the role of altered striatal function in the manifestation of ASD-associated motor behaviors. In particular, these chapters highlight corticostriatal synapses as a point of potential convergent change across a diverse number of ASD risk gene mutations. Identifying convergence in ASD is difficult for several reasons, one of which being the large variability of developmental timepoints, recording techniques and behavioral assays used across different studies. To reconcile this in the striatum, a comprehensive study of a diverse range of ASD mouse models should be performed across developmental timepoints, utilizing consistent physiological methods to assess the function of primary cell types in multiple striatal subregions. Similarly, at the behavioral level, a battery of behavioral assays of both social and motor behaviors in these models, performed at the same developmental timepoints, would best complement this data. Together, this type of study would provide the most cohesive understanding to date of the striatum as a region of potential convergent functional change in ASD.

**References**


Anderson, G. R., Galfin, T., Xu, W., Aoto, J., Malenka, R. C., & Sudhof, T. C. (2012). Candidate autism gene screen identifies critical role for cell-adhesion molecule CASPR2 in dendritic arborization and spine development. *Proc Natl Acad Sci U S A*, *109*(44), 18120-18125. https://doi.org/10.1073/pnas.1216398109

APA. (2022). *Diagnostic and Statistical Manual of Mental Disorders* (5th ed., text rev. ed.). https://doi.org/https://doi.org/10.1176/appi.books.9780890425787

Baez-Mendoza, R., & Schultz, W. (2013). The role of the striatum in social behavior. *Front Neurosci*, *7*, 233. https://doi.org/10.3389/fnins.2013.00233

Bey, A. L., & Jiang, Y. H. (2014). Overview of Mouse Models of Autism Spectrum Disorders. *Current Protocols in Pharmacology*, *66*(1). https://doi.org/10.1002/0471141755.ph0566s66

Cording, K. R., & Bateup, H. S. (2023). Altered motor learning and coordination in mouse models of autism spectrum disorder. *Front Cell Neurosci*, *17*, 1270489. https://doi.org/10.3389/fncel.2023.1270489

Dang, M. T., Yokoi, F., Yin, H. H., Lovinger, D. M., Wang, Y., & Li, Y. (2006). Disrupted motor learning and long-term synaptic plasticity in mice lacking NMDAR1 in the striatum. *Proc Natl Acad Sci U S A*, *103*(41), 15254-15259. https://doi.org/10.1073/pnas.0601758103

Delevich, K., Hoshal, B., Zhou, L. Z., Zhang, Y., Vedula, S., Lin, W. C., Chase, J., Collins, A. G. E., & Wilbrecht, L. (2022). Activation, but not inhibition, of the indirect pathway disrupts choice rejection in a freely moving, multiple-choice foraging task. *Cell Rep*, *40*(4), 111129. https://doi.org/10.1016/j.celrep.2022.111129

Fuccillo, M. V. (2016). Striatal Circuits as a Common Node for Autism Pathophysiology. *Front Neurosci*, *10*, 27. https://doi.org/10.3389/fnins.2016.00027

Graybiel, A. M., & Grafton, S. T. (2015). The striatum: where skills and habits meet. *Cold Spring Harb Perspect Biol*, *7*(8), a021691. https://doi.org/10.1101/cshperspect.a021691

Gunaydin, L. A., & Deisseroth, K. (2014). Dopaminergic Dynamics Contributing to Social Behavior. *Cold Spring Harb Symp Quant Biol*, *79*, 221-227. https://doi.org/10.1101/sqb.2014.79.024711

Hassler, R. (1978). Striatal control of locomotion, intentional actions and of integrating and perceptive activity. *J Neurol Sci*, *36*(2), 187-224. https://doi.org/10.1016/0022-510x(78)90082-5

Inda, M. C., DeFelipe, J., & Munoz, A. (2006). Voltage-gated ion channels in the axon initial segment of human cortical pyramidal cells and their relationship with chandelier cells. *Proc Natl Acad Sci U S A*, *103*(8), 2920-2925. https://doi.org/10.1073/pnas.0511197103

Izquierdo, A., Brigman, J. L., Radke, A. K., Rudebeck, P. H., & Holmes, A. (2017). The neural basis of reversal learning: An updated perspective. *Neuroscience*, *345*, 12-26. https://doi.org/10.1016/j.neuroscience.2016.03.021

Kupferschmidt, D. A., Augustin, S. M., Johnson, K. A., & Lovinger, D. M. (2019). Active Zone Proteins RIM1alphabeta Are Required for Normal Corticostriatal Transmission and Action Control. *J Neurosci*, *39*(8), 1457-1470. https://doi.org/10.1523/JNEUROSCI.1940-18.2018

Li, W., & Pozzo-Miller, L. (2020). Dysfunction of the corticostriatal pathway in autism spectrum disorders. *J Neurosci Res*, *98*(11), 2130-2147. https://doi.org/10.1002/jnr.24560

Lin, W. C., Liu, C., Kosillo, P., Tai, L. H., Galarce, E., Bateup, H. S., Lammel, S., & Wilbrecht, L. (2022). Transient food insecurity during the juvenile-adolescent period affects adult weight, cognitive flexibility, and dopamine neurobiology. *Curr Biol*, *32*(17), 3690-3703 e3695. https://doi.org/10.1016/j.cub.2022.06.089

Martin-de-Saavedra, M. D., Dos Santos, M., Culotta, L., Varea, O., Spielman, B. P., Parnell, E., Forrest, M. P., Gao, R., Yoon, S., McCoig, E., Jalloul, H. A., Myczek, K., Khalatyan, N., Hall, E. A., Turk, L. S., Sanz-Clemente, A., Comoletti, D., Lichtenthaler, S. F., Burgdorf, J. S., . . . Penzes, P. (2022). Shed CNTNAP2 ectodomain is detectable in CSF and regulates Ca(2+) homeostasis and network synchrony via PMCA2/ATP2B2. *Neuron*, *110*(4), 627-643 e629. https://doi.org/10.1016/j.neuron.2021.11.025

Nestler, E. J., & Hyman, S. E. (2010). Animal models of neuropsychiatric disorders. *Nat Neurosci*, *13*(10), 1161-1169. https://doi.org/10.1038/nn.2647

Nisenbaum, E. S., Xu, Z. C., & Wilson, C. J. (1994). Contribution of a slowly inactivating potassium current to the transition to firing of neostriatal spiny projection neurons. *J Neurophysiol*, *71*(3), 1174-1189. https://doi.org/10.1152/jn.1994.71.3.1174

Poliak, S., Gollan, L., Martinez, R., Custer, A., Einheber, S., Salzer, J. L., Trimmer, J. S., Shrager, P., & Peles, E. (1999). Caspr2, a new member of the neurexin superfamily, is localized at the juxtaparanodes of myelinated axons and associates with K+ channels. *Neuron*, *24*(4), 1037-1047. https://doi.org/10.1016/s0896-6273(00)81049-1

Poliak, S., Salomon, D., Elhanany, H., Sabanay, H., Kiernan, B., Pevny, L., Stewart, C. L., Xu, X., Chiu, S. Y., Shrager, P., Furley, A. J., & Peles, E. (2003). Juxtaparanodal clustering of Shaker-like K+ channels in myelinated axons depends on Caspr2 and TAG-1. *J Cell Biol*, *162*(6), 1149-1160. https://doi.org/10.1083/jcb.200305018

Ramirez-Armenta, K. I., Alatriste-Leon, H., Verma-Rodriguez, A. K., Llanos-Moreno, A., Ramirez-Jarquin, J. O., & Tecuapetla, F. (2022). Optogenetic inhibition of indirect pathway neurons in the dorsomedial striatum reduces excessive grooming in Sapap3-knockout mice. *Neuropsychopharmacology*, *47*(2), 477-487. https://doi.org/10.1038/s41386-021-01161-9

Rothwell, P. E., Fuccillo, M. V., Maxeiner, S., Hayton, S. J., Gokce, O., Lim, B. K., Fowler, S. C., Malenka, R. C., & Sudhof, T. C. (2014). Autism-associated neuroligin-3 mutations commonly impair striatal circuits to boost repetitive behaviors. *Cell*, *158*(1), 198-212. https://doi.org/10.1016/j.cell.2014.04.045

Satterstrom, F. K., Kosmicki, J. A., Wang, J., Breen, M. S., De Rubeis, S., An, J.-Y., Peng, M., Collins, R., Grove, J., Klei, L., Stevens, C., Reichert, J., Mulhern, M. S., Artomov, M., Gerges, S., Sheppard, B., Xu, X., Bhaduri, A., Norman, U., . . . Walters, R. K. (2020). Large-Scale Exome Sequencing Study Implicates Both Developmental and Functional Changes in the Neurobiology of Autism. *Cell*, *180*(3), 568-584.e523. https://doi.org/10.1016/j.cell.2019.12.036

Scott, R., Sanchez-Aguilera, A., van Elst, K., Lim, L., Dehorter, N., Bae, S. E., Bartolini, G., Peles, E., Kas, M. J. H., Bruining, H., & Marin, O. (2019). Loss of Cntnap2 Causes Axonal Excitability Deficits, Developmental Delay in Cortical Myelination, and Abnormal Stereotyped Motor Behavior. *Cereb Cortex*, *29*(2), 586-597. https://doi.org/10.1093/cercor/bhx341

Shen, W., Hernandez-Lopez, S., Tkatch, T., Held, J. E., & Surmeier, D. J. (2004). Kv1.2-containing K+ channels regulate subthreshold excitability of striatal medium spiny neurons. *J Neurophysiol*, *91*(3), 1337-1349. https://doi.org/10.1152/jn.00414.2003

Varea, O., Martin-de-Saavedra, M. D., Kopeikina, K. J., Schurmann, B., Fleming, H. J., Fawcett-Patel, J. M., Bach, A., Jang, S., Peles, E., Kim, E., & Penzes, P. (2015). Synaptic abnormalities and cytoplasmic glutamate receptor aggregates in contactin associated protein-like 2/Caspr2 knockout neurons. *Proc Natl Acad Sci U S A*, *112*(19), 6176-6181. https://doi.org/10.1073/pnas.1423205112

Yin, H. H., Mulcare, S. P., Hilário, M. R. F., Clouse, E., Holloway, T., Davis, M. I., Hansson, A. C., Lovinger, D. M., & Costa, R. M. (2009). Dynamic reorganization of striatal circuits during the acquisition and consolidation of a skill. *Nature Neuroscience*, *12*(3), 333-341. https://doi.org/10.1038/nn.2261

Zeidan, J., Fombonne, E., Scorah, J., Ibrahim, A., Durkin, M. S., Saxena, S., Yusuf, A., Shih, A., & Elsabbagh, M. (2022). Global prevalence of autism: A systematic review update. *Autism Research*, *15*(5), 778-790. https://doi.org/10.1002/aur.2696

Zhang, Y. F., Vargas Cifuentes, L., Wright, K. N., Bhattarai, J. P., Mohrhardt, J., Fleck, D., Janke, E., Jiang, C., Cranfill, S. L., Goldstein, N., Schreck, M., Moberly, A. H., Yu, Y., Arenkiel, B. R., Betley, J. N., Luo, W., Stegmaier, J., Wesson, D. W., Spehr, M., . . . Ma, M. (2021). Ventral striatal islands of Calleja neurons control grooming in mice. *Nat Neurosci*, *24*(12), 1699-1710. https://doi.org/10.1038/s41593-021-00952-z